



Technische Universität München

Fakultät für Chemie

Professur für Molekulare Katalyse

Heavier *N*-Heterocyclic Tetrylenes in Platinum-Catalyzed Alkene Hydrosilylation

SEBASTIAN MARTIN HÖLZL

Vollständiger Abdruck der von der Fakultät für Chemie der Technischen Universität München zur Erlangung des akademischen Grades eines

Doktors der Naturwissenschaften (Dr. rer. nat.)

genehmigten Dissertation.

Vorsitzender:

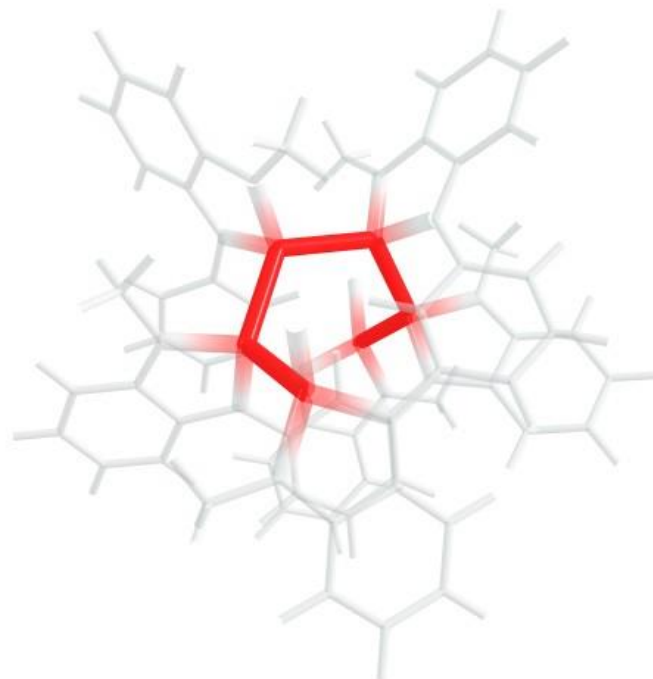
Prof. Dr. Tom Nilges

Prüfer der Dissertation:

1. Prof. Dr. Fritz E. Kühn

2. Prof. Dr. Shigeyoshi Inoue

Die Dissertation wurde am 11.07.2019 bei der Technischen Universität München eingereicht und durch die Fakultät für Chemie am 16.09.2019 angenommen.



„Wenn will geht Alles“

Die vorliegende Arbeit wurde im Zeitraum von September 2016 bis Juli 2019 im Fachgebiet Molekulare Katalyse der Technischen Universität München angefertigt.

Mein ganz besonderer Dank gilt meinem Doktorvater

Herrn Prof. Dr. Fritz E. Kühn

für die Möglichkeit meine Promotion in seiner Arbeitsgruppe anzufertigen, für die Freiheiten und das Vertrauen im Rahmen der Kooperation mit der Wacker Chemie AG sowie die exzellenten Arbeitsbedingungen und bereitgestellten Mittel im Katalysezentrum der Technischen Universität München. Die spannenden Gespräche waren für mich Wegbereiter meiner Doktorarbeit und haben mir neue Einblicke in die Welt der Wissenschaft und darüber hinaus gegeben.

Darüber hinaus möchte ich mich herzlich bedanken bei

Herrn. Prof. Dr. Shigeyoshi Inoue

für seinen steten wissenschaftlichen Rat zu meiner Doktorarbeit sowie kontinuierliche Diskussionen über die Welt der niedervalenten Verbindungen. Die vielen konstruktiven Gespräche waren für den Erfolg meiner Arbeit von entscheidender Bedeutung.

Diese Arbeit ist im Rahmen einer Kooperation der TU München mit der Wacker Chemie AG entstanden.

DANKSAGUNG

Durch die Hilfe von vielen verschiedenen Personen wurde diese Arbeit erst möglich. Zahllose Gespräche, aufmunternde Worte und Rückhalt auch abseits der Arbeit haben mir die nötige Zuversicht und den Optimismus gegeben, um meine Doktorarbeit erfolgreich zu gestalten.

Mein Dank gilt **Herrn Dr. Richard Weidner, Frau Dr. Elke Fritz-Langhals** und **Herrn Dr. Jan Tillmann** der WACKER Chemie AG für den regen Austausch und aufschlussreiche Diskussionen. Insbesondere Herrn Dr. Richard Weidner für die kontinuierliche Unterstützung in der Funktion als Mentor meiner Promotion.

Herausstellen möchte ich **Frau Hifinger**, die mir in vielen Situationen des oft undurchsichtig erscheinenden Promotionsalltags mit unerschütterlicher Geduld weitergeholfen hat.

Bei meinem Labor samt **Lorenz, Christiane** und **Nadine**, die mir die 3 Jahre im CRC2010 extrem angenehm und unkompliziert gestaltet haben. Besonders meinen Nachbarn **Marco** und **Daniela**, die es nie langweilig werden lassen und wirklich zu jedem Zeitpunkt mehr als hilfsbereit waren. Ich finde jeder sollte einmal einen Marco als Laborpartner erleben dürfen!

Besonders möchte ich mich an dieser Stelle bei meinem Laborpartner **Lorenz** bedanken, der mir nicht nur im Labor ein wichtiger Rückhalt war sondern auch sonst ein steter Freund und Ratgeber ist. In unzähligen Gesprächen und Stunden hat er meine Begeisterungen geteilt und oft den Blick fürs Wesentliche gehabt – auch wenn er von Silylenen bis zum Schluss nicht überzeugt werden konnte.

Bei **Jens O.**, der ein Eckpfeiler meiner Promotionszeit war und ist. Danke Jens, dass du auch nach 1000 Kristallen die Geduld nicht verloren hast und uns auch einmal an die wichtigen Dinge des Lebens erinnerst.

Danke **Bruno** für deine italienischen Weisheiten und deutschen Tugenden.

Bei **Robert**, der so etwas wie der Anker unserer Gruppe ist, sich für jedes Problem Zeit nimmt und mit Rat und Tat zur Seite steht. Über die drei Jahre hast du mir in vielen Situationen weitergeholfen und immer für Harmonie in der Gruppe gesorgt.

Felix und **Ben**, die innerhalb der Kooperation mit der Wacker Chemie AG essenzielle Hilfen zu meiner Arbeit geleistet haben und mir in vielen fachlichen Fragen weitergeholfen haben. Insbesondere bei Ben, der mir in den letzten beiden Jahren entscheidend beim Aufsetzen von Katalysen und mit umfangreichen theoretischen Studien unter die Arme gegriffen hat. Vielen Dank für die Zeit, die du dir genommen hast.

Dem gesamten **AK Kühn**, bei der jeder Einzelne zu einer wirklich besonderen Atmosphäre beiträgt. Bedanken möchte ich mich für die vielen Hilfen bei technischen Problemen, bei **Flo D.** fürs Messen von Kristallen und Hilfen bei den Katalysen, bei **Chris** für ESIs zu jeder Tag- und Nachtzeit, bei **Jonas** für die Zeit am Raman und fachliche Diskussionen – und natürlich fürs Mittagessen. Besonders möchte ich mich bei **Andi**, der guten Seele unserer Gruppe, und **Pauline** bedanken – wichtige Vertreter der Münchner Altlappensammlung und mitreißende Sportler/innen (auch **Anja** und **Flo G.** seien an dieser Stelle nicht unerwähnt). Danke, dass ihr von Anfang an für den Zusammenhalt unserer Arbeitsgruppe gesorgt habt. Ein großes Danke an **Lilli**, die auch bei schlechter Stimmung die richtigen Worte findet, und natürlich bei den beiden **Alex**, die schlechte Stimmung erst gar nicht aufkommen lassen. Danke, dass Ihr & alle anderen unseren AK zu einem wirklich Besonderen gemacht habt. Danke auch **Julius & Konsn** vom **AK Fischer** für die Hilfen beim Messen am verflixten LIFDI und Stunden abseits der Arbeit.

Meinen Praktikanten, Bacheloranden und Masteranden, die wichtige Beiträge und Ideen zu verschiedenen Projekten geliefert haben und Freundschaften entstehen haben lassen. Es war einfach eine Freude mit euch zusammenzuarbeiten, von euch zu lernen und gemeinsam Erfolge zu feiern.

Bei **Jürgen, Maria** und **Olaf**, ohne die wir Doktoranden oft mehr als hilflos wären. Danke für die vielen Stunden, in denen Ihr mir Geräte bis ins Detail erklärt habt und die Basis unserer Arbeit erst ermöglicht. Bei **Dr. Markus Drees** und **Dr. Alexander Pöthig**, für die vielen hilfreichen Diskussionen, sei es bei DFT Rechnungen, XRD Messungen oder einfach im alltäglichen Leben.

An dieser Stelle möchte ich mich auch noch einmal bei meinen Betreuern aus der Studiumszeit, **Steven L., Jens K., Lavinia, Teresa, Korbi** und **Tobi**, herzlich bedanken. Letztlich habt Ihr mir den Weg zu einer erfolgreichen Doktorarbeit geebnet und wart Vorbild für meine eigene Promotionszeit in vielerlei Hinsicht. Danke **Jens** und **Tobi**, dass ihr mich bis heute als Freunde unterstützt und ich mich zu jeder Zeit bei euch melden kann.

Meine Studienkollegen und sehr guten Freunden **Zani, Lara, Fabi, Kaddl, Michl, Mara, Lorenz, Jens** und **Annika** nehmen hier noch eine ganz besondere Rolle ein. Ihr habt meine Studentenzzeit in und neben der Uni unvergesslich gemacht. Danke Kaddl, Jens, Lenz & Zani fürs geduldige Lesen der Arbeit!

Mein besonderer Dank gilt **Christina**, für die liebevolle Unterstützung, den unerschütterlichen Rückhalt und Ausgleich. Danke, dass du gerade an den schwierigen Tagen an meiner Seite stehst und mir dann Auftrieb gibst wenn ich verzweifle.

Ich möchte mich am Schluss von Herzen bei meiner ganzen Familie bedanken. Erst durch euch konnte ich diesen Weg gehen. Meinen beiden Brüdern **Andreas** und **Michael**, dass ihr die Familie nie außer Acht lässt und mir helft wann immer ich euch brauche. Meinen Eltern **Evi** und **Hans**, die mir bis heute Vorbild sind, mich begleiten und in jeder Entscheidung unterstützen.

KURZZUSAMMENFASSUNG

Große Mengen an wertvollem Platin werden jährlich in der katalytischen Hydrosilylierung von Olefinen verwendet und verbraucht. Die Vision dieser Arbeit war es deshalb effizientere Prozesse durch maßgeschneiderte Liganden zu entwickeln und damit den Verbrauch dieses Edelmetalls zu reduzieren. Durch den gezielten Einsatz von Liganden können die stereoelektronischen Eigenschaften von katalytisch aktiven Übergangsmetallen optimiert werden. Schwere Homologe von Carbenen können dabei aufgrund ihres Singulett-Grundzustands starke σ -Bindungen zu Metallen aufbauen und lassen gleichzeitig π -Rückbindungen zu. In diesem Zusammenhang eignen sich insbesondere mehrfach koordinierende, *N*-heterozyklische Tetrylene für die Synthese von thermodynamisch stabilen Koordinationsverbindungen.

Im Rahmen dieses Projekts wurden verschiedene *N*-funktionalisierte Dihalogenasilane und -germane synthetisiert und charakterisiert. Arylverbrückte Bis(dibromsilane) können bei sehr niedrigen Temperaturen mit KC_8 zu kinetisch stabilisierten Si_4^- - und Si_6^- -Polysilanbausteinen reduziert werden. Die detaillierte Analyse der molekularen Struktur mittels spektroskopischer Methoden, DFT-Rechnungen und Einkristallanalysen bestätigt den kovalenten Charakter der entstehenden helikalen Siliziumketten. Die Funktionalisierung der terminalen Silizium-Bromid-Gruppen eröffnet neue Möglichkeiten für die Synthese von neuartigen makromolekularen Polysilanen.

In Reaktionen von Pyridyl-funktionalisierten *N*-heterozyklischen Tetrylenen mit Übergangsmetallen wurde eine Vielzahl unterschiedlich koordinierter Germaniumverbindungen charakterisiert. Diese weisen elektronisch-flexible Eigenschaften auf und können im festen Zustand zwei- bis sechsfach koordinierte Zustände einnehmen. Ligand-gebundene Pyridylgruppen sind dazu in der Lage Germylene intramolekular zu stabilisieren – können aber auch als Chelatligand Übergangsmetalle inter- oder intramolekular koordinieren oder in einem nicht-bindenden Zustand verbleiben. Die Stabilisierung von Tetrylenen durch Pyridindonoren verändert dabei die elektronischen Eigenschaften des Liganden signifikant, wodurch beispielsweise die Bindung von *Lewis*-Säuren über Imidazol-Stickstoffatome oder die Insertion in Metallhalogenidbindungen ermöglicht wird.

Funktionalisierte *N*-heterozyklische Germylene können den Verlauf von platin-katalysierten Olefinhydrosilylierungen erheblich verändern. Katalytische Hydrosilylierungen mit *Karstedt's Katalysator* und verschiedenen Ligandadditiven zeigen das große Potenzial von chelatbildenden Tetrylenen in der selektiven Olefinhydrosilylierung. Wie im festen Zustand gezeigt, können Platincluster durch verbrückende Germylene stabilisiert werden. Diese stellen möglicherweise aktive Spezies des Katalysezyklus von Olefinhydrosilylierungen dar.

ABSTRACT

Tremendous amounts of platinum are still consumed in catalytic industrial olefin hydrosilylation processes. The vision of this work was the design and implementation of novel steering ligands, creating more efficient processes and minimizing waste production. As such, heavier tetrylenes comprise unmatched properties considering their capability to bind transition metals as Lewis base and simultaneously enable significant metal-to-ligand backbonding. In this context, the major goal of this thesis was the synthesis of novel silylenes and germylenes, the study of their coordinative properties and their application in platinum-catalyzed olefin hydrosilylation. In particular, chelating *N*-heterocyclic ligands are applied to synthesize thermodynamically stable complexes and to modify the stereoelectronic properties of transition metals.

In the course of this project, synthetic protocols towards several different *N*-functionalized dihalogenesilanes have been developed. Thereby, aryl-bridged bis(dibromosilanes) can be reduced with KC_8 at low temperatures to give kinetically-stabilized Si_4^- - and Si_6^- -polysilane building blocks. The molecular structure investigated by means of spectroscopic methods, SC-XRD analysis and DFT calculations confirm the covalent nature of the helical silicon chain therein. Functionalization of the terminal silicon-bromide bonds opens up new possibilities for the synthesis of unprecedented macromolecular polysilane molecules.

From reactions of pyridyl-functionalized *N*-heterocyclic germylenes with transition metals, a great variety of differently coordinated germanium compounds ranging from dicoordinate to six-fold coordinated motifs are characterized. The flexible pyridyl moieties can stabilize germylenes intramolecularly, coordinate transition metals inter- or intramolecularly or comprise a non-binding state. Thereby, binding of germylenes by pyridine donors changes their electronic properties significantly and enables new reactivities such as coordination of Lewis acids *via* the imidazole nitrogen atoms or insertion into metal halide bonds.

Pyridine-functionalized *N*-heterocyclic germylenes can substantially alter platinum-catalyzed olefin hydrosilylation. In catalytic screenings with *Karstedt's catalyst*, the effect of several different additives is presented, validating the huge potential of chelating NHGes in regard of selective olefin hydrosilylation. Moreover, it is shown that NHGes are capable of stabilizing small platinum clusters forming bonds to several central metals. Such platinum clusters are suggested to play a key role in the catalytic cycle of hydrosilylation chemistry.

LIST OF ABBREVIATIONS

AIOX	aluminum oxide
BTSA	bis(trimethylsilyl)amide
Bu	butyl
COSY	correlated spectroscopy
Cy	cyclohexyl
δ	chemical shift
DABCO	1,4-diazabicyclo[2.2.2]octan
DFT	density functional theory
DIPEA	<i>N,N</i> -diisopropylethylamine
DIPP	diisopropylphenyl
^{DiPP} NHC	bis(2,6-diisopropylphenyl)benzimidazol-2-ylidene
DMAP	4-(dimethylamino)pyridine
dvtms	divinyltetramethyldisiloxane
eq.	equivalents
<i>et al.</i>	<i>et alia</i>
FG	functional group
GC	gas chromatography
HMBC	heteronuclear multiple bond correlation
HOMO	highest occupied molecular orbital
HSi	heptamethyltrisiloxane
HT	heavier tetrylene
INEPT	insensitive nuclei enhancement by polarization transfer
^{iP} NHC	1,3-diisopropylbenzimidazol-2-ylidene
LIFDI	liquid injection field desorption ionization
LiHMDS	lithium bis(trimethylsilyl)amide
LUMO	lowest unoccupied molecular orbital
M	molar (mol/l)
<i>m/z</i>	mass to charge ratio
Mes	mesitylene
^{Mes} NHC	bis(2,4,6-trimethylphenyl)imidazol-2-ylidene

MHz	mega hertz
MS	mass spectrometry
N3Ge	<i>N,N'</i> -neopentyl(pyridin-2-ylmethyl)benzimidazolin-2-germylene
N4Ge	<i>N,N'</i> -bis(pyridin-2-ylmethyl)benzimidazolin-2-germylene
NeoGe	<i>N,N'</i> -bis(neopentyl)benzimidazolin-2-germylene
NHC	<i>N</i> -heterocyclic carbene
NHGe	<i>N</i> -heterocyclic germylene
NHSi	<i>N</i> -heterocyclic silylene
NMR	nuclear magnetic resonance
ppm	parts per million
Py	pyridyl
QTAIM	quantum theory of molecules and atoms
r.t.	room temperature
SC-XRD	single crystal X-Ray diffraction
<i>t</i>	<i>tert</i>
TLC	thin layer chromatography
TMS	tetramethylsilane
UV	ultraviolet
ViSi	1-vinyl-1,1,3,3,3-pentamethyldisiloxan
XRD	X-Ray diffraction

CONTENT

Danksagung	IV
Kurzzusammenfassung	VI
Abstract	VII
List of Abbreviations	VIII
Content	X
1 Introduction	1
1.1 Catalysis	1
1.2 Homogeneous Catalysis	2
1.3 Industrial Homogeneous Catalysis	3
1.4 Heavier Tetrylenes in Homogeneous Catalysis	4
1.5 Platinum-Catalyzed Alkene Hydrosilylation	11
1.6 Tetrylenes in Platinum-Catalyzed Alkene Hydrosilylation	13
1.7 Pincer-Type Ligands in Non-Precious Metal-Catalyzed Olefin-Hydrosilylation	16
2 Objective	18
3 Discussion of Results	20
3.1 From a Bissilylene Precursor to a Kinetically Stabilized Polysilane Molecule	20
3.2 Versatile Coordination Behavior of a Pyridyl-Functionalized NHGe	36
3.3 Pyridyl-Functionalized NHGe Ligands – Reactivity and Coordination Chemistry	48
3.4 Novel Late Transition Metal Complexes of Pyridyl-Functionalized NHGes	65
3.5 Pyridyl-Substituted NHGes as Additives in Alkene Hydrosilylation	73
4 Conclusion and Outlook	82
5 Experimental Section	85
5.1 General Remarks	85
5.2 Synthetic Procedures	89
6 Supplementary Data	118
	X

6.1	LIFDI Mass Spectrometry	118
6.2	NMR Spectroscopy	122
6.3	DFT Calculations	125
6.4	X-Ray Diffraction Analysis	127
6.5	Infrared Spectroscopy	139
6.6	Catalytic Experiments	140
7	References	142

1 INTRODUCTION

1.1 Catalysis

Megatrends of the 21st century are closely connected to the worldwide growing population, the ongoing climate change and developing markets in former third world countries.^{1,2} These challenges can only be addressed by the development of highly efficient, ecologically-friendly processes on large scales. Thereby, catalytic reactions ensure the mass production of basic chemicals as well as the continuous manufacturing of fine chemicals, high performance materials and pharmaceuticals.³⁻⁷ Therefore, the development of new catalysts and processes is of fundamental importance for ensuring high-quality of life also in the future.⁸ More than that, catalytic processes could possibly render fossil fuels abundant and improve the efficient usage of renewable resources.⁹

The discovery of the catalytic activity of certain substances in chemical reactions dates back to the 1830s, when Jakob Berzelius studied the oxidation of coal gas by platinum and J.W. Döbereiner observed the enlightenment of hydrogen.¹⁰ "Catalysis is defined as a process in which the rate and/or the outcome of the reaction is influenced by the presence of a substance (the catalyst) that is not consumed during the reaction and that is subsequently removed if it is not to constitute as an impurity in the final product."¹¹ Already in the past century, catalysts have changed life on Earth. For example, billions of people depend on the Haber-Bosch process, which enables the extraction of nitrogen from air and the production of ammonia-containing fertilizers.¹² Catalytic processes already contribute significantly to the protection of nature as well.^{9, 13, 14} Greater precision and higher efficiencies in industrial processes lead to fewer waste products, less air pollution and reduce the need for the transportation and storage of bulk chemicals. While loads of discussions about air pollution by the automobile industry have dominated the media scene over the past years, platinum-containing catalytic converters have reduced air polluting of NO_x gases by 90%, emissions of hydrocarbons by 97% and CO emissions by 96%.^{9, 15} Another important contribution to sustainable economic growth was the development of olefin hydrosilylation on an industrial scale.^{16, 17} The latter process is crucial to the production of a great variety of daily life applications by the controlled synthesis of functionalized silanes. However, the process generates high costs on an industrial scale as it is still based on platinum catalysts with low selectivity.¹⁸ Thus, research into the development of highly selective catalysts has been ongoing continuously for decades.¹⁹ Thereby, the development of novel homogeneous processes including catalytically active small molecules could be key for achieving the effective usage of a wide range of substrates and efficient transformations thereof.

1.2 Homogeneous Catalysis

One of the greatest challenges in catalytic research is still to pick the exact right conditions of a catalytic system, balancing production and investment costs, efficiency and effectivity.²⁰ The dream of predicting the perfect properties of a catalyst for a desired reaction remains, so far, a dream.²¹ More than that, a highly active and selective catalyst for a certain reaction cannot be designed from scratch by virtue of the theoretical requirements, but has to be probed under practical conditions – once synthesized in usable yield and purity.

Therefore, the development of a novel catalyst is still connected to high investment costs and risks. The global demand for refining catalysts is predicted to reach 4.7×10^3 million \$ by 2020.²² The worldwide investments in catalysts is about 10^4 million € per year while kicking off an estimated market volume of 10^6 million € in products of catalytic processes.⁹ Each improvement of a catalytic reaction therefore pays back over and over again and, thus, there is a great economic drive for the improvement of established processes and the development of new catalysts. Therefore, it is the task of the present and upcoming community to unravel the mere endless multilayers of catalytic mechanisms in order to get deeper understandings and allow accurate reactivity predictions of catalytically active molecules.

During the past decades, understanding of both heterogeneous and homogeneous catalysis has improved significantly, accounting for higher atom economy and greater energy efficiency in the production of chemicals.^{9, 23, 24} Homogeneous catalysis in comparison to still predominant heterogeneous catalysis benefits from a deeper mechanistic understanding driven from the characterization of catalytic active intermediate species.^{25, 26} However, separation of the catalytic material from the product remains one of the major drawbacks in comparison to heterogeneous catalysis.²⁷

The theoretical modeling of catalysis on a molecular level has significantly enhanced in recent years. With a growing understanding of the mechanisms present in catalytic processes, scientists have started to develop a unified molecular basis for all chemical processes.⁹ In combination with continuously improving synthetic methods for molecular catalysts, the custom-fit manufacturing of individual catalysts comes within reach.^{28, 29} So far try and error-based approaches evolve increasingly into computer-assisted approaches.^{21, 30, 31} However, computational techniques and calculations remain sumptuous and are thus not available on a broad scale in the research and development of new catalysts. So far, computers cannot predict the ideal molecular shape in regard to steric demand and electronic properties.²¹ Yet, the development of effective and efficient homogeneous catalysts has significantly improved due to deeper understandings into the nature of a catalytic active molecule.

1.3 Industrial Homogeneous Catalysis

A chemical reaction's nature is highly diverse and thus only perfectly matching catalysts yield high-quality chemicals on a large scale.²⁰ The modification of the catalyst's architecture directly shapes the course of a catalytic reaction.²¹ In homogeneous catalysis, steering ligands enable the customization of the stereoelectronic properties of a catalyst to force the selective manufacturing of the desired product in short times.^{32, 33} In the past decades, new dimensions of chemo- and stereoselectivity have been reached due to the research into new molecules and development of modified ligands.^{34-38;a} Thereby, the industrial production of specialty chemicals, high-performance materials or fine chemicals has significantly improved quantitatively and qualitatively. In the first decade of the 21st century, already three Nobel Prizes in chemistry have been awarded for major achievements in the field of homogeneous catalysis. In 2001, *B. Sharpless, S.W.S. Knowles* and *R. Noyori* have been awarded for their development of homogeneous catalysts which enable chiral hydrogenation and oxidation reactions.³⁹ In 2005, the Nobel prize in chemistry was awarded to *Y. Chauvin, R. H. Grubbs* and *R. R. Schrock* for their research in the field of metathesis catalysts.⁴⁰ The third has been awarded to *R. F. Heck, A. Suzuki* and *E. Negishi* for their contributions to palladium-catalyzed cross-coupling reactions.⁴¹

The properties of transition metal complexes in homogeneous catalysis are mainly determined by the central metal, its oxidation state, and the properties of coordinating ligands.²⁰ Most of the important industrially applied processes are based on cost-intensive and ecologically questionable precious metals.^{20, 32} While the simple substitution of precious metals by benign metals such as iron or copper comes with a lot of difficulties, the application of tailor-made ligands allows for the controlled and predictable shaping of a catalytic reaction.^{32, 42} Consequently, more efficient processes allow for a more selected usage of transition metals and simplified manufacturing of industrial goods.

A great variety of homogeneous catalysts and ligands has thus been developed over the past decades in laboratories worldwide. While many of these wait for further investigation under industrial conditions, only few can potentially be applied in large scale processes, mainly due to economic reasons. A catalytic reaction comprises a large manifold of different interactions, which have to be studied and understood as a whole.²¹ Nowadays, systematic approaches to new applicable catalysts are possible thanks to major progress in the understanding of catalytic reactions and molecular interactions. The design and synthesis of ligands featuring customized properties is, thus, key to the improvement of catalytic reactions.

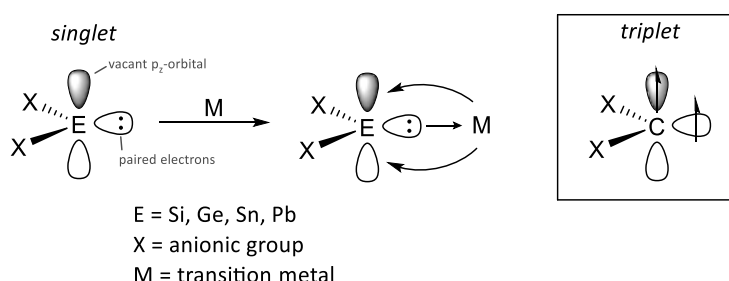
^a Selected examples of recent reviews.

1.4 Heavier Tetrylenes in Homogeneous Catalysis

Significant progress in the understanding and utilization of organometallic chemistry has brought major advantages in homogeneous catalysis over the past two decades.^{20, 28, 32, 43-45} Specifically, the application of *N*-heterocyclic carbenes has been a milestone in the development of various transition metal complexes featuring excellent catalytic properties in fundamental reactions such as cross-coupling reactions, C-H oxidations, or hydrosilylations.⁴⁶⁻⁴⁹ Most important advantages are the ease of shaping their steric and electronic properties through modification of the wingtip moieties (substituents on the imidazole nitrogen atoms) in combination with great thermodynamic stability of transition metal complexes thereof. The major success of NHCs in homogeneous catalysis has triggered the further exploration of stable heavier tetrylenes and their properties as steering ligands in transition metal catalysts.⁵⁰⁻⁵⁴ In recent years, decisive advances in the understanding, synthesis and application of such low-valent tetrylenes have been made. These molecules feature unique properties which potentially enable the development of new catalytic applications.⁵⁵⁻⁵⁸

1.4.1 Properties of Heavier Tetrylenes

Heavier tetrylenes (sometimes called heavier analogs of carbenes) are molecules which contain silicon, germanium, tin or lead in the oxidation state +II.^{44, 59} They significantly differ from their lighter relatives in their altered electronic properties.⁶⁰ The higher elements in the period show a pronounced singlet state due to the inert pair effect and a lower degree of hybridization.⁶⁰⁻⁶⁴ Already in 1990 *Trinquier* has predicted the latter in theoretical calculations of heavier ethylene analogs.⁶⁵ In general, HTs of the formula MX_2 , where M represents the metal and X any anionic group, can act as electron donor and/or acceptor as they possess both a lone-pair of electrons and an empty p_z orbital (Scheme 1).^{66, 67} Compared to carbenes, the polarization of the M-X bond is significantly increased.



Scheme 1: Singlet heavier tetrylenes acting as σ -donor/ π -acceptor in transition metal complexes (left). Triplet carbene shown in the frame (right).⁶⁷

HTs are characterized by their unique reactivity in comparison to their lighter analogs. In recent years, a broad variety of reactions has been reported comprising low-valent tetrylenes in substitution,⁶⁸

insertion,^{69, 70} cycloaddition,^{71, 72} redox-,^{73, 74} or Lewis acid-base reactions.^{75, 76} In transition metal complexes, they can play a valuable role as strong σ -donor- π -acceptor ligands leading to high electronic versatility. The history of HTs in transition metal complexes dates back more than half a century when a silyliron complex has been isolated by *Welz et al.* from the reaction of $\text{Fe}(\text{CO})_5$ with a cyclic dichlorosilane in 1977.^{77, 78} Interestingly, due to their unique electronic properties, heavier analogs of carbenes have been isolated in a dicoordinate state – similarly to carbenes – but also in higher binding modes.⁷⁹⁻⁸³ This variability allows for the development of new ligand/metal combinations customized to the requirements of catalytic processes.

1.4.2 *N*-Heterocyclic Tetrylenes - Stabilizing Strategies

In contrast to their lighter carbene analogs, HTs have a singlet ground state with a pair of electrons in the outermost shell and a vacant p_z orbital.^{60, 84} While the lone pair is relatively inert due to its high s -character, six-electron low-valent HTs easily react with other molecules as well as themselves. Thus, it is a prerequisite to employ either kinetic or thermodynamic stabilization of the reactive p_z orbital in order to isolate HTs at ambient conditions (Figure 1).⁸⁵⁻⁸⁷

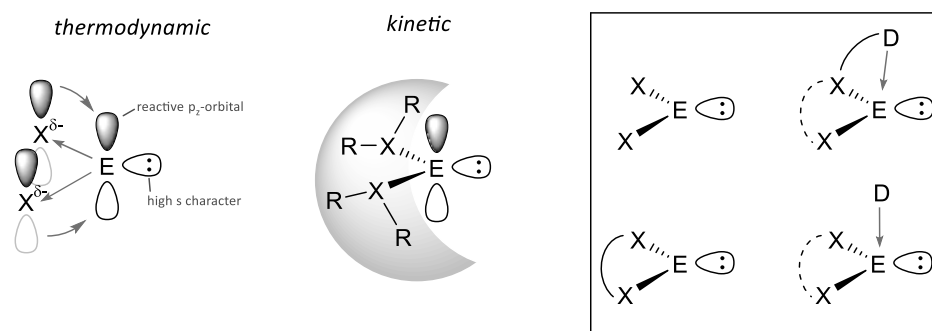


Figure 1: Thermodynamic and kinetic stabilization leading to room temperature stable HTs (left). Cyclic and non-cyclic HTs, non-donor- as well as intramolecularly- and intermolecularly-stabilized. E = Si, Ge; X = anionic group; D = donor group.⁸⁸

Several different ligands have been designed in the past decade with the aim to isolate tetrylenes with formal low oxidation state at ambient conditions.^{58, 88-91;^a} Due to their flexible electronic structure, it is possible to isolate donor-free as well as intramolecularly and intermolecularly stabilized tetrylenes under inert atmosphere. Thus, the family of HTs nowadays comprises a broad variety of cyclic and acyclic motifs, stabilizing the low-valent metal thermodynamically and/or kinetically.^b Typically employed substituents in non-cyclic HTs are for example amides, NHCs, *N*-heterocyclic imines or halides, offering interesting reactivity towards small molecule activation and further functionalization.^{64, 88, 92-96} The application of such ligands in homogeneous catalysis, however, has

^a Selected examples.

^b In the literature it is not consistent whether intramolecularly donor stabilized HTs are counted as cyclic.

proven to be difficult due to low kinetic and/or thermodynamic stability.⁹⁷ Most applied tetrylenes in transition metal chemistry can be related to cyclic HTs – including intramolecularly stabilized tetrylenes – usually ranging from three- to six-membered ring systems.^{67, 98, 99}

The history of NHSi ligands dates to 1994 when *Denk et al.* published the first stable silylene $\text{Si}[(\text{N}^t\text{Bu})_2\text{C}_2\text{H}_5]$.¹⁰⁰⁻¹⁰² Two years in advance, *Herrmann et al.* already reported the synthesis of stable cyclogermynes.¹⁰³ Since germanium is a scarce element in the Earth crust, most research has been done on silylene chemistry over the past two decades. Prominent examples of ligand structures nowadays comprise four-membered amidinate and guanidinate, five-membered imidazole and six-membered diketinimates, while also the donor-stabilized HTs thereof are usually accounted into this group (Figure 2).⁵⁸

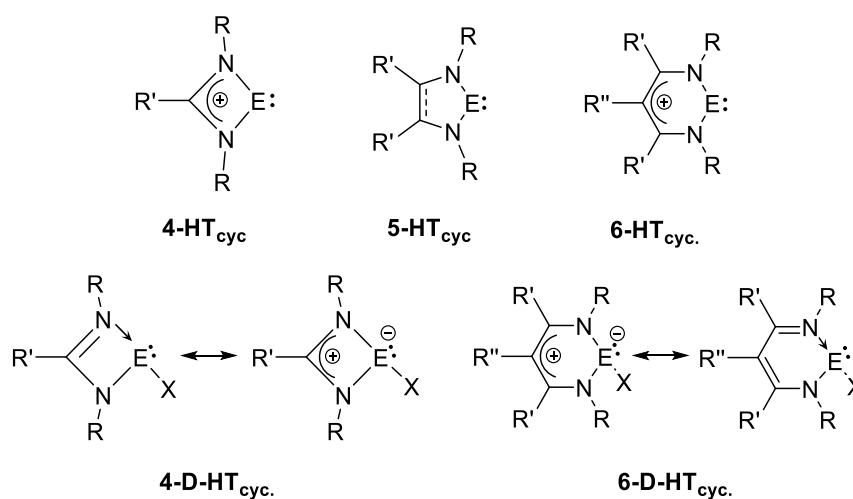


Figure 2: *N*-heterocyclic four-, five- and six-membered tetrylenes. X = donor group; E = Si, Ge.⁵⁸

While four-membered cationic amidinate silylenes have not been isolated yet, donor-stabilized four-membered HTs have been the focus of numerous publications over the past years, allowing for various reactivities and properties.⁶⁷ Thereby, the broad diversity of five-membered NHC analogs has been increasingly disregarded. The library of this ligand class comprises unsaturated as well as saturated compounds, while benzannulated, pyridoannulated, or aminotroponimate ligands have been added over the past years, offering a broad range of structural and electronic properties (Figure 3).⁵⁸

Apart from kinetic stabilization by the bulky wingtips, five-membered HTs receive significant stabilization through an inductive effect from the neighbored more electronegative nitrogen atoms as well as through π -electron donation of the unshared electron pairs into the vacant p_z orbital.^{47, 104, 105} In addition, the delocalized π -electron system contributes to the overall stability, while it is usually not crucial.^{106, 107} In recent publications, the effect of ring expansion on the stability of the ligand has been under investigation.¹⁰⁸⁻¹¹² According to *Phukan et al.* and others, benzannulation leads to further

thermodynamic stabilization and increases metal-to-ligand backbonding within transition metal complexes.

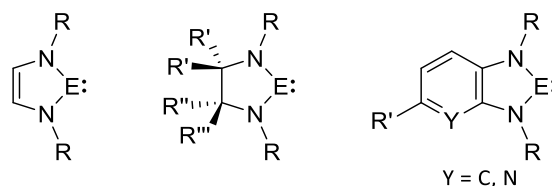


Figure 3: General structures of most common five-membered NHSis and NHGes. E = Si, Ge; R = sterically demanding aliphatic and arylene group.

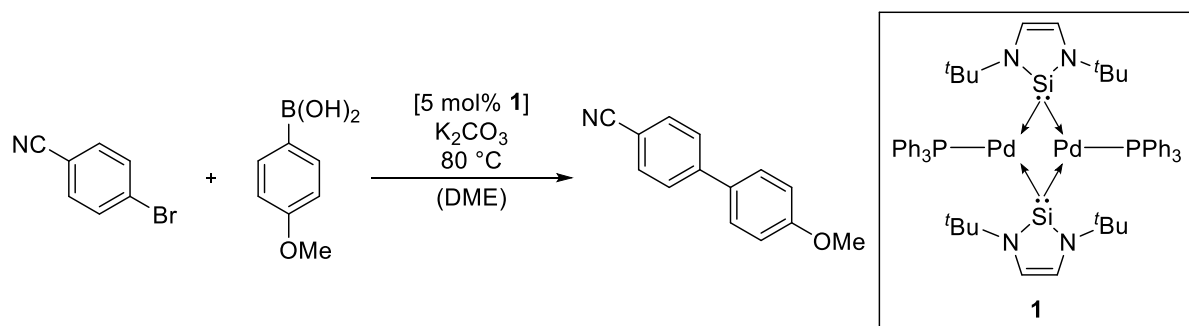
The first germylene, stabilized by a four-membered *N*-heterocyclic ring diamino ligand, has been isolated by *Lappert et al.* already in 1976 when working on the synthesis of isolable heavier carbene analogs.¹¹³ However, they were not successful in the synthesis of low-valent silylenes at that time due to their lower kinetic stabilities.¹¹⁴ Various NHGe metal complexes are known to date, comprising similar ligand structures as NHSis.¹¹⁵ The versatile electronic properties of germylenes allow interesting reactions of small molecules such as CO₂ to methanol reduction, ammonia activation or the catalytic hydroboration of aldehydes.^{69, 92, 116-119}

1.4.3 *N*-Heterocyclic Tetrylenes in Homogeneous Catalysis

HTs are able to bind to a metal center due to their paired electron pair. Depending on the ligand structure, the σ -donor strength of NHSis and NHGes is slightly reduced compared to a carbene, however, their p_z orbital remains almost free of electron density, which makes them interesting for homogeneous catalysis.^{56, 57} The unique properties of HTs render them also potential candidates for metal-free catalysis as mentioned above, however, this will not be discussed in the following. Despite growing numbers of publications on the use of stabilized silylenes and germylenes as ligands in homogeneous catalysis, they remain far from being studied as extensively as their lighter carbene analogs.⁵⁶ While several available synthetic protocols allow the facile isolation of NHC complexes, the marked sensitivity of HTs render their synthesis and handling a lot more challenging.⁶⁷ Transition metal complexes are usually synthesized *via* reaction of the isolated free HT with respective metal precursors. Much more research has been conducted on the application of silylenes rather than germylenes in homogeneous catalysis due to the reasons mentioned above. In the following, the development of catalytically applied NHSi ligands shall be given.

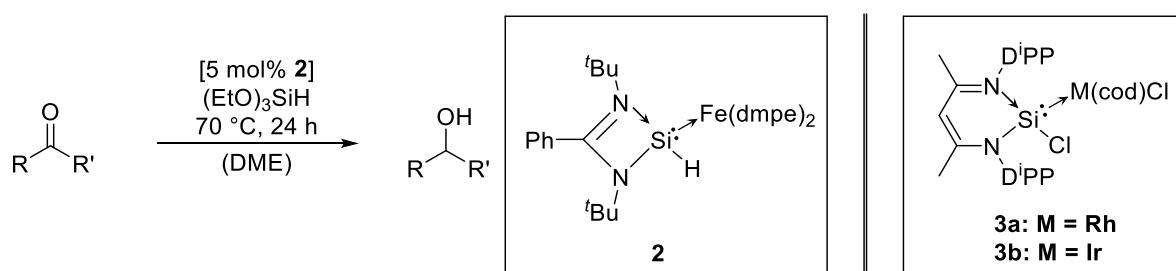
The application of HTs in homogeneous catalysis dates to 2001 when *Fürstner et al.* used a bis-palladium complex coordinated by bridging NHSi ligands for the catalytic conversion of aryl boronic acids with bromoarenes (Scheme 2).¹²⁰ It took another seven years until *Roesky et al.* published the

second example of a catalytically active NHSi palladium complex.¹²¹ The group was able to show the distinct activity of the latter in Heck-type couplings of styrene with bromoacetophenone. Both complexes have been prepared by reacting the free NHSi with a metal precursor and subsequent crystallization of the product.



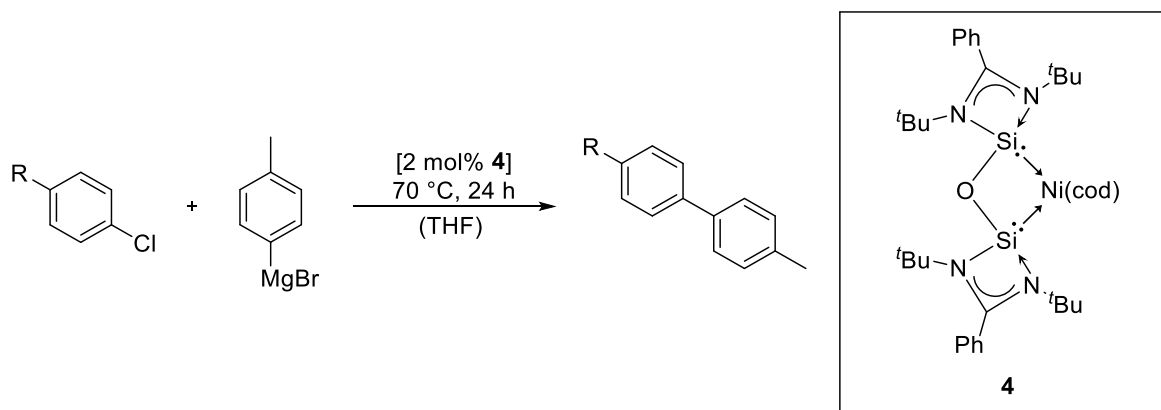
Scheme 2: Conversion of aryl boronic acids with bromoarenes catalyzed by **1** as reported by Fürstner *et al.*¹²⁰

Donor-stabilized four-membered NHSis have first been published by Roesky *et al.* in 2006 and broadly established in homogeneous catalysis by Driess *et al.* in the following years.^{55-57, 122} An important example of the catalytic application of such amidinate-based HTs was given in 2013 (Scheme 3).¹²³ The group was able to use hydride-stabilized **2** in the catalytic hydrosilylation of ketones, after reacting the chloro-silylene precursor with Superhydride[®]. The authors proposed a catalytic cycle which involves hydride migration onto the metal center and coordination of the ketone substrate at the positively charged silylene. In the same year, Driess *et al.* also employed a six-membered diketiminato ligated HT in rhodium- and iridium- catalyzed amide reductions (Scheme 3).¹²⁴



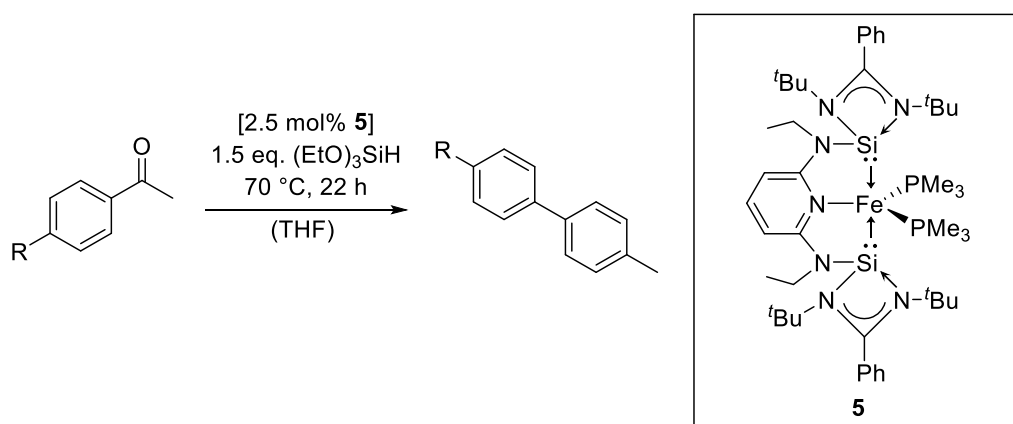
Scheme 3: Catalytic hydrosilylation of ketones catalyzed by **2** as reported by Driess *et al.* (left).¹²³ Rhodium and iridium complexes **3a/b** of six-membered NHSis active in the catalysis of amide reductions (right).¹²⁴

The thermodynamic stability of transition metal complexes is a predominant factor of an efficiently working catalyst. Several chelating HTs have been created over the past years and applied in homogeneous catalysis already.¹²⁵⁻¹²⁹ Thereby, the versatile reactivity of substituted amidinate HTs was key to the synthesis of several ligand motifs. The first chelating bis-NHSi ligand was reported by Driess *et al.* in 2010 and further coordinated onto $Ni(cod)_2$ (Scheme 4).¹³⁰ The isolated complex was successfully applied in carbon-carbon bond coupling reactions, benefiting from the strong electron donating properties of the ligand.



Scheme 4: Carbon-carbon coupling reaction catalyzed with 2 mol% of **4** as reported by *Driess et al.* in 2010.¹³⁰

In the following years, the group was able to isolate a series of chelating NHSis and NHGes, including pincer-type ligands and mixed NHSi/NHC chelators.¹²² Utilizing these as steering ligands of transition metal complexes, they were successful in the catalysis of a broad scope of chemical reactions of high relevance such as the borylation of arenes, hydroformylation reactions or carbonyl hydrosilylations (Scheme 5).¹³¹



Scheme 5: Ketone hydrosilylation reaction catalyzed with 2.5 mol% of **5** as reported by *Driess et al.* in 2010.¹³¹

All these examples demonstrate the high potential of HTs in transition metal catalysis as tunable steering ligands, featuring versatile electronic properties. The so far predominantly employed tricoordinate amidinate-HTs possess significantly reduced π -backbonding capabilities due to intramolecular donor-stabilization. Dicoordinate five-membered NHSis and NHGes in contrast, feature relatively high thermodynamic stabilities due to the efficient π -electron delocalization (including the empty out-of-plane p_z orbital) but also allow for the efficient metal-to-ligand backbonding as mentioned above.^{101, 102, 132}

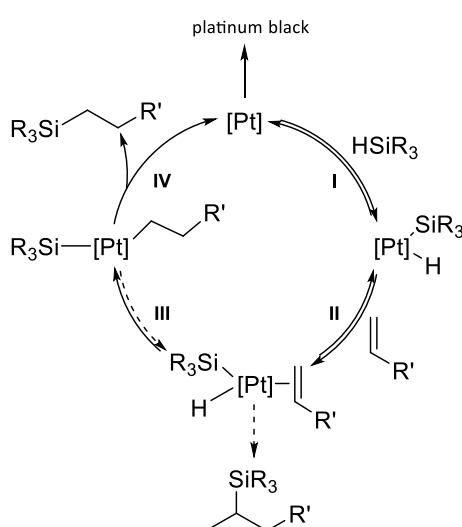
Thus, the ligand properties of five-membered NHSis and NHGes can outrange their lighter analogs and other cyclic HTs in certain catalytic applications. *Szilvási et al.* have performed a detailed theoretical study of a vast number of NHSis as well as NHGes ligated by different structural motifs, comparing

their ligand properties.^{98, 99} Thereby, it was concluded that donor-substituted HTs can easily outperform their lighter analogs in terms of donor-strength, while the latter is only slightly reduced in five-membered NHSis and NHGes. Moreover, these ligands are characterized by significant π -backbonding, facilitating the efficient reductive elimination of other substrates. Most conspicuously, only very few examples of chelating ligands bearing multiple five-membered HTs have been published over the past years, while applications in homogeneous catalysis remain even more rare.¹³³⁻¹³⁹

1.5 Platinum-Catalyzed Alkene Hydrosilylation

The hydrosilylation of olefins is a key technology of the industrial manufacturing of consumer products such as adhesives, coatings, or surfactants, and thereby basis to daily-life applications.^{16, 140, 141} For example, silicon polymers are the basic ingredients for lubricating oils, resins, and release coatings, while there are also applications in medicinal chemistry and semiconducting industry.¹⁴² Therefore, hydrosilylation has emerged as a widely applied reaction, belonging to the largest-scale applications of homogeneous catalysis.¹⁴³ Alkene hydrosilylation comprises of the addition of a hydrosilane to a carbon-carbon multiple bond, and therefore constitutes a highly atom-economical reaction.

The first homogeneous platinum catalysts for the industrial application in alkene hydrosilylation were developed by *Speyer et al.*, involving transition metal salts of platinum, ruthenium and iridium such as hydrochloric platinum acid.¹⁴⁴ Until today, the most established catalyst is *Karstedt's catalyst*, $[\text{Pt}_2(\text{dvtms})_3]$, which has already been developed in 1973.¹⁴⁵ Due to its superior catalytic properties, high versatility and ease in handling, the latter still serves as benchmark system.¹⁴⁶ Over the past half century only few mechanistic studies in the field of platinum-catalyzed hydrosilylation have been conducted, thus, the widely accepted mechanism is still based on the early studies of *Chalk and Harrod* in 1965 (Scheme 6).¹⁴⁷ They claimed that the catalytic cycle comprises four consecutive steps: I) the oxidative addition of the hydrosilane; II) the coordination of the olefin; III) the olefin migration into the platinum-hydride bond; IV) the reductive elimination of the product. The first three steps are generally believed to be reversible, while reductive elimination of the product would be the rate-determining, irreversible step.



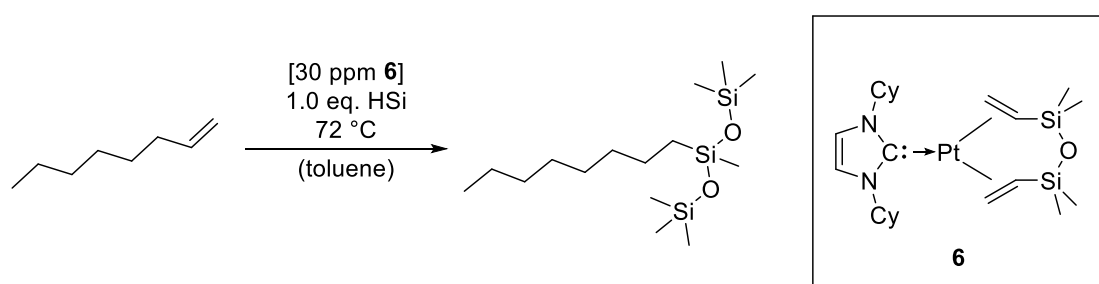
Scheme 6: Catalytic cyclic of platinum-catalyzed olefin hydrosilylation. Recent studies of *Kühn et al.* show that the third step of the mechanism most likely belongs to the rate-determining step.¹⁴⁸

Mechanistic studies remain scarce due to various difficulties that are connected to platinum catalysis, such as its high activity and the sensitivity of the active species. Also, *Karstedt's catalyst* is usually stored in an organic solvent as it tends to form catalytically inactive colloids (platinum black).^{146, 149} Besides theoretical studies, major breakthroughs have been achieved by *Lewis* and *Stein et al.*,¹⁵⁰ *Roy et al.*¹⁵¹ and *Herrmann* and *Kühn et al.*,¹⁴⁸ that provide proof of the classical *Chalk-Harrod* mechanism. Some publications rather refer to the so-called *modified Chalk-Harrod* mechanism, which comprises olefin insertion into the platinum-silicon bond, however, most have been discussed using other metal centers such as iron.¹⁵²⁻¹⁵⁵ The majority of research indeed indicates that the active species contains platinum-silicon and platinum-carbon bonds, that olefin insertion into the platinum-silicon bond is not favored, and that platinum black is formed if no excess olefin is present, which is associated with deactivation. Quite interestingly, there is also evidence that demonstrates a beneficial oxygen effect onto the catalysis through breaking multiple platinum bonds in platinum(0) colloids.¹⁵⁶ Making use of different techniques, such as isotope labeling, NMR spectroscopic investigations and kinetic experiments, *Kühn et al.* have contributed significantly to the overall understanding of the mechanism.¹⁴⁸ Thereby, the authors were able to demonstrate proof that the insertion of the olefin into the metal-hydride bond is included in the rate-determining step of platinum-catalyzed olefin hydrosilylation.

Over the past decade, research efforts into eco-friendly “green chemistry” have been intensified massively.¹⁵⁷ Thereby, numerous d^8 , d^9 and d^{10} metal-containing catalysts have been found.^{16, 158, 159} However, no match for the unparalleled catalytic properties of platinum has been reported so far. Due to the high difficulties in separating the catalyst of the product in a homogeneously driven hydrosilylation reaction, an enormous amount of platinum is continuously withdrawn from the value chain.¹⁶⁰ Thus, the improvement of this catalytic process is one of the major goals of homogeneous catalysis-related research. One of the most promising approaches is the design and application of tailor-made ligands, which are capable of improving the performance of a catalytic active transition metal by steering its stereoelectronic properties in the right direction.

1.6 Tetrylenes in Platinum-Catalyzed Alkene Hydrosilylation

Steering ligands are essential to developing precise and efficient catalytic processes, enabling the exact tailoring of material properties and the development of novel technical applications.^{20, 21, 32} The widely applied olefin hydrosilylation still depends on the highly active, but poorly selective *Karstedt's catalyst*. Thus, a strong drive for improvement has led to the development of a series of new ligand motifs. In 2002, *Markó et al.* have published the successful application of NHC ligated platinum(0) complexes in olefin hydrosilylation, yielding a marked increase in terms of yield and selectivity.¹⁶¹ Under ideal conditions, the authors reported up to 96% yield in the hydrosilylation of 1-octene with heptamethyltrisiloxane when **6** was added in catalytic amounts, while only 78% have been reached with *Karstedt's catalyst* (Scheme 7).

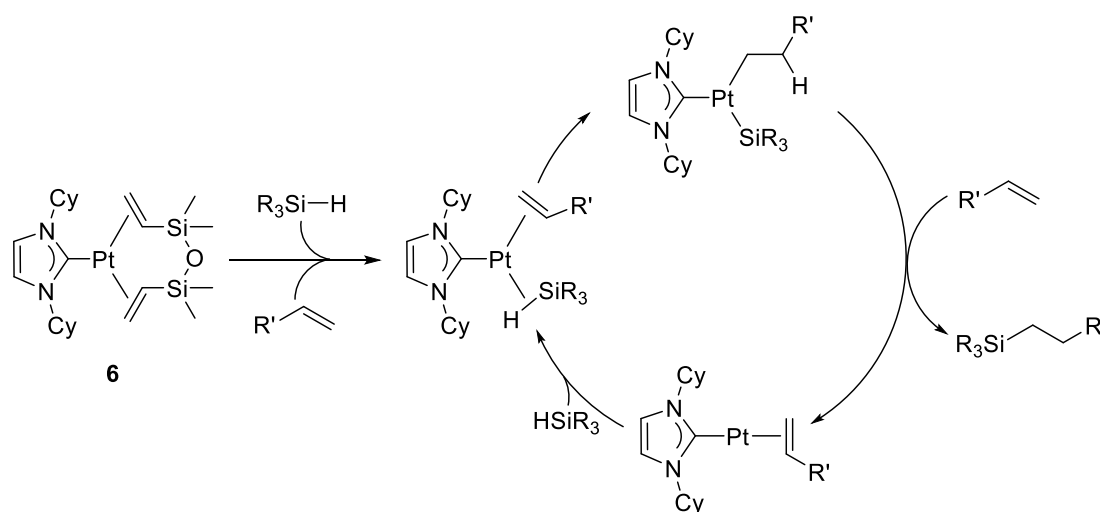


Scheme 7: Hydrosilylation of *n*-octene with HSi under typical reaction conditions applying 30 ppm of **6** as reported by *Markó et al.* in 2002.²¹

The highly efficient catalytic reaction benefits from strong σ -donating properties of the applied NHCs, forming strong metal-carbon bonds. *Markó's catalyst* can be synthesized easily, is stable towards air and moisture, and provides facile modification opportunities of the stereoelectronic properties through altering of the wingtips.¹⁶² With the ultimate goal to develop more stable and reusable catalysts several modifications of *Markó's catalyst* have been published over the past years.¹⁶³⁻¹⁷³

The group of *Markó* also suggested a mechanistic cyclic for the catalytic conversion of olefins using NHC ligated platinum(0) complexes.¹⁶⁸ They proposed that the catalytic active species is formed through oxidation of the dtvms ligand, which is by far the slowest step of the entire catalytic reaction (Scheme 8). The overall activity is thus dictated by the dissociation of the dtvms ligand. Thereby, the (NHC)Pt(dtvms) precursor would act as a stable reservoir of catalytically active species, leading to significantly increased selective catalysis.¹⁷⁴ Furthermore, the isomerization of the alkene, which usually constitutes the major side-reaction, was observed to be strongly dependent on the turnover rate of the reaction. Variation of the steric demand of the NHC ligand results in altered induction periods.¹⁷⁰ In general, sterically crowded NHC ligands lead to prolonged initiation times and higher selectivity. Remarkably, after dissociation and hydrosilylation of the chelating dtvms ligand, a greater

steric demand of the NHC substituents accelerates the reductive elimination step within the catalytic cycle.¹⁶⁹ In addition, the strong electron-donating nature of the NHC ligand has an impact on the activity and selectivity of the catalyst. *Markó et al.* proposed that the selectivity of the catalytic reaction and the formation of colloidal platinum depends on the binding of the NHC ligand in the active species. In reaction series regarding NHC ligands with increasing σ -donation capability, the afforded catalytic systems were improved significantly in selectivity while being slightly lowered in activity.¹⁷⁰



Scheme 8: Catalytic cycle of olefin hydrosilylation catalyzed by NHC platinum(0) dtms complexes as proposed by *Markó et al.*¹⁶⁸

In course of their unique electronic properties, HTs have already been applied to olefin hydrosilylation. Interesting results on a novel hydrosilylation mechanism, with participation of a reactive non-cyclic silylene, have been published by *Tilley et al.* in 2003.^{175, 176} Major improvements in hydrosilylation catalysis with regard to established systems have been achieved by *Kato and Baceiredo et al.* using a silycyclopropyliden ligand in 2016.¹⁷⁷ The latter, which comprises a highly nucleophilic, donor-stabilized silylene, readily reacts with *Karstedt's catalyst* to form the highly active and selective hydrosilylation catalyst **7** (Figure 4). The catalyst benefits from the strong σ -donating properties of the silylene ligand in combination with significant π -backbonding from the metal. Exemplary, 81% isolated yield was achieved in the hydrosilylation of 1-octene with heptamethyltrisiloxane, using 50 ppm of the complex as catalytic precursor. Most interestingly, however, the catalytic reaction proceeded significantly quicker compared to similar NHC complexes. In the same year, *Iwamoto et al.* succeeded in synthesizing a novel platinum(0) complex coordinated by a dialkylsilylene ligand **8**.¹⁷⁸ Due to the absent nitrogen atoms and consequently missing π -donation of electrons into the empty p_z orbital of the silylene, the ligand is capable of even stronger metal-to-ligand backbonding. According to the authors, the catalytic properties of the complex are significantly improved due to its electronic design and catalyzes a wide range of substrates with great efficacies. Only one year later, an asymmetrically substituted platinum(0) complex **9** was published by the same group.¹⁷⁹ Therein, the adjacent nitrogen

atom reduces the π -backbonding from the metal to the coordinated silylene and, thus, reduces its catalytic activity slightly. The latter complex tolerates a wide range of functional groups, such as ethers, epoxides, or esters. However, the authors were not able to identify the active species within the catalytic cycle and also included small platinum clusters into their discussion.

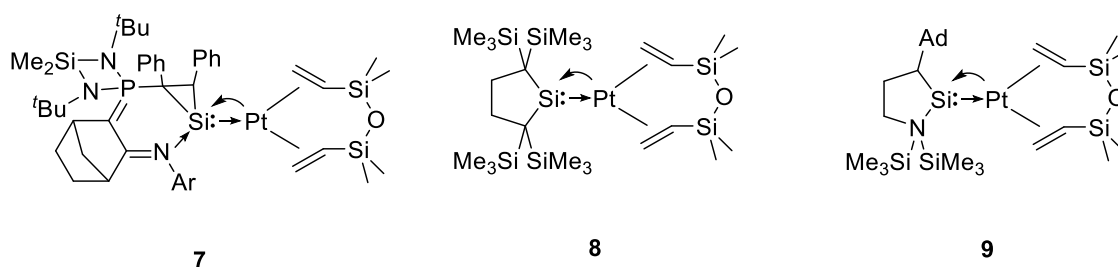
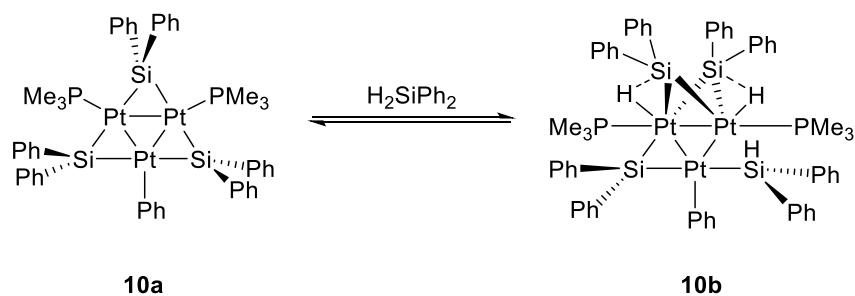


Figure 4: HT ligated platinum(0) dtms complexes reported as active precursors in the hydrosilylation of olefins.^{177, 178 179}

Quite interestingly, stabilized platinum clusters have been applied as precursors in catalytic hydrosilylations already. In 2017, *Osakada et al.* reported the synthesis and reactivity of a triangular triplatinum complex.¹⁸⁰ The latter comprises four bridging diphenylsilylenes, acting as divalent ligands. The symmetrical complex adds one equivalent of H_2SiPh_2 in an oxidative addition, which is bound by two platinum atoms (Scheme 9). Using this complex, the authors were able to perform the catalytic conversion of benzaldehyde with diphenylsilane. Already in 2012, a trinuclear platinum complex, coordinated by dtms-related η^2 -alkyne ligands, has been reported by *Marciniak et al.*¹⁸¹ This complex even exceeded *Karstedt's catalyst* in terms of catalytic activity at 50 °C.

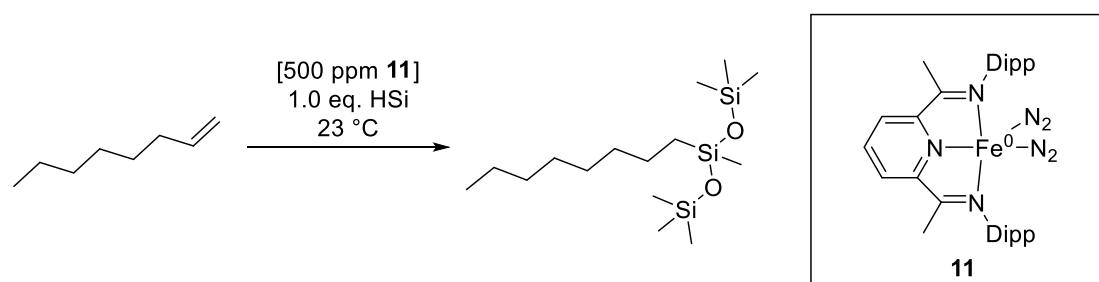


Scheme 9: Reversible oxidative addition of H_2SiPh_2 at a trinuclear platinum complex.¹⁸⁰

1.7 Pincer-Type Ligands in Non-Precious Metal-Catalyzed Olefin-Hydrosilylation

Besides known problems, such as numerous side-reactions and cost-intensive purification methods, *Karstedt's catalyst* is based on one of the most precious and toxic transition metal. The long-term supply of platinum is thus uncertain which is mirrored in its high price.^{182, 183} A broad scope of ligand motifs that allows the application of environmentally benign metals have been designed and applied to find alternative catalytic active metal centers.^{143, 159} The very first application of iron as catalyst in hydrosilylation dates back to 1962 when *Nesmeynov et al.* utilized small amounts of pure $\text{Fe}(\text{CO})_5$ to react unsaturated olefins with hydrosilanes.¹⁸⁴ Based on these results, research into hydrosilylation catalysis focused on iron carbonyl chemistry for a long time.¹⁸⁵⁻¹⁸⁸ However, these systems are difficult to be applied in homogeneous catalysis, as they constitute a high manifold of reactivity and their activation often requires high temperatures or external energy sources.^{152, 154}

Significant improvements have been achieved over the past years utilizing multiple-coordinating ligands. A major breakthrough in iron-mediated hydrosilylation of olefins has been achieved by *Chirik et al.* in 2004 by introduction of non-innocent bisiminopyridines (Scheme 10).¹⁸⁹



Scheme 10: Room temperature hydrosilylation of *n*-octene catalyzed with 500 ppm of **11** as reported by *Chirik et al.*¹⁸⁹

The group was able to reduce ligated iron(II) halide complexes under nitrogen atmosphere, giving remarkably active precatalysts as exemplified in Scheme 10. With catalyst loadings down to 0.004 mol% and at room temperature, the authors were able to demonstrate the efficient hydrosilylation of primary silanes with unactivated alkenes and alkynes.¹⁸⁹ Subsequently, a broad variety of highly active catalysts, comprising metal centers such as cobalt, iron or nickel has been developed.^{171, 190-194} Modification of the structural motif included, for example, terpyridines, biscarbenes or mixed variations such as phosphinite-iminopyridines. Thereby, only the reduction of the size of the wingtip substituents of the imines, allowed for the effective hydrosilylation of industrially relevant tertiary silanes such as Et_3SiH with unactivated terminal alkenes.¹⁷¹

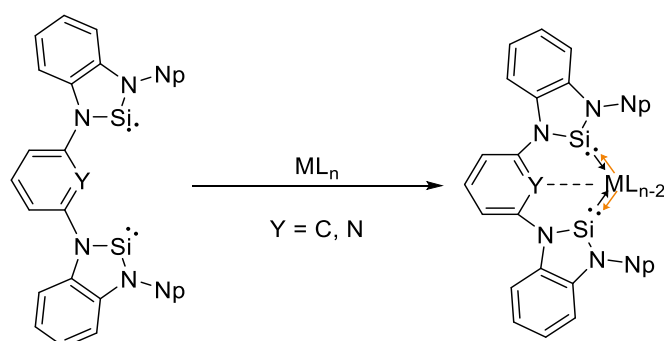
To some extent, these catalysts exceed existing platinum-based catalysts by far in terms of efficient catalysis, speaking of the combination of high turnover numbers and high selectivity. However, only few exceptions are catalytic active under aerobic conditions as the great majority suffers from pronounced sensitivity to air and moisture. In order to solve this and enable the use of catalytic systems that rely on other metals than platinum, further research into new ligation concepts has to be performed.

2 OBJECTIVE

Taking these developments into account, the major aim of this thesis was the development of new *N*-heterocyclic silylenes and *N*-heterocyclic germynes matching the demands of transition metal-catalyzed olefin hydrosilylation.

As outlined above, great expenses have been incurred over the past years pursuing two major goals: I) The improvement of platinum-catalyzed olefin hydrosilylation utilizing strongly coordinating as well as shielding ligands to yield more stable and thus more selective catalysis. Thereby, recently developed catalysts benefit from strong metal-ligand bonds based on σ -donating capabilities of the latter as well as significant metal-to-ligand π -backbonding. II) The application of chelating, non-innocent ligands has enabled the efficient hydrosilylation catalysis with non-precious metals such as iron and cobalt. Major drawbacks of these systems are either small substrate scopes, lack of robustness or impracticability in consequence of their extreme sensitivity.

Compared to other HT motifs, *N*-heterocyclic silylenes and germynes are most interesting in regard to applied catalysis in course of their elevated thermodynamic stability. First objective of this thesis was thus to find novel synthetic pathways towards so far unprecedented free *N*-heterocyclic bissilylenes (Scheme 11).

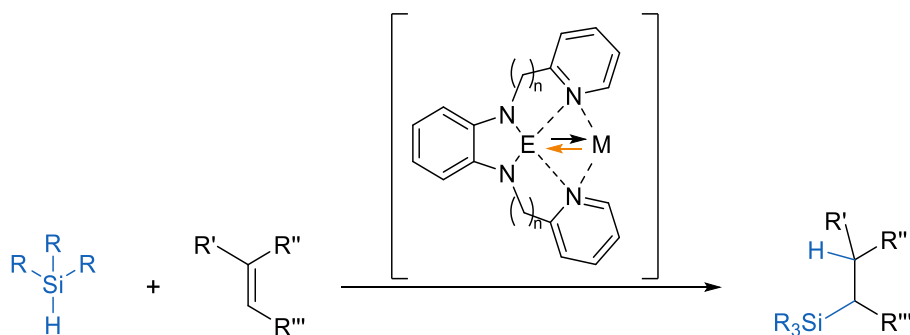


Scheme 11: Aimed *N*-phenylene bridged bissilylenes as unprecedented chelating motifs in transition metal complexes.

Transition metal complexes coordinated by such ligands would benefit from high electron density on the metal center through the overall strong σ -donation from two coordinating silylenes, high thermodynamic stabilities in course of the chelating motif of the ligand, and allow for the facile reductive elimination of substrates in catalytic reactions through pronounced metal-to-ligand backbonding. Known donor-stabilized amidinate bissilylenes have not allowed for the efficient catalysis of olefin hydrosilylation so far, while applications of donor-free multidentate NHGes have remained scarce. Inspired by non-innocent bisiminopyridine ligands and modifications thereof, novel synthetic routes towards unprecedented donor-free bissilylenes will be investigated in this thesis.

Applying various known procedures for the synthesis of free NHSi ligands, two major results will be presented in the following, including the characterization of an unprecedented helical hexasilane.

Platinum compounds are still by far the most important applied catalysts as they offer industrially-relevant properties, which are unmatched by all other systems. Platinum(0) complexes can usually be used under air, as they are not prone to undergo oxidation, exhibit unparalleled activity, and tolerate a wide range of functional groups. Based on recent developments, the second objective of this thesis was to further exploit the potential of HTs as steering ligands in platinum-catalyzed olefin hydrosilylation. *N*-heterocyclic germylenes offer comparably high thermodynamic stabilities and can easily be modified in their stereoelectronic properties. More than that, dicoordinate HTs are highly flexible regarding their electronic state, pushing the boundaries of electronic movements in homogeneous transition metal catalysis (Scheme 12).



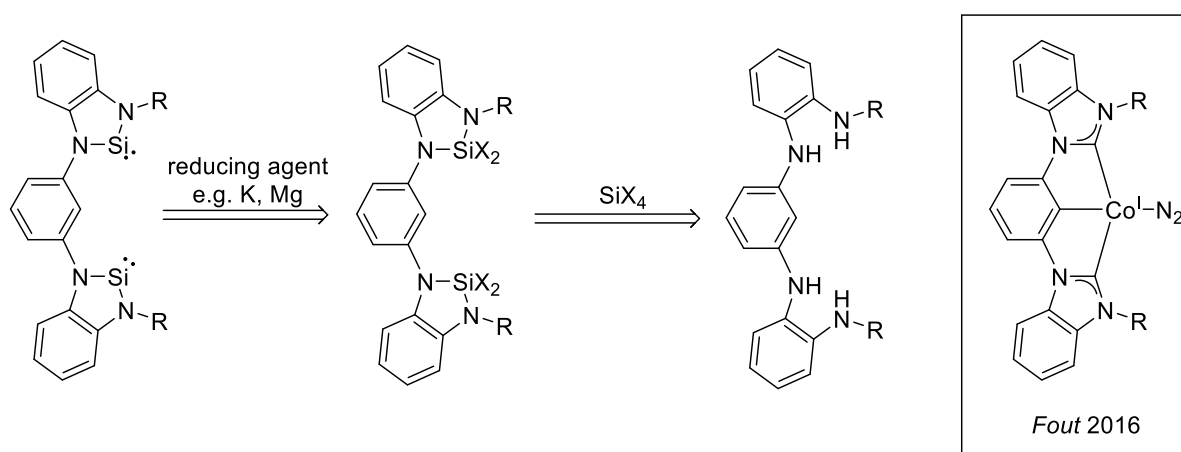
Scheme 12: Aimed *N*-functionalized five-membered heavier tetrylenes as steering ligands in transition metal-catalyzed olefin hydrosilylation.

As recent publications have outlined, the expansion of the delocalized aromatic system of NHGers by benzannulation can increase π -backbonding capabilities as well as lead to increased thermodynamic stability. Thereby, the effect of chelating wingtips has not been investigated in depth so far. Bearing this in mind, a series of pyridyl-substituted, benzannulated NHGers will be presented in this work and investigated in their reactivity and coordinative properties. In addition, the isolated ligands will be used to study their potential to improve the catalytic performance of *Karstedt's catalyst* in olefin hydrosilylation under standard conditions and compared with established systems such as NHCs and phosphines.

3 DISCUSSION OF RESULTS

3.1 From a Bissilylene Precursor to a Kinetically Stabilized Polysilane Molecule

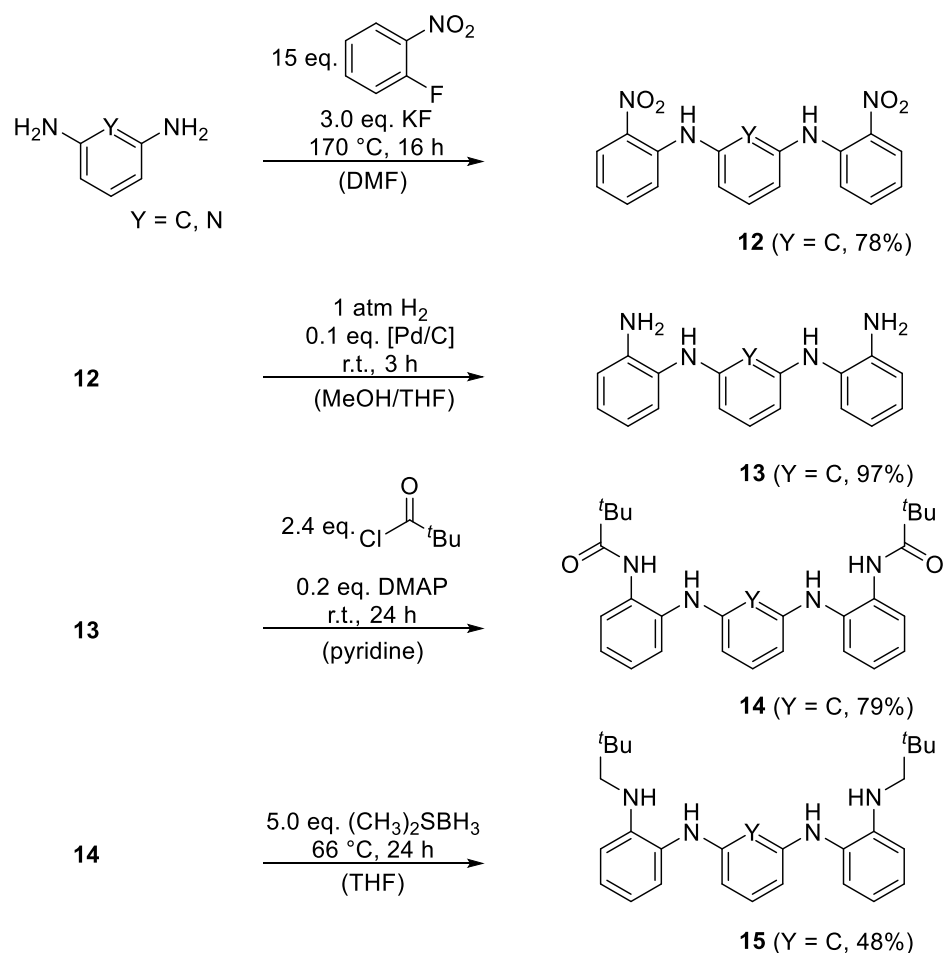
In recent years, several different types of chelating HT ligands have been reported. Prominent examples have been synthesized by *Driess et al.*,^{130, 195} *Hahn et al.*^{133-136, 196-199} and *Tacke et al.*,^{81, 82, 122} and applied in catalysis.^{55, 127, 200-204} Interestingly, the majority of these ligands is based on donor-substituted amidinate ligands, including mixed tetrylenes.¹²² Catalytic applications of bidentate five-membered *N*-heterocyclic tetrylenes have not been reported to date, although they are capable of forming comparably strong bonds with transition metals.²⁰⁵ Thus, the aim of the first project step was the synthesis of a free bissilylene ligand and its reaction with various metal precursors towards coordination complexes with the ultimate goal of olefin hydrosilylation catalysis. In particular, five-membered NHSis should be connected *via* imidazole nitrogen atoms yielding a free bissilylene ligand which is capable of strong electronic interaction with transition metals due to its donor-free p_z orbitals. In comparison to existing *N*-heterocyclic bisgermylenes, connected *via* aliphatic methylene groups, sp^2 -phenylene bridged ligands supposedly act more rigid in transition metal complexes while also exhibiting higher thermodynamic stabilities.^{134, 197} Thereby, meta-substituted phenylene bridged NHCs have already been proved to act as superior steering ligands in alkene hydrosilylation as reported by *Fout et al.* in 2016 (Scheme 13).^{206, 207}



Scheme 13: Synthetic approach of *N*-bridged bissilylenes *via* reduction of bis(dihalogen)silanes (left). General structure of a catalytically active cobalt(I) complex ligated by a pincer-type biscarbene published by *Fout et al.* (right).^{206, 207}

The isolation of free *N*-heterocyclic silylenes is possible through different synthetic approaches. The reduction of halogenated silanes is still most common, reflecting the key step (Scheme 13). Cyclic

dihalogeno silanes can easily be synthesized from the corresponding amines, either through lithiation or *in-situ* deprotonation and subsequent reaction with tetrahalogensilanes. Therefore, several synthesis routes towards phenylene-bridged benzannulated tetraamines have been evaluated, where starting from *m*-phenylenediamine turned out most feasible (Scheme 14).

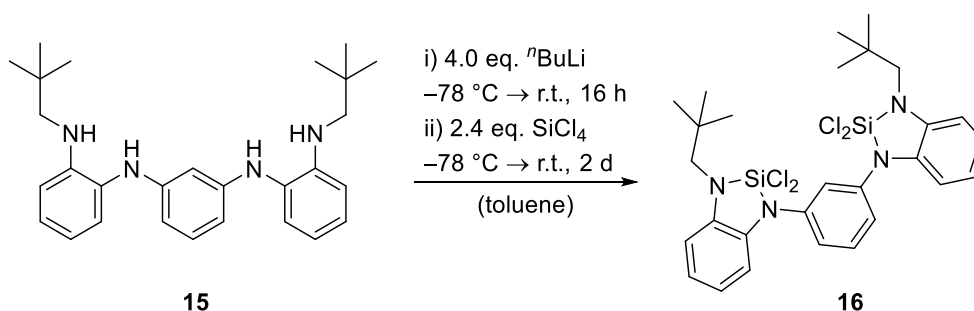


Scheme 14: Four-step synthesis route towards **15** starting from 1,3-bisaminobenzene.

Starting from *m*-phenylenediamine, the targeted compound **15** can be synthesized following a four-step protocol. By use of a large excess of 1-fluoro-2-nitrobenzene and at elevated temperature, the amine groups can be coupled in a high ratio to give **12**. The latter can easily be reduced with hydrogen in a Pd-catalyzed reaction to give the *N*¹,*N*³-bis(2-aminophenyl)benzene-1,3-diamine (**13**). In the next step, the primary amino groups are functionalized in a DMAP-catalyzed nucleophilic substitution reaction with pivaloyl chloride to give the *N*¹,*N*³-bis(2-*N*-neopentylamidophenyl)-benzene-1,3-diamine (**14**) in 79% yield. Borane dimethyl sulfide has been deployed for the final reduction step yielding the *N*¹,*N*³-bis(2-*N*-neopentylaminophenyl)benzene-1,3-diamine (**15**). The sulfide is known for its gentle reducing properties, allowing for the selective reduction of the amide groups.^{208, 209} The equivalent pyridyl-bridged tetraamine has been synthesized according to the same synthetic protocol, however, as it is not part of the following chapter it will not be discussed in detail herein.

N,N-Bridged Bis(dihalogen)silanes

The bis(dichloro)silane **16** was synthesized following standard procedures reported by *Heinicke et al.*²¹⁰ Therein, the tetraamine **15** is cooled down to $-78\text{ }^{\circ}\text{C}$ and lithiated by *n*-butyl lithium (Scheme 15). The product is obtained in a substitution reaction with tetrachlorosilane.



Scheme 15: Synthesis of **16** via lithiation with *n*-butyl lithium and subsequent reaction with SiCl_4 .

The product can be precipitated from the reaction mixture and extracted into hexane. However, NMR spectroscopy showed that impurities, such as incompletely substituted silanes, are still incorporated. Its pronounced sensitivity towards air and moisture – hydrolyzed products can be generated in the LIFDI mass spectrum (Figure 5) – and the high viscosity of the product impeded further workup and usage in subsequent reactions. All chosen reducing agents (potassium, lithium/sodium alloy: 8% and 15% lithium, *Rieke-magnesia*²¹¹ and KC_8) did not lead to the desired free bisilylene ligand, regardless of varied temperatures and quantities. Related bis(dihydro)silanes and bis(hydrochloro)silanes were synthesized from the tetraamine **15** as well, however, no improvement in terms of reactivity towards the aimed free bisilylene was observed.

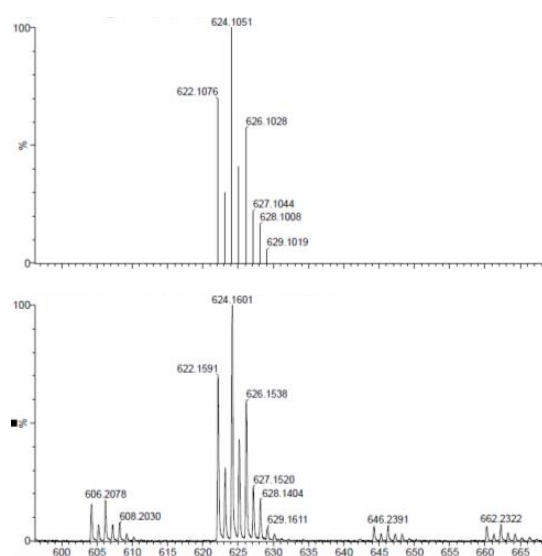
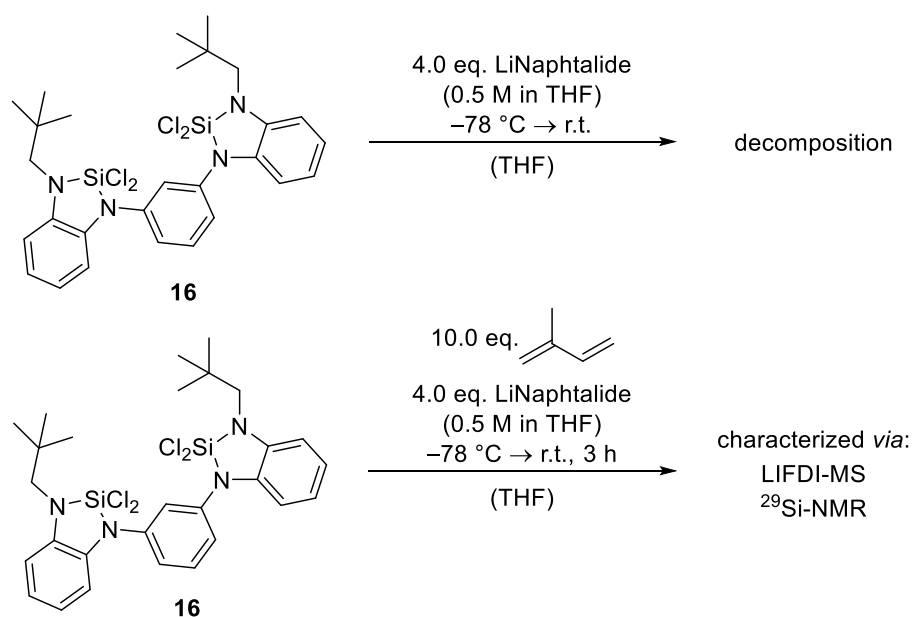


Figure 5: Calculated isotopic pattern corresponding to $\text{C}_{28}\text{H}_{34}\text{Cl}_4\text{N}_4\text{Si}_2$ (top) and measured LIFDI mass spectrum of **16** showing hydrolyzed products as well (bottom). The complete spectrum can be found in the supplementary data (SD 1).

HTs have been shown to easily add unsaturated olefins.⁷¹ To investigate whether the ligand structure is degraded during the reduction step or the bissilylene forms initially but decomposes subsequently, isoprene was added to the reaction mixture in large excess. The trapping agent is capable of binding free tetrylenes in a concerted 1,4-addition reaction. Following literature procedures,²¹² lithium naphthalide was added stoichiometrically at $-78\text{ }^{\circ}\text{C}$ to a solution of **16** in THF, which is allowed to warm to room temperature afterwards (Scheme 16).



Scheme 16: Reduction of **16** with lithium naphthalide with (top) and without (bottom) presence of 10.0 eq. isoprene.

At low temperatures, immediate reaction of lithium naphthalide and the silane takes place yielding an orange suspension, while a brown reaction mixture is obtained if no isoprene is present. The reducing agent is added dropwise until no further discoloration of the intensively green-colored reagent can be observed. The successful trapping of the free bissilylene was confirmed *via* LIFDI mass spectrometry and ^{29}Si -NMR spectroscopy. Signals in the mass spectrum are relatively weak, however, ions corresponding to $[\text{C}_{38}\text{H}_{50}\text{N}_4\text{Si}_2]$ and $[\text{C}_{33}\text{H}_{40}\text{N}_4\text{Si}_2]$ can be detected clearly (Figure 6). In addition, a significant downfield shift of the ^{29}Si signal was found ($-27.63\text{ ppm} \rightarrow 27.33\text{ ppm}$).

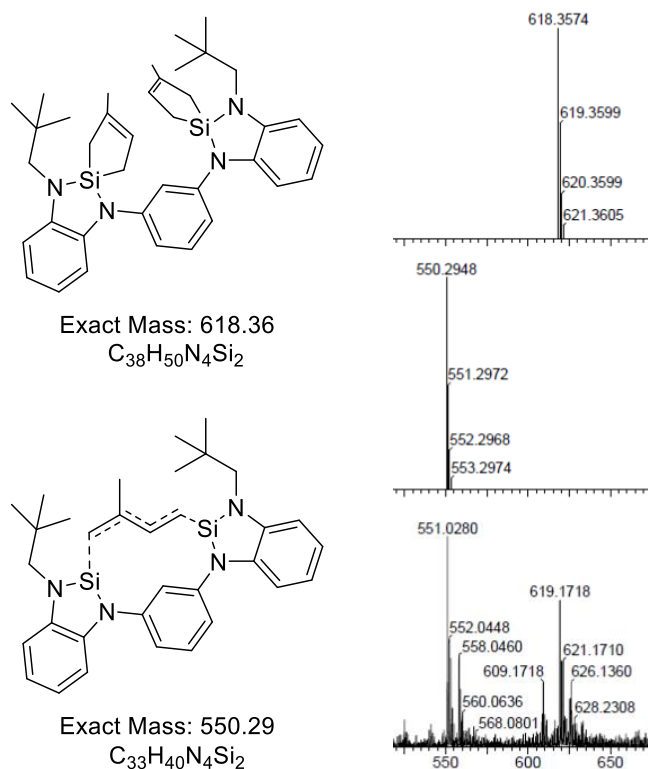
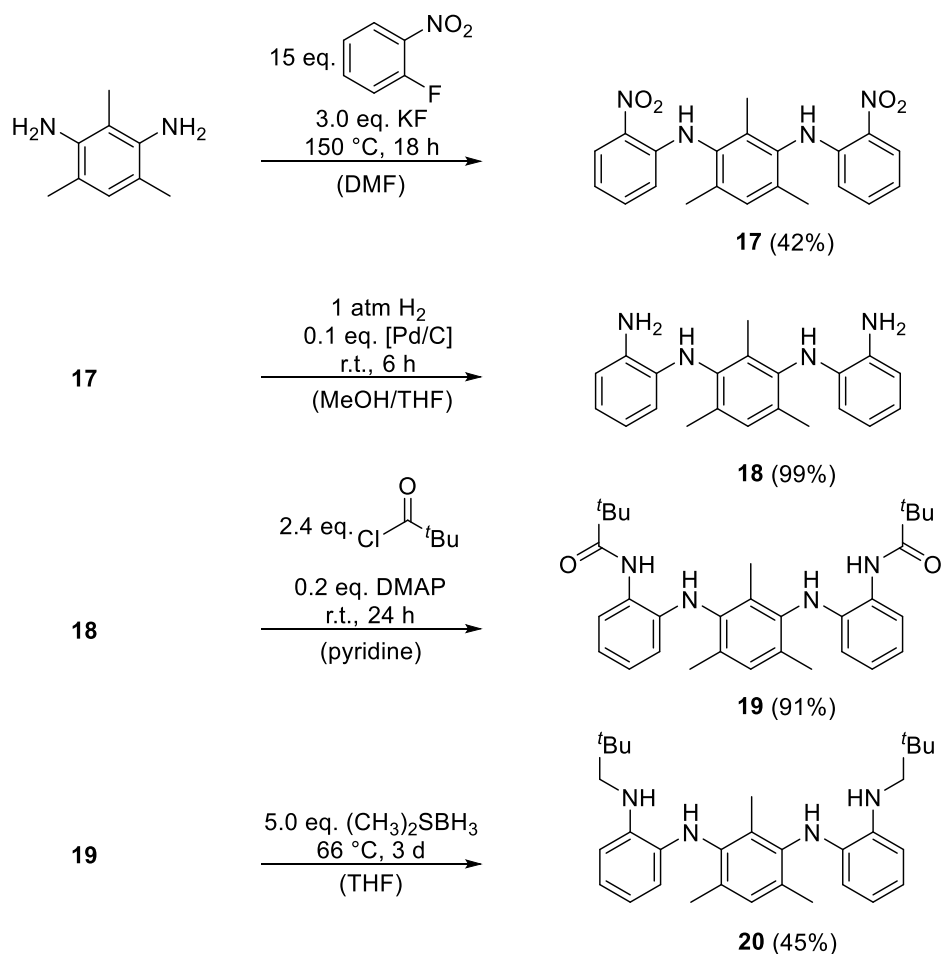


Figure 6: Calculated mass distribution corresponding to $C_{38}H_{50}N_4Si_2$ and $C_{33}H_{40}N_4Si_2$ (top, middle) and measured LIFDI mass spectrum of the reaction mixture of the reduction of **16** in presence of 10.0 eq. isoprene measured in toluene (bottom). The complete spectrum can be found in the supplementary data (SD 2).

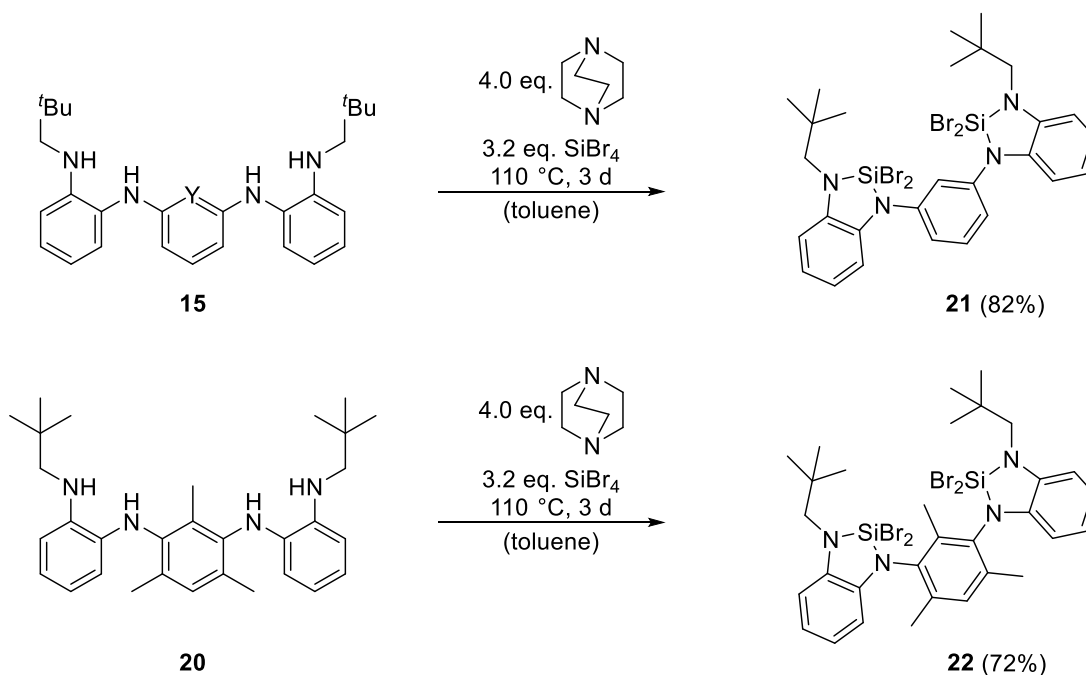
Following these results, the reduction of halogenesilanes towards low-valent silylenes will be addressed at low temperatures in the subsequent experiments. Moreover, further kinetic stabilization of the silicon atom shall be introduced in order to enable the isolation of the free ligand at room temperature. For this purpose, two different approaches were pursued. While functionalization of the exterior wingtips by sterically more demanding groups such as mesitylene has not been successful, it was possible to synthesize the mesitylene-bridged tetraamine 2,4,6-trimethyl- N^1, N^3 -bis(2-*N*-neopentylaminophenyl)-benzene-1,3-diamine (**20**) (Scheme 17).



Scheme 17: Four-step synthesis route towards **20** starting from 1,3-bisamino-2,4,6-trimethylbenzene.

Analogous to the tetraamine **15**, the product **20** can be obtained in a four-step synthesis starting from 1,3-diamino-2,4,6-trimethylbenzene in good yields. Similar to known room temperature stable NHSis featuring large wingtip groups, the additional steric bulk of the mesitylene potentially leads to a higher kinetic stabilization of the respective bisilylene.

Starting from **15** and **20** the respective bis(dibromo)silanes **21** and **22** can be synthesized selectively in a reaction with tetrabromosilane in presence of an amine base (Scheme 18). Using DABCO as trapping agent for the developing hydrobromide, the synthetic protocol for the synthesis of cyclic dihalogenesilanes was improved, circumventing selectivity problems due to the exceptional reactivity of a fourfold lithiated amine.



Scheme 18: Synthesis of **21** and **22** via reaction of **15** and **20** with SiBr₄ at elevated temperatures in presence of DABCO.

Both compounds, **21** and **22** can be synthesized at elevated temperatures under inert atmosphere in high yields. The product can be separated from the ammonium salt simply by filtration as the latter is not soluble in toluene. Both products can be extracted into hexane, residual bromosilanes are removed *in vacuo*.

Interestingly, while the ¹H-NMR signals of **21** remain unchanged in benzene throughout several days, significant shifts are detected in THF after 24 h (Figure 7). This Lewis acid-base interaction of **21** with THF molecules is evidenced by a significant upfield shift of the ²⁹Si-NMR signal (−46.45 ppm → −55.35 ppm). In contrast, the methylated phenylene bridge of **22** inhibits such an interaction as the NMR signals remain unchanged for several days in THF.

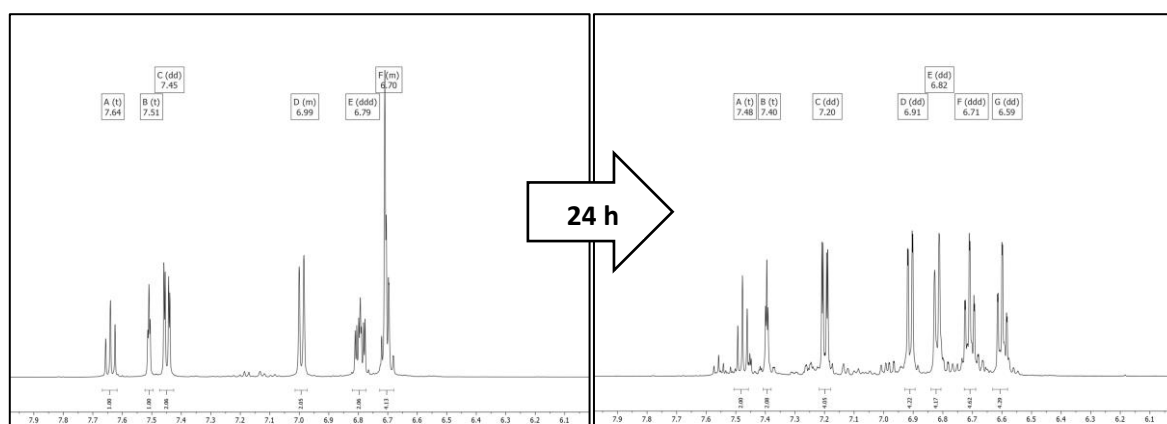


Figure 7: Aromatic region of the ¹H-NMR spectrum of **21** in THF-d₈ after 10 min and after 24 h. Full spectra are available in the supplementary data (SD 12, SD 13).

It is possible to crystallize the bis(dibromo)silanes from a saturated benzene solution at low temperatures. The molecular structure of **21** is depicted in Figure 8.

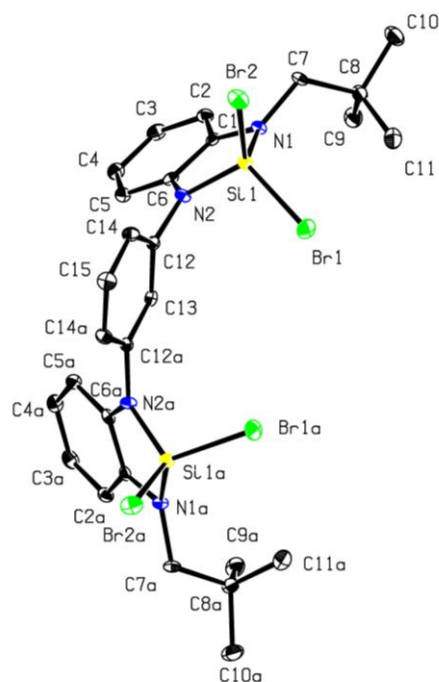


Figure 8: Molecular structure of **21**. Ellipsoids are shown at the 50% probability level. Hydrogen atoms are omitted for clarity. Grey = carbon, blue = nitrogen, yellow = silicon, green = bromide. Selected bond lengths (Å) and angles (°): Si1-Br1 2.1923(6), Si1-Br2 2.2136(6), Si1-N2 1.7020(17), Si1-N1 1.7041(17), C12-N2 1.431(2), Br1-Si1-Br2 103.9, N2-Si1-N1 94.87(8), C14-C12-N2 118.92(18), Si1-N2-C12 125.76(13), Si1-N2-C12-C14 62.3.

The molecular structure of **21** illustrates the bent nature of the phenylene- sp^2 bridge, anchoring at the imidazole nitrogen atoms. The angle between C14-C12-N2 amounts 119° while the phenylene bridge is turned out of plane significantly (Si1-N2-C12-C14 62.3°). The molecule features a mirror plane through the phenylene bridge, while the coordination sphere of the silane atoms can be described as distorted tetragonal.

Synthesis of Polysilane **24**

In the following, several reducing agents mentioned above have been tested at different temperatures in reactions with the dibromosilanes **21** and **22**. The elevated reactivity of bromosilanes enables the gentle reduction at low temperatures with a broad variety of reactants. After a screening, KC_8 has been selected for further experiments as it can easily be applied in very precise amounts and showed the most promising reactivity. Table 1 summarizes observations when reacting **21** with varying stoichiometries of KC_8 . All reactions have been prepared in the glove box under inert atmosphere by mixing **21** with KC_8 and adding the given solvent at -78 °C.

Table 1: Screening reactions of **21** with KC_8 .

entry	reducing agent	solvent	temperature	time	observation
1	4.0 eq. KC_8	THF	$-30\text{ }^\circ\text{C}$	3d	orange solution
2	4.0 eq. KC_8	DME	$-40\text{ }^\circ\text{C}$	3d	orange solution
3	excess KC_8	DME	$-40\text{ }^\circ\text{C}$	3d	orange solution
4	4.0 eq. KC_8	toluene	$-30\text{ }^\circ\text{C}$	3d	no reaction
5	3.33 eq. KC_8	DME	$-37\text{ }^\circ\text{C}$	3d	red solution

Conversion of **21** with the reducing agent at low temperatures was only detected in ethereal solvents such as THF and DME, while no reaction takes place in toluene at temperatures up to $-30\text{ }^\circ\text{C}$ (Table 1, entry 4). After the indicated reaction time, the mixtures were filtered in the cold and analyzed *via* LIFDI mass spectrometry (Figure 9).

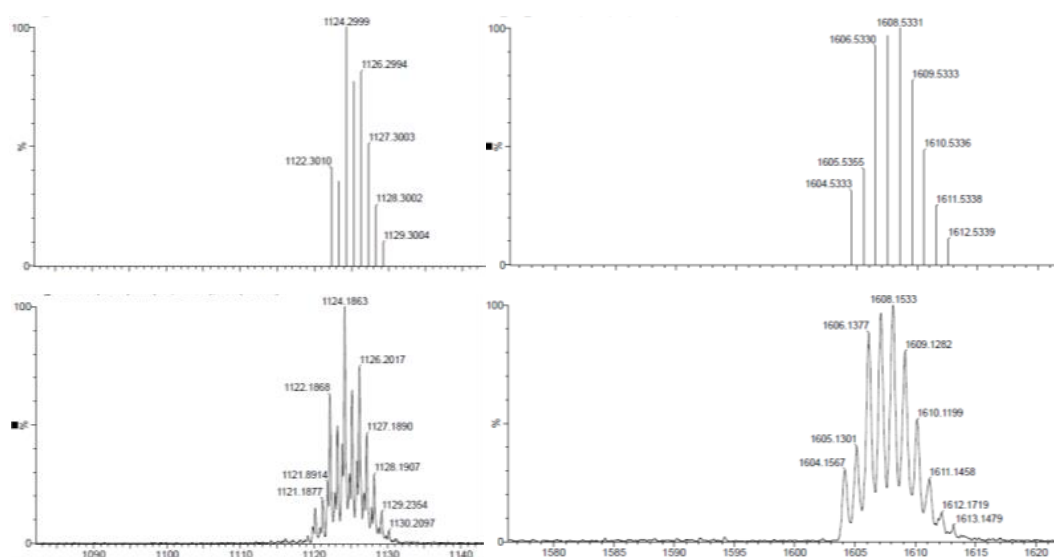
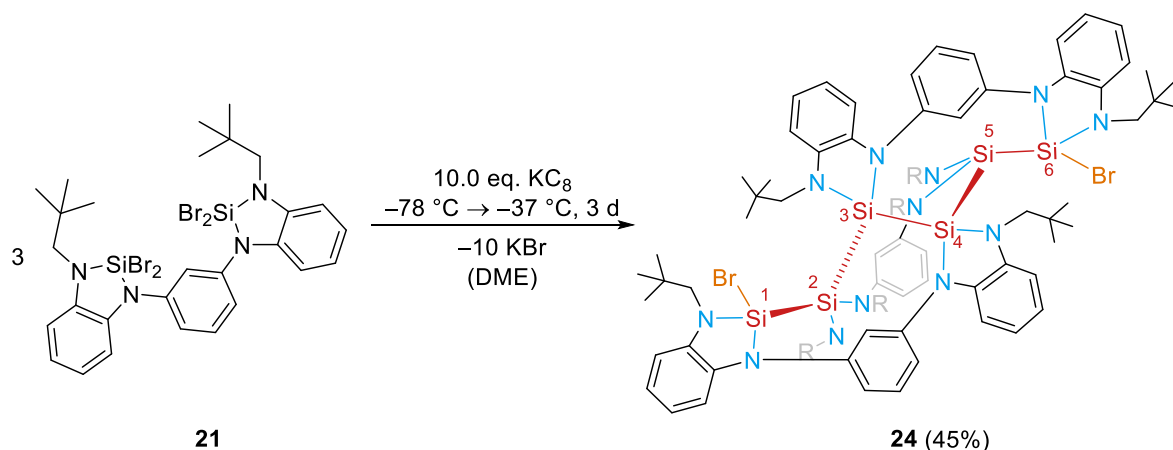


Figure 9: Calculated mass distribution corresponding to $(\text{C}_{28}\text{H}_{34}\text{N}_4\text{Si}_2)_2\text{Br}_2$ and $(\text{C}_{28}\text{H}_{34}\text{N}_4\text{Si}_2)_3\text{Br}_2$ (top from left to right) and measured LIFDI mass spectra corresponding to Table 1 entry 2 and 5. The complete spectra can be found in the supplementary data (SD 3, SD 4).

When letting react **21** with four equivalents KC_8 , an intensively orange-colored solution was obtained, independently of the solvent (THF, DME) and the temperature ($-30\text{ }^\circ\text{C}$ to $-40\text{ }^\circ\text{C}$; Table 1, entry 1-3). Selective formation of the free bissilylene ligand could not be detected *via* mass spectrometry. As shown in Figure 9S, signals at higher m/z have been found in different reaction mixtures, which can be assigned to silane oligomers of the formula $(\text{C}_{28}\text{H}_{34}\text{N}_4\text{Si}_2)_2\text{Br}_2$ (**23**) and $(\text{C}_{28}\text{H}_{34}\text{N}_4\text{Si}_2)_3\text{Br}_2$ (**24**). As the latter is equal to a reduction of 10/12 of the total bromides of one starting molecule, a reaction of **21** with 3.33 eq. KC_8 was performed under similar conditions (Scheme 19).



Scheme 19: Reduction of **21** with 3.33 eq. KC_8 giving the polysilane molecule $(\text{C}_{28}\text{H}_{34}\text{N}_4\text{Si}_2)_3\text{Br}_2$ (**24**). Parts of the latter molecule have been shortened (R) for clarity.

The intensively red-colored solution was filtered through a filter pad, the solvent removed *in vacuo*, and the product extracted into hexane, from which crystals, suitable for X-ray diffraction analysis, grew after one week. However, the molecules within the crystal were highly disordered. Thus, only the molecular structure of compound **24** is given in Figure 10, while atom distances and angles cannot be determined accurately. Numerous attempts, applying different techniques to grow crystals of higher quality, have remained unsuccessful.

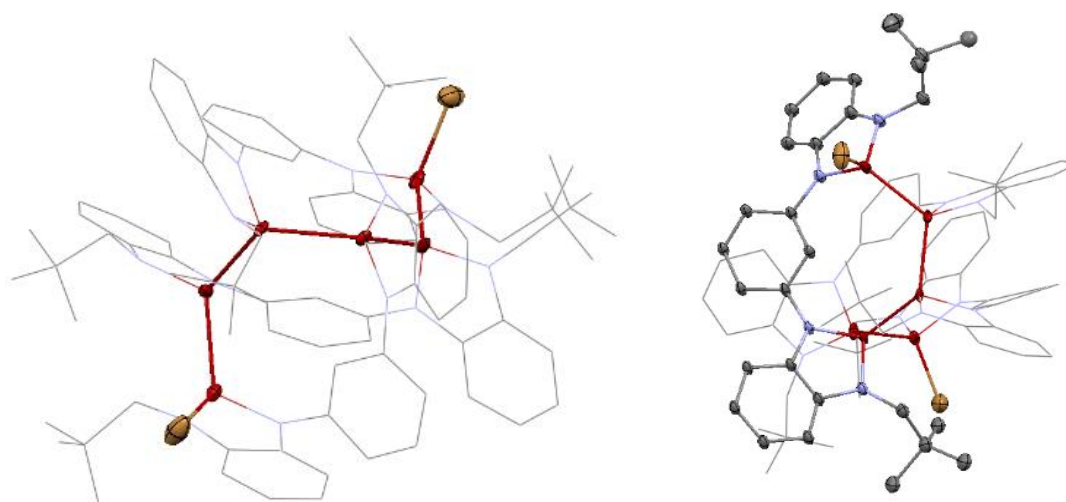


Figure 10: Molecular structure of **24**. Ellipsoids are shown at the 50% probability level. Hydrogen atoms are omitted for clarity. Bulky ligand residues are depicted as wireframes. The helical silicon chain is highlighted in the left picture. The intramolecular linkage *via* the benzimidazole ligands is depicted in the right picture ($\text{Si}_1\text{-Si}_4$). Grey = carbon, blue = nitrogen, red = silicon, orange = bromide.

As can be seen from the LIFDI mass spectrum, the main product of the reaction as shown in Scheme 19 is **24** (SD 4). The selective synthesis of the smaller analog **23** has not been addressed so far. Its formation, however, can be related to substrate concentration and temperature. **24** can be separated off and isolated purely by crystallization at $-32 \text{ }^\circ\text{C}$. The product can be stored at room temperatures under inert gas for weeks without detectable degradation. In the solid state, reaction with moisture

takes place relatively slowly (\approx 10% degradation after three hours). Further analysis, including NMR spectroscopy and DFT calculations, have been conducted to get a deeper insight into the properties of this molecule. In particular, the question arises whether **24** comprises a stabilized bissilylene or can be described as polysilane featuring covalent silicon-silicon bonds.

NMR Spectroscopy of **24**

The compound **24** is best described as a helical Si₆ chain capped by bromine atoms. Most interestingly, the aromatic backbone of each former bissilane wraps around this chain providing steric shielding and connecting two silicon atoms, namely Si₁-Si₄, Si₂-Si₅, and Si₃-Si₆ (Scheme 19, assignment as given in the experimental section). Thereby, the first and the third "unit" within **24** are chemically identical, while the inner unit acts as binding element. In ¹H-NMR and ¹³C-NMR spectroscopy equivalent positions of the first and third unit as well as equivalent positions within the second unit are represented by a single signal (SD 14 and SD 15). In the aliphatic region two singlets of 36 and 18 protons can be found, originating from the inner and outer laying *tert*-butyl groups, respectively (CH₃-32,33;34, CH₃-17;18;19)^a. The methylene protons of the neopentyl groups are given as two singlets (4 protons each) and two doublets (2 protons), which arise from vicinal coupling of the most inner laying protons (CH₂-15';15'''). Proton signals can easily be assigned to a certain unit of the silicon chain by help of ²⁹Si-HMBC spectroscopy (Figure 11). Therein, coupling of three distinct silicon signals with different aliphatic proton signals can be observed, while only weak interaction with aromatic protons takes place. On account of the electronegative bromine substituents, the outer laying silicon atoms are shifted upfield the most (-20.57 ppm), while all signals lay in the area typical for halogenesilanes.²¹³ The most inner laying phenylene bridge, represents the center of the chain and generates unique proton signals. As expected, 28 distinct signals can be found in the aromatic region of the ¹³C-NMR (SD 15). In addition, and in agreement with three chemically distinct positions, three signals of each neopentyl carbon atom are displayed.

^a Exact assignment can be found in the experimental section.

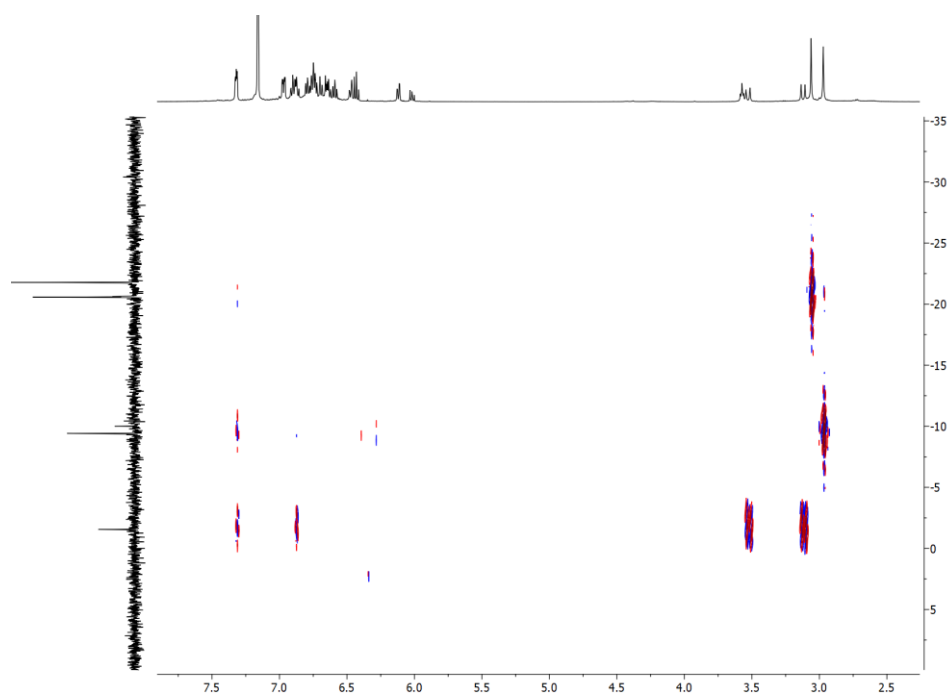


Figure 11: ^{29}Si -HMBC spectrum of **24**. The ^{29}Si -NMR contains not assigned signals arising from contained grease (-21.3 ppm). As shown above, the free bissilylene ligand can be trapped at low temperatures in presence of unsaturated reagents, however, formation of larger molecules such as **24** seems to be kinetically favored. Shifts in ^{29}Si -NMR indicate the formation of a true polysilane featuring covalent silicon-silicon bonds, however, further research has been conducted by means of DFT calculations.

DFT Calculations of **24**^a

Details of DFT calculations can be found in the experimental section, selected data in the supplementary data (SD 18-SD 21). The following conclusions are based on two significant simplifications: I) The neopentyl groups have been replaced by methyl groups. II) Bromine atoms have been replaced by chlorine atoms, in order to reduce the total number of electrons. In the course of the DFT calculations, the ligated Si_6 molecule **24** is compared to a) hexasilane C_6H_{14} and b) chlorohexasilane C_6Cl_{14} by means of QTAIM. The strength of the silicon-silicon bonds is assessed by two predicted properties: I) The electron density given by ρ , which is related to the bond critical point^b between the binding partners. II) The integral of the bond separating surface, defined as $[\int A \cap B \rho(r)]$, which represents diffuse bonds with higher correctness. From the obtained data it is concluded that the strength of the silicon-silicon bond strongly depends upon the substituents at the Si atoms. The highest electron density can be found on average between the silicon atoms of the $\text{Si}_6\text{Cl}_{14}$ molecule, while **24**

^a Performed by M.Sc. Benjamin Hofmann, Prof. Fritz E. Kühn, Molecular Catalysis, TUM

^b Atomic expectation value of the electron density. Decrease in electron density in two spatial directions of the Hessian Matrix and accumulation of electron density in the third direction.

comprises the lowest electron density, barely deviating from the covalently bound hydrosilane. The outer silicon-silicon bonds, Si₁-Si₂ and Si₅-Si₆, of **24** accumulate significantly more electron density compared to the inner laying bonds -which is in contrary to C₆H₁₄ and C₆Cl₁₄. The integral of the electron density confirms this trend. $\int A\cap B\rho(r)[\text{Si}_1\text{-Si}_2; \text{Si}_5\text{-Si}_6]$ of the outer silicon-silicon bonds and $\int A\cap B\rho(r)[\text{Si}_6\text{Cl}_{14}]$ exceed the integral value of the hydrosilane significantly, as electron density of the silicon-chloride and the silicon-nitrogen bonds is donated into the silicon-silicon bonds. K_{tot} , the potential and kinetic energy of electrons along the bonding path, is lowest for the ligated Si₆ chain and highest for the hydrosilane molecule. The negative value indicates a covalent nature of the silicon-silicon bonds within **24**, which therefore would be more stable than Si₆H₁₄ and Si₆Cl₁₄ (Figure 12).

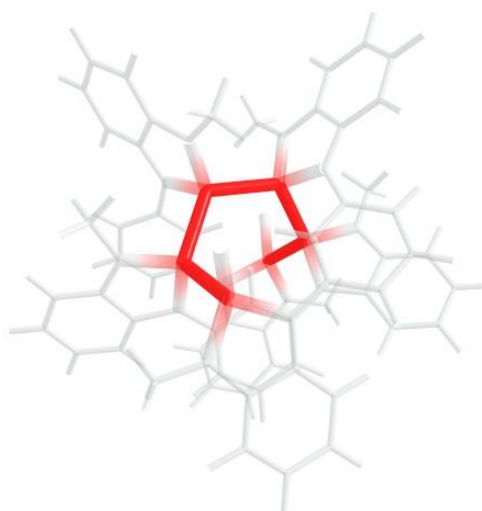


Figure 12: Covalently bound Si₆-chain within **24** as calculated by DFT. Visualized with *Chemcraft*.²¹⁴

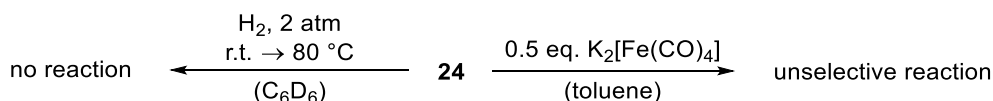
The potential energy of **24** is predicted to be significantly lower compared to the other silanes. Thus, the surrounding electron density causes decisive stabilization. It is possible to conclude that **24** represents a bromine capped polysilane molecule with true covalent bonds. As a result, the inner silicon-silicon bonds of **24** are distinctly weaker compared to Si₁-Si₂ and Si₅-Si₆. Thereby, relatively small ellipticity represents significant hyperconjugation from all sides (SD 20). The ellipticity of the outer silicon-silicon bonds is higher compared to the inner laying bonds by about one magnitude, originating from a pronounced π -character in one direction only. Significantly lower potential energies of the outer laying bonds can be related to the comparably high binding strength.

Reactivity of **24**

The bromine capped **24** features interesting potential reactivities to yield so far unprecedented molecules and complexes. Quite interestingly, in the LIFDI mass spectrum, bromine substitution can be observed, indicating the possibility of further reduction (SD 4). Therefore, experiments have been

performed, to investigate the reactivity of **24** towards nucleophiles, reducing agents, and molecular hydrogen.

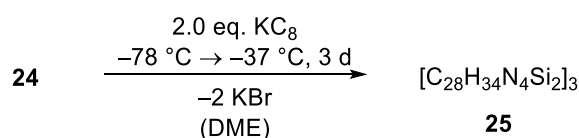
Reaction with hydrogen has been investigated as the so far experimentally unprecedented hydrosilane Si_6H_{14} could possibly be synthesized starting from kinetically stabilized **24**. Nevertheless, no reaction takes place at temperatures as high as $80\text{ }^\circ\text{C}$ and 2 bar hydrogen (Scheme 20). Thus, only the usage of a catalyst might enable such hydrogenation reactions.



Scheme 20: Reactivity of **24** towards molecular hydrogen and *Collman's* reagent different reactants.

The bromine capped hexasilane **24** could also function as monomeric unit towards different oligomers such as ring structures and strands. One experiment regarding the reactivity of the polysilane with nucleophiles has been conducted so far. 0.5 equivalents of *Collman's* reagent, $\text{K}_2[\text{FeCO}_4]$, were added to a solution of **24** in toluene at $-78\text{ }^\circ\text{C}$, without any reaction being observed. When allowing to warm to room temperature, the reaction mixture turned intensively purple. LIFDI mass spectrometry and NMR spectroscopy indicate an unselective reaction, which is probably related to the relatively weak inner laying silicon-silicon bonds. However, the selective substitution of halogenesilanes and-silylenes with nucleophiles is well known.^{67, 215} Therefore, future experiments, such as the stoichiometric hydrolysis, possibly yielding oxo-bridged polysilanes, hold great potential towards unprecedented polysilanes.

As can be seen from the LIFDI mass spectrum shown in SD 4, bromides can be cleaved off the hexasilane **24** easily. Thus, reactions of the latter with two equivalents KC_8 have been performed to investigate the possibility to remove the remaining bromides selectively and finally synthesize novel *N*-bridged bissilylenes (Scheme 21).



Scheme 21: Reaction of **24** with 2.0 eq. KC_8 yielding a room temperature instable trimer **25** of the desired bissilylene.

The reaction has been performed analogously to the procedure described for the synthesis of the hexasilane **24**. After filtration of the reaction mixture, NMR spectroscopy and mass spectrometry were performed. The isotopic pattern and m/z ratio of the most abundant signal of the LIFDI mass spectrum correspond to a molecular formula of $(\text{C}_{28}\text{H}_{34}\text{N}_4\text{Si}_2)_3$ (Figure 13). Thus, the terminal bromides have been removed successfully. The main product is not stable at room temperature, as signals in NMR spectra

broaden over time, which inhibited an exact assignment. This might indicate oligomerization of the low-valent compound towards higher silanes as observed before.^{87, 216-219}

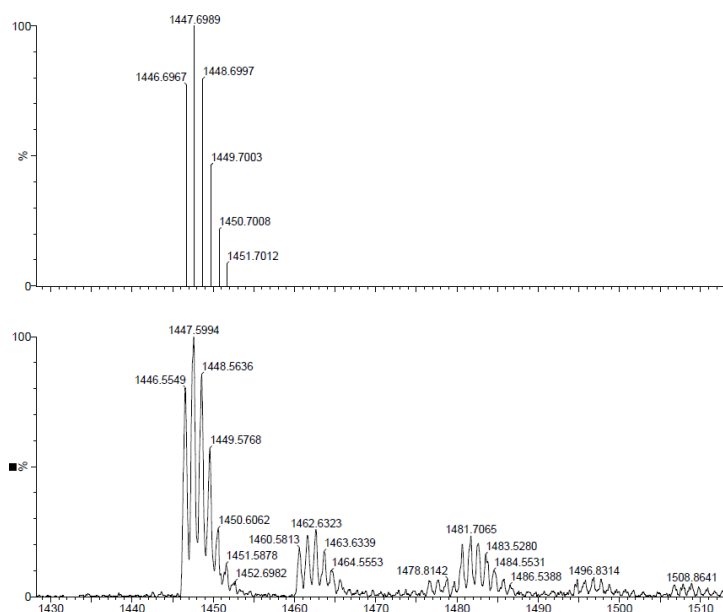


Figure 13: Calculated mass distribution corresponding to $(C_{28}H_{34}N_4Si_2)_3$ (top) and measured LIFDI mass spectrum corresponding to the reaction of **24** with 2.0 eq. KC_8 in DME. The complete spectrum can be found in the supplementary data (SD 5).

Two remarkable signal sets can be seen in the mass spectrum additionally. On the one side, the product shows distinct sensitivity to air and moisture as numerous hydrolyzed side-products can be detected during the LIFDI mass spectrometry measurement under high vacuum (10^{-7} bar). Moreover, the isotopic pattern of the second most abundant signal ($m/z = 481$) can be assigned to $C_{28}H_{34}N_4Si_2$, the molecular formula of the free bissilylene. It seems likely that the main product and the free bissilylene are in equilibrium in solution. However, it was not possible to determine whether the monomeric bissilylene is already present in the reaction solution or forms during ionization in mass spectrometry. Several efforts to crystallize the products have not been successful so far. However, further experiments, including attempts to isolate the reaction product at low temperatures could lead to unprecedented low-valent bissilylene molecules. In addition, transition metal complexes could possibly be synthesized by addition of suitable metal precursors to the reaction mixture as trapping agents.

Summary

Over the past decades, polysilane molecules have been studied intensively, as their unique properties render them interesting for applications in the rising semiconductor industry.²²⁰⁻²²⁶ Insertion reactions of *N*-heterocyclic silylenes yielding stable silanes as well as reversible oligomerization reactions such as dimerization and tetramerization have already been reported before.^{87, 216-219} However, the

synthesis and isolation of a silicon chain connected intramolecularly *via* a *N,N*-substituted aromatic ring system has not been known to literature so far. In the previous chapter, several synthetic approaches towards free *N*-bridged bissilylenes have been studied. While the latter could only be trapped at low temperatures, the kinetically favored bromine-capped hexasilane **24** offers interesting reactivities towards novel polymeric molecules and materials. In future experiments, deeper insights into the reactivity of the silicon-bromine bond, aiming for the interconnection of several Si₆ units, will be targeted. Reactivity studies of **24** with KC₈ have shown that the isolation of *N,N*-substituted bissilylenes might be possible at low temperatures, while stabilization through trimerization (**25**) occurs.

3.2 Versatile Coordination Behavior of a Pyridyl-Functionalized NHGe

As outlined in the introduction, *N*-heterocyclic silylenes and germynes feature exclusive flexible donor-acceptor properties, rendering them interesting steering ligands in homogeneous catalysis.⁷⁹⁻⁸³ In particular donor-stabilized HTs, have already been applied in various catalytic reactions, outperforming their lighter analogs in terms of activity and selectivity (Figure 14).^{131, 201, 204}

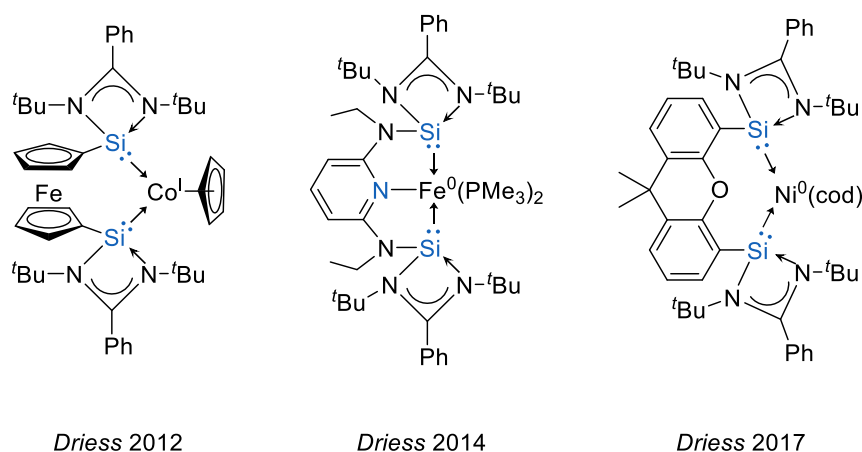
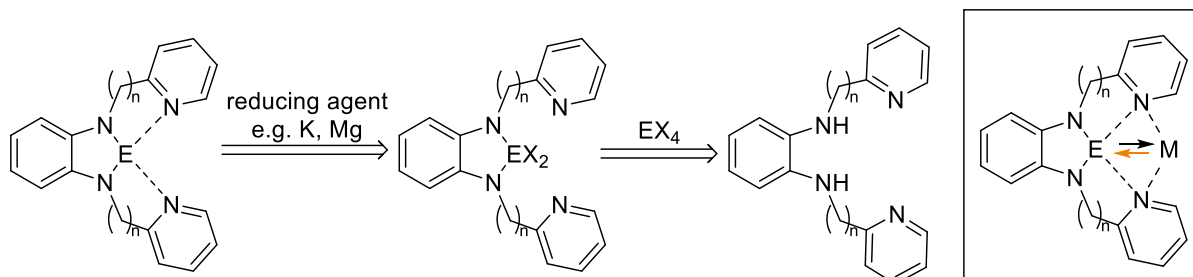


Figure 14: Examples of catalytically active transition metal complexes ligated by chelating HT ligands.^{131, 201, 204}

Rather surprisingly, the potential of less coordinated tetrylenes such as long-known five-membered NHSis and NHGes towards higher electronic versatility has been quite disregarded over the past years.^{55, 113, 114, 227, 228} Noteworthy, the catalytic hydrosilylation of olefins potentially benefits from an unhindered electron exchange. Within the catalytic cycle, the substrate is usually added to the metal center in an oxidative addition, while the hydrosilylated product is eliminated reductively, returning electron density to the metal center. In the following chapters, novel five-membered *N*-heterocyclic tetrylenes functionalized by flexible intramolecular donors should be designed and applied as steering ligands in the catalytic hydrosilylation of olefins (Scheme 22). The donor moiety could possibly ensure the ideal balance between electron donation to the metal center and metal-to-ligand backbonding.



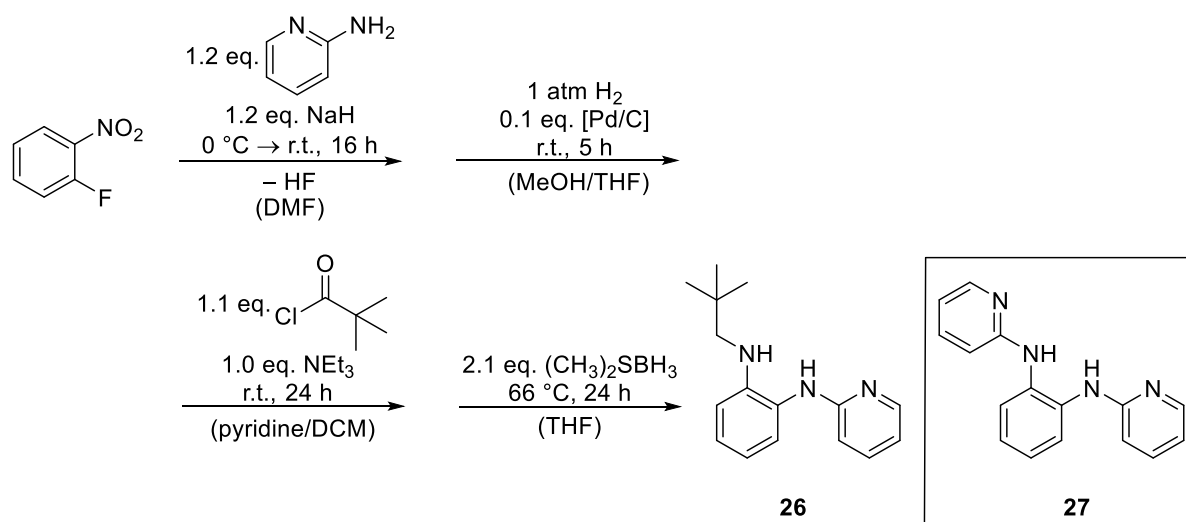
Scheme 22: Synthetic approach towards pyridyl-functionalized five-membered *N*-heterocyclic tetrylenes as steering ligands in transition metal complexes. E = Si, Ge; n = 0, 1.

Nitrogen donors have been proven to be suitable candidates for coordinating and stabilizing low-valent tetrylenes.^{74, 229-231} *Driess et al.*, among others, reported the very first pyridine-stabilized germanone accessible through oxygenation of a DMAP adduct of a six-membered *N*-heterocyclic germylene.⁷⁴ HT ligated transition metal complexes usually suffer from their tendency to undergo oxidation and hydrolyzation reactions, to the extent that applications in alkene hydrosilylation have remained scarce.^{56, 177-179, 232} Benzannulated NHGes, including pyrido[b]annulated five-membered germylenes, undergo significant stabilization due to delocalization of the electron density. Thus, binding of an external donor is hampered.¹¹² In contrast, the reduced aromaticity of pyrido[c]annulated NHGes allows for strong intermolecular donation to the germanium atom, even leading to air stability.²³³

Pyridyl-functionalized NHGes, thus, represent a so far poorly investigated field with high potential with respect to electronically more versatile, thermodynamically stable ligands. Promising results have been reported by *Kühn et al.* recently.^{234, 235} Therein, the reactivity of a *N*-heterocyclic silane with a pyridine-2-ylmethyl wingtip has been investigated. Interestingly, the latter features an unexpected change in coordination when reacted with late transition metals. Based on these results, novel pyridyl-substituted *N*-heterocyclic ligated tetrylenes have been synthesized in the following and studied in reactions with different Lewis acids. In comparison to known macrocyclic NHGes, the introduction of flexible pyridyl wingtips allows for the development of electronically more versatile transition metal complexes.^{135, 197}

Synthesis of Novel NHGe 33

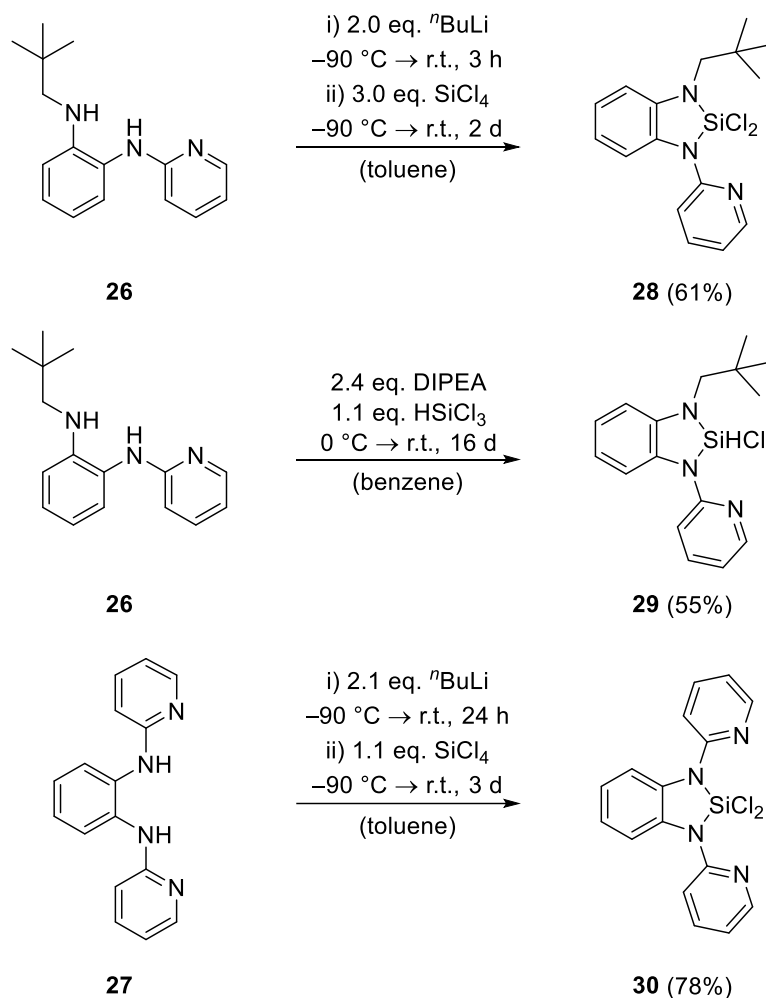
For the synthesis of novel pyridyl-substituted HTs, *N*-substituted pyrido-1,2-diaminobenzenes **26** and **27** have been synthesized following synthetic procedures as already described above (Scheme 23). The annellation of the ligand potentially increases the thermodynamic stability of tetrylenes through electron delocalization. In comparison to known *N*-pyridine-2-ylmethyl-substituted diamines, the direct binding of the pyridyl at the nitrogen atom would change the coordination behavior of the latter significantly.



Scheme 23: Synthesis of the diaminobenzene **26** following synthetic procedures as described above. *N,N*-Bis(pyridine)-1,2-diaminobenzene (**27**) as highlighted in the box was synthesized by a member of the working group of Prof. Fritz E. Kühn.

As described above, HTs can be synthesized starting from diamino compounds *via* the reduction of the respective dihalogenosilane with alkali metals. The *N,N*-bis(pyridine)-1,2-diaminobenzene (**27**) has been synthesized within the laboratories of Prof. Fritz E. Kühn (Scheme 23).^a The asymmetric diaminobenzene **26** has been manufactured following an altered four-step synthesis as described above for the tetraamines **15** and **20**. In order to increase the reactivity, 1-aminopyridine was reacted with NaH prior to its addition to a solution of 1-nitrofluorobenzene. In the third step, introducing the 2-*N*-neopentylamide group, triethylamine was used instead of DMAP, to prevent the otherwise observed double substitution. Starting from the asymmetric diaminobenzene **26**, the dichlorosilane **28** and the hydrochlorosilane **29** were synthesized and isolated following synthetic procedures as described in the previous chapter (Scheme 24). Lithiation of **27** and subsequent reaction with tetrachlorosilane gives the dichlorosilane **30** in high yields. Selected SC-XRD analysis is given in the supplementary data (SD 22), however will not be part of the following discussion.

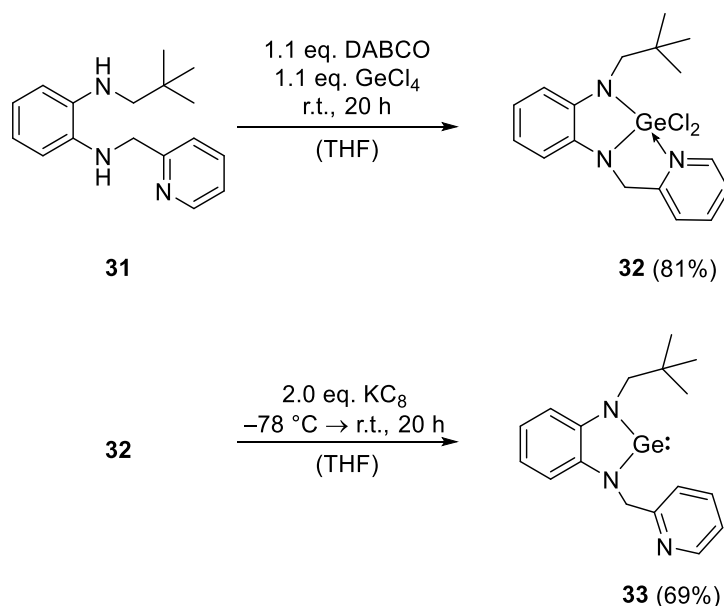
^a M.Sc. Han Li, Prof. Fritz E. Kühn, Molecular Catalysis, TUM



Scheme 24: Synthesis of novel dichloro- and hydrochlorosilanes **28**, **29** and **30**.

Dehydrochlorination of hydrochlorosilanes with carbenes to give donor-stabilized silylenes has already been reported before.^{236, 237} Reaction of **29** with $\text{DIP}^{\text{P}}\text{NHC}$, however, did not result in the free silylene but gives a mixture of products. Moreover, several attempts to reduce the dichlorosilanes **28** and **30** with common reducing agents to give the free NHGes were not successful. Thus, dichlorogermanes were synthesized in the following and subsequently reduced to give free NHGes, as their pronounced stabilities render them suitable substitutes for NHSi ligands.

Since the discovery of the first NHGe, several synthetic approaches have been discussed in the literature over the past decades.⁸⁸ Similar to NHSis, the most common approach is the reduction of the corresponding dihalogenegermanes. Starting from literature known diamine **31**, the free *N*-pyridine-2-ylmethyl-substituted NHGe **33** can be synthesized in a two-step protocol *via* reduction of the dichlorogermane **32** (Scheme 25).



Scheme 25: Synthesis of novel *N*-heterocyclic germylene **33** from the corresponding diamine **31** in a two-step procedure *via* reduction of the dichlorogermene **32** with KC_8 .

The synthesis of the dichlorogermene **32** using common literature-known procedures like the transmetalation of the corresponding diamine with *n*-butyl lithium and GeCl_2 -dioxane were not successful.^a Upon treatment of the diamine **31** with a slight excess of DABCO and GeCl_4 , the product can be obtained as a green solid in high yield.²³⁴ Reduction of the latter with two equivalents of KC_8 leads to the *N*-heterocyclic germylene **33** which can be isolated as yellow solid by crystallization from diethyl ether at low temperatures ($-32 \text{ }^\circ\text{C}$). The new compounds **32** and **33** are highly sensitive to air and moisture and were both fully characterized by NMR spectroscopy, LIFDI mass spectrometry, elemental analysis and single crystal X-ray diffraction analysis.

Mass spectrometry confirmed the proposed composition $\text{C}_{17}\text{H}_{21}\text{N}_3\text{GeCl}_2$ of **32**. The ^1H -NMR spectrum shows a broad singlet for the neopentyl moiety, indicating hindered rotation. Determination of the structure by SC-XRD unequivocally confirmed the structure of **32** and revealed the presence of a pentavalent germanium with the pyridyl moiety as donating ligand (Figure 15). Examples of hypervalent germanium atoms have been reported to literature before, including dative bonding of nitrogen-containing ligands.^{231, 238-241}

^a Similar NHGers have been synthesized *via* deprotonation of the corresponding diamine before, however, in this case only methylene deprotonation is observed.

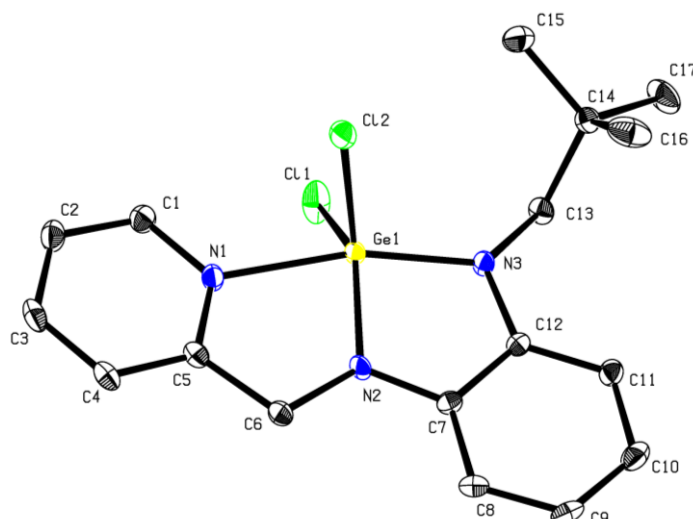


Figure 15: Molecular structure of **32**. Ellipsoids are shown at the 50% probability level. Hydrogen atoms are omitted for clarity. Grey = carbon, blue = nitrogen, yellow = germanium, green = chloride. Selected bond lengths (Å) and angles (°): Ge1-N1 2.101(2), Ge1-N2 1.825(2), Ge1-N3 1.874(2), Ge1-Cl1 2.1934(7), Ge1-Cl2 2.2017(6), N3-Ge1-N2 86.94(8), N1-Ge1-N2 79.62(7), N1-Ge1-N3 165.54(7), Cl2-Ge1-N2 115.58(6), Cl2-Ge1-Cl1 107.32(2), Cl1-Ge1-N2 134.26(6), N2-C6-C5-N1 1.3(3).

In contrast to the well-known symmetric ^tBu-NHGe, which slowly releases ^tBu-NH₂, the five-fold coordinated germane **32** is stable in solution.²⁴² Due to the dative binding, the four rings in **32** form a coplanar, annular system and, thus, the coordination sphere of the germane is best described as distorted trigonal bipyramidal. The bond length Ge1-N1 is significantly longer than Ge1-N2 and Ge1-N3 (2.101 Å versus 1.825 Å and 1.874 Å), indicating a polar dative interaction in contrast to the covalent bonds Ge1-N2 and Ge1-N3.^{238, 239, 241} Of these, Ge1-N3 is 0.049 Å longer, which is attributed to the *trans*-influence of the pyridyl moiety. The distances Ge1-Cl1 and Ge1-Cl2 amount 2.1934 Å and 2.2017 Å, and thus lay between typical tetra- and pentavalent germanium compounds.²⁴⁰⁻²⁴³

The mass spectrum of the free germylene **33** shows one major signal at $m/z = 342$ and an isotopic distribution pattern matching the predicted values for the free germylene. SC-XRD unequivocally reveals the formation of the non-coordinated bivalent germylene **33**, wherein the pyridyl wingtip is tilted by about 90 degrees (Figure 16).

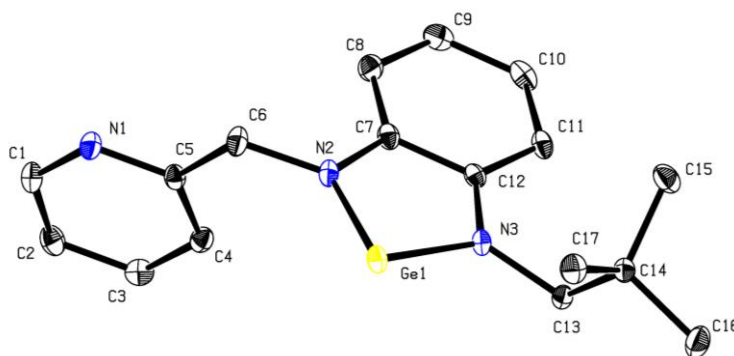


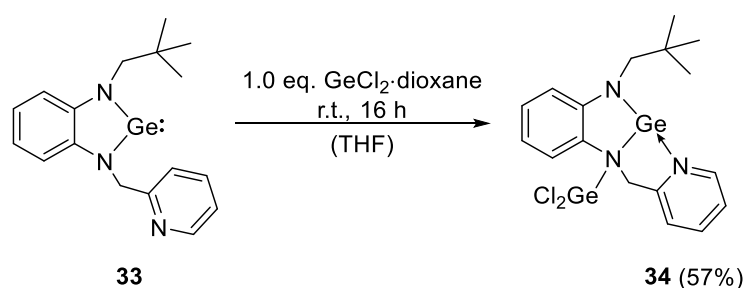
Figure 16: Molecular structure of **33**. Ellipsoids are shown at the 50% probability level. Hydrogen atoms are omitted for clarity. Grey = carbon, blue = nitrogen, yellow = germanium. Selected bond lengths (Å) and angles (°): Ge1-N2 1.851(2), Ge1-N3 1.863(1), N2-Ge1-N3 85.07(6), Ge1-N2-C6-C5 104.7(7).

The wingtips in **33** are rotated to opposite sides, which is attributed to crystal packing effects.¹¹² Comparable to lighter *N*-heterocyclic carbenes and donor-free cyclic tetrylenes, the annulated system is not tilted as the germanium lies in plane with the aromatic backbone. The bond lengths Ge1-N2 and Ge1-N3 (1.851 Å, 1.863 Å) are comparable to typical covalent germanium-nitrogen distances and non-donor stabilized NHGes.²⁴² The germylene is dicoordinate only, as the pyridyl moiety faces away from the germanium and remains uncoordinated. This is in agreement with literature known benzannulated NHGes such as pyrido[b]annulated *N*-heterocyclic germylenes, where no interaction with the backbone nitrogen atom takes place due to the high thermodynamic stability of the germylene.²¹⁰

The ¹H-NMR signals of **33** are shifted significantly compared to the dichlorogermene **32** confirming the electronic influence of the donor group in the latter. In accordance with the absent coordination of the pyridyl moiety to the germylene, the signal of the *ortho*-proton is shifted high-field (8.63 ppm → 8.47 ppm). The pyridyl-bound methylene bridge at 5.29 ppm shows a significant down field shift of 1.54 ppm compared to **32**, suggesting significantly reduced electron density through a pronounced electron pull of the chlorides in the latter. The pyridyl moiety can thus act as a flexible intramolecular Lewis base, which donates electron density to the germanium under certain conditions.

Reactivity Studies with Lewis Acids

Pyridyl-substituted germylene **33** represents a novel asymmetric ligand, exhibiting multiple possible interactions with Lewis acids. To investigate its coordination behavior and to prove the potential stabilization through pyridine coordination, reactions of the novel NHGe with two Lewis acids were conducted and investigated by means of NMR spectroscopy and SC-XRD. In recent years, several reactions of HTs with germanium dichloride and other low-valent tetrylenes have been performed in order to investigate their coordination chemistry.^{116, 244-247} Interestingly, HTs are able to stabilize intramolecular adducts due to their ambivalent electron donor/acceptor properties.^{129, 248-255} Thus, the reaction of **33** with an equimolar amount of GeCl₂·dioxane has been conducted at room temperature (Scheme 26).



Scheme 26: Reaction of **33** with GeCl₂·dioxane leading to the *N*-dichlorogermene-substituted **34**.

No significant visible changes were observed upon stirring in dichloromethane overnight. LIFDI mass spectrometry of the solution shows two signals, the main signal matching the free ligand **33** and a second smaller signal which corresponds to the chlorinated germane **32**. Crystals suitable for X-ray diffraction analysis, obtained from a hexane layered THF solution of the reaction mixture, revealed the molecular structure of compound **34** – a coordination compound consisting of GeCl_2 and the free ligand **33** (Figure 17).

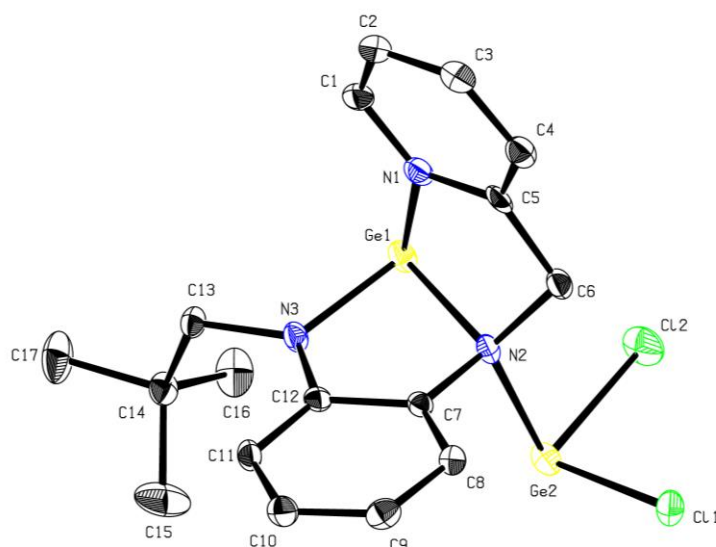


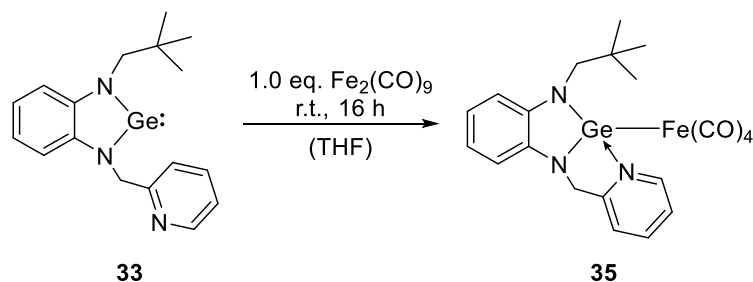
Figure 17: Molecular structure of **34**. Ellipsoids are shown at the 50% probability level. Hydrogen atoms are omitted for clarity. Grey = carbon, blue = nitrogen, yellow = germanium, green = chloride. Selected bond lengths (Å) and angles (°): N1-Ge1 2.129(3), N2-Ge1 2.036(3), N3-Ge1 1.881(3), N2-Ge2 2.098(3), N2-Ge1-N3 84.0(1), N2-Ge1-N1 77.7(1), N3-Ge1-N1 96.0(1).

Ligand **33** coordinates GeCl_2 in a rather unexpected way. Instead of the germanium atom, the tertiary nitrogen N2 acts as Lewis base. Furthermore, the pyridyl moiety coordinates to the germanium, comparable to the situation in the chlorinated germane **32** and in contrast to the free germylene. Accordingly, the *ortho*-proton of the pyridyl-moiety is shifted low-field in $^1\text{H-NMR}$ spectroscopy when compared to **33** (8.47 ppm \rightarrow 8.70 ppm). In addition, also the pyridine-bound methylene bridge is shifted low-field due to the additional coordination of GeCl_2 .

The aromatic N2-Ge1 bond is significantly weakened, as an elongation of the bond from 1.851 Å to 2.036 Å takes place. In fact, this bond length is closer to a dative rather than a covalent bond (N1-Ge1: 2.101 Å in **32**, 2.129 Å in **34**).^{241, 256} Due to the coordination of GeCl_2 at N2, the π -donor strength of the latter towards Ge1 is reduced which leads to an elongation of the N2-Ge1 bond. Thus reduction in aromaticity can only be rationalized through the intramolecular interaction of the pyridyl donor.

To further investigate the reactivity with different kinds of Lewis acids, **33** was reacted with iron carbonyl. Similar reactions of simple NHCs, NHSis, and NHGes with iron carbonyl have been reported in the literature before, leading to the isolation of a broad variety of mononuclear transition metal(0)

complexes.^{246, 257-267} By treatment with one equivalent of $\text{Fe}_2(\text{CO})_9$ in THF, the clear yellow solution of **33** starts to turn dark orange after a few minutes (Scheme 27).



Scheme 27: Reaction of **33** with $\text{Fe}_2(\text{CO})_9$ in THF leading to the respective iron carbonyl complex **35**.

Decarbonylation of $\text{Fe}(\text{CO})_5$ leads to the iron complex **35**, which crystallizes in pure form from THF/diethyl ether in high yields. In strong accordance with the isotopic pattern, LIFDI-MS shows a maximum signal set corresponding to $[(\mathbf{33})\text{Fe}(\text{CO})_3]$ beside the second most abundant signal corresponding to $[(\mathbf{33})\text{Fe}(\text{CO})_4]$ and further signals stemming from carbonyl dissociation (SD 6). The carbonyl ligand seems to be labilized due to the *trans*-effect of the germylene ligand. Single crystal X-Ray diffraction analysis confirmed this assertion and revealed the molecular structure of the product (Figure 18). In fact, the NHGe **33** binds as a monodentate ligand *via* Ge1 while the pyridyl moiety again binds in a dative fashion to the germylene.

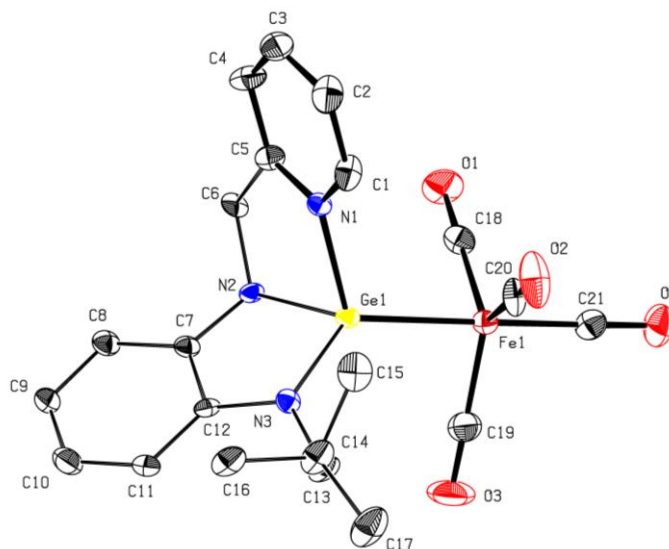


Figure 18: Molecular structure of **35**. Ellipsoids are shown at the 50% probability level. Hydrogen atoms are omitted for clarity. Grey = carbon, blue = nitrogen, yellow = germanium, dark red = iron, red = oxygen. Selected bond lengths (Å) and angles (°): Ge1-N1 2.101(2), Ge1-N2 1.87(1), Ge1-N3 1.86(1), Ge1-Fe1 2.2897(4), Fe1-C21 1.785(6), N2-Ge1-N3 88.4(7) N1-Ge1-N2 82.6(3), N1-Ge1-N3 107.9(4), N1-Ge1-Fe1 110.55(5), N2-Ge1-Fe1 132.0(3), N3-Ge1-Fe1 126.3(4), Ge1-Fe1-C21 176.85(4), C12-N3-Ge-N1 86.9(6), C7-C12-N3-C13 169.2(1).

The molecular structure of complex **35** is slightly distorted trigonal bipyramidal around the iron center with an axial angle of 176.85° (Ge1-Fe1-C21). Stabilized by the neutral, intramolecular pyridyl-moiety, the Ge1-Fe1 bond length amounts 2.2897 \AA , which is comparable to germanium-iron complexes stabilized by external Lewis bases such as hydroxide, fluoride or chloride.^{261, 262, 268-270} Remarkably, the

pyridyl moiety binds to the germylene ligand plane almost orthogonally while the neopentyl wingtip remains in plane. The benzannulated plane of the germylene is tilted with respect to the Ge1-Fe1 bond by about 40°. Thus, coordination of the pyridyl moiety at the germylene does not only lead to a stabilization but can also provoke an alteration of the binding mode of the tetrylene. In fact, the coordination sphere of the germylene is best described as distorted tetrahedral. The Ge1-N1 separation (2.101 Å) matches the determined Ge1-N1 distance in the dichlorogermene **32** and is comparable to measured intermolecular distances in pyrido[c]annulated germylenes (2.104 Å).²³³ The atom distance is elongated when compared to covalent bonds (1.864(2) Å - 1.955(2) Å, 2.088(2) Å in Ge[N(SiMe)₃]₂),^{241, 256, 271} however, significantly shorter than typical donor-acceptor distances (2.3 Å - 3.5 Å).^{134, 233, 272}

NMR experiments at elevated temperatures were performed to gain further insight into the thermodynamic stability of the pyridyl-substituted complex in solution. Quite remarkably, shifts in the ¹H-NMR spectrum are reversible and therefore no thermodynamic conversion takes place - no matter if performed in pure benzene or pyridine. Addition of the latter, however, leads to a reversible shift of the neopentyl and methylene protons of the ligand at elevated temperatures, indicating reversible coordination of a solvent molecule (Figure 19). In the ¹³C-NMR spectrum, the carbonyl signal appears at 214.2 ppm which is in accordance with literature-known base-stabilized tetrylene iron carbonyl complexes.^{261, 268}

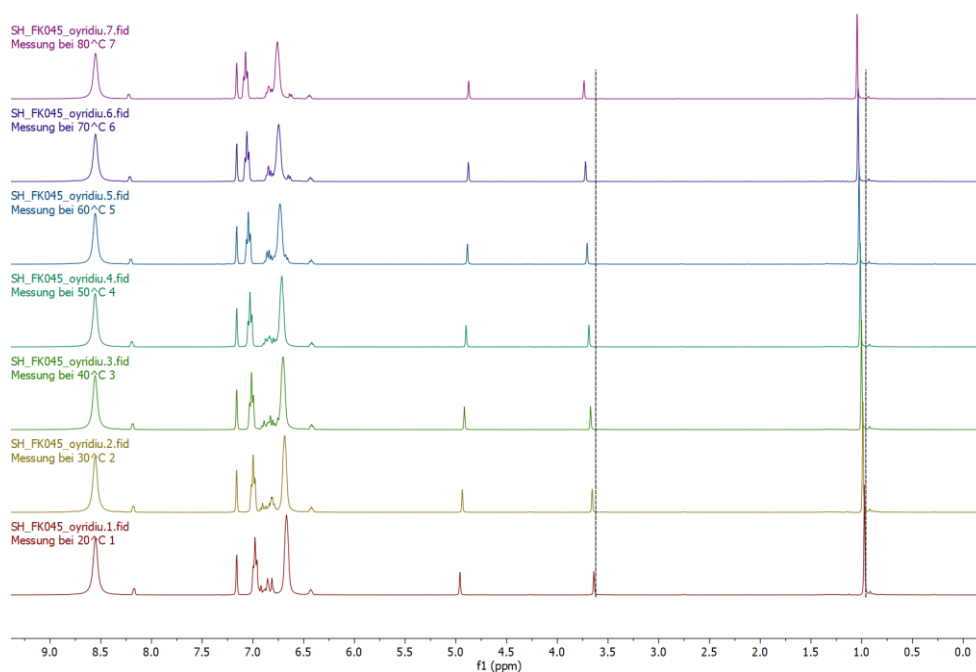


Figure 19: ¹H-NMR spectra of **35** in C₆D₆ and pyridine at variable temperatures (20 °C - 80 °C).

The stretching frequency of the respective *trans*-carbonyl ligand allows insights into the donor strength of the novel pyridine-substituted germylene. As the iron(0) carbonyl complex **35** is highly sensitive to

air and moisture, the IR-spectrum was recorded in solution and can be found in the supplementary data (SD 37). In comparison with other cyclic germylenes and donor-stabilized HTs, carbonyl stretching frequencies indicate strong electron donation to the metal center due to the additional coordination of the pyridyl moiety.²⁶² In comparison to pure σ -donating carbene ligands, donation through **33** is only slightly reduced ($\nu(\text{CO})[(\mathbf{33})\text{Fe}(\text{CO})_4] = 2041, 1967, 1933 \text{ cm}^{-1}$ versus $\nu(\text{CO})[(^{\text{Mes}}\text{NHC})\text{Fe}(\text{CO})_4] = 2035, 1947, 1928, 1919 \text{ cm}^{-1}$).²⁶⁶

Metal carbonyl compounds depict an interesting class of transition metal complexes, as their catalytic activity has already been found and investigated more than 50 years ago – including the catalytic carbonylation, hydrogenation and hydrosilylation of olefins.^{147, 184, 273, 274} Thereby, the photolytic activation towards the catalytic transformation of silanes and alkenes has been reported in several examples.^{152, 155, 185-188} Moreover, the catalytic activity of lighter *N*-heterocyclic carbene complexes such as $(^{\text{Mes}}\text{NHC})\text{Fe}(\text{CO})_4$ has already been demonstrated in hydroboration and carbonyl reduction reactions.^{266, 275} Complex **35** features an intense absorption band in UV/VIS spectroscopy at 302 nm. Thus, irradiation experiments were examined to reveal the reactivity of the iron carbonyl bond. Exposition of both a benzene and a THF solution to UV-light with a wavelength of $\lambda = 300 \text{ nm}$ led to a change in color into deep red after several hours. Mass spectrometry analysis indicated the formation of a diiron carbonyl complex coordinated by either one or two equivalents of **33**. NMR spectroscopy also shows more than one product, but the selective separation and structural characterization has not been successful so far. Further experiments, such as the activation of the complex in presence of silane molecules or the catalytic conversion of alkenes, have not been addressed so far.

Summary

In summary, a novel pyridine-substituted *N*-heterocyclic germylene has been synthesized and utilized as electronically flexible ligand of Lewis acids such as $\text{Fe}(\text{CO})_4$ (**35**) and GeCl_2 (**34**). The ligand has been synthesized starting from the respective dichlorogermane *via* reduction with KC_8 . Full characterization of the compounds reveals the electronically flexible behavior of the *N*-heterocyclic germylene as both deficits as well as excesses in electron density can be balanced *via* flexible coordination of the pyridyl moiety. The unexpected coordination of the GeCl_2 by the nitrogen atom N2 instead of the designated Lewis base Ge1 is quite surprising as the *N*-heterocyclic germylene partly loses its aromatic ring structure. This can be attributed to the asymmetric nature of the NHGe **33** and could possibly open up reactivities of thermodynamically stable, five-membered germylenes towards small molecules. The effect of the flexible pyridine-2-ylmethyl wingtip has also been investigated by means of DFT calculations.^a Studies of the binding strength, molecular orbitals, and total energies have settled three

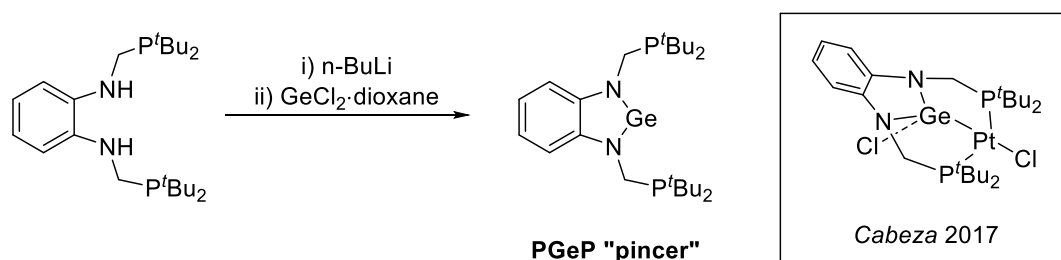
^a Performed by M.Sc. Benjamin Hofmann, Prof. Fritz E. Kühn, Molecular Catalysis, TUM

major findings: I) Binding of the Lewis acid GeCl_2 by the nitrogen atom N2 can only take place due to the dative coordination of the pyridyl moiety at the germylene. II) The thermodynamic stability of the germylene iron(0) metal complex **35** is significantly increased due to the intramolecular pyridine donor. III) The binding of the germylene at transition metals can alter dramatically due to the intramolecular coordination of the pyridyl moiety, thus losing pure σ -donor character. Further work is ongoing, investigating the potential of such asymmetric tetrylenes in reactions with coordination compounds and activation of small molecules. So far, the synthesis of NHGes based on the pyridyl-functionalized diamines **26** and **27** has not been addressed.

3.3 Pyridyl-Functionalized NHGe Ligands – Reactivity and Coordination Chemistry

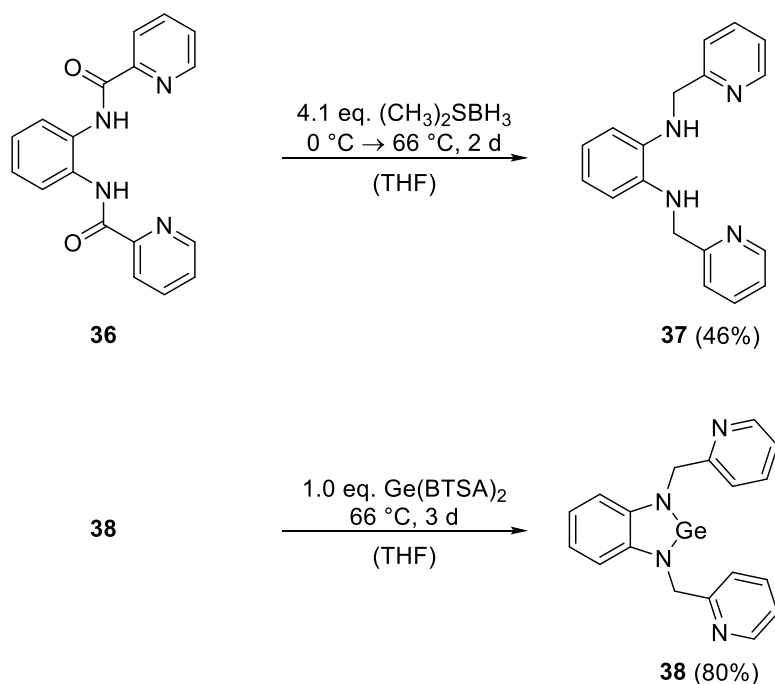
Synthesis of Novel NGeN Pincer-Type Ligand **38**

NHC-based pincer-type ligands have paved the way towards the stable catalysis of a broad variety of catalytic reactions.²⁷⁶ As mentioned above, several examples of silyl-based pincer ligands and donor-stabilized amidinate pincer ligands have already been applied in catalysis.^{131, 195, 213, 277-279} Only recently, *Garcia-Álvarez et al.* and *Cabeza et al.* successfully synthesized of the very first PGeP pincer-ligand and its coordination chemistry within transition metal complexes (Scheme 28).^{276, 280, 281} Within the free benzannulated ligand, the phosphine wingtips are directed towards the germanium (Ge-P 3.320 Å, 0.6 Å shorter than the sum of van der Waals radii), while the atom distance is still significantly higher than dative phosphine germanium bonds.²⁸² Interestingly, coordination of the phosphine substituents at the germanium occurs neither in the free ligand nor in transition metal complexes thereof.



Scheme 28: Synthesis of the benzannulated PGeP pincer-type NHGe as reported by *Cabeza et al.* and a PGeP platinum(I) chloride complex highlighted in the box.²⁷⁶

Five-membered *N*-heterocyclic HTs display interesting electronic properties considering novel steering ligands as described in the previous section. In comparison with the asymmetrically functionalized pyridine-2-ylmethyl NHGe **33**, the synthesis and reactivity of a symmetrically-substituted bis(pyridine-2-ylmethyl) NHGe was pursued in the following. Since pyridine donation of low-valent germanium atoms has been observed before, also within **33**, the properties of the novel ligand presumably differ significantly from the recently reported PGeP pincer ligand. Starting from the literature known bisamide **36**,²⁸³ the pincer-type NGeN *N,N'*-di(pyridin-2-ylmethyl)benzimidazolin-2-germylene (**38**) has been synthesized following a two-step procedure (Scheme 29).



Scheme 29: Synthesis of novel bis(pyridin-2-ylmethyl) NHGe **38** following a two-step procedure *via* reaction of the corresponding diamine **37** with Ge(BTSA)₂.

The reduction of **36** to give the diamine **37** was achieved with borane dimethyl sulfide following synthetic procedures as already described above in the synthesis of **15** and **20**.^{208, 209} Analogous to the synthesis of **16** the corresponding dichlorogermane of **37** can easily be synthesized in a one-pot reaction with DABCO and tetrachlorogermane. However, reduction with various agents such as potassium and KC₈ in different solvents does not result in the free germylene selectively. Thus, Ge[N(SiMe₃)₂]₂ has been synthesized according to *Mathur et al.*²⁸⁴ and reacted with the diamine **37**. The amide acts as internal base, leading to the desired product **38** in good yields after three days at elevated temperatures. The resulting amine can be removed easily *in vacuo*. The product features excellent thermodynamic stability allowing its sublimation at 250 °C in high vacuum (10⁻⁸ bar). The product was fully characterized by NMR spectroscopy, LIFDI mass spectrometry, and elemental analysis. Crystals, suitable for SC-XRD were grown from a THF solution at -30 °C (Figure 20). Interestingly, THF coordination at low temperatures changes the color of the orange solution into dark green.

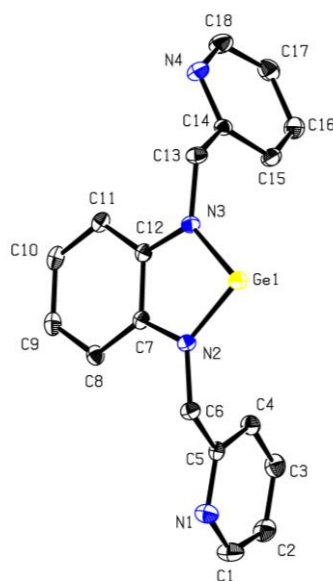
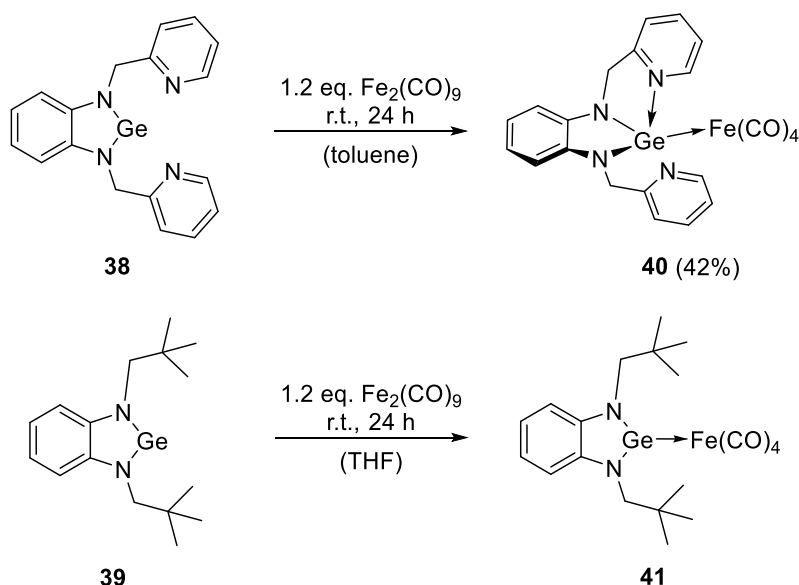


Figure 20: Molecular structure of **38**. Ellipsoids are shown at the 50% probability level. Hydrogen atoms and co-crystallized THF are omitted for clarity. Grey = carbon, blue = nitrogen, yellow = germanium, green = chloride. Selected bond lengths (Å) and angles (°): Ge1-N2 1.8667(9), Ge-N3 1.8568(9), N3-C13 1.4571(13), N2-C6 1.4552(13), N2-Ge1-N3 84.73(4), C6-N2-Ge1 125.61(7), C13-N3-Ge1 125.68(7), C5-C6-N2 114.99(8), C14-C13-N3 114.77(9), Ge1-N2-C6-C5 109.35(9), Ge1-N3-C13-C14 112.23(9).

In the molecular structure of **38**, it is remarkable to see that the pyridyl moieties are pointing to opposite directions and away from the germylene. This stands in stark contrast to the PGeP pincer-type ligand reported by *Cabeza et al.*²⁷⁶ Thus, the torsion angles between the germylene plane and the pyridyl moieties amount more than 105° each. The distances between the nitrogen atoms N2 and N3 and the germylene are in the same range as in **33** while the N2-Ge1-N3 angle is slightly decreased (84.7°). Signal shifts in NMR spectroscopy are very similar to the asymmetric **33**.

Synthesis and Properties of Novel NHGe Iron(0) Carbonyl Complexes

As already observed in reactions of the asymmetric NHGe **33** with Lewis acids, the pyridyl moiety can influence the electronic properties of germylene ligands significantly. To compare these effects, the donor-free bisneopentyl-substituted NHGe **39** was synthesized according to *Kühl et al.* (Scheme 30).¹¹² The latter can be prepared *via* lithiation of the corresponding diamine and subsequent treatment with GeCl₂-dioxane. To get a deeper insight into the coordination properties of the novel pincer-type germylene **38** and the influence of the pyridyl moiety, both **38** and **39** were reacted with iron nonacarbonyl (Scheme 30).



Scheme 30: Synthesis of the iron(0) carbonyl complexes **40** and **41** via reaction of **38** and **39** with $\text{Fe}_2(\text{CO})_9$.

Analogous to the already described iron(0) carbonyl complex **35**, $[(\mathbf{38})\text{Fe}(\text{CO})_4]$ (**40**) and $[(\mathbf{39})\text{Fe}(\text{CO})_4]$ (**41**) can be synthesized by treatment of the corresponding ligands with a slight excess of $\text{Fe}_2(\text{CO})_9$ in a THF solution. However, the pincer-type NGeN ligand **38** does not react with iron carbonyl at room temperature but only at elevated temperatures. From a toluene solution, in contrary, it was possible to isolate the product in moderate yields after 24 h stirring at room temperature. Interestingly, multiple substitution of carbonyl ligands at the iron center by a NHGe was only observed with the donor free bisneopentyl germylene **39** (SD 7). In contrary, multiple carbonyl substitution at iron(0) does not take place with donor free NHSi ligands as reported in the literature.²⁸⁵

Shifts in ^1H -NMR spectroscopy are in the same range as **35**, while the ^{13}C signal of the carbonyl ligand of **40** is shifted high-field slightly. Interestingly, the pyridyl moieties are chemically identical in solution as equivalent positions are represented by one signal only. Crystals, suitable for SC-XRD analysis, of both **40** and **41** can be grown from diluted solutions in diethyl ether at cold temperatures ($-30\text{ }^\circ\text{C}$, Figure 21).

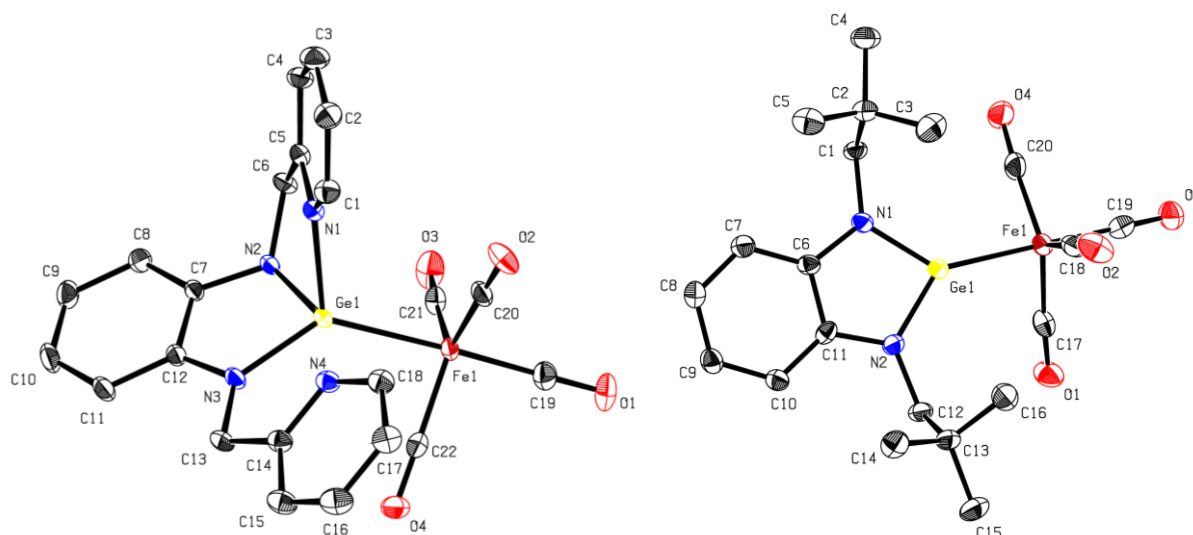


Figure 21: Molecular structures of **40** and **41**. Ellipsoids are shown at the 50% probability level. Hydrogen atoms are omitted for clarity. Grey = carbon, blue = nitrogen, yellow = germanium, dark red = iron, red = oxygen. Selected bond lengths (Å) and angles (°): [**40**, left] N1-Ge1 2.1028(13), N2-Ge1 1.8917(13), N3-Ge1 1.8580(13), Ge1...N4 2.489(4), Ge1-Fe1 2.3343(3), Fe1-C19 1.7864(17), N3-Ge1-N2 85.76(5), N2-Ge1-N1 81.22(5), C7-N2-C6 119.05(12), N3-Ge1-N1 113.76(5), N1-Ge1-Fe1 112.59(4), N3-Ge1-Fe1 131.73(4), C12-C7-N2-C6 142.34(13), C7-C12-N3-C13 176.80(13), C7-N2-Ge1-N1 110.03(10), C12-N3-Ge1-Fe1 121.37(9); [**41**, right] N1-Ge1 1.819(2), N2-Ge1 1.815(2), Ge1-Fe1 2.2760(5), Fe1-C19 1.787(3), N1-Ge1-N2 89.03(11), N2-Ge1-Fe1 134.86(8), N1-Ge1-Fe1 136.01(7), C6-C11-N2-C12 177.3(3), C11-C6-N1-C1 179.1(3), C11-N2-Ge1-Fe1 171.31(15).

The coordinative environment of both iron complexes features trigonal bipyramidal symmetry, comparable to similar tetrylene iron tetracarbonyl complexes. The dicoordinate germylene in **41** is bound in a trigonal planar fashion, while the germylene in **40** features a distorted tetragonal symmetry (smallest angles: N1-Ge1-N2 81.2°, N2-Ge1-N3 85.8°; biggest angle: N3-Ge1-Fe1 131.8°). Due to binding of the germylene at the iron center, the bond lengths N2-Ge1 and N3-Ge1 in **40** are slightly increased compared to the free ligand. No intramolecular interaction between pyridyl moieties and germylene centers can be seen in the crystal structure. The Ge1-N1 bond length is in the same range as observed before (2.103 Å; **40**: Ge1-N1 2.101 Å).

The overall iron carbonyl bond lengths are in the same range for all obtained iron(0) carbonyl complexes **35**, **40** and **41**. However, the distance between the germylene and the iron center is significantly elongated in the donor-stabilized complexes **35** and **40**. (**41** Ge1-Fe 2.276 Å, **35** Ge1-Fe1 2.289 Å, **40** Ge1-Fe1 2.334 Å). This can be related to an increased electron density on the germylene due to the binding of the pyridyl moiety and, thus, reduced π -backbonding of the metal. Largest bond length is consequently observed in the bis(pyridine-2-ylmethyl)-functionalized **40**. Most remarkably, the wingtips in **41** are almost in plane with the backbone of the ligand. In contrary, the intramolecularly donating pyridyl moiety in **40** is tilted by almost 90° comparably to the situation in **35**, while the second remains in plane with the benzannulated ring system (C7-N2-Ge1-N1 110.0°, C12-C7-N2-C6 142.4°, C7-C12-N3-C13 176.8°). Due to binding of the pyridine at the germylene, the angle N2-Ge1-N3 in **40** is reduced compared to **41**. Moreover, the iron center is tilted out of plane even further when compared to **35**, while the iron center lays almost in plane with the ligand backbone within the donor-free **41**

(**40** C₁₂-N₃-Ge₁-Fe₁ 121.4°; **41** C₆-N₁-Ge₁-Fe₁ 171.4°). Further insights into the stability of the highly air and moisture sensitive complexes were gained by means of LIFDI mass spectrometry (Figure 22).

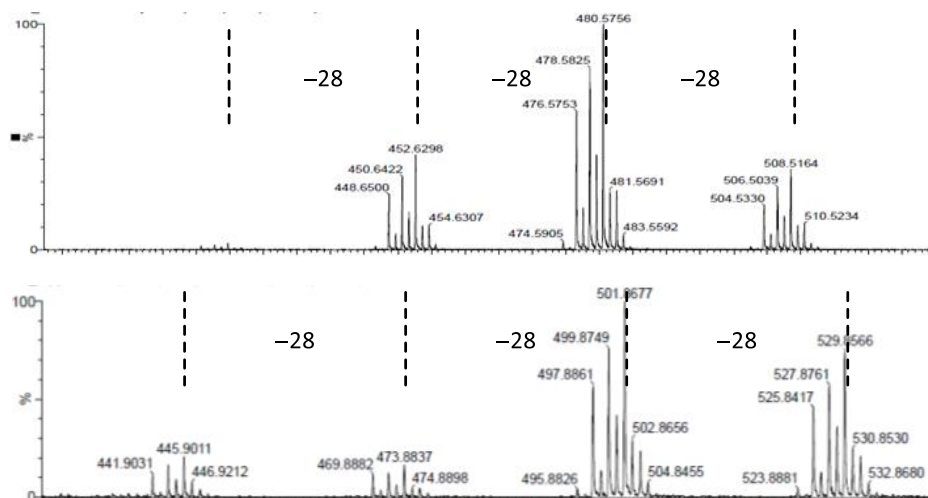


Figure 22: Cut-outs of the LIFDI mass spectra of **35** ($m/z = 509.01$) and **40** ($m/z = 529.97$) measured in THF, wherein CO cleavage can be observed. The complete spectra of **35**, **40** and **41** can be found in the supplementary data (SD 6-SD 8).

Mass spectrometry of **35** and **40** show multiple signals, while the most abundant signals fit the mass to charge ratio of [**35-28u**] and [**40-28u**], which is characteristic of carbonyl dissociation. Besides, signals fitting the m/z and the isotopic pattern of the products, C₂₁H₂₁N₃GeFeO₄ [**35**] and C₂₂H₁₆N₄GeFeO₄ [**40**], can be observed as well as further carbonyl fragmentation. In contrary to that, the mass spectrum of **41** shows the product signal only (SD 7).^a Thus, the pyridyl moieties significantly alter the reactivity of the carbonyl complexes, as they are capable of stabilizing lower coordinated transition metal complexes. The hemilabile binding behavior of the pincer-type NGeN is of high interest for catalytic applications, rendering unprecedented electronically flexible processes possible. All NHGe iron(0) carbonyl complexes are highly sensitive to air and moisture and decompose in solution within a few weeks. Interestingly, **40** is significantly more stable when compared to the bulkier but donor free bisneopentyl complex **41**. The bond strength of NHGes with iron carbonyls, thus, benefits from donating groups such as the pyridyl moiety in **35** and **40**, as DFT calculations of the latter have already shown.

Reactivity of **33** and **38** with Lewis Acids

As already discussed above, HTs are capable of stabilizing other tetrylenes.^{242, 248} As the asymmetric **33** features surprising coordination of GeCl₂ by the imidazole nitrogen atom, it was interesting to investigate whether the symmetrically substituted bis(pyrido-2-ylmethyl) NHGe **38** is capable of

^a The m/z of the free ligand **39** as well as of side-product [(**38**)₂Fe(CO)₃] can be seen as well, however, these are already present in the reaction mixture.

forming stable germanium-germanium bonds, potentially stabilized by interaction of the pyridyl moieties.

Stirring of the ligand with equimolar amounts of GeCl_2 -dioxane in THF at room temperature slowly yields an off-white precipitate. From the filtered solution, intensively orange-colored crystals of the product **42** can be grown at low temperatures, suitable for SC-XRD analysis (Figure 23).

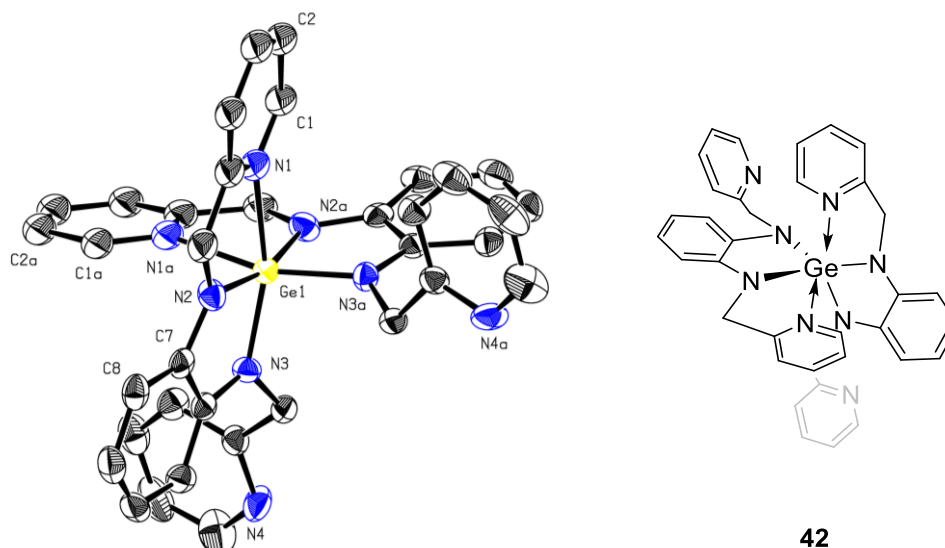
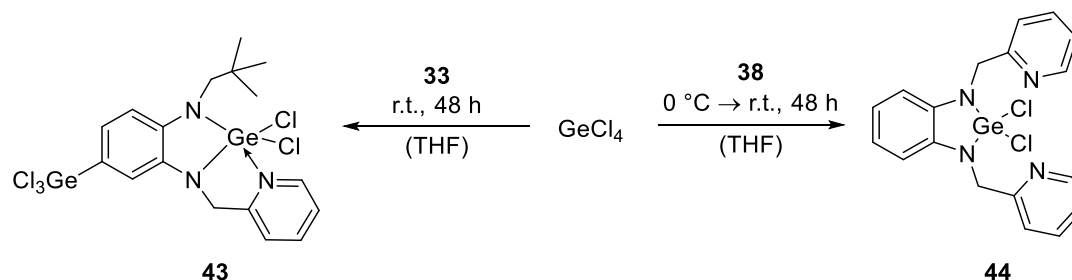


Figure 23: Molecular structure of **42**.(left) Ellipsoids are shown at the 50% probability level. Hydrogen atoms are omitted for clarity. Grey = carbon, blue = nitrogen, yellow = germanium. Selected bond lengths (Å) and angles (°): N1-Ge1 2.213(8), N2-Ge1 1.885(8), Ge1-N3 1.915(7), N1-Ge1-N2 76.9(4), N2-Ge1-N3 83.9(4), N3-Ge1-N2a 105.1(6), N2a-Ge1-N1a 92.4(8), N1-Ge1-N1a 84.0(9), N1a-Ge1-N3 90.2(3). Structural representation of compound **42**.(right)

The germanium in **42** features a distorted octahedral coordination sphere, ligated by two bis(pyridine-2-ylmethyl)diamine ligands that are almost orthogonal to each other. Compared to the dative bonds observed in **32** and **40**, the Ge1-N1 bond is slightly elongated. As can be seen from NMR spectroscopy, **42** features high symmetry as equivalent positions are reflected by one sharp signal only. Thus, no distinction between bound and loose pyridyl moieties can be made in solution.

The precipitate, which forms during the reaction, has not been characterized so far. The latter is only partially soluble in pyridine, which hinders structural elucidation of the aromatic signals by means of NMR spectroscopy. Signals at $m/z = 525$ in LIFDI mass spectrometry indicate successful coordination of the germanium dichloride prior to further reaction yielding **42**. Interestingly, *Rivard et al.* recently reported the stabilization of low-valent tetrylenes with non-cyclic germylenes.⁷⁶ The authors revealed that coordinative solvents, such as THF, can break weak germanium-germanium bonds, which might be the reason for the slow formation of **42** in a THF solution.

To gain further insight and a better understanding of the reactivity of pyridyl-functionalized NHGes with Lewis acids, **35** and **38** were reacted with a different, more reactive germanium compound. Upon treatment of the ligands with GeCl_4 a yellow suspension form (Scheme 31).



Scheme 31: Reactions **33** and **38** with GeCl_4 resulting in the dichlorogermanes **43** and **44**.

Two distinct signal patterns are present in the LIFDI mass spectrum of the reaction of **33** with GeCl_4 after three hours (Figure 24). Extending the reaction time to three days, the quantitative composition of the mixture changed with more of the heavier product being formed. Analysis of the mass to charge ratio and the isotopic distribution pattern suggests the lower signal to relate to the dichlorogermane **32**, the signal at higher m/z to a product **43**, which exhibits a composition of $[\mathbf{33} + \text{GeCl}_3]$. Analyses based on $^1\text{H-NMR}$ spectroscopy confirmed the presence of **43** in the reaction mixture. Further signals were found; however, assignment was not possible due to low quality of the spectra.

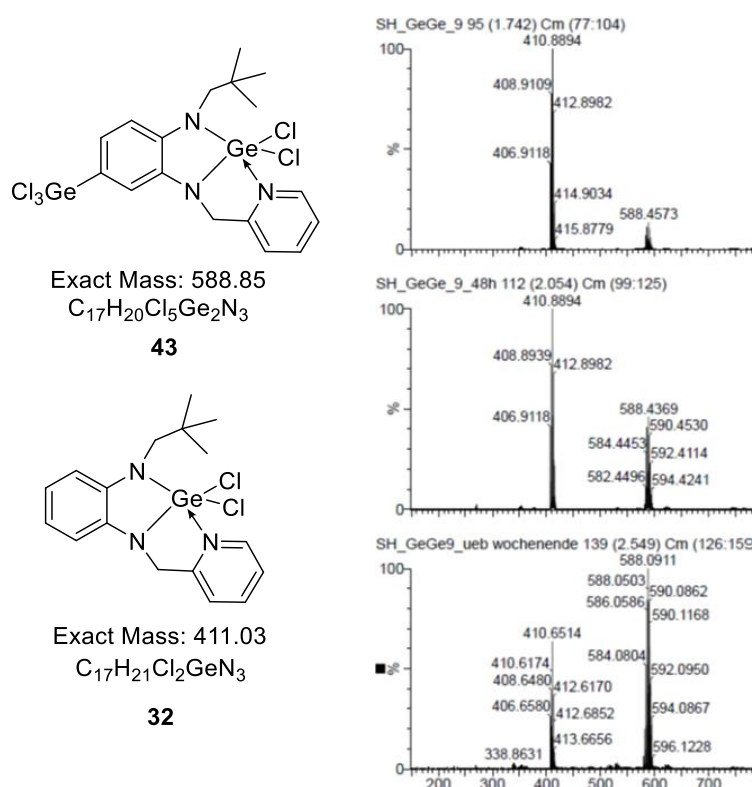


Figure 24: LIFDI MS of the reaction of **33** with GeCl_4 in THF after 3 h (top), 48 h (middle), 3 d (bottom).

Crystals of **43**, suitable for SC-XRD analysis were obtained from a hexane layered solution of the reaction mixture (Figure 25). Therein, the aromatic proton *CH*-11 is substituted for a GeCl_3 moiety. The pyridyl moiety is bent towards the dichlorogermane, forming a dative bond (N1-Ge1 2.131 Å), comparable to **32** (N1-Ge1 2.101 Å). The second germanium atom is bound covalently, while the bond

length is comparably short.²⁸⁶ As observed before, the symmetry of the dichlorogermane is best described as distorted bipyramidal (equatorial: N2, Cl1, Cl2, axial: N1, N3) while the second germanium is coordinated distorted tetragonal.

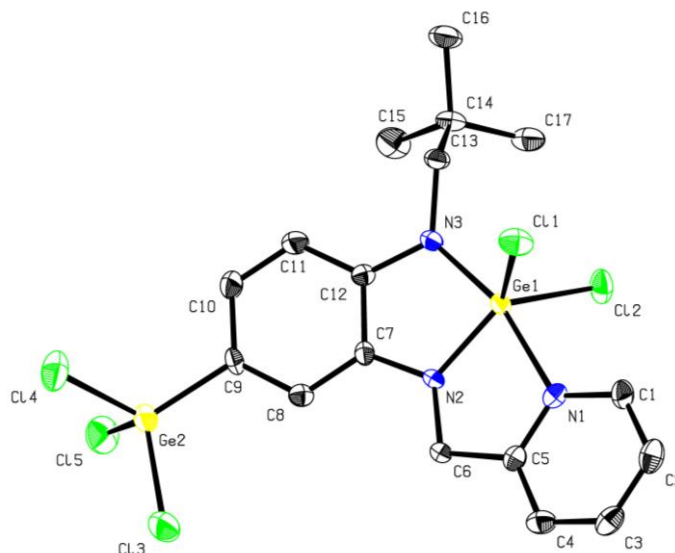


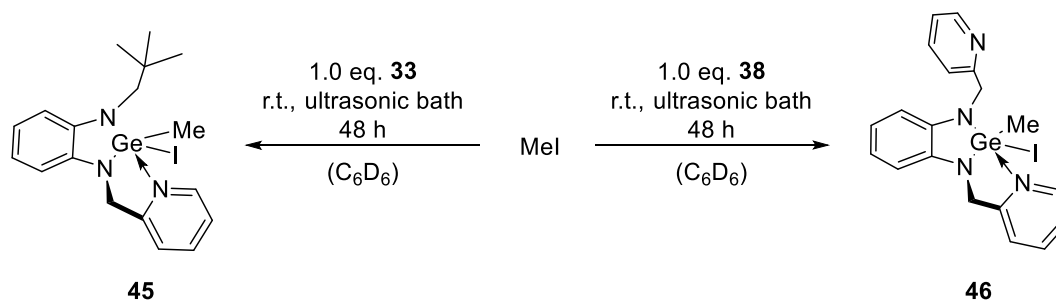
Figure 25: Molecular structure of **43**. Ellipsoids are shown at the 50% probability level. Hydrogen atoms are omitted for clarity. Grey = carbon, blue = nitrogen, yellow = germanium, green = chlorine. Selected bond lengths (Å) and angles (°): Ge1-Cl1 2.2044(13), Ge1-Cl2 2.157(14), N3-Ge1 1.892(4), N2-Ge1 1.828(4), N1-Ge1 2.131(4), C9-Ge2 1.909(5), Ge2-Cl3 2.1386(14), Ge2-Cl4 2.1248(15), Ge2-Cl5 2.1352(16), Cl1-Ge1-Cl2 105.2(6), N1-Ge1-N2 78.70(16), N2-Ge1-N3 86.51(17), C9-Ge2-Cl4 113.00(15), Cl4-Ge2-Cl5 104.05(6), Cl4-Ge2-Cl3 106.1(7), C7-N2-Ge1-N1 166.3(3).

Given this result, the question of the reaction pathway arose. After addition of GeCl_4 , **32** is formed initially in a redox reaction. As side-product probably GeCl_2 is formed. Product **43** was only obtained after addition of excess GeCl_4 , indicating reaction of the latter with **32**. This might include the formation of a complex $(\text{NN})\text{Ge}-\text{Cl}^+\text{GeCl}_3^-$ salt, in resemblance to a previously reported reaction of a dichlorogermane with GeCl_2 .²⁴² Further experiments into the elucidation of the mechanism have not been performed so far. Considering the reaction of **38** with GeCl_4 , however, only the 2,2-dichloro-*N,N'*-di(pyridin-2-ylmethyl)benzimidazolin-2-germane (**44**) forms. C-H activation, as observed in the reaction of **33**, can therefore be related to the asymmetric nature of the latter NHGe .

44 precipitated from the reaction mixture as a yellow solid and was characterized by NMR spectroscopy and LIFDI mass spectrometry. Crystals, grown from a THF/diethyl ether solution at cold temperatures, were too distorted for high-quality SC-XRD analysis; however, structural elucidation was possible. One pyridyl moiety is coordinated at the germylene comparable to dichlorogermanes obtained before (**32** and **43**). Proton signals in the NMR spectrum are shifted as expected compared to the free ligand **38**. The chlorination of the germanium center leads to an increased electron pulling effect at the adjacent nitrogen atoms and the bound methylene bridges. Proton signals of the latter are therefore shifted to higher fields.

Reactivity of **33** and **38** with Oxidative Reactants

In recent years, several reports on the oxidation of low-valent tetrylenes have been reported, including the synthesis of heavier analogs of carboxylic acid derivatives such as esters and amides.^{267, 287-291} In the following, reactions of the pyridyl-substituted NHGes **33** and **38** with methyl iodide and elemental sulfur were performed (Scheme 32 and Scheme 33).



Scheme 32: Reactions of **33** and **38** with MeI giving the iodomethylgermanes **45** and **46**.

The asymmetrically substituted NHGe **33** features surprising coordination of Lewis acids *via* the ring nitrogen atom and the pyridyl moiety. The versatile reactivity could possibly open up novel activation pathways of small molecules. The reaction of the asymmetric **33** as well as the symmetric **38** with methyl iodide, should give insights whether the activation *via* nitrogen atoms can be controlled by the coordination of the pyridyl moiety. As observed *via* LIFDI mass spectrometry, reaction in deuterated benzene at room temperature takes place only in an ultrasonic bath. After 48 h the product solution was analyzed by NMR spectroscopy. Dilution with diethyl ether and storage at low temperatures leads to intensively yellow-colored crystals, suitable for SC-XRD analysis (Figure 26).

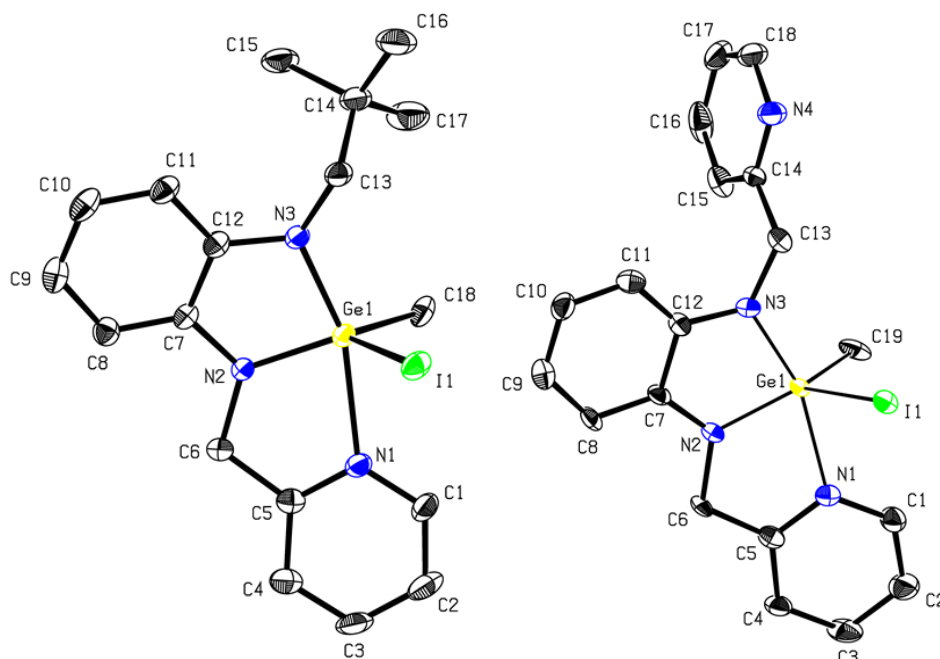
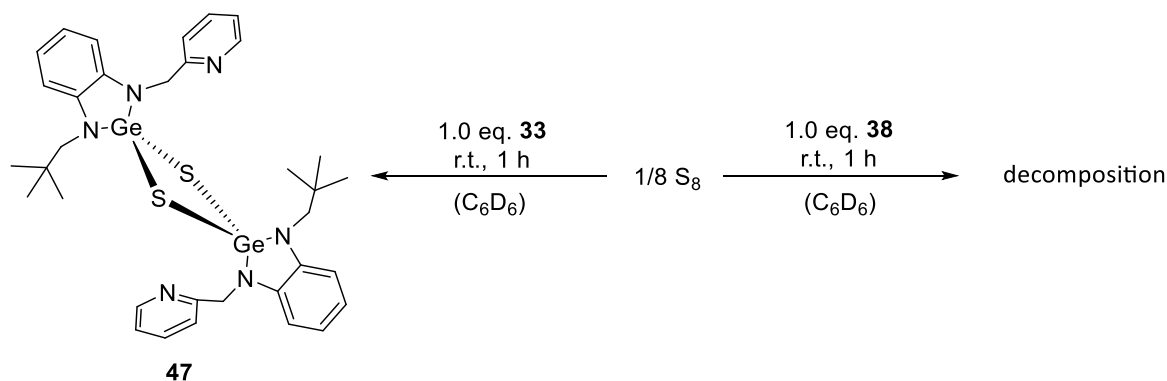


Figure 26: Molecular structure of **45** and **46**. Ellipsoids are shown at the 50% probability level. Hydrogen atoms are omitted for clarity. Grey = carbon, blue = nitrogen, yellow = germanium, green = chlorine. Selected bond lengths (Å) and angles (°): [**45** left] N3-Ge1 1.904(3), N2-Ge1 1.854(3), N1-Ge1 2.275(3), Ge1-I1 2.618(5), Ge1-C18 1.965(4), N3-Ge1-N2 85.7(14), N1-Ge1-N2 76.32(12), I1-Ge1-C18 108.50(12), C12-C7-N2-C6 166.7(6), C7-N2-Ge1-N1 162.9(3), C7-C12-N3-C13 165.9(3); [**46** right] N3-Ge1 1.890(5), N2-Ge1 1.843(5), N1-Ge1 2.182(5), Ge1-I1 2.6141(10), Ge1-C19 1.927(13), N3-Ge1-N2 84.7(2), N2-Ge1-N1 77.8(2), C19-Ge1-I1 107.5(4), C12-C7-N2-C6 175.2(6), C7-N2-Ge1-N1 165.8(5), C7-C12-N3-C13 173.3(6), C12-N3-C13-C14 79.2(8).

The molecular structures of **45** and **46** unequivocally reveal addition of methyl iodide at the germanium atom in both cases as observed before for similar low-valent tetrylenes. Therein, dative bonding of one pyridyl-moiety takes place as already observed before. The atom distances are comparable to related dihalogengermanes described above. The Ge1-N1 distance is shorter than in **32**, as lesser electron density is accumulated on the bis(pyridine-2-ylmethyl)germanium. The coordinating pyridyl moieties are almost in plane with the respective benzannulated ring systems, while the free pyridine-2-ylmethyl wingtip in **46** is tilted out of plane by 79°. Compared to the free ligands, the methylene protons of **45** and **46** appear significantly high-field shifted due to the increased electron pull of the germanium(IV). Interestingly, the introduction of an enantiotopic center leads to a geminal coupling of the methylene protons of the neopentyl moiety in **45**. The reactivity of the pyridine-functionalized NHGes was also studied by reaction with elemental sulfur (Scheme 33).



Scheme 33: Oxidation reaction of **33** and **38** with elemental sulfur to result in the dithiadigermetane **47** and decomposition of **38**.

Reaction of the asymmetric **33** already takes place at room temperature. Conversion has been confirmed by LIFDI mass spectrometry and NMR spectroscopy. Remarkably, two products with $m/z = 744$ and the same isotopic pattern matching the chemical formula $C_{34}H_{42}N_6Ge_2S_2$ can be detected in the NMR spectrum. Crystals, suitable for SC-XRD analysis, were grown from a diluted solution at low temperatures (Figure 27).

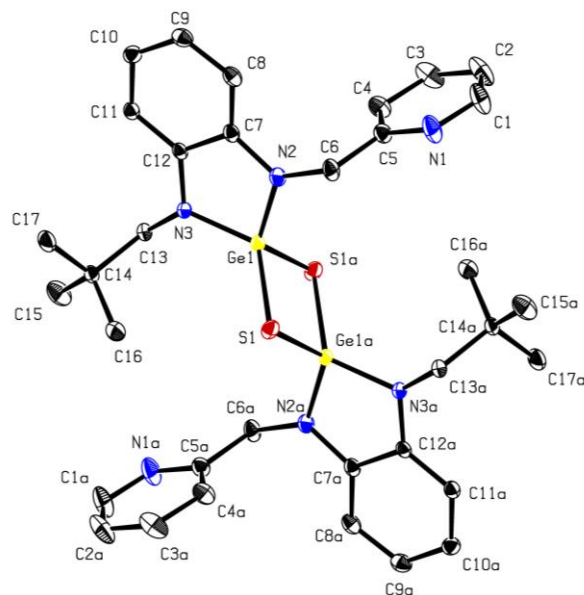


Figure 27: Molecular structure of **47**. Ellipsoids are shown at the 50% probability level. Hydrogen atoms are omitted for clarity. Grey = carbon, blue = nitrogen, yellow = germanium, red = sulfur. Selected bond lengths (Å) and angles (°): Ge1-S1 2.2300(4), Ge1-S1a 2.2179(4), N3-Ge1 1.8171(11), Ge1-N2 1.8109(12), Ge1...Ge2 2.973, N3-Ge1-N2 90.90(5), S1-Ge1-S1a 96.090(13), Ge1-S1-Ge1a 83.909(13), S1-Ge1-N2 121.35(4), S1-Ge1-N3 114.45(4).

In compound **47**, two ligand motifs are connected with each other *via* a planar Ge_2S_2 four-membered ring. The distances of the germanium atoms to sulfur amount 2.218–2.230 Å, comparable to previously reported single Ge-S bonds.^{229, 247, 292} The molecule features an inversion center analogous to a previously reported sulfur oxidized amidinate ligated germylene.²⁹¹ In stark contrast, the tetracoordinated germanium atoms in **47** feature tetragonal symmetry, as the pyridyl moieties are not coordinated at the germanium atoms but aim to the opposite sides. The latter exemplifies the high

flexibility of the pyridyl-substituted five-membered NHGe ligand, which is not given in the base-stabilized amidinate.

Reactivity of **33** and **38** with First-Row Transition Metals

Due to their free electron pair, HTs are capable of binding transition metals and form strong coordinative bonds. Iron(II) bromide depicts an interesting catalytically active precursor, which has been ligated by several HT based ligands already. In particular, donor-stabilized amidinate ligands have been used recently.^{78, 82, 129, 245, 293} In resemblance to well-known pincer-type complexes of iron, nickel and cobalt (Figure 28),^{171, 193, 206, 294-298} the coordinative behavior of the novel pyridyl-substituted NHGe ligands has been investigated in the following.

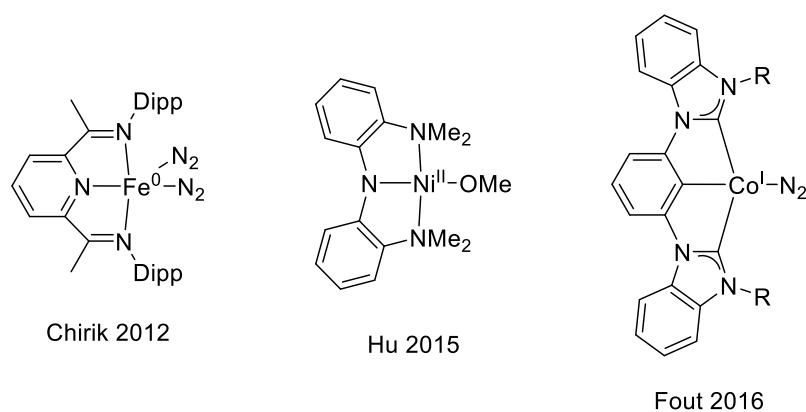
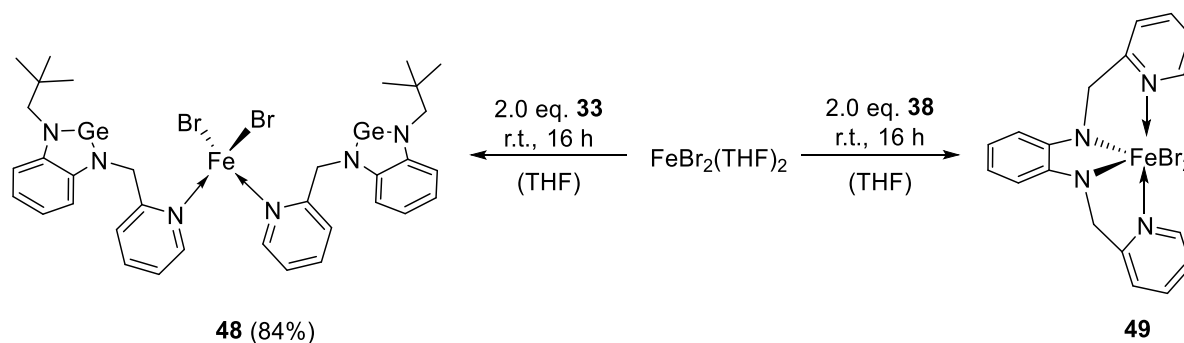


Figure 28: Complexes of iron, nickel and cobalt catalytically active in the hydrosilylation of olefins.^{171, 207, 294}

In the following, the pyridyl-substituted ligands **33** and **38** were reacted with $\text{FeBr}_2(\text{THF})_2$ (Scheme 34).



Scheme 34: Reaction of **33** and **38** with $\text{FeBr}_2(\text{THF})_2$ giving the iron(II) bromide complexes **48** and **49**.

The addition of two equivalents **33** to a solution of $\text{FeBr}_2(\text{THF})_2$ in THF leads to a clear yellow solution. Conversion of the ligand was observed by means of LIFDI mass spectrometry. Full conversion is reached after 24 h and the product **48** can be separated off by extraction into toluene and crystallization at low temperatures. The molecular structure is given in Figure 29.

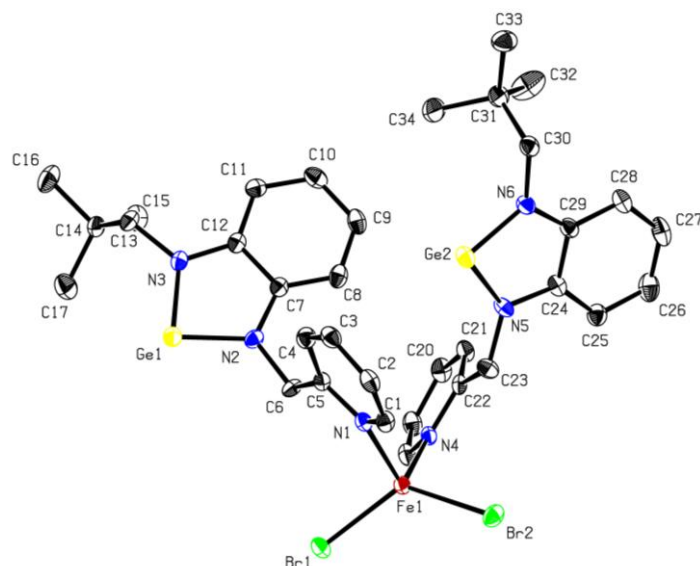


Figure 29: Molecular structure of **48**. Ellipsoids are shown at the 50% probability level. Hydrogen atoms are omitted for clarity. Grey = carbon, blue = nitrogen, yellow = germanium, green = bromide, dark red = iron. Selected bond lengths (Å) and angles (°): Fe1-Br1 2.3907(8), Fe1-Br2 2.4099(7), Fe1-N1 2.130(3), Fe1-N4 2.132(2), Br1-Fe1-Br2 125.83(2), Br2-Fe1-N1 107.37(7), Br2-Fe1-N4 103.69(7), N4-Fe1-Br1 111.33(7), Br1-Fe1-N1 102.45(7), N1-Fe1-N4 104.35(9).

Quite surprisingly, the pyridyl moieties of two NHGe ligands are coordinating the iron(II) bromide – leaving the germylene in a dicoordinate state. No intramolecular interaction can be observed from the molecular structure. This is in contrast to known, donor-stabilized bis(tetrylene)pyridine ligands, which have been shown to easily coordinate iron halides. Therein, the bridging pyridine is not even involved in the coordination of the metal center.¹³¹ In the molecular structure of **48** the wingtips of one ligand are bent to the same side of the ligand plane while the wingtips of the other one are aiming to opposite directions. Thereby, the bound pyridyl moieties are tilted with respect to the benzannulated plane by 84.6° and 77.3°, respectively. The germanium atom features a distorted tetragonal coordination sphere, while the angle between the two bromides and the iron center is rather large (Br1-Fe1-Br2 125.8°).

The most abundant signal in the mass spectrum of **48** at $m/z = 405.08$ features a very distinct isotopic pattern with two signals of approximately the same intensity (Figure 30). Most likely, the signal can be related to a doubly charged fragment of the complex, namely $[(\mathbf{33})\text{FeBr}]^{2+}$, fitting the isotopic pattern very well. The observed deviation of the expected mass most likely arises from inaccuracies of the mass spectrometer or proton addition to the cation.

In contrary, the two most abundant signals in the LIFDI mass spectrum of the reaction of **38** with $\text{FeBr}_2(\text{THF})_2$ can be related to the bisamine iron(II) bromide complex **49**, featuring the formula $[\text{C}_{16}\text{H}_{18}\text{N}_4\text{FeBr}_2]$ (Scheme 34, SD 9). Due to bromide dissociation, the main signal is very weak. Without the steric bulk of at least one neopentyl moiety, complexes of **38** with iron(II) halides seem to be thermodynamically instable leading to decomposition of the NHGe. Crystals of **49** can be grown from

a hexane layered THF solution at room temperature. The molecular structure is depicted in the supplementary data (SD 24). However, as the initial bright yellow crystals quickly turned dark green when separating off the reaction mixture, it is not clear whether **49** is the main product of the reaction or decomposition of the latter took place.

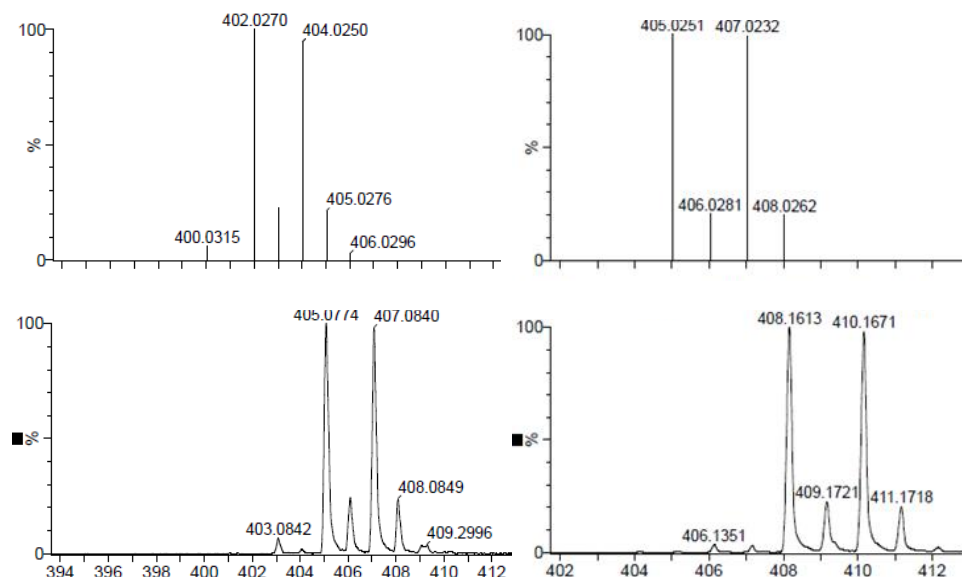
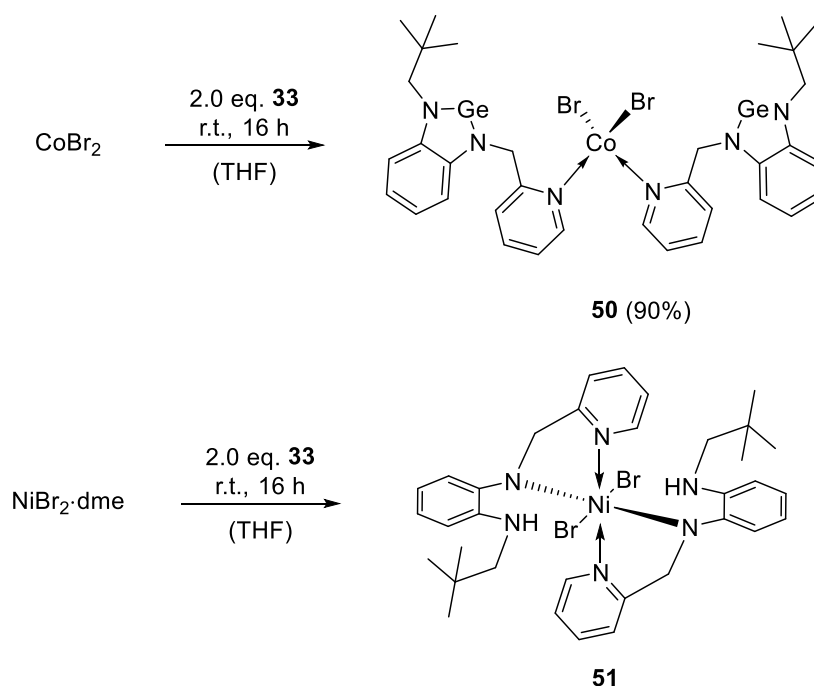


Figure 30: Calculated mass distribution corresponding to $C_{17}H_{21}N_3FeBr$ (top, left) and $C_{17}H_{21}N_3CoBr$ (top, right) and cut-outs of the measured LIFDI mass spectra of **48** and **50** in toluene. The complete spectra can be found in the supplementary data (SD 10, SD 11).

The uncommon coordination of **33** to iron(II) bromide rises the unexpected possibility for the synthesis of new bi- and trimetallic compounds, *via* binding of the free germylene. Due to the high affinity of the pyridine moiety to bind iron(II) halide, the electron pair of the low-valent germylene remains free. So far, only very few examples of bimetallic compounds ligated by *N*-heterocyclic tetrylenes are known.²⁹⁹ Complex **48** was thus reacted with $GeCl_2$ and $Fe_2(CO)_9$; however, in the former case no reaction took place while in the latter only the formation of $[(\mathbf{33})Fe(CO)_4]$ (**35**) could be detected. Further studies into the synthesis of novel bimetallic complexes are ongoing.

Applying similar conditions as described above, **33** has also been reacted with $CoBr_2$ and $NiBr_2 \cdot dme$ to further elaborate the coordination chemistry of the novel ligand within first-row transition metal complexes (Scheme 35).



Scheme 35: Reaction of **33** with CoBr_2 and $\text{NiBr}_2 \cdot \text{dme}$ giving the complexes **50** and **51**.

Similar to **48**, reaction of **33** with CoBr_2 gives the bispyridine cobalt(II) bromide complex **50** in high yields. The intensively green-colored compound can easily be crystallized from a toluene solution and was characterized by means of SC-XRD analysis, NMR, and EA (SD 23). In the LIFDI mass spectrum a signal with $m/z = 408$ can be seen, featuring an isotopic pattern that fits the doubly charged $[(\mathbf{33})_2\text{CoBr}]^{2+}$ cation (Figure 30). Both complexes, **48** and **50**, are paramagnetic and sensitive to air and moisture. Further experiments regarding the reactivity of these unusual complexes have not been performed so far. However, further functionalization such as reduction of the bromides could be possible. From the reaction mixture of **33** with nickel(II) bromide, only the germanium-free, diamine complex **51** could be crystallized from a diluted THF solution at low temperatures. Immediate darkening of the reaction mixture upon addition of the NHGe **33** to a solution of $\text{NiBr}_2 \cdot \text{dme}$ indicates decomposition of the ligand. The molecular structure of **51** is given in the supplementary data (SD 25) but will not be discussed in detail.

Summary

In the previous chapter, the novel NGeN pincer-type NHGe ligand has been synthesized and fully characterized. Most remarkably, the pyridyl moieties show a pronounced flexibility regarding the intramolecular electron donation to the germylene. Through coordination of the latter at Lewis acids, reaction with nucleophiles or oxidation, additional electron density can be donated by the flexible pyridyl moieties. In particular, in solution no distinction between bound and donating pyridyl moieties was possible. Starting from the pyridyl-functionalized NHGes **33** and **38** examples of dicoordinate (**48**;

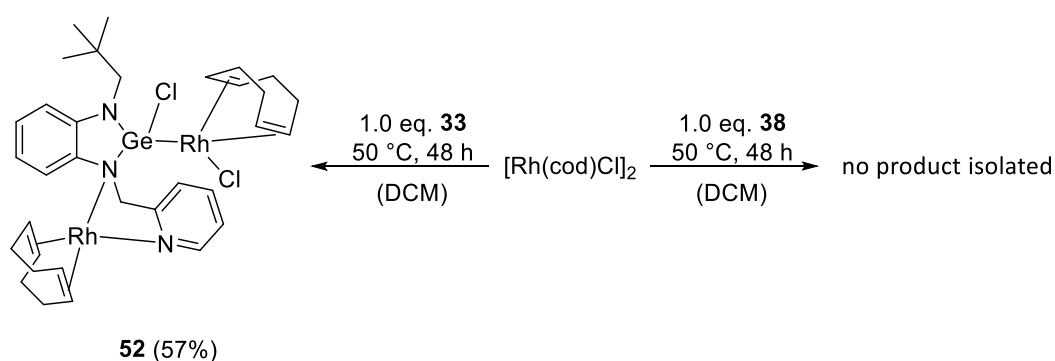
50), tricoordinate (**35**; **41**), four-fold coordinated (**47**), five-fold coordinated (**43**; **45**; **46**), and six-fold coordinated (**42**) germanium compounds were obtained and characterized in the solid state.

Comparison of the bis(pyridyl-2-ylmethyl) NHGe **38** with the asymmetric, mono pyridyl-functionalized NHGe **33** reveals distinct differences regarding reactivity and stability. Hence, the steric neopentyl group of the latter plays a decisive role in stabilizing coordination compounds of first-row transition metals such as **48**. The unexpected coordination compounds of **33**, received in reactions with iron(II) bromide and cobalt(II) bromide, are promising candidates for further synthetic approaches of so far unprecedented complex compounds and catalytic applications thereof. As sterically bulky wingtips are not available in **38** - the pyridyl moieties are significantly less steric compared to neopentyl groups - only germanium-free amine complexes were obtained. However, in comparison to the donor-free NHGe **39**, both pyridyl-functionalized HTs allow the successive dissociation of carbonyl ligands as observed in the LIFDI mass spectra of **35** and **40**.

3.4 Novel Late Transition Metal Complexes of Pyridyl-Functionalized NHGes

Rhodium Complexes of **33** and **38**

In the following chapter, the coordination chemistry of the novel pyridyl-functionalized NHGe ligands **33** and **38** within late transition metal complexes has been investigated. As flexible steering ligands, novel coordinative motifs thereof could potentially direct the catalytic activity of such metals towards higher selectivity and activity in homogeneous processes. Already in the past, five-membered *N*-heterocyclic tetrylenes have been studied in reactions with catalytically active metal precursors.^{115, 300} Interestingly, even at elevated temperatures, no conversion could be observed in a reaction mixture of a donor-free NHSi and $[\text{Rh}(\text{cod})\text{Cl}]_2$. In contrary, complexes of donor-stabilized silyliumylidenes, silyl pincer ligands and phosphor-stabilized germylenes have been reported recently.³⁰¹⁻³⁰³ Therefore, it was interesting to see whether the flexible pyridyl-donor moieties would allow for an insertion of the germylene into metal halide bonds and the selective formation of novel coordination compounds. In a DCM solution, $[\text{Rh}(\text{cod})\text{Cl}]_2$ was reacted with equimolar amounts of **33** or **38** (Scheme 36).



Scheme 36: Reaction of **33** and **38** with $[\text{Rh}(\text{cod})\text{Cl}]_2$ leading to complex **52**.

No reaction takes place until heating to 50 °C. At this temperature, the mixtures turned dark orange after two days. No product could be detected by means of LIFDI mass spectrometry though. Thus, diluted solutions (DCM/diethyl ether) were stored at -30 °C for several days, resulting in an orange crystalline solid from the reaction of **33**, suitable for SC-XRD analysis (Figure 31). The yield of the product **52** can be increased by addition of hexane, enabling full characterization by NMR spectroscopy and elemental analysis.

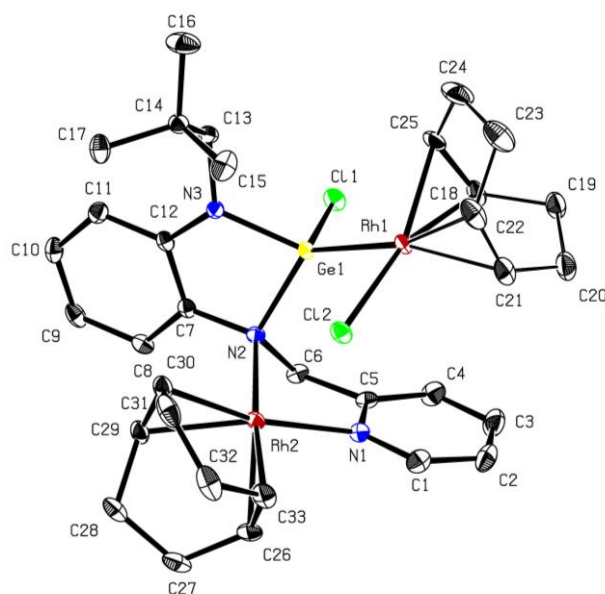


Figure 31: Molecular structure of **52**. Ellipsoids are shown at the 50% probability level. Hydrogen atoms are omitted for clarity. Grey = carbon, blue = nitrogen, yellow = germanium, green = chlorine, red = rhodium. Selected bond lengths (Å) and angles (°): Ge1-Rh1 2.3910(2), Ge1-Cl1 2.3297(4), Rh1-Cl2 2.3579(4), N3-Ge1 1.8625(14), N2-Ge1 1.9581(14), N1-Rh2 2.1084(15), N2-Rh2 2.2330(14), N3-Ge1-N2 86.37(6), N3-Ge1-Rh1 125.33(4), Rh1-Ge1-N2 129.64(4), Rh1-Ge1-Cl1 113.510(13), Rh1-Ge1-N2 129.64(4), Ge1-Rh1-Cl2 87.228(12), Ge1-N2-Rh2 108.27(6), Cl1-Ge1-Rh1-Cl2 163.6(2), C8-C7-N2-Rh2 78.1(3).

In the molecular structure of **52**, two rhodium atoms are bound by a single NHGe ligand, involving the germanium atom and two nitrogen atoms. Thereby, the germanium inserts into a rhodium-chloride bond and coordinates one rhodium atom. The latter is ligated additionally by one cyclooctadiene molecule and one chloride. In this process, the germanium is formally oxidized. The second rhodium is ligated by one cyclooctadiene molecule and additionally by the pyridyl moiety and one ring nitrogen atom. As observed before, the coordination sphere of the four-fold coordinated germanium is distorted tetragonal, however, angles comprising the rhodium center are relatively large. The chlorine atoms are almost in a right angle with respect to the rhodium atom and in plane while aiming to opposite directions. (Rh1-Ge1-Cl1 113.5°, Ge1-Rh1-Cl2 87.2°, Cl1-Ge1-Rh1-Cl2 163.6°). The second rhodium atom is significantly tilted out of the benzannulated ring (C8-C7-N2-Rh2 78.1°).

Most remarkably, the aromatic germanium-nitrogen bonds differ in their lengths by 0.1 Å, similar to the GeCl₂ coordinated **34**. The asymmetric binding of the second rhodium atom results in a weakening of the σ -bond of the N2-Ge1 bond (1.958 Å). The germanium-rhodium bond length is comparable to literature known values, however, shorter than a related phosphine-stabilized germylene complex.³⁰² Interestingly, the latter publication also reports the rearrangement of phosphine-stabilized chlorogermylene rhodium(I) complexes towards dichlorogermene rhodium metallacycles. Complex **52** is stable in solution which might be related to the binding of the second rhodium atom by the pyridyl moiety. Thus, rearrangement through coordination of the pyridyl at the rhodium(I) cannot take place.

The germanium-chloride bonds are in the same range and rather large when compared to related compounds.²⁴⁰⁻²⁴³

In the $^1\text{H-NMR}$ spectrum shifts of the unsaturated C-H bonds of the cyclooctadiene ligands can be observed between 3.56-5.37 ppm, comparable to literature known compounds (SD 16). Assertion of the signals was not possible due to overlapping. The carbon spectrum clearly shows coupling with the ^{103}Rh (spin $\frac{1}{2}$, $^2J = 13\text{Hz}$, Figure 32).³⁰⁴

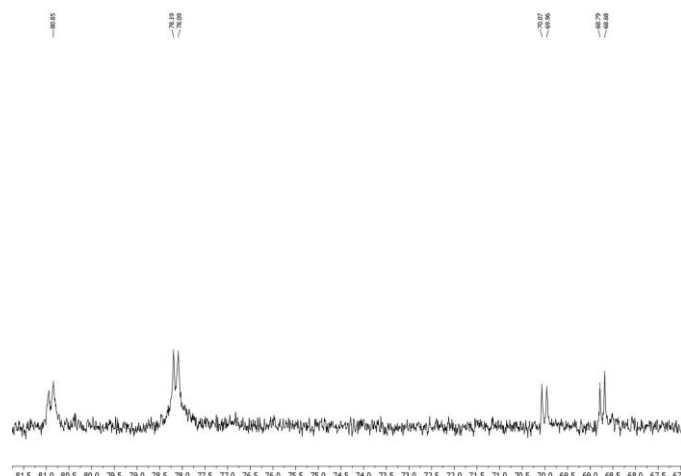
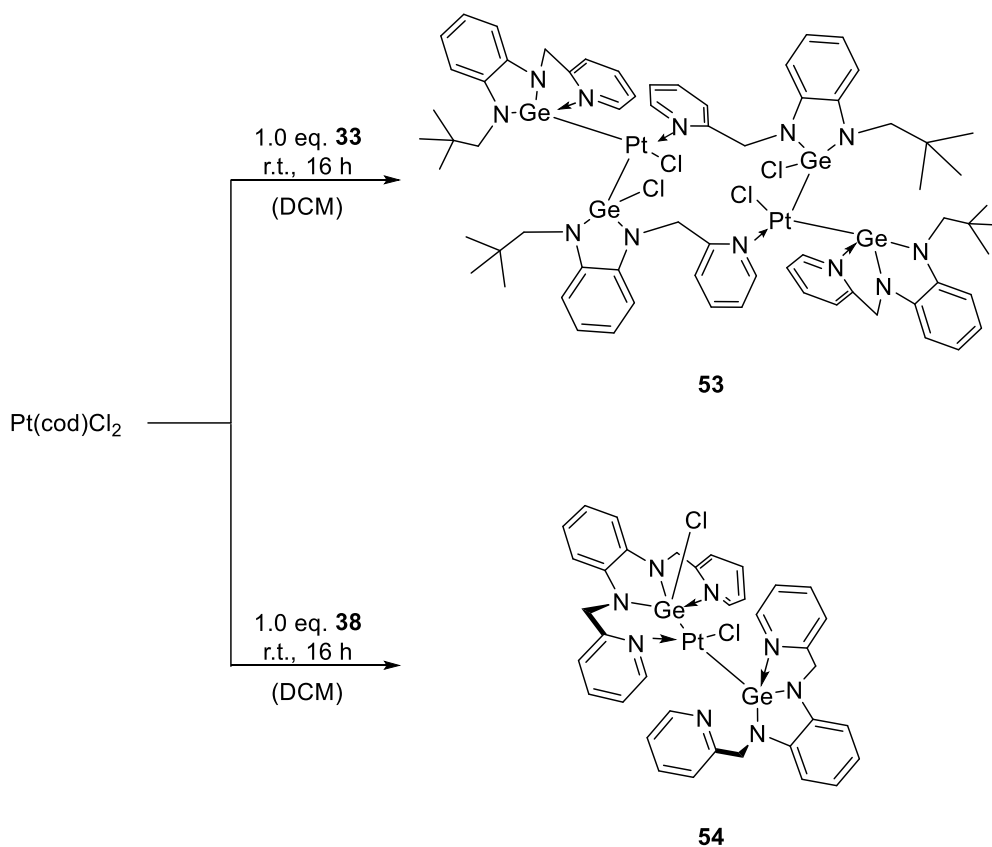


Figure 32: Cut-out of the $^{13}\text{C-NMR}$ spectrum of **52**. Full spectra are given in the supplementary data (SD 16, SD 17).

No product has been obtained from the reaction of **38** with $[\text{Rh}(\text{cod})\text{Cl}]_2$, indicating unselective reaction. Compared to the recently published PGeP pincer-type ligand, however, the coordination chemistry of pyridyl-substituted **33** significantly differs.³⁰² As shown above, insertion into metal halide bonds is possible through interaction of the pyridyl moiety. Thereby, the ligand does not act as chelating motif of a single metal center but rather forms a bimetallic complex.

Platinum Complexes of **33** and **38**

To further elaborate the coordination chemistry of pyridyl-substituted NHGe ligands, reactions with various platinum-containing metal precursors were performed. Vinylsiloxane-ligated platinum(0) (*Karstedt's catalyst*) still remains the most widely used catalytic source in industrial olefin hydrosilylation processes.^{145, 146} Therefore, novel coordination compounds thereof could be interesting candidates for improving homogeneous catalytic reactions. *Cabeza et al.* recently reported the synthesis and structural properties of group 10 transition metal complexes ligated by the previously described pincer-type PGeP NHGe ligand.²⁷⁶ Therein, the latter acts as chelating ligand of halide salts to give square planar complexes of the type $\text{Ge},P,P\text{-}[(\text{N},\text{N})\text{Ge}]\text{MCl}$ ($\text{M} = \text{metal}$). In the following, the ligands **33** and **38** have thus been reacted with equimolar amounts of $\text{Pt}(\text{cod})\text{Cl}_2$ (Scheme 37).



Scheme 37: Reaction of **33** and **38** with $\text{Pt}(\text{cod})\text{Cl}_2$ resulting in the complexes **53** and **54**.

In DCM the reaction mixture turns intensively yellow at room temperature. Products, however, were not detectable *via* LIFDI mass spectrometry. After stirring overnight, both solutions were filtered and diluted with diethyl ether. Storage at low temperatures ($-30\text{ }^\circ\text{C}$) yields crystals, suitable for SC-XRD analysis (Figure 33, Figure 34).

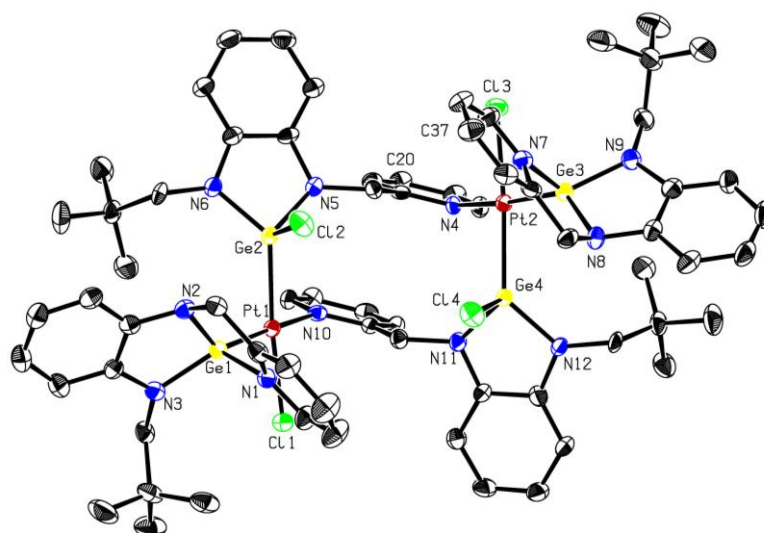


Figure 33: Molecular structure of **53**. Ellipsoids are shown at the 50% probability level. Hydrogen atoms are omitted for clarity. Grey = carbon, blue = nitrogen, yellow = germanium, green = chlorine, red = platinum. Selected bond lengths (Å) and angles (°): Ge4-Cl4 2.288(14), Ge2-Cl2 2.2749(13), N7-Ge3 2.043(4), N8-Ge3 1.864(4), N9-Ge3 1.844(4), N1-Ge1 2.042(2), N2-Ge1 1.865(4), N3-Ge1 1.856(4), Pt2-Ge3 2.3233(8), Pt2-Ge4 2.3339(8), Pt2-Cl3 2.3609(13), Pt2-N4 2.129(4), Pt1-Ge1 2.3320(8), Pt1-Ge2 2.3330(7), Pt1-Cl1 2.3745(13), Pt1-N10 2.124(4), C21...C52 3.539, C18...C55 3.567, Cl3-Pt2-Ge3 89.86(3), Ge3-Pt2-Ge4 91.52(2), Ge4-Pt2-N4 94.04(10), N4-Pt2-Cl3 84.89(10), Cl1-Pt1-Ge1 91.31(4), Ge1-Pt1-Ge2 91.53(3), Ge2-Pt1-N10 91.62(10), N10-Pt1-Cl1 85.77(10), Cl4-Ge4-N12 107.68(13), Cl4-Ge4-N11 100.57(12), Cl2-Ge2-N5 99.76(12), Cl2-Ge2-N6 106.10(13), N4-C22-N10-C5 3.4.

The molecular structure of **53** reveals a binuclear complex, wherein each platinum atom is coordinated by two germynes and one pyridyl moiety. The latter acts as a bridging unit binding the opposite platinum center. At each metal center, one gemyne inserts into a platinum-chloride bond. One NHGe is thus intermolecularly donor-stabilized by the chloride while the other one is stabilized intramolecularly by a pyridyl moiety. Due to the binding of an additional donor, all present gemyne platinum bonds are tilted out of the respective ligand plane. The platinum centers, the chloride-stabilized NHGes and the bridging pyridyl moieties build a twelve-membered ring system. The gemyne-bound chlorides point to the same side of the ligand plane while the chlorides on the platinum atoms are in plane aiming to opposite directions. The bridging pyridyl moieties are planar to each other, indicating π -interactions between the aromatic systems (N4-C22-N10-C5 3.5°, C21-C52 3.539 Å, C18-C55 3.567 Å). All gemyne atoms are coordinated in a strongly distorted tetragonal motif, the platinum center features square planar symmetry.

Bond lengths and angles of equivalent atoms are similar to each other and in the range of previously obtained complex compounds. The platinum-germanium bonds are very similar to each other (2.323-2.334 Å) and slightly increased when compared to related compounds known to literature.²⁷⁶ The shortest bond to the platinum center is formed by the nitrogen atom of the pyridyl moiety (Pt1-N10 2.12 Å). Due to the interaction of the gemyne with the platinum center, the dative bonds of the intramolecular pyridyl donors to the germanium atoms are comparably short (N1-Ge1 2.042 Å). In

course of this electron pull, protons of the methylene groups are significantly shifted high-field in NMR-spectroscopy (3.46 ppm - 5.48 ppm).

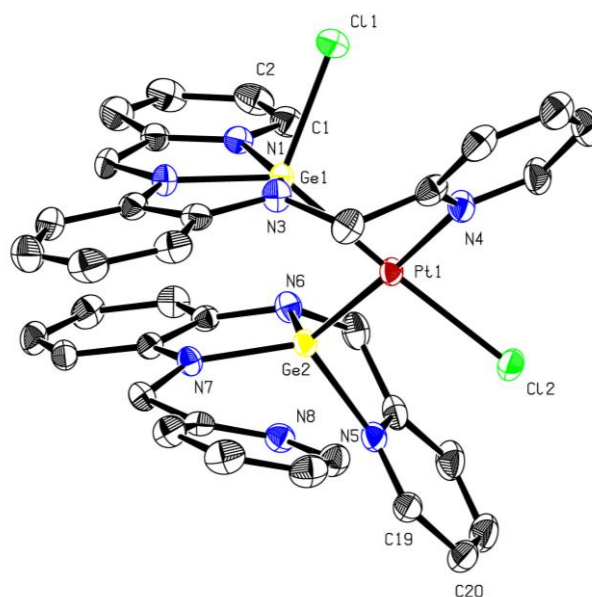


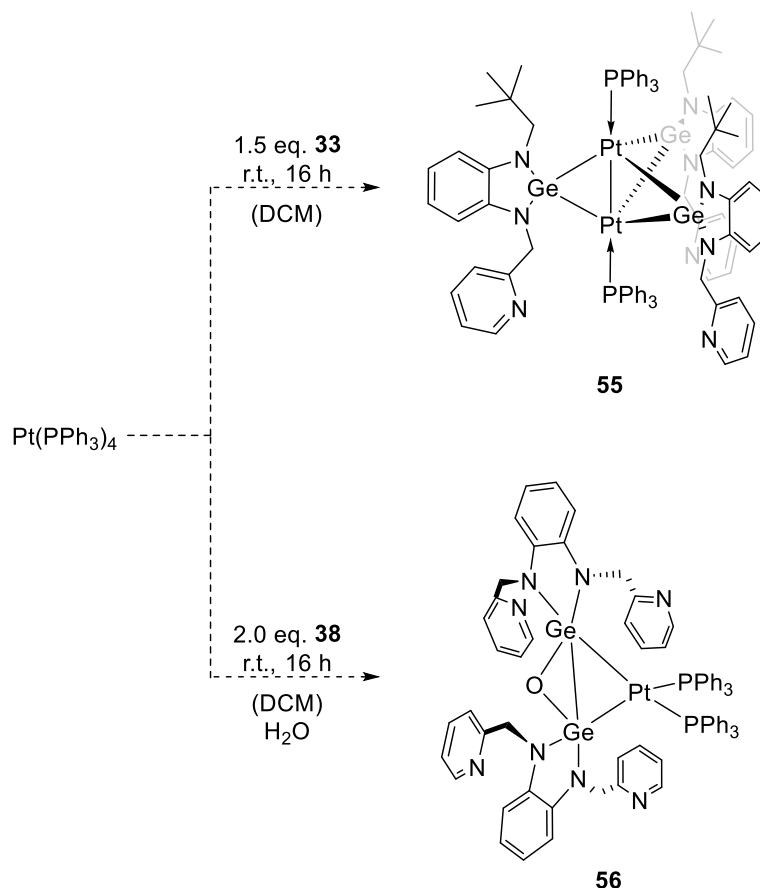
Figure 34: Molecular structure of **54**. Ellipsoids are shown at the 50% probability level. Hydrogen atoms are omitted for clarity. Grey = carbon, blue = nitrogen, yellow = germanium, green = chlorine, red = platinum. Selected bond lengths (Å) and angles (°): N5-Ge2 2.080(3), N6-Ge2 1.888(3), N7-Ge2 1.857(3), N1-Ge1 2.253(3), N2-Ge1 1.857(3), N3-Ge1 1.938(3), Cl1-Ge1 2.2696(8), Pt1-Cl2 2.4122(8), Pt1-Ge1 2.3455(4), Pt1-Ge2 2.3255(4), Pt1-N4 2.117(3), N8⋯Ge2 2.496, Cl2-Pt1-Ge2 95.69(2), Ge2-Pt1-Ge1 89.944(15), Ge1-Pt1-N4 86.66(7), Cl2-Pt1-N4 87.57(8), Ge1-N2-Ge2-N7 176.8.

Due to the sensitivity of **54**, no high-quality NMR spectrum has been obtained so far. In the molecular structure, a platinum(I) chloride center is coordinated by two NHGe ligands. Thereby, one germylene has inserted into a platinum-chloride bond, resulting in a five-fold coordinated germanium (including the bond to platinum and intramolecular donation of one pyridyl moiety). In contrast, the second germylene is only four-fold coordinated featuring intramolecular donation of one pyridyl moiety as well. The second wingtip aims towards the germanium atom; however, no covalent bond is formed (N8⋯Ge2 2.496 Å).

As already observed before, the five-fold coordinated germanium features a distorted trigonal bipyramidal symmetry, while the coordination sphere of the four-fold coordinated germanium is best described as distorted tetragonal. The platinum atom remains in a square planar symmetry. Remarkably, the pyridyl moiety, bound at the tetragonal germanium, is tilted out of the ligand plane by far, while the pyridyl donor of the five-fold coordinated germanium is almost in plane. Comparably to **53**, the platinum-nitrogen bond of the pyridyl moiety is relatively short (Pt1-N4 2.12 Å), while the dative bond of the intramolecular pyridyl donor is significantly increased in the chloride-donated germanium (N5-Ge2 2.080 Å versus N1-Ge1 2.253 Å). The platinum-germanium bond lengths are comparable to previously observed values, while Pt1-Ge1 is comparably large due to the additional

donor (2.346 Å). The same trend can be observed in the platinum-chloride bond lengths (**53** Pt2-Cl3 2.361 Å versus **54** Pt1-Cl2 2.412 Å).

In both cases, $[\text{Rh}(\text{cod})\text{Cl}]_2$ and $\text{Pt}(\text{cod})\text{Cl}_2$, the asymmetric pyridyl-functionalized NHGe **33** is capable of stabilizing a dinuclear transition metal complex. Contrary to that, the symmetric bis(pyridyl-2-ylmethyl) NHGe **38** gives a mononuclear complex with $\text{Pt}(\text{cod})\text{Cl}_2$, analogous to literature known mononuclear platinum complexes of the PGeP pincer-type ligand.²⁷⁶ This trend could also be confirmed in reactions of the novel NHGes **33** and **38** with $\text{Pt}(\text{PPh}_3)_4$, resulting in **55** and **56** (Scheme 38).



Scheme 38: Reaction of **33** and **38** with $\text{Pt}(\text{PPh}_3)_4$. From the reaction mixtures, **55** and **56** have been crystallized and characterized *via* X-Ray diffraction analysis.

The addition of the ligands to a DCM solution of $\text{Pt}(\text{PPh}_3)_4$ results in a deep red solution in both cases already at room temperature. Crystals, suitable for SC-XRD analysis, can be obtained from diluted solutions at low temperatures (diethyl ether, $-30\text{ }^\circ\text{C}$). Several attempts to selectively isolate the products in quantitative yields were not successful though. This might indicate unselective reactions due to a high number of different possible coordination motifs. The found molecular structures are shown in the supplementary data (SD 26, SD 27). **55** depicts an interesting coordination compound, wherein multiple binding of three NHGes at a bimetallic platinum center takes place. The platinum atoms and the coordinated triphenylphosphine ligands are located on a rotation axis. Most

remarkably, the germylene atoms remain free of intramolecular donation, as the pyridyl moieties aim to opposite directions. This might be related to the relatively electron rich platinum(0) centers. Similar examples, where heavier tetrylenes coordinate transition metals in a divalent fashion are already known to literature.¹²⁰

The molecular structure of **56** exemplifies the diverse reactivity of pyridyl-substituted NHGes with transition metals. The mononuclear complex is coordinated by two NHGe ligands which are connected *via* an oxygen bridge. The latter probably originates from impurities in used solvents or water bound to the surface of glassware. Most interestingly, no interaction of both pyridyl moieties with the coordinated germylenes take place in the solid state, comparable to **55**. The latter complexes, **55** and **56**, have not been fully characterized and are thus not discussed in detail. However, the molecular structures confirm the distinct coordination behavior of **33** and **38** in transition metal complexes and the significant effect of intramolecular pyridyl donors.

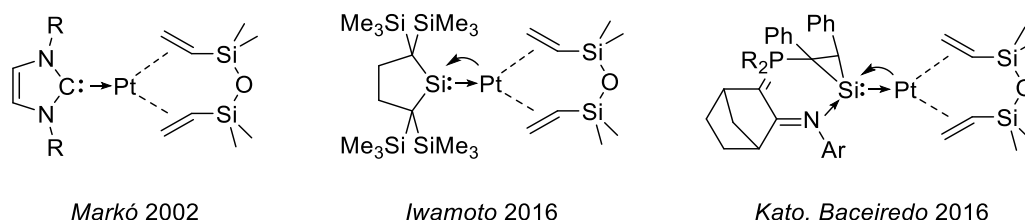
Summary

The complexes of **33** and **38**, described in the previous chapter, exemplify the diverse coordination chemistry of the latter and the flexible nature of the present pyridine-2-ylmethyl wingtips. The molecular structures of the complexes prove the electronic diversity of the *N*-heterocyclic germylene ligands, as both deficits and excesses in electron density can be balanced *via* flexible intramolecular coordination of the pyridyl moiety. Bond lengths to the stabilizing *N,N*-benzimidazole ligands and bond angles are altered correspondingly thereby. The application of non-innocent ligands has opened new ways in homogeneous catalysis already in the past. Thus, further experiments and studies into the catalytic activity of the latter complexes have to be performed in the future, allowing insights into the influence of intramolecular donor groups and the optimized design of steering ligands.

3.5 Pyridyl-Substituted NHGes as Additives in Alkene Hydrosilylation

Reactivity of **33** and **35** with *Karstedt's Catalyst*

As described before, the platinum-catalyzed hydrosilylation of olefins is of paramount importance for the synthesis of organosilicon compounds.^{17, 140, 141} The highly atom-economical addition of a hydrosilane to a carbon-carbon double bond to form functionalized silanes is commonly used in the synthesis and cross-linking of silicones and sol-gel silicates like silicon rubbers or liquid injection molding products. Over the past decades, a great variety of catalytic active transition metal complexes has been reported. However, platinum complexes were found to surpass other metals in activity and/or selectivity.^{16, 18, 157, 305-307} Consequently, *Karstedt's catalyst* remains the most conventionally applied industrial catalyst.^{145, 146} The latter exhibits unmatched activity but the system is not stable when exposed to reaction conditions. The rapid formation of catalytically inactive platinum colloids is accompanied by color changes and varying amounts of undesired byproducts.^{150, 161} In consequence of colloid formation, these catalysts cannot be recycled and the metal remains in the product. To suppress these side reactions, research efforts have been directed to the design of steering ligands that are capable of improving the stability of such platinum catalysts. Most promising candidates have already been discussed in the introduction (Scheme 39).^{161, 168, 170, 177-179, 308}

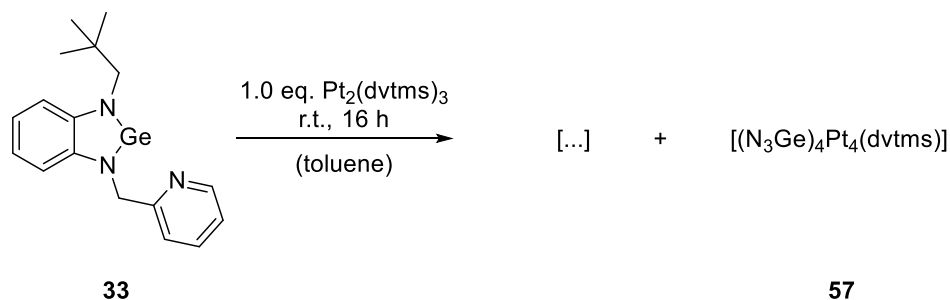


Scheme 39: Examples of catalytically active platinum complexes ligated by different cyclic tetraylene ligands.^{161, 177, 178}

As discussed in the previous chapter, the novel pyridyl-substituted NHGe ligands **33** and **38** display interesting candidates for steering platinum-catalyzed alkene hydrosilylation into the right direction. Due to their proven electronic flexibility, they potentially facilitate key steps of the catalytic cycle while also stabilizing the catalytic active species. In particular, their elevated π -accepting properties can lead to an acceleration of the reductive elimination of the hydrosilylated product, which has shown to be the rate-determining step of common platinum-catalyzed olefin hydrosilylation.¹⁴⁸ In addition, the novel germynes are capable of binding more than one metal center, allowing for metal-metal interactions in the catalytic cycle.

As reactions with $\text{Pt}(\text{PPh}_3)_4$ showed, the novel ligands **33** and **38** feature various coordination modes with platinum(0) metal centers. Therefore, the selective formation of complex compounds is most unlikely. Several test reactions with *Karstedt's catalyst* were performed, however, only one molecular

structure could be enlightened from the reaction of **33** with equimolar amounts of $\text{Pt}_2(\text{dvtms})_3$ (Scheme 40).



Scheme 40: Reaction of the *N*-heterocyclic germylene **33** with $\text{Pt}_2(\text{dvtms})_3$ in toluene to result in an undefined mixture of products. From the reaction mixture, $[(\text{N}_3\text{Ge})_4\text{Pt}_4(\text{dvtms})]$ (**57**) has been crystallized and characterized *via* X-ray diffraction analysis.

After addition of the ligand to a solution of *Karstedt's catalyst* in toluene, the reaction mixture turns dark red immediately. Similar observations were been made using the second bis(pyridyl-2-ylmethyl)-functionalized NHGe **38** no product could be isolated though. In both cases, it was not possible to detect products *via* LIFDI mass spectrometry or NMR spectroscopy due to multiple product formation. From the reaction mixture of **33** the crystals, suitable for SC-XRD analysis, could be obtained *via* dilution with hexane and storage at $-30\text{ }^\circ\text{C}$ for several days (Figure 35).

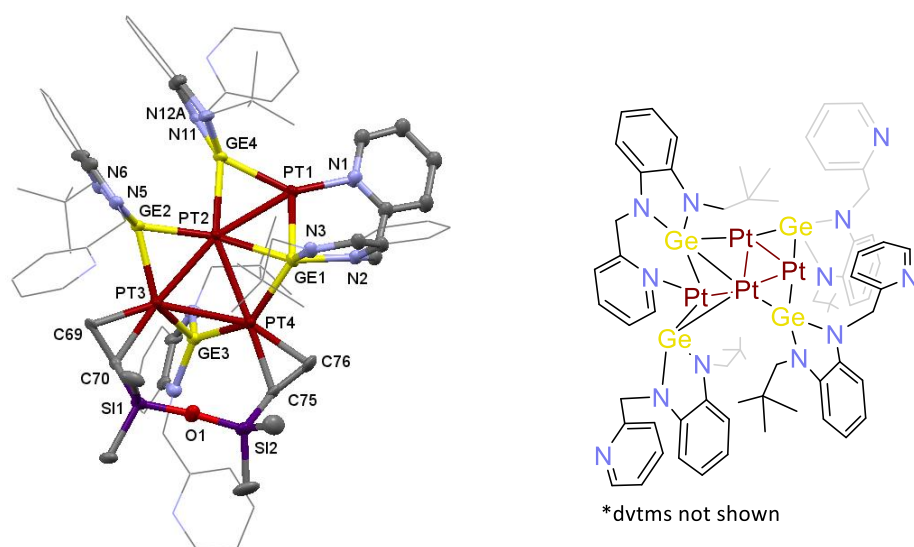


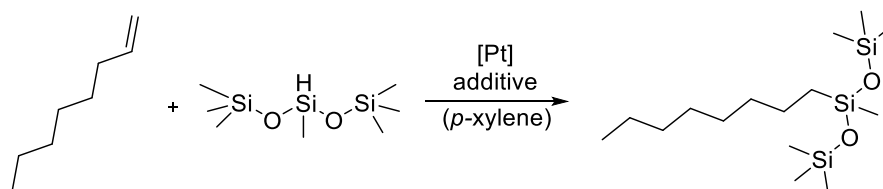
Figure 35: Molecular structure of **57**. Ellipsoids are shown at the 50% probability level. Hydrogen atoms are omitted for clarity. Bulky ligand residues are depicted as wireframes. Grey = carbon, blue = nitrogen, yellow = germanium, dark red = platinum, red = oxygen, purple = silicon. Selected bond lengths (Å) and angles (°): Pt4-C76 2.155(11), Pt4-C75 2.156(11) Pt3-C69 2.121(10), Pt3-C70 2.144(10), C69-C70 1.392(15), C76-C75 1.405(16), Pt4-Pt3 2.8470(7), Pt4-Pt2 2.7708(7), Pt3-Pt2 2.6764(6), Pt2-Pt1 2.6747(6), Ge3-Pt4 2.3969(14), Ge3-Pt3 2.4230(14), Ge2-Pt3 2.3909(13), Ge2-Pt2 2.3835(13), Ge4-Pt2 2.3604(12), Ge4-Pt1 2.3645(13), Ge1-Pt1 2.471(13), Ge1-Pt2 2.5203(13), Ge1-Pt4 2.413(14), N1-Pt1 2.10(3), C76-Pt4-C75 38.4, C70-Pt3-C69 38.1, Pt4-Ge3-Pt3 72.41(4), Pt3-Ge2-Pt2 68.19(4), Pt2-Ge4-Pt1 68.95(4), Pt1-Ge1-Pt2 64.73(3), Pt2-Ge1-Pt4 68.29(4), Pt1-Pt2-Pt3-Pt4 171.5. Structural representation of compound **57**. (right) Further representations of the molecular structure of **57** are given in the supplementary data (SD 28).

The molecular structure of **57** displays a tetranuclear complex, featuring four NHGe and one dtms ligand. In contrary to known tetrylene-ligated platinum(0) dtms complexes, the vinyl groups of the dtms ligand are not coordinated at the same metal center but two platinum atoms are bound. Thereby, these platinum atoms form together with the dtms ligand a seven-membered ring system, which adopts a typical chair-like structure (similar to common six-membered ring structures of platinum dtms complexes). The platinum atoms Pt2, Pt3 and Pt4 are six-fold coordinated while Pt1 forms four bonds only. Within **57**, three NHGes (Ge2-Ge4) feature divalent coordination of two platinum centers, while Ge1 even binds three different metal centers. The flexible pyridyl wingtips are either bound at a platinum acting as chelating side arm or remain non-coordinated similar to the situation in **55**. Remarkably, intramolecular donation to a germanium atom does not take place.

One feature of the molecular structure of **57** is that all platinum atoms almost lay in the same plane (Pt1-Pt2-Pt3-Pt4 171.5). Platinum-platinum distances range from 2.675-2.847 Å. The germanium-platinum bonds of the divalent germylene atoms range from 2.360-2.423 Å including angles from 68.19-72.41°. In comparison to donor-stabilized germylenes coordinating platinum(I), bond lengths are thus slightly elongated (**53**: Ge-Pt 2.323-2.333 Å). The germanium-platinum distances of the trivalent germanium are significantly increased due to a weaker interaction and range from 2.414-2.520 Å comprising angles of 64.73-68.29°. In comparison to benchmark tetrylene ligated platinum(0) dtms complexes, the Pt-C_{vinyl} bonds ranging from 2.121-2.156 Å belong to the shortest observed distances, suggesting strong interaction of the platinum with the dtms ligand.^{168, 169, 177, 178} In stark contrast to known complexes, the carbon-carbon bond lengths of the vinyl groups remain very small (1.392-1.405 Å, literature from 1.415-1.425 Å to 1.426-1.434 Å). This peculiarity might be related to the binding of two platinum by the vinyl groups in **57** instead of a single metal center. As the cleavage of the metal-dtms bond most likely depicts a key step in the activation of the catalyst, this might influence the performance of such NHGe-supported catalytic hydrosilylations decisively.

NHGes **33**, **38** and **39** as Additives in Olefin Hydrosilylation

As complex compounds could not be isolated in quantitative yields from reactions of **33** and **38**, the latter were used as sole additives in the catalytic hydrosilylation of alkenes with Pt₂(dtms)₃. As model reaction, the hydrosilylation of *n*-octene with heptamethyltrisiloxane has been performed in *p*-xylene (Scheme 41).



Scheme 41: Model hydrosilylation reaction of *n*-octene with heptamethyltrisiloxane in *p*-xylene.

The reaction depicts a standard reaction for the evaluation of homogeneous catalysts. In the following, ligands have been added in equimolar amounts as well as in excess to a solution of *Karstedt's catalyst* in *p*-xylene. To start the catalytic reaction, certain amounts of the tempered catalyst solution (50 ppm [Pt], 66 ppm [Pt], 133 ppm [Pt]) were added to a substrate mixture in *p*-xylene at various temperatures (72 °C, 100 °C, 130 °C) and subsequently analyzed *via* GC in certain time intervals. Besides the novel pyridyl-substituted NHGes **33** (N3Ge) and **38** (N4Ge), the donor-free bisneopentyl germylene **39** (NeoGe), as well as two NHCs (^DiPPNHC and ⁱPNC) and one phosphine (PPh₃) were utilized (Figure 36).

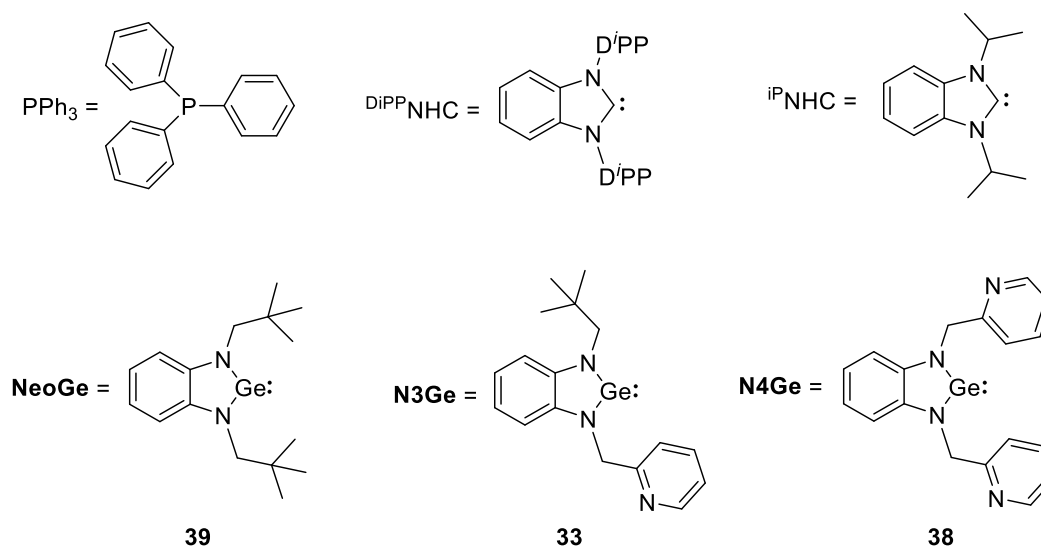


Figure 36: Applied additives in the following catalytic experiments.

Common tetraylene platinum(0) dtms complexes, as introduced in Scheme 39, are usually synthesized simply by mixing of equimolar amounts of the free ligand with *Karstedt's catalyst* and subsequent crystallization. The catalyst solution used in the following experiments was thus stirred after addition of the respective ligand for three hours at elevated temperatures in order to reach full conversion of the platinum precursor. It has to be considered that free platinum(0) dtms might still be present in the catalyst solution though.

The systematic alteration of the wingtip groups of the NHGes allows insights into the effect of flexible electron donors onto the catalytic hydrosilylation of olefins. As can be seen from the reaction depicted above in Scheme 40, most likely several different cluster-like complex compounds will be present in the catalytic solutions with *N*-heterocyclic germylene additives. Thereby, the comparison with

common ligands such as NHCs and phosphines, used as additives in the exact same manner, provides insights into the effect of heavier tetrylenes as steering ligands. Noteworthy, amine groups are known to influence the activity of platinum-based catalysts.³⁰⁹ As it was not clear whether the pyridyl-functionalized NHGes decompose in the reaction with Pt₂(dvtms)₃ in significant amounts, the respective diamines **31** and **37** were tested as additives as well (Table 2). Selected reactions have been performed twice under the exact same conditions, validating the received data (error circa 3%). However, a more detailed study will have to be performed in the future including the exact determination of the course of the reaction by means of *in-situ* NMR spectroscopy or IR spectroscopy. Exact turnover frequencies were thus not determined. Major results of the performed catalytic screenings and effects of the additives on product formation and yield are discussed in the following.

Table 2: Hydrosilylation of *n*-octene (1.5 eq.) with HSi (1.0 eq., 0.5 M) in *p*-xylene with 50 ppm [Pt] and 1.0 eq. additives at 72 °C. Selected conversion versus time graphs are given in the supplementary data (SD 38).

entry	catalytic system	conversion ^a [%]	yield ^b [%] 72 °C
1	<i>Karstedt's catalyst</i>	100	83
2	1.0 eq. 31	100	82
3	1.0 eq. 37	100	83
4	1.0 eq. ⁱ P-NHC	100	84
5	1.0 eq. ^{Di} PP-NHC	100	89
6	1.0 eq. PPh ₃	100	87
7	1.0 eq. NeoGe	100	93
8	1.0 eq. N3Ge	100	95

All reactions were performed with an excess of olefin to ensure full conversion of the silane, which allows for a more precise determination of the yield. As can be seen from Table 2, the reaction of *n*-octane with HSi catalyzed by *Karstedt's catalyst* (50 ppm) at 72 °C yields 83% of the hydrosilylated product (entry 1). The addition of the diamines **31** or **37** did not affect the course of the reaction as the observed yield did not change (entries 2,3). Conversion versus time graphs, created from the measured points, are given in the supplementary data. Exact turnover frequencies have not been determined as not enough data was available. The graph shown in SD 38 unequivocally reflect the effect of NHC and phosphine additives on the performance of *Karstedt's catalyst* – without prior

^a Defined as the concentration of HSi divided by the starting concentration of HSi₀.

^b Defined as the concentration of product divided by the starting concentration of HSi₀.

isolation of the respective tetraylene platinum(0) dvtms complexes. Thereby, sterically demanding ligands such as ^{DiPP}NHC lead to an ample initiation phase reaching 89% yield in product. In comparison, smaller ligands such as ^{iP}NHC result in a shortened initiation phase as well as lower yields, which is in accordance with the literature (84%, entries 4,5).^{161, 168-170} 87% yield was obtained after addition of triphenylphosphine correlating with previously reported catalytic reactions with phosphine platinum(0) dvtms complexes under similar conditions.¹⁶¹

Addition of the NHGe ligands leads to a further increase in product (Table 2 entries 7,8). The initiation phase of both catalytic reactions is significantly shorter compared to the catalytic reactions with NHC and phosphine ligands although reaching higher yields. This is contrary to previous reports on the performance of NHC platinum(0) complexes by *Markó et al.*, who observed that faster reactions always led to a decrease in product yield.^{161, 168-170} Remarkably, the substitution of a neopentyl moiety by a pyridine-2-ylmethyl group (**33** versus **39**) results in a slower but more selective reaction (SD 38). Thus, the electronic effect of the pyridyl moiety outweighs the steric stabilization effect of the neopentyl moiety – either through chelation or through intramolecular donation to the binding germanium atom.

As the reaction of the NHGe ligands with Pt₂(dvtms)₃ is not selective, the molecular structure of the compounds present in the catalytic solution cannot be clarified. The NHGe ligands have thus been used in excess to ensure full ligation of the platinum(0) atoms (Table 3).

Table 3: Hydrosilylation of *n*-octene (1.5 eq.) with HSi (1.0 eq., 0.5 M) in *p*-xylene with 50 ppm [Pt] and 1.0 eq./2.0 eq. additives at 72 °C/100 °C.

entry	catalytic system*	conversion [%]	yield [%] 72 °C	yield [%] 100 °C
1	1.0 eq. NeoGe	100	93	
2	2.0 eq. NeoGe	100	96	
3	2.0 eq. NeoGe ^a	100		89
4	1.0 eq. N3Ge	100	95	
5	2.0 eq. N3Ge	100	98	
6	2.0 eq. N3Ge ^a	100		95

Addition of excess ligand leads in both cases to a further increase in product yield by circa 3% (Table 3, entries 1,2,4,5). At the same time, the initiation phase is prolonged by far (SD 39). The addition of

^a 133 ppm [Pt]

further ligand possibly leads to a lower concentration of free platinum(0) dtms in solution and, thus, higher yields. Despite higher additive loadings and prolonged initiation phases, comparable activities can be reached at later times. Thus, the excess of NHGe ligand does not hinder the catalytic reaction through oversaturation of the active species, but rather inhibits its formation in the first place. In course of the presence of excess ligand, it is possible that altered platinum clusters are being formed in the catalyst solution. The significantly prolonged initiation phase indicates a decelerated formation/slower release of the active species.

At elevated temperatures, the active species of both catalytic systems are formed already after a few minutes. Adding NeoGe, no induction period was detectable within the chosen intervals. However, formation of a ligated platinum center takes place, as the yield in product differs significantly compared to catalytic reactions with *Karstedt's catalyst*. Thus, formation of the catalytic active species is significantly accelerated through the additional input of energy. To further elaborate the effect of the pyridyl moieties and the formation of the active species, hydrosilylation reactions with *Karstedt's catalyst* and excess N3Ge and N4Ge were performed at different temperatures (72 °C, 100 °C, 130 °C, Table 4).

Table 4: Hydrosilylation of *n*-octene (1.5 eq.) with HSi (1.0 eq., 0.5 M) in *p*-xylene with 66 ppm [Pt] and 2.0 eq. additives at 72 °C, 100 °C, and 130 °C.

entry	catalytic system	yield [%] 72 °C	yield [%] 100 °C	yield [%] 130 °C
1	<i>Karstedt's catalyst</i>	82	79	78
2	2.0 eq. N3Ge	95	93	93
3	2.0 eq. N4Ge	98	97	94

As observed before, the addition of NHGes to *Karstedt's catalyst* leads to a significant increase in product yield. Thereby, the substitution of the neopentyl moiety of N3Ge by a second pyridine-2-ylmethyl wingtip (N4Ge), further increases the stability of the catalytic reaction reaching yields as high as 98% (Table 4, entries 1-3). The increase of the temperature leads to a decrease in yield in all three cases, while the initiation phase is reduced to very short times as already observed before (SD 41). With the bis(pyridine-2-ylmethyl) additive N4Ge, 94% yield in product can still be reached at 130 °C, while pure *Karstedt's catalyst* only reaches 78%. The latter screening confirms the finding that the electronic effect of an intramolecular donor plays a significant role in stabilizing catalysis to give high yields. Thereby, it is possible that the pincer-type ligand either coordinates several active metal centers allowing for platinum-platinum interactions or acts as intramolecular donor at the germanium atom strengthening the germanium-platinum bond thereby. As already determined by *Markó et al.*, the

stability of the ligand-metal bond is decisive for a stable catalytic reaction and high yields of the hydrosilylated product.¹⁶⁸

One of the most prominent enigmas of nowadays platinum-catalyzed hydrosilylation of olefins remains the identity of the catalytic active species. Applying mononuclear tetraylene platinum(0) dtms complexes, most likely the dtms ligand gets hydrosilylated in the first step, leaving a free coordination sphere at the ligated platinum(0) metal center.^{168, 174} *Markó et al.* proposed that the initiation phase, obtained with tetraylene ligated complexes, can be related to the slow release of the active species. In the present case, the question arises whether cluster-like platinum species are present as active species or platinum-platinum bonds are being broken initially, giving mononuclear complexes in strong reliance to reported catalysts. Already before, the marked potential of platinum clusters in hydrosilylation catalysis has been reported.^{180, 181}

As demonstrated, addition of the NHGes has a significant influence on the catalytic output of the reaction, while pure diamines **31** and **37** did not have an effect. Thus, clusters comparable to **57** are formed initially in the catalytic solutions used while the NHGes do not decompose. The initiation phase of the catalytic reactions with HTs are short when compared to NHCs and phosphines. This is in accordance with earlier reports by *Kato*, *Baceiredo* and *Iwamoto* on HT platinum(0) complexes featuring similar electronic properties.^{177, 178} The donor properties of tetraylenes allow for an easier hydrosilylation of the dtms ligand and formation of the active species thereby. However, bond lengths of the platinum-C_{vinyl} bonds in **57** ranging from 2.121-2.156 Å indicate comparably strong interactions, thereby hindering the hydrosilylation of the dtms ligand. In addition, excess ligand decelerates the activation process of the precatalysts significantly. Therefore, it is likely that the presence of additional NHGes leads to the formation of several cluster-like platinum compounds, ultimately slowing down formation of the active species. The dramatic shortening of the initiation phase at higher temperatures can thus be related to the formation of the active species through breaking of platinum-platinum bonds. As the platinum-C_{vinyl} bond is relatively strong, so far unknown platinum clusters are probably involved in the catalytic cycle of *N*-heterocyclic germylene-featured olefin hydrosilylation catalysis. Moreover, the presence of additional donor groups in the pyridyl-functionalized N₃Ge and N₄Ge ligands stabilizes the catalytic reaction even further. This prevents the formation of colloidal platinum black and gives significantly increased yields in hydrosilylated product.

Summary

In summary, functionalized NHGes were used as additives in the catalytic hydrosilylation of olefins. The molecular structure of the tetranuclear platinum cluster **57** indicates the formation of various cluster-like platinum compounds, ligated by polyvalent germylene ligands, in reaction mixtures of

pyridyl-functionalized NHGes and *Karstedt's catalyst*. Pyridyl moieties, as either functioning as additional intramolecular donors or chelating wingtips, stabilize such complex compounds and catalytic active species thereof.

In the platinum-catalyzed hydrosilylations of olefins, functionalized germylene additives prevent formation of catalytically inactive platinum colloids and ensure higher yields in product in comparison to donor-free NHGes. It seems probable that multinuclear platinum-clusters featuring metal-metal interactions are also involved in the catalytic cycle. Three key observations are drawn into consideration: I) The initiation phase of NHGe featured platinum-catalyzed olefin hydrosilylation is significantly shorter when compared to common ligands such as NHCs and phosphine while reaching higher yields in product. II) The initiation phase is prolonged by far with excess additives, contradicting dtms hydrosilylation in the rate-determining step of the activation process. III) At higher temperatures, formation of the active species is accelerated dramatically.

Further work has to be done to elaborate the molecular size of the active species for example by means of DSC measurements. In addition, *in-situ* spectroscopic measurements might help to clarify the formation of the active species and the possible hydrosilylation of the dtms ligand. Thereby, it would be interesting to see what role flexible donor groups such as pyridyl moieties can play within the catalytic cycle. The presented catalytic system can also be extended to other substrates as well as other metal precursors, potentially allowing for unprecedented reactivities. Further catalytic experiments will also include [(NHGe)Fe(CO)₄] complexes presented in chapter 3.2, which showed interesting reactivities in strong dependence of the wingtip groups.

4 CONCLUSION AND OUTLOOK

On the way of synthesizing novel functionalized *N*-heterocyclic tetrylenes, interesting insights into the formation of unprecedented polysilanes, the structure of transition metal complexes of tetrylenes and the steering influence of HTs in the platinum-catalyzed hydrosilylation of olefins have been gained.

In the first chapter, a unique hexasilane molecule **24** consisting of three equivalent bissilane units has been synthesized and fully characterized in a six-step synthesis (Figure 37). Reduction of the respective bis(bromo)silanes at low temperatures yields a helical silicon chain, connected intramolecularly *via* a *N,N*-substituted aromatic ring system. The end-to-end bromine functionalization allows for interesting reactivities towards novel polymeric molecules and materials. In times of fast-growing semiconductor industries, polysilanes have received an increasing interest in recent years. In future experiments, deeper insights into the reactivity of the silicon-bromine bond have to be targeted, aiming for the interconnection of several Si₆ units. Also, reactivity studies of **24** with KC₈ have already shown that the synthesis of *N,N*-substituted bissilylenes might be possible at low temperatures.

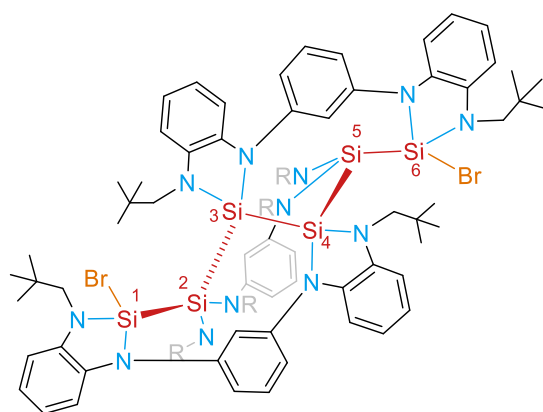


Figure 37: Structural presentation of the bromine-capped hexasilane **24** as presented in chapter 3.1.

In the second project part, two novel pyridyl-2-ylmethyl-functionalized *N*-heterocyclic germynes were synthesized and studied in their reactivity with various substrates. The molecular structures of the ligands in the solid state reveal their elevated thermodynamic stabilities, as the *N*-heterocyclic germylene atoms remain in a dicoordinate state. In reactions with different Lewis acids, such as GeCl₂-dioxane, GeCl₄ or Fe₂(CO)₉, the high flexibility of the wingtip groups could be shown and analyzed in detail *via* multiple analytical methods including NMR spectroscopy, SC-XRD analysis and DFT calculations. The pyridyl moieties can thereby act either as intramolecular donor at the germanium atom, coordinate other metal centers as chelating side arm or remain free of coordination.

In the course of this thesis, examples of dicoordinate, tricoordinate, four-fold coordinated, five-fold coordinated as well as six-fold coordinated germanium compounds could be synthesized and

characterized due to the flexible donating behavior of the pyridyl moieties (Figure 38). In transition-metal complexes, the coordination sphere of the germanium atom can thereby be altered through intramolecular donation usually leading to distorted tetragonal or trigonal bipyramidal symmetry. The donating pyridyl moiety is tilted orthogonally with respect to the ligand plane in the former case, while it remains in plane in the latter.

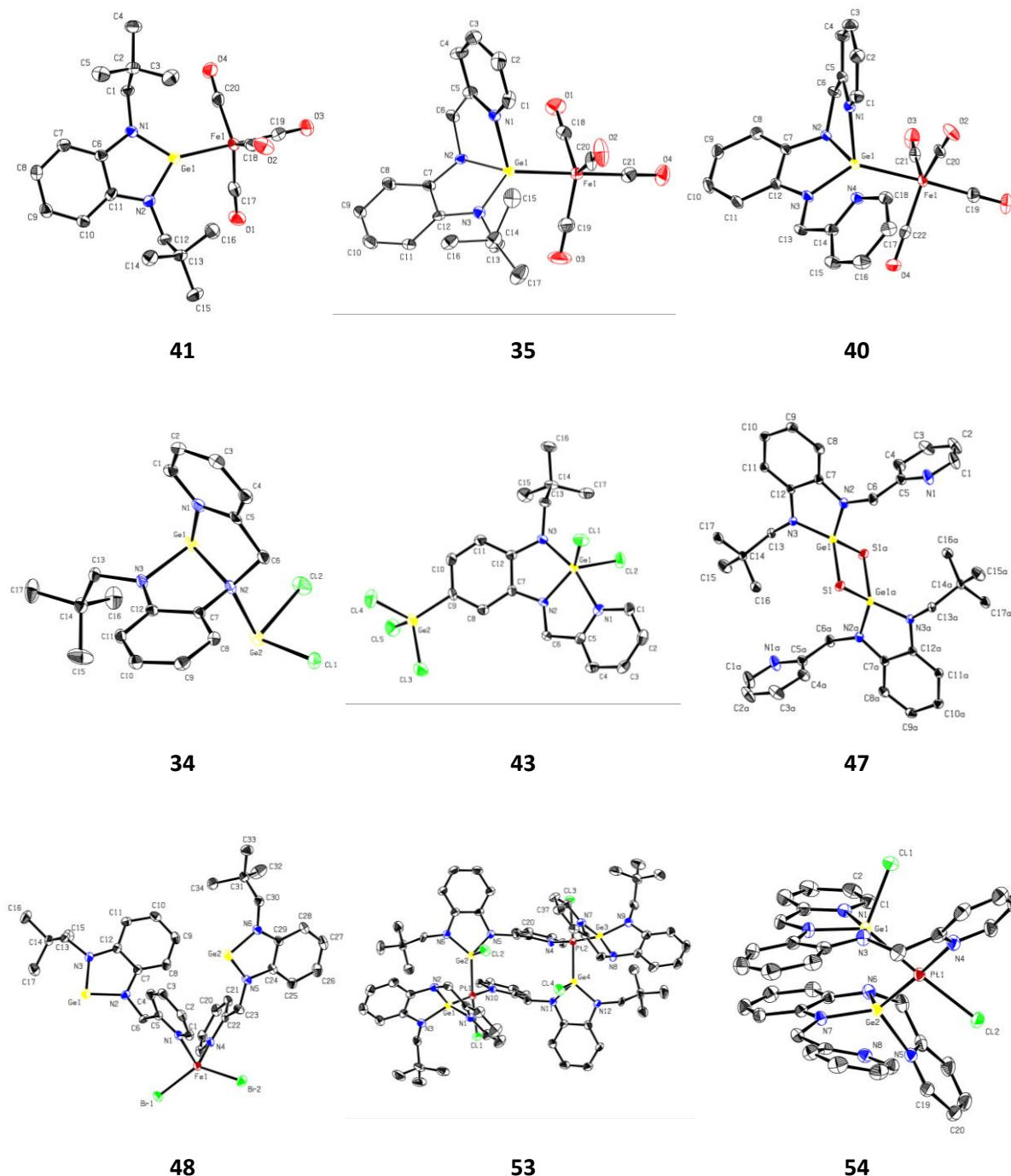


Figure 38: Selected examples of presented complex compounds involving five-membered *N*-heterocyclic germynes in several different coordination spheres ranging from dicoordinate to five-fold coordinated germanium atoms.

Most surprisingly, coordination of Lewis acids cannot only take place at the divalent germylene but also at tertiary nitrogen atoms of the benzannulated ring and the pyridyl moiety, which can even result

in a degraded aromaticity of the NHGe (**34** and **43**). In several reactions with transition metal precursors, the asymmetrically functionalized NHGe **33** is capable of stabilizing dinuclear complexes. In contrast to known PGeP pincer-type NHGe ligands, the symmetrically functionalized bis(pyridyl-2-ylmethyl) NHGe **38** forms intramolecularly stabilized complexes with metal precursors such as Pt(cod)Cl₂.

Pyridyl-functionalized NHGes were shown to significantly affect the platinum-catalyzed hydrosilylation of olefins, outperforming common ligands such as NHCs and phosphines in terms of reactivity and selectivity. Within this thesis, the molecular structure of a tetranuclear platinum cluster could be found, that is showing the ambivalent coordination behavior of the novel ligands towards catalytically active platinum(0) centers (Figure 39). Through the flexible binding of the wingtip groups, the steering ligands potentially allow for an optimized electron balance between the germylene and the transition metal center. In catalytic screenings of various additives, evidence for the involvement of NHGe-stabilized platinum clusters was found.

The presented results may potentially trigger the development of new homogeneous catalytic systems involving functionalized *N*-heterocyclic germylenes. These are capable of steering the electronic properties of transition metal compounds flexibly while even allowing for metal-metal interactions in multinuclear complex compounds. In future projects, the wingtip groups could be altered in their steric demand as well as their donating properties to optimize the transition metal-catalyzed transformation of various substrates.

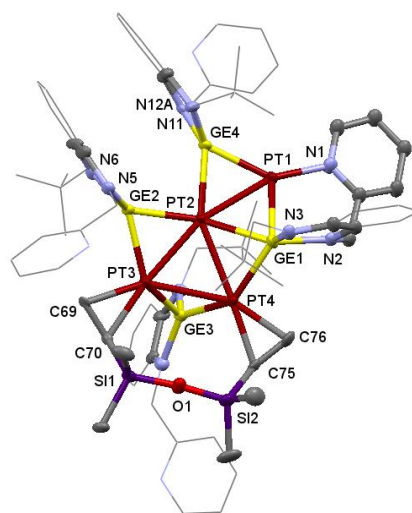


Figure 39: Molecular structure of **57** involving a tetranuclear platinum core and multi-valent germylene ligands. Ellipsoids are shown at the 50% probability level. Hydrogen atoms are omitted for clarity. Bulky ligand residues are depicted as wireframes.

5 EXPERIMENTAL SECTION

5.1 General Remarks

All reactions were carried out under argon (99,996%, Westfalen) in heated glassware and within a glove box if necessary unless otherwise stated. Synthesized complexes and low-valent HTs have been stored under exclusion of light at 4 °C and argon atmosphere. Selected NMR, IR and MS spectra, as well as crystallographic data, can be found as Supplementary Data. Solvents and chemicals were obtained from *TCI Deutschland GmbH*, *Alfa Chemicals*, *Sigma-Aldrich* or *ABCR* and used as received without prior purification unless otherwise stated. Benzene, diethyl ether, DME, hexane, toluene, THF, and pentane were purified with a *Grubbs*-type solvent purification system, MeOH was distilled prior to use. In addition, DME, DMF, hexane, toluene, THF, benzene, and pyridine were distilled over potassium and stored over molecular sieve under argon atmosphere prior to use. Pentane and diethyl ether were pre-dried and stored over molecular sieve under argon atmosphere prior to use. Heptamethyltrisiloxane, 1-vinyl-1,1-3,3,3-pentamethyldisiloxane, tetrachlorosilane, trichlorosilane, and tetrabromosilane have been distilled prior to use and stored under argon atmosphere at 4 °C. Deuterated solvents besides chloroform were distilled over potassium prior to use and stored over molecular sieve under argon atmosphere. Thin-layer chromatography (TLC) was carried out either on pre-coated ALUGRAM SIL G silica gel plates or on POLYGRAM ALOX N plates manufactured by *Macherey-Nagel*. Column chromatography was performed using silica or aluminum oxide 90 active neutral by *Merck*. Visual detection was performed using UV ($\lambda = 254$ nm) in combination with KMnO_4 (0.75 g KMnO_4 , 5.0 g K_2CO_3 , 0.6 mL NaOH_{aq} (10 weight-%), 100 mL H_2O). The following compounds have been prepared following literature procedures: **31**,²³⁴ **36**,²⁸³ $\text{Ge}[\text{N}(\text{SiMe}_3)_2]_2$,²⁸⁴ **Lithium naphthalide**,²¹² **39**,³¹⁰ DiPP/iP/MesNHC.³¹¹

NMR Spectroscopy

^1H -NMR and $^1\text{H}/^{13}\text{C}$ -2D spectra were obtained on a *Bruker* AVHD-300 (300.13 MHz), a *Bruker* AVHD-400 (400.13 MHz), a *Bruker* DPX-400 (400.13 MHz), a *Bruker* Avance III 400 (400.13 MHz), a *Bruker* AVHD-500 (500.13 MHz) and a *Bruker* AVHD-500C (500.13 MHz) at room temperature unless otherwise stated. ^{13}C -NMR spectra were obtained on the *Bruker* AVHD-500C with a frequency of 126 MHz. ^{29}Si -NMR spectra were obtained on the *Bruker* AVHD-500C with a frequency of 99 MHz. Signals are given in *ppm* and are calibrated to the residual resonance of the deuterated solvent with respect to tetramethylsilane. ^{13}C -NMR spectra are proton-decoupled. For the declaration of the signal

multiplicities, the following abbreviations were used: s (singlet), d (doublet), t (triplet), q (quartet), quint (quintet), m (multiplet), br (broad). The coupling constants J are the mean values of the experimentally found values given in Hz. Discussed NMR signals are assigned following the numbering in the corresponding figure. Equivalent positions are indicated with a superscripted bar.

LIFDI Mass Spectrometry

Liquid injection field desorption ionization mass spectrometry measurements were performed on a Waters LCT device equipped with a LIFDI source to enable measurements of air-sensitive compounds. Thereby the probe was coated onto a tungsten wire and a field voltage of 5-7 kV was applied. Heating the wire by increasing the current constantly (30mA/min) leads to ionization. Calibration of the LIFDI-MS has to be performed for each measurement utilizing external standards such as polyethyleneglycol.

Crystallographic Data

Crystallographic data can be found in the supplementary data (SD 29-SD 36). Errors of bond lengths and angles are indicated in brackets if given. Data were collected on a X-ray single-crystal diffractometer equipped with a CCD detector (APEX II, κ -CCD), a Bruker D8 Kappa APEX II system equipped with a fine-focused sealed tube with MoK α radiation ($\lambda = 0.71073 \text{ \AA}$) and a Triumph monochromator, or a rotating anode FR591 (Bruker TXS) equipped with a Montel mirror optic by using the APEX software package.³¹² The measurements were performed on single-crystals coated with perfluorinated ether. The crystals were fixed on top of a glass fiber and transferred to the diffractometer. The measured crystals were frozen under a stream of cold nitrogen (100 K). A matrix scan was used to determine the initial lattice parameters. Reflections were merged and corrected for Lorentz and polarization effects, scan speed, and background using SAINT.³¹³ Absorption corrections, including odd and even ordered spherical harmonics were performed using SADABS.³¹³ Space group assignments were based upon systematic absences, E statistics, and successful refinement of the structures. Structures were solved by direct methods with the aid of successive difference Fourier maps,³¹⁴ and were refined against all data using the APEX 2 software³¹² and SHELXL³¹⁵ in conjunction with SHELXL-2014.³¹⁶ Methyl hydrogen atoms were refined as part of rigid rotating groups, with a C–H distance of 0.98 \AA and $U_{\text{iso}}(\text{H}) = 1.5 \cdot U_{\text{eq}}(\text{C})$. Other H atoms were placed in calculated positions and refined using a riding model, with methylene and aromatic C–H distances of 0.99 and 0.95 \AA , respectively, and $U_{\text{iso}}(\text{H}) = 1.2 \cdot U_{\text{eq}}(\text{C})$. If not mentioned otherwise, non-hydrogen atoms were refined with anisotropic displacement parameters. Full-matrix least-squares refinements were carried out by minimizing $\sum w(\text{Fo}2 - \text{Fc}2)^2$ with SHELXL-97³¹⁴ weighting scheme. Neutral atom scattering factors for all atoms and anomalous dispersion corrections for the non-hydrogen atoms were taken from

International Tables for Crystallography.³¹⁷ Images of the crystal structures were generated by PLATON and Mercury.³¹⁸

DFT Calculations

All calculations were performed with Gaussian16.³¹⁹ The pure functional B97 was applied with a Grimme's D3PJ dispersion and the DEF2-SVP basis for all atoms.^{320, 321} This level of theory was used for geometry optimization and frequency calculation. No symmetry or coordinate constraints were applied during optimizations. All reported optimized geometries were verified as being true minima by the absence of eigenvalues in the vibrational frequency analysis. NBO calculations were performed with NBO3.1 as implemented in Gaussian16. The AIMALL program was used for all QTAIM calculated key figures.³²²⁻³²⁴

Infrared Spectroscopy

IR spectroscopy has been performed using a Mettler-Toledo ReactIR 45m and a SiComp probe attached *via* a K8-Conduit-to-Sentinal arm.

Gas Chromatography

The catalytic reactions mixtures have been segregated and analyzed *via* gas chromatography using a gas chromatograph 7890B *Agilent Technologies* equipped with a HP-5 column. The GC method starts with 60 °C for 7 minutes to strip off the volatile substances first. Afterwards, the GC was heated to 260 °C with a ramp of 15 °C/min to separate the educts, products and byproducts. The temperature of 260 °C is maintained for 15 min to remove the residues from the column of the GC.

Elemental Analysis

Elemental analyses were carried in the central analytical department of the TUM chemistry department. Value are given in per cent.

Catalytic Reactions

The catalytic reaction used as benchmark within this thesis is the hydrosilylation of 1-octene (375 mg, 3.34 mmol, 1.65 eq.) with heptamethyltrisiloxane (450 mg, 2.03 mmol, 1.0 eq.) in 4 mL *para*-xylene (0.5 M HSi). All experiments were filled and performed in heated glassware under inert gas. The reactions were monitored *via* GC. using *n*-decane (405 mg) as internal standard for the determination

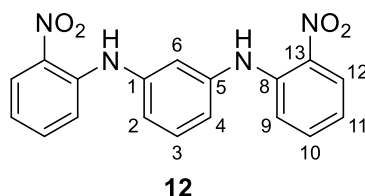
of the conversion and yield. Samples (0.1 mL) were taken with an applied argon counterflow with a 1 mL syringe, filtered through a pad of silica and diluted with *n*-hexane.

To prepare the catalyst solution, 6.41 mg $\text{Pt}_2(\text{dvtms})_3$ (9.6 μmol) are dissolved in 1.0 mL para-xylene. To this solution either 1.0 eq. (9.6 μmol) additive (1.98 mg $^i\text{P}^i\text{NHC}$; 4.26 mg $^{\text{DiPP}}\text{NHC}$; 2.54 mg PPh_3 ; 3.08 mg NeoGe; 3.28 mg N3Ge, 3.49 mg N4Ge) or 2.0 eq. (19.2 μmol , 3.96 mg $^i\text{P}^i\text{NHC}$; 8.52 mg $^{\text{DiPP}}\text{NHC}$; 3.19 mg $^{\text{tBu}}\text{NHSi}$; 6.16 mg NeoGe; 6.56 mg N3Ge; 6.98 mg N4Ge, 5.18 mg **31**, 4.76 mg **37**) are added as from a stock solution.

The catalyst solution was stirred for 3 h at room temperature after which 150 μL (50 ppm [Pt]), 200 μL (66 ppm [Pt]) or 400 μL (133 ppm [Pt]) are added to the substrate mixture at the respective temperature. Catalyst solutions can be stored in the freezer for a week without noticeable changes in catalytic activity. Before catalysis was started by injection of the catalyst solution, each substrate mixture was stirred at the respective temperature for 20 min after which a sample was taken and the quantity of educts measured.

5.2 Synthetic Procedures

5.2.1 *N*¹,*N*³-Bis(2-nitrophenyl)benzene-1,3-diamine (**12**)



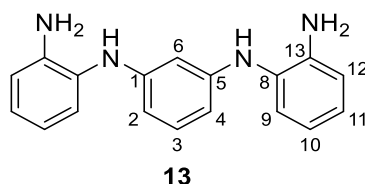
m-Phenylenediamine (1.50 g, 13.9 mmol, 1.0 eq.) is dissolved in 20 mL DMF. After addition of 2.42 g potassium fluoride (41.6 mmol, 3.0 eq.), 21.9 mL 1-fluoro-2-nitrobenzene (29.4 g, 208 mmol, 15.0 eq.) are added slowly and the reaction mixture is stirred at 170 °C for 16 h. After cooling to room temperature, the remaining potassium fluoride is filtered off and the residue washed with cold THF. The product can be collected in form of a red crystalline solid from the concentrated filtrate after storage at 4 °C for 48 h and is washed with cold pentane and dried *in vacuo* (3.81 g, 10.9 mmol, 78.4%).

R_f (SiO₂, hexane/EtOAc: 4/1): 0.39.

¹H-NMR (CDCl₃): δ = 9.46 (s, 2H, NH), 8.21 (dd, ³J = 8.6, ⁴J = 1.6, 2H, CH-12;12'), 7.43 (m, 3H, CH-3;10;10'), 7.31 (dd, ³J = 8.7, ⁴J = 1.3, 2H, CH-9;9'), 7.20 (t, ⁴J = 2.1, 1H, CH-6), 7.13 (dd, ³J = 8.0, ⁴J = 2.1, 2H, CH-2;4), 6.83 (ddd, ³J = 8.4, ³J = 6.9, ⁴J = 1.3, 2H, CH-11;11').

¹³C-NMR (CDCl₃): δ = 142.3 (*C_{arom.}*), 140.5 (*C_{arom.}*), 135.9 (*C_{arom.}*), 133.8 (*C_{arom.}*), 131.0 (*C_{arom.}*), 126.9 (*C_{arom.}*), 120.7 (*C_{arom.}*), 118.9 (*C_{arom.}*), 118.3 (*C_{arom.}*), 116.4 (*C_{arom.}*).

5.2.2 *N*¹,*N*³-Bis(2-aminophenyl)benzene-1,3-diamine (**13**)



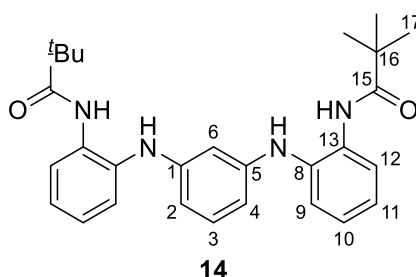
To a solution of 3.80 g **12** (10.9 mmol, 1.0 eq.) in 140 mL THF and 40 mL MeOH are added 578 mg Pd/C (10 weight-%) and H₂-gas is bubbled through the suspension for 3 h. The clear product solution is filtered through a filter pad under argon and concentrated *in vacuo*. The precipitated residue can be washed with cold pentane under argon and dried *in vacuo*. The product can be isolated in form of a white powder (3.05 g, 10.5 mmol, 96.7%).

R_f (SiO₂, hexane/EtOAc/NEt₃ 4/1/0.1): 0.26.

¹H-NMR (CDCl₃): δ = 7.13 (dd, ³J = 7.78, ³J = 1.51, 2H, CH-9;9'), 7.02 (m, 3H, CH-3;11;11'), 6.79 (dd, ³J = 7.9, ⁴J = 1.0, 2H, CH-12;12'), 6.75 (ddd, ³J = 7.8, ³J = 7.2, ⁴J = 1.0, 2H, CH-10;10'), 6.22 (t, ³J = 8.0, ⁴J = 2.1, 2H, CH-2;4), 6.13 (t, ⁴J = 2.1, 1H, CH-6), 5.11 (s, 2H, NH), 3.72 (s, 4H, NH₂).

¹³C-NMR (CDCl₃): δ = 146.75 (C-13;13'), 142.2 (C-8;8'), 130.3 (C-3), 128.6 (C-1;5), 125.9 (C-11;11'), 125.3 (C-19;19'), 119.2 (C-10;10'), 116.8 (C-12;12'), 116.3 (C-2;4), 114.8 (C-6).

5.2.3 N¹,N³-Bis(2-N-neopentylamidophenyl)benzene-1,3-diamine (**14**)

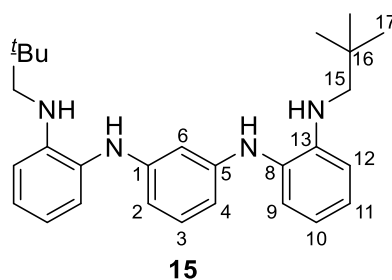


In 80 mL are dissolved 3.05 g **13** (10.5 mmol, 1.0 eq.) and 260.9 mg DMAP (2.15 mmol, 0.2 eq.). After cooling the solution with an ice bath 3.15 mL pivaloyl chloride (3.09 g, 25.6 mmol, 2.4 eq.) are added dropwise. The mixture is allowed to warm to room temperature and stirred overnight. After addition of 50 mL H₂O and 100 mL DCM, the organic layer is washed with 1 M HCl (5 × 200 mL), 5% NaOH (4 × 200 mL) and brine (2 × 200 mL). The combined organic layers are dried over MgSO₄ and reduced *in vacuo* giving the product as white solid (3.81 g, 8.32 mmol, 79.1%).

R_f (SiO₂, hexane/EtOAc/NEt₃ 4/2/0.1): 0.54

¹H-NMR (CDCl₃): δ = 8.06 (dd, ³J = 8.4, ⁴J = 1.6, 2H, CH-12;12'), 7.92 (s, 2H, CONH), 7.14 (m, 4H, CH-9;9';11;11'), 7.06 (ddd, ³J = 8.5, ³J = 7.0 Hz, ⁴J = 1.6, 2H, H-10;10'), 7.02 (t, ³J = 8.0, 1H, CH-3), 6.20 (dd, ³J = 8.0, ⁴J = 2.0, 2H, CH-2;4), 6.11 (t, ⁴J = 2.2, 1H, CH-6), 5.57 (s, 2H, NH) 1.18 (s, 18H, C(CH₃)₃).

¹³C-NMR (CDCl₃): δ = 177.1 (C-15), 146.4 (C-13;13'), 133.4 (C-8;8'), 132.5 (C-8;8';12;12'), 130.6 (C-3), 125.9 (C-9;9';11;11'), 125.0 (C-10;10'), 122.0 (C-12;12'), 107.9 (C-2;4), 102.9 (C-6), 39.9 (C(CH₃)₃), 27.6 (C(CH₃)₃).

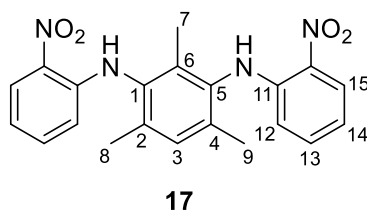
5.2.4 N^1,N^3 -bis(2-*N*-neopentylaminophenyl)benzene-1,3-diamine (**15**)

To a cooled solution of 3.81 g **14** (8.32 mmol, 1.0 eq.) in 65 mL THF are added 20.8 mL (3.16 g, 41.5 mmol, 5.0 eq.) borane dimethyl sulfide (2 M in THF) carefully. The resulting grey suspension is allowed to warm to room temperature and heated to reflux overnight. The solvent is removed in vacuo and the residue dissolved in 50 mL DCM. After cooling to 0 °C excess borane is reacted with 50 mL aqueous NaHCO₃. The aqueous layer is extracted with DCM (2 × 100 mL) and the combined organic layers are washed with 1 M HCl (3 × 100 mL), saturated aqueous NaHCO₃ (2 × 100 mL) and brine (1 × 100 mL). The organic layers are dried over MgSO₄ and the solvent evaporated under reduced pressure giving a grey-white solid. This solid can be purified *via* column chromatography (AIOX, hexane/EtOAc, gradient 15/1, 10/1, 5/1, 1% NH₃). The product can be isolated as grey solid after drying *in vacuo* (1.70 g, 4.02 mmol, 47.7%).

R_f (TLC, AIOX, hexane/EtOAc: 5/1, 1% NH₃): 0.66.

¹H-NMR (CDCl₃): δ = 7.08 (m, 4H, CH_{arom.}), 7.00 (t, ³J = 7.97, 1H, CH-3), 6.70 (dd, ³J = 8.55, ⁴J = 1.37, 2H, CH_{arom.}), 6.63 (td, ³J = 7.52, ⁴J = 1.36, 2H, CH_{arom.}), 6.18 (dd, ³J = 7.97, ⁴J = 2.20, 2H, CH-2;4), 6.09 (t, ³J = 2.17, 1H, CH-6), 5.01 (s, 2H, NH), 4.18 (s, 2H, NH), 2.88 (s, 4H, CH₂), 0.92 (s, 18H, CH₃).

¹³C-NMR (CDCl₃): δ = 147.0 (C-1;5), 145.0 (C_{arom.}), 130.1 (C-3), 127.9 (C_{arom.}), 126.4 (C_{arom.}), 125.5 (C_{arom.}), 116.9 (C_{arom.}), 110.8 (C_{arom.}), 106.7 (C-2;4), 102.2 (C-6), 55.6 (CH₂), 32.1 (C(CH₃)₃), 27.1 (C(CH₃)₃).

5.2.5 2,4,6-Trimethyl- N^1,N^3 -bis(2-nitrophenyl)benzene-1,3-diamine (**17**)

Fluoronitrobenzene (21.0 mL, 200 mmol, 15.0 eq.) and KF (2.32 g, 39.9 mmol, 3.0 eq.) are dissolved in 25 mL DMF. Add 2,4,6-trimethyl-1,3-benzenediamine (2.00 g, 13.3 mmol, 1.0 eq.) to the resulting

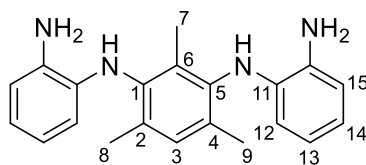
yellow suspension while stirring at room temperature and stir for another 8 h at 150 °C. The solution is allowed to cool to room temperature and KOH (1.49 g, 26.6 mmol, 2.0 eq.) is added to give a purple suspension which is heated again to 165 °C for 4 d. The still warm suspension is filtered and concentrated to 30 mL under reduced pressure, resulting in a yellow precipitate. The filtrate is cooled to 0 °C, filtered cold and rinsed with cold EtOH (4 × 10 mL) and diethyl ether (1 × 10 mL). The yellow solid is dried *in vacuo*, which provides 2.27 g of the product (2.12 g, 5.59 mmol, 42% yield).

R_f (SiO₂, hexane/EtOAc: 4/1): 0.67.

¹H-NMR (CDCl₃): δ = 9.18 (s, 2H, NH), 8.24 (dd, ³J = 8.3, ⁴J = 1.4, 2H, CH-15;15'), 7.27-7.39 (m, 2H, CH-13;13'), 7.18 (s, CH-3), 6.73 (d, ³J = 8.3, ³J = 7.0, ⁴J = 1.2, 2H, CH-14;14'), 6.38 (dd, ³J = 8.6, ⁴J = 1.3, 2H, CH-12;12'), 2.21 (s, 6H, CCH₃).

¹³C-NMR (CDCl₃): δ = 144.4 (C-16;16'), 136.5 (C-13;13'), 135.8 (C-11;11'), 134.5 (C-1;5), 131.0 (C-3), 126.9 (C-15;15'), 116.9 (C-14;14'), 115.1 (C-12;12'), 96.4 (C-2;4), 91.5 (C-6), 18.3 ((CH₃C)-8;9), 13.7 (CH₃C-7).

5.2.6 2,4,6-Trimethyl-*N*¹,*N*³-bis(2-aminophenyl)benzene-1,3-diamine (**18**)



18

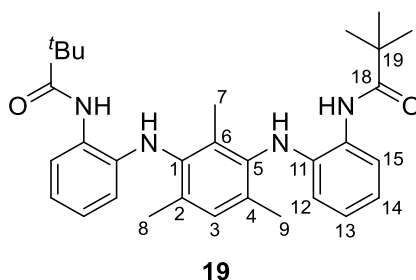
To a solution of 2.27 g **17** (5.78 mmol, 1.0 eq.) in 100 mL THF and 25 mL anhydrous MeOH are added 1.3 g Pd/C (10weight%) and H₂-gas is bubbled through the stirred suspension at room temperature for 6 h until the yellow-colored suspension turns colorless. The reaction mixture is filtered through a filter pad under argon and the solvent evaporated *in vacuo* to yield the product as a light yellow solid (1.92 g, 5.78 mmol, 99%).

R_f (SiO₂, hexane/EtOAc: 4/1): 0.71.

¹H-NMR (CDCl₃): δ = 7.05 (s, 1H, CH-3), 6.78 (dd, ³J = 7.5, ⁴J = 1.5, 2H, CH-15;15'), 6.74 (dd, ³J = 7.5, ³J = 7.4, 2H, CH-14;14'), 6.65 (dd, ³J = 7.8, ³J = 7.4, ⁴J = 1.5 2H, CH-13;13'), 6.25 (dd, ³J = 7.8, 2H, CH-12;12'), 4.87 (s, 2H, NH), 3.65 (s, 4H, NH₂), 2.16 (s, 6H, ((CH₃C)-8;9), 1.96 (s, 3H, ((CH₃C)-7).

¹³C-NMR (CDCl₃): δ = 140.4 (C-16;16'), 135.7 (C-11;11'), 130.4 (C-3), 123.1 (C-1;5), 120.5 (C-14;14'), 120.5 (C-3;3'), 116.5 (C-15;15'), 115.1 (C-12;12'), 96.4 (C-2;4), 91.5 (C-6), 18.1 ((CH₃C)-8;9), 13.7 (CH₃C-7).

5.2.7 2,4,6-Trimethyl-*N*¹,*N*³-bis(2-*N*-neopentylamidophenyl)benzene-1,3-diamine (**19**)



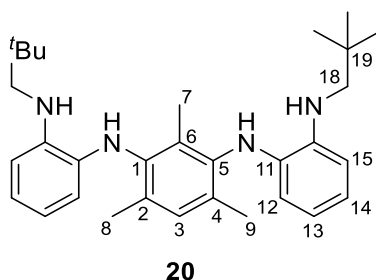
DMAP (141 mg, 1.67 mmol, 0.2 eq.) and 1.92 g **18** (5.77 mmol, 1.0 eq.) are dissolved in 20 mL pyridine. Pivaloyl chloride (1.71 mL, 13.9 mmol, 2.4 eq.) is added drop by drop to the resulting dark orange solution while stirring at 0 °C. After addition, the reaction solution is stirred for 24 h at room temperature. To the brownish solution is added 40 mL H₂O and the organic layer is extracted with DCM (3 × 10 mL). The combined organic phase is washed with 1 M HCl_{aq.} (2 × 10 mL) until the aqueous phase has a pH=1 (colored dark blue). The DCM phase is neutralized with 3 M NaOH_{aq.} (2 × 20 mL) and brine (2 × 200 mL). The combined organic layers are dried over MgSO₄ and reduced *in vacuo* giving the product as dark green solid (2.62 g, 5.28 mmol, 91%).

R_f (SiO₂, hexane/EtOAc/NEt₃: 4/2/0.1): 0.70.

¹H-NMR (CDCl₃): δ = 7.61 (s, 2H, CONH), 7.33 (d, ³J = 7.9, 2H, CH-15;15'), 7.02 (s, 1H, CH-3), 6.98 (dd, ³J = 8.1 ³J = 7.7, 2H, CH-13;13'), 6.82 (dd, ³J = 7.9, ³J = 7.7, 2H, CH-14;14'), 6.40 (dd, ³J = 8.1, 2H, CH-12;12'), 5.69 (s, 4H, NH₂), 2.17 (s, 6H, ((CH₃C)-8;9), 1.96 (s, 3H, ((CH₃C)-7), 1.36 (s, 18H, C(CH₃)₃)

¹³C-NMR (CDCl₃): δ = 177.7 (CONH), 140.3 (C-16;16'), 138.3 (C-11;11'), 130.4 (C-3), 126.8 (C-13;13'), 125.8 (C-1;5), 124.6 (C-15;15'), 119.9 (C-14;14'), 116.4 (C-12;12'), 107.9 (C-2;4), 102.9 (C-6), 39.7 (C(CH₃)₃), 28.0 (C(CH₃)₃), 18.3 ((CH₃C)-8;9), 13.5 (CH₃C-7).

5.2.8 2,4,6-Trimethyl-*N*¹,*N*³-bis(2-*N*-neopentylaminophenyl)-benzene-1,3-diamine (**20**)

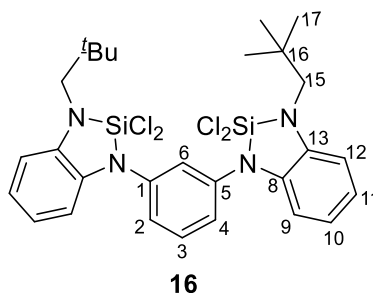


To a cooled solution of 2.12 g **19** (4.22 mmol, 1.0 eq.) in 50 mL THF are added 10.6 mL borane dimethyl sulfide (2 M in THF, 1.61 g, 21.2 mmol, 5.0 eq.) carefully. The resulting yellow solution is allowed to warm to room temperature and heated to reflux for 3 d. The solvent is removed in vacuo and the residue dissolved in 30 mL MeOH and 30 mL H₂O are added slowly. After addition of another 20 mL 3 M HCl the suspension is heated to 100 °C for 16 h resulting in a green suspension. The solid is separated off, dissolved in 3 M NaOH (20 mL) and extracted into diethyl ether (4 × 10 mL). The aqueous layer is extracted with DCM (2 × 100 mL) and the combined organic layers are washed with 1 M HCl (3 × 100 mL), 3 M NaOH_{aq.} (2 × 100 mL) and brine (2 × 50 mL) and dried over MgSO₄. The solvent is evaporated under reduced pressure giving a yellow solid which is dried *in vacuo* (0.91 g, 1.89 mmol, 45%).

¹H-NMR (CDCl₃): δ = 7.21-7.15 (m, 3H, CH-3, CH_{arom.}), 7.01 (t, ³J = 7.8, 2H, CH-13;13'), 6.90 (dt, ³J = 7.5, ⁴J = 3.8, 2H, CH-14;14'), 6.62 (t, ³J = 7.1, 2H, CH-15;15'), 3.67 (s, 4H, NH), 2.07 (s, 6H, CH-8;9), 1.69 (s, 3H, CH-7), 0.99 (s, 18H, C(CH₃)₃).

¹³C-NMR (CDCl₃): δ = 138.4 (C_{arom.}), 137.0 (C_{arom.}), 136.8 (C_{arom.}), 134.5 (C_{arom.}), 129.7 (C_{arom.}), 119.0 (C_{arom.}), 118.6 (C_{arom.}), 109.7 (C_{arom.}), 109.2 (C_{arom.}), 55.8 (CH₂), 33.9 (C(CH₃)₃), 28.4 (C(CH₃)₃), 18.1 (CH₃C), 13.4 (CH₃C).

5.2.9 N^1,N^3 -Bis((2,2-dichloro-3-neopentyl)benzimidazolin-2-silane)-1,3-diaminobenzene (**16**)



To a stirring solution of 140 mg **15** (325 μmol , 1.0 eq.) in 5 mL toluene are added 520 μL *n*-BuLi (2.5 M in hexane, 83.3 mg, 1.30 mmol, 4.0 eq.) dropwise at -78 $^{\circ}\text{C}$. The resulting mixture is allowed to warm to room temperature and stirred overnight. After cooling to 0 $^{\circ}\text{C}$, 90 μL SiCl_4 (132 mg, 780 μmol , 2.4 eq.) are added slowly and the solution stirred for 2 d at room temperature. The resulting suspension is filtered through a filter pad and concentrated *in vacuo*. The precipitated yellow residue is separated off, extracted into hexane and dried *in vacuo* giving the product as orange oil. Small amounts of side-products were still detected in the NMR spectrum, signals are therefore only assigned to the benzannulated backbone (arom.) and the phenylene bridge (phenyl). Yield has not been determined.

$^1\text{H-NMR}$ (C_6D_6): δ = 7.61 (t, 3J = 7.96, 1H, $\text{CH}_{\text{phenyl}}$), 7.45 (t, 3J = 2.12, 1H, $\text{CH}_{\text{phenyl}}$), 7.39 (d, 3J = 7.95, 2H, $\text{CH}_{\text{arom.}}$), 6.97 (d, 3J = 7.96, 2H, $\text{CH}_{\text{phenyl}}$), 6.81 (td, 3J = 7.54, 1.88, 2H, $\text{CH}_{\text{arom.}}$), 6.72 (m, 4H, $\text{CH}_{\text{arom.}}$), 3.39 (s, 4H, CH_2), 1.12 (s, 18H, CH_3).

$^{13}\text{C-NMR}$ (C_6D_6): δ = 141.1 (C_{phenyl}), 139.5 ($\text{C}_{\text{arom.}}$), 137.6 ($\text{C}_{\text{arom.}}$), 132.3 (C_{phenyl}), 125.7 (C_{phenyl}), 121.1 ($\text{C}_{\text{arom.}}$), 120.2 ($\text{C}_{\text{arom.}}$), 111.9 ($\text{C}_{\text{arom.}}$), 110.9 ($\text{C}_{\text{arom.}}$), 56.2 (CH_2), 34.5 ($\text{C}(\text{CH}_3)_3$), 29.3 ($\text{C}(\text{CH}_3)_3$).

INEPT- $^{29}\text{Si-NMR}$ (C_6D_6): δ = -27.63 (SiCl_2).

HRMS (LIFDI, toluene): m/z = 625.6582 [**16**] $^+$ (calc. $\text{C}_{28}\text{H}_{34}\text{N}_4\text{Si}_2\text{Cl}_4$: 624.1051).

Elemental analysis: calc. **16** (%): C 53.51, H 5.15, N 10.23; found: C 49.95, H 5.25, N 9.92.

5.2.10 Reduction of **16** in Presence of Isoprene

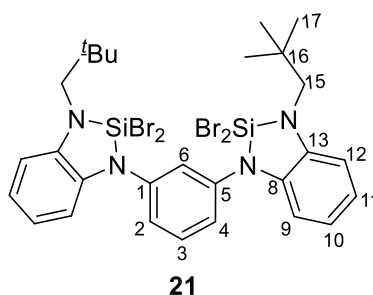
25.0 mg **16** (40.0 μmol , 1.0 eq.) and 40 μL isoprene (27.3 mg, 400 μmol , 10.0 eq.) are dissolved in 3 mL THF and cooled to -78 $^{\circ}\text{C}$ in an acetone/dry ice bath. Lithium naphthalide (534 mM in THF, 534 mM in THF, 300 μL , 21.5 mg, 4.0 eq.) is added dropwise over a period of 10 min until no discoloration of the

reagent can be observed while the reaction mixture turns orange. The reaction is allowed to warm to room temperature and stirred for 3 h. The solvent of the reaction mixture was removed *in vacuo* and extracted into deuterated THF.

INEPT-²⁹Si-NMR (THF-*d*₈): $\delta = 27.33$.

HRMS (LIFDI, THF): $m/z = 551.0280$ (calc. C₃₃H₄₀N₄Si₂: 550.2948), 619.1718 (calc. C₃₈H₅₀N₄Si₂: 618.3574).

5.2.11 *N*¹,*N*³-Bis((2,2-dibromo-3-neopentyl)benzimidazolin-2-silane)-1,3-diaminobenzene (**21**)



To a stirring solution of 200 mg **15** (464 μ mol, 1.0 eq.) and 208 mg DABCO (1.85 mmol, 4.0 eq.) in 6 mL toluene are added 186 μ L SiBr₄ (518 mg, 1.49 mmol, 3.2 eq.) dropwise at -78 °C. The resulting mixture is allowed to warm to room temperature and heated to reflux for 3 d. Afterwards, the orange suspension is filtered through a filter pad and the solvent evaporated *in vacuo*. The orange residue can be extracted into hexane and dried *in vacuo* giving the product as off-white solid (305 mg, 380 μ mol, 82%). Crystals suitable for X-ray analysis can be grown from a benzene solution at 0 °C.

¹H-NMR (C₆D₆): $\delta = 7.51$ (t, ⁴*J* = 2.1, 1H, CH-6), 7.26 (dd, ³*J* = 7.9, ⁴*J* = 2.1, 2H, CH-2;4), 7.09 (t, ³*J* = 8.0, 1H, CH-3), 6.85 – 6.77 (m, 6H, CH_{arom.}), 6.74 (ddd, ³*J* = 8.0, 6.8, ⁴*J* = 1.7, 2H, CH_{arom.}), 3.21 (s, 4H, CH₂), 0.99 (s, 18H, CH₃).

¹³C-NMR (C₆D₆): $\delta = 140.3$ (C-1;5), 139.3 (C-13;13'), 137.7 (C-8;8'), 131.5 (C-3), 126.7 (C-6), 125.7 (C-2;4), 120.4 (C_{arom.}), 119.9 (C_{arom.}), 111.4 (C_{arom.}), 110.8 (C_{arom.}), 56.1 (CH₂), 33.6 (C(CH₃)₃), 29.2 (C(CH₃)₃).

INEPT-²⁹Si-NMR (C₆D₆): $\delta = -46.45$ (SiBr₂).

¹H-NMR (THF-*d*₈): $\delta = 7.64$ (t, ³*J* = 8.0 Hz, 1H, CH-3), 7.51 (t, ⁴*J* = 2.1, 1H, CH-6), 7.45 (dd, ³*J* = 7.9, ⁴*J* = 2.1, 2H, CH-2;4), 7.02 – 6.97 (m, 2H, CH_{arom.}), 6.79 (ddd, ³*J* = 8.0, 6.2, ⁴*J* = 2.7, 2H, CH_{arom.}), 6.74 – 6.68 (m, 4H, CH_{arom.}), 3.41 (s, 4H, CH₂), 1.15 (s, 18H, CH₃).

¹H-NMR (THF-*d*₈, **24h)^a:** δ = 7.48 (t, ³J = 8.0 Hz, 1H, CH-3), 7.40 (t, ⁴J = 2.1, 1H, CH-6), 7.20 (dd, ³J = 8.0, ⁴J = 2.2, 2H, CH-2;4), 6.91 (dd, ³J = 7.7, ⁴J = 1.4, 2H, CH_{arom.}), 6.82 (dd, ³J = 7.8, ⁴J = 1.3, 2H, CH_{arom.}), 6.71 (ddd, ³J = 7.9, 5.7, ⁴J = 2.3, 2H, CH_{arom.}), 6.59 (dd, ³J = 7.7, ⁴J = 1.3, 2H, CH_{arom.}), 3.25 (s, 4H, CH₂), 1.08 (s, 18H, CH₃).

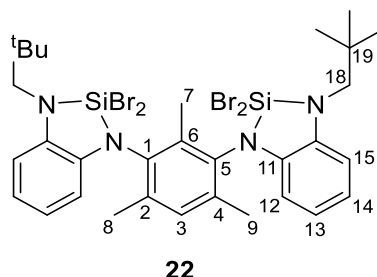
¹³C-NMR (THF-*d*₈, **24h):** δ = 143.70 (C_{arom.}), 140.36 (C_{arom.}), 136.73, (C_{arom.}), 131.71 (C_{arom.}), 121.63, (C_{arom.}), 121.59 (C_{arom.}), 120.10 (C_{arom.}), 118.40 (C_{arom.}), 110.46 (C_{arom.}), 110.08 (C_{arom.}), 56.21 (CH₂), 34.66 (C(CH₃)₃), 28.92 (C(CH₃)₃).

INEPT-²⁹Si-NMR (THF-*d*₈, **24h):** δ = -55.35 (SiBr₂).

HRMS (LIFDI, toluene): m/z = 803.1056 [**21**]⁺ (calc. C₂₈H₃₄N₄Si₂Br₄: 801.9019).

Elemental analysis: calcd. for **21 (%):** C 41.91, H 4.27, N 6.98; found: C 41.24, H 4.58, N 6.23.

5.2.12 2,4,6-Trimethyl-*N*¹,*N*³-Bis((2,2-dibromo-3-neopentyl)benzimidazolin-2-silane)-1,3-diaminobenzene (**22**)



To a stirring solution of 250 mg **20** (529 μ mol, 1.0 eq.) and 190 mg DABCO (2.12 mmol, 4.0 eq.) in 10 mL toluene are added 211 μ L SiBr₄ (588 mg, 1.69 mmol, 3.2 eq.) dropwise at -78 °C. The resulting mixture is allowed to warm to room temperature heated to reflux for 3 d. The resulting suspension is filtered through filter pad and the solvent evaporated *in vacuo* giving an orange oil. The residue can be extracted into hexane and dried *in vacuo* giving the product as orange oil (321 mg, 380 μ mol, 72%).

¹H-NMR (THF-*d*₈): δ = 7.24–7.22 (m, 3H, CH-3;12;12'), 6.95 (td, J = 7.7, 1.3 Hz, 1H, CH-13;13'), 6.84 (ddd, J = 7.8, ⁴J = 1.1, 2H, CH-14;14'), 6.56 (dd, ³J = 7.8, ⁴J = 1.2, 2H, CH-15;15'), 3.72 (d, 4H, CH-18;18'), 2.06 (s, 6H, CH-8;9), 1.69–1.67 (m, 3H, CH-7), 1.01–0.99 (m, 18H, CH₃).

¹³C-NMR (THF-*d*₈)^b: δ = 139.4; 139.4* (C_{arom.}), 138.2; 138.1* (C_{arom.}), 137.6; 137.6* (C_{arom.}), 135.4, 135.4* (C_{arom.}), 135.0; 134.9* (C_{arom.}), 130.7, 130.7* (C_{arom.}), 120.1; 120.1* (C_{arom.}), 119.8; 119.7* (C_{arom.}), 110.9;

^a NMR measured after 24 h.

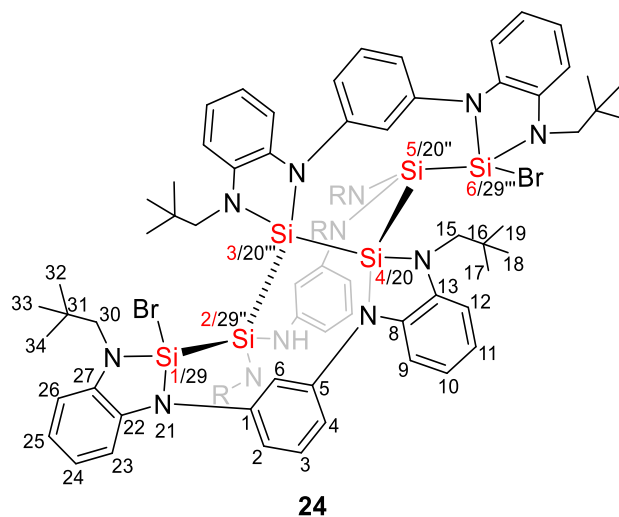
^b ¹³C NMR signals of second conformer are marked with a *.

110.9* ($C_{arom.}$), 110.5; 110.3* ($C_{arom.}$), 56.3 (CH_2), 34.6 ($C(CH_3)_3$), 28.71 ($C(CH_3)_3$), 18.3 (C-8;9), 13.57; 13.5* (C-7).

INEPT- ^{29}Si -NMR (THF- d_8): $\delta = -40.28$ (SiBr $_2$).^a

HRMS (LIFDI, toluene): $m/z = 844.8578$ [**22**]⁺ (calc. $C_{28}H_{34}N_4Si_2Br_4$: 843.9488).

5.2.13 [$C_{28}H_{34}N_4Si_2$] $_3Br_2$ (**24**)



For the synthesis of **24**, 50.0 mg **21** (62.4 μ mol, 1.0 eq.) and 30.1 mg KC_8 (229 μ mol, 3.7 eq.) are mixed and cooled in an acetone/dry ice bath. *Via* a pre-cooled, dry cannula are added 5 mL of cold DME. The reaction mixture is allowed to warm to -37 °C and stirred at this temperature for 3 d. The reaction mixture is filtered through a filter pad at cold temperatures giving an intensively red-colored solution. The solvent is evaporated *in vacuo* and the residue extracted into hexane (3 \times 3 mL). The solution is concentrated to 2 mL and stored in the freezer for 7 d resulting in a red microcrystalline precipitate (15.1 mg, 9.4 μ mol, 45%). Suitable crystals for X-ray analysis can be grown from a concentrated solution in hexane at 4 °C.

1H -NMR (THF- d_8):^b $\delta = 7.33$ – 7.31 (m, 4H, $CH_{arom.}$), 6.98–6.95 (m, 4H, $CH_{arom.}$), 6.94–6.83 (m, 6H, $CH_{arom.}$), 6.77–6.72 (m, 6H^c, $CH_{arom.}$), 6.70–6.68 (m, 2H, $CH_{arom.}$), 6.67–6.63 (m, 4H, $CH_{arom.}$), 6.63–6.57 (m, 3H, $CH_{arom.}$), 6.49–6.41 (m, 4H, $CH_{arom.}$), 6.12 (dd, $^3J = 7.9$, $^4J = 2.1$, 2H, CH -2'';4''), 6.02 (dd, $^3J = 8.5$, 7.4, 1H, CH -3''), 3.53 (d, $^2J = 14.5$, 2H, CH_2 -15';15'''), 3.12 (d, $^2J = 14.5$, 2H, CH_2 -15';15'''), 3.06 (s, 4H, CH_2 -

^a The product still contained impurities which could not be assigned.

^b Signals have been assigned by referencing to the three bissilane units as indicated by superscripted bars.

^c Signal contains impurities

30';30'''), 2.97 (s, 4H, CH-15'';30''), 1.10 (s, 18H, (CH₃-32;33;34)';(CH₃-32;33;34)'''), 0.90 (s, 36H, (CH₃-17;18;19)';(CH₃-17;18;19;32;33;34)''';(CH₃-17;18;19)''').

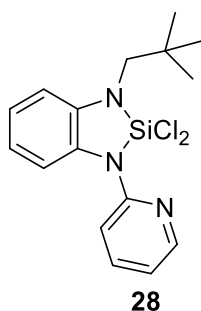
¹³C-NMR (THF-*d*₈): δ = 144.3 (*C*_{arom.}), 143.8 (*C*_{arom.}), 142.0 (*C*_{arom.}), 140.9 (*C*_{arom.}), 140.7 (*C*_{arom.}), 139.3 (*C*_{arom.}), 137.2 (*C*_{arom.}), 136.4 (*C*_{arom.}), 134.4 (*C*_{arom.}), 131.0 (*C*_{arom.}), 130.0 (*C*-2;4), 120.1 (*C*_{arom.}), 119.7 (*C*_{arom.}), 119.4 (*C*_{arom.}), 119.4 (*C*_{arom.}), 119.3 (*C*_{arom.}), 118.6 (*C*_{arom.}), 118.4 (*C*_{arom.}), 118.1 (*C*_{arom.}), 116.4 (*C*_{arom.}), 116.4 (*C*_{arom.}), 115.4 (*C*-3), 112.8 (*C*_{arom.}), 112.1 (*C*_{arom.}), 111.4 (*C*_{arom.}), 110.9 (*C*_{arom.}), 110.4 (*C*_{arom.}), 109.6 (*C*_{arom.}), 62.5 (*C*-30;30'), 58.0 (*C*-15;15'), 55.0 (*C*-38;38'), 34.5 (C(CH₃)₃), 34.2 (C(CH₃)₃), 34.0 (C(CH₃)₃), 30.2 (C(CH₃)₃), 29.8 (C(CH₃)₃), 29.1 (C(CH₃)₃).

INEPT-²⁹Si-NMR (THF-*d*₈): δ = -1.55 (*Si*-1;6), -9.42 (*Si*-2;5), -20.57 (*Si*-3;4).

HRMS (LIFDI, toluene): m/z = 1608.1533 [24]⁺ (calc. C₈₄H₁₀₂N₁₂Si₆Br₂: 1608.5331).

Elemental analysis: calcd. for 24·1.9(KBr·THF) (%): C 55.66, H 5.98, N 8.49; found: C55.27 H 6.32, N 8.21.

5.2.14 2,2-Dichloro-*N,N'*-neopentyl(pyridin-2-yl)benzimidazolin-2-silane (**28**)



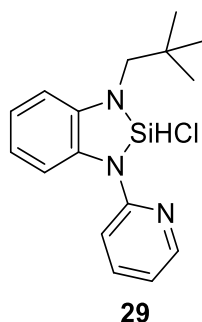
The diamine **26** (187 mg, 732 μ mol, 1.0 eq.) is dissolved in 5 mL toluene and cooled to -90 °C in an acetone/dry ice bath. *n*-BuLi (2.5 M in hexane, 586 μ L, 93.8 mg, 1.46 mmol, 2.0 eq.) is added dropwise to give a light yellow solution. The reaction mixture turns orange when allowed to warm to room temperature and is stirred for 3 h. After cooling to -90 °C SiCl₄ (252 μ L, 2.20 mmol, 3.0 eq.) is added slowly and the reaction mixture is allowed to warm to room temperature over a period of 1 h. The reaction mixture is stirred for 24 h at room temperature to give an orange suspension which is filtered and evaporated to dryness *in vacuo*. The residue is washed with hexane (1 mL) and extracted into warm hexane (3 \times 3 mL) and filtered. The concentrated yellow solution is stored at -32 °C for 48 h to give a light yellow crystalline solid which is separated off and dried *in vacuo* (157 mg, 447 μ mol, 61%).

¹H-NMR (C₆D₆): δ = 8.16 (dt, ³J = 5.1, ⁴J = 1.4, 1H, CH_{pyr.}), 7.24 (dd, ³J = 7.9, ⁴J = 1.3, 1H, CH_{arom.}), 6.99-6.92 (m, 3H, CH_{arom.}), 6.85 (d, ³J = 8.1, 1H, CH_{arom.}), 6.79 (t, ³J = 7.7, 1H, CH_{arom.}) 6.37 (dd, ³J = 4.4, 1H, CH_{pyr.}), 3.23 (s, 2H, CH₂), 0.99 (s, 9H, CH₃).

¹³C-NMR (C₆D₆): δ = 153.8 (C_{arom.}), 148.3 (C_{arom.}), 140.5 (C_{arom.}), 138.6 (C_{arom.}), 131.7 (C_{arom.}), 121.6 (C_{arom.}), 118.9 (C_{arom.}), 118.2 (C_{arom.}), 111.9 (C_{arom.}), 111.7 (C_{arom.}), 111.5 (C_{arom.}), 55.4 (CH₂), 33.7 (C(CH₃)₃), 29.2 (C(CH₃)₃).

²⁹Si NMR (C₆D₆): δ = -29.09.

5.2.15 2,2-Hydrochloro-*N,N'*-neopentyl(pyridin-2-yl)benzimidazolin-2-silane (**29**)

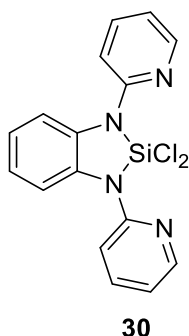


150 mg of the diamine **26** (587 μ mol, 1.0 eq.) and 182 mg DIPEA (244 μ L, 1.41 mmol, 2.4 eq.) are dissolved in 5 mL benzene. At 0 °C 65.3 μ L HSiCl₃ (87.5 mg, 646 μ mol, 1.1 eq.) are added dropwise to give a green solution which turns yellow when allowed to warm to room temperature. The resulting suspension is stirred for 16 h at room temperature after which the solvent is evaporated *in vacuo*. The product is extracted into hexane (3 \times 2.5 mL) which is filtered and stored at -32 °C to give a light yellow crystalline solid (103 mg, 323 μ mol, 55%).

¹H-NMR (C₆D₆): δ = 8.05 (ddd, ³J = 5.1, ⁴J = 1.8, ⁴J = 1.0, 1H, CH_{pyr.}), 7.24 (dd, ³J = 7.7, ⁴J = 1.3, 1H, CH_{arom.}), 7.04-6.99 (m, 1H, CH_{arom.}), 6.99-6.95 (m, 2H, CH_{arom.}), 6.86-6.79 (m, 2H, CH_{arom.}), 6.62 (s, 1H, SiHCl) 6.33 (d, ³J = 6.6, ³J = 4.9, ⁴J = 1.4, 1H, CH_{pyr.}), 3.22-3.12 (m, 2H, CH₂), 0.88 (s, 9H, CH₃).

¹³C-NMR (C₆D₆): δ = 155.1 (C_{arom.}), 147.9 (C_{arom.}), 142.6 (C_{arom.}), 138.8 (C_{arom.}), 130.9 (C_{arom.}), 121.6 (C_{arom.}), 117.9 (C_{arom.}), 116.7 (C_{arom.}), 112.3 (C_{arom.}), 110.6 (C_{arom.}), 109.4 (C_{arom.}), 54.2 (CH₂), 34.4 (C(CH₃)₃), 28.5 (C(CH₃)₃).

²⁹Si NMR (C₆D₆): δ = -28.21.

5.2.16 2,2-Dichloro-*N,N'*-bis(pyridin-2-yl)benzimidazolin-2-silane (**30**)

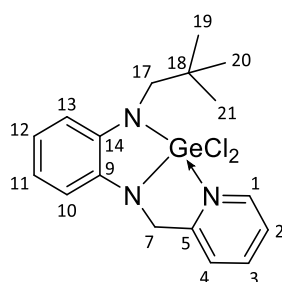
The diamine **27** (350 mg, 1.33 mol, 1.0 eq.) is partly dissolved in 15 mL toluene and cooled to $-90\text{ }^{\circ}\text{C}$ in an acetone/dry ice bath. *n*-BuLi (2.5 M in hexane, 1.1 mL, 175 mg, 2.74 mmol, 2.05 eq.) is added dropwise to give a light yellow solution. The reaction mixture turns green when allowed to warm to room temperature and is stirred for 24 h. After cooling to $-90\text{ }^{\circ}\text{C}$ SiCl_4 (148 μL , 1.47 mmol, 1.1 eq.) is added slowly and the reaction mixture is allowed to warm to room temperature over a period of 1 h. The reaction mixture is stirred for 3 d at room temperature to give a yellow suspension which is filtered and concentrated *in vacuo* to give an off-white precipitate. The solid is separated off, washed with hexane ($2 \times 1\text{ mL}$) dried *in vacuo* (371 mg, 1.04 mmol, 78%)

$^1\text{H-NMR}$ (C_6D_6): $\delta = 8.18$ (dt, $^3J = 4.8$, $^4J = 1.5$, 1H, $\text{CH}_{\text{arom.}}$), 7.92 (dd, $^3J = 5.9$, $^4J = 3.4$, 1H, $\text{CH}_{\text{arom.}}$), 7.87 (ddd, $^3J = 4.9$, $^4J = 2.0$, $^5J = 0.9$, 1H, $\text{CH}_{\text{arom.}}$), 7.30 (dd, $^3J = 5.9$, $^4J = 3.4$, 1H, $\text{CH}_{\text{arom.}}$), 7.11 (dd, $^3J = 8.3$, $^4J = 1.0$, 1H, $\text{CH}_{\text{arom.}}$), 7.06 (dd, $^3J = 6.0$, $^4J = 3.4$, 1H, $\text{CH}_{\text{arom.}}$), 7.02-6.97 (m, 2H, $\text{CH}_{\text{arom.}}$), 6.85 (dd, $^3J = 6.0$, $^4J = 3.3$, 1H, $\text{CH}_{\text{arom.}}$), 6.78 (ddd, $^3J = 8.3$, 7.3, $^4J = 2.0$, 1H, $\text{CH}_{\text{arom.}}$), 6.38 (ddd, $^3J = 6.3$, 4.9, $^4J = 2.1$, 1H, $\text{CH}_{\text{arom.}}$), 6.16 (ddd, $^3J = 7.3$, $^4J = 4.8$, $^5J = 0.9$, 1H, $\text{CH}_{\text{arom.}}$).

$^{13}\text{C-NMR}$ (C_6D_6): $\delta = 155.2$ ($\text{C}_{\text{arom.}}$), 154.0 ($\text{C}_{\text{arom.}}$), 148.7 ($\text{C}_{\text{arom.}}$), 148.3 ($\text{C}_{\text{arom.}}$), 138.3 ($\text{C}_{\text{arom.}}$), 137.6 ($\text{C}_{\text{arom.}}$), 134.1 ($\text{C}_{\text{arom.}}$), 133.3 ($\text{C}_{\text{arom.}}$), 121.2 ($\text{C}_{\text{arom.}}$), 121.1 ($\text{C}_{\text{arom.}}$), 118.3 ($\text{C}_{\text{arom.}}$), 117.5 ($\text{C}_{\text{arom.}}$), 114.5 ($\text{C}_{\text{arom.}}$), 113.1 ($\text{C}_{\text{arom.}}$), 113.1 ($\text{C}_{\text{arom.}}$), 112.2 ($\text{C}_{\text{arom.}}$).

$^{29}\text{Si NMR}$ (C_6D_6): $\delta = -36.86$.

5.2.17 2,2-Dichloro-*N,N'*-neopentyl(pyridin-2-ylmethyl)benzimidazolin-2-germane (**32**)

**32**

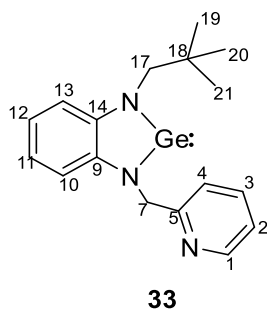
The diamine **31** (912 mg, 3.39 mmol, 1.0 eq.) and DABCO (399 mg, 3.55 mmol, 1.1 eq.) are dissolved in 15 mL THF. GeCl_4 (402 μl , 755 mg, 3.52 mmol, 1.1 eq.) is added, upon which a bright yellow suspension forms immediately. The reaction is stirred for 20 h at room temperature, filtered through a filter pad and reduced to approximately 6 mL. 12 mL of pentane are added and the solution is stored at -30°C . After 1 d, a large quantity of green crystals, suitable for single crystal X-ray diffraction, has formed. The crystals are filtered off, washed with pentane (2×5 mL) and dried *in vacuo*. The product is isolated as a green crystalline solid (1.12 g, 2.73 mmol, 81%).

$^1\text{H-NMR}$ (C_6D_6): δ = 8.63 (dt, 3J = 5.6, 4J = 1.4, 1H, CH-1), 7.14 – 7.03 (m, 2H, CH-12;13), 6.96 (td, 3J = 7.6, 4J = 1.4, 1H, CH-11), 6.65 (td, 3J = 7.6, 4J = 1.4, 1H, CH-3), 6.54 (dd, 3J = 7.6, 4J = 1.3, 1H, CH-10), 6.38 (ddd, 3J = 7.3, 5.6, 4J = 1.2, 1H, CH-2), 6.02 (dt, 3J = 7.6, 1H, CH-4), 3.89 (br, 2H, CH-17), 3.75 (s, 2H, CH-7), 1.34 (s, 9H, CH-19;20;21).

$^{13}\text{C-NMR}$ (C_6D_6): δ = 150.7 (C-5), 143.5 (C-1), 141.2 (C-9), 139.1 (C-3), 133.6 (C-14), 123.7 (C-2), 122.0 (C-4), 119.2 (C-12), 116.1 (C-11), 109.3 (C-13), 108.6 (C-10), 57.4 (C-17), 44.3 (C-7), 34.3 (C-18), 30.2 (C-19-21).

HRMS (LIFDI, toluene): m/z = 411.0242 [**32**] $^+$ (calc. $\text{C}_{17}\text{H}_{21}\text{N}_3\text{GeCl}_2$: 411.04320).

Elemental analysis: calc. **32** (%): C 49.69, H 5.15, N 10.23; found: C 49.95, H 5.25, N 9.92.

5.2.18 *N,N'*-Neopentyl(pyridin-2-ylmethyl)benzimidazolin-2-germylene (**33**)

To a mixture of compound **32** (224 mg, 545 μmol , 1.0 equiv.) and KC_8 (147 mg, 1.09 mmol, 2.0 equiv.) are added 10 mL of THF at $-78\text{ }^\circ\text{C}$. The suspension turns yellow when allowed to warm to room temperature and is stirred for another 20 h. The resulting suspension is filtered, evaporated to dryness, dissolved in 2 mL diethyl ether and filtered again. The solution is stored at $-32\text{ }^\circ\text{C}$ for 24 h, after which a large amount of solid, containing crystals, suitable for single crystal X-ray diffraction analysis, has formed. The crystals are filtered off, washed with pentane ($2 \times 5\text{ mL}$) and dried *in vacuo*. The product is isolated as a yellow crystalline solid (128 mg, 376 μmol , 69%).

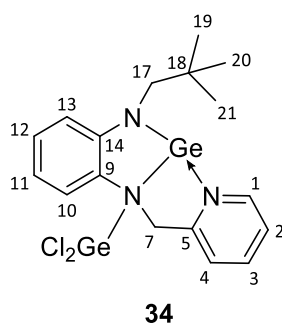
$^1\text{H-NMR}$ (C_6D_6): $\delta = 8.47$ (ddd, $^3J = 4.9$, $^4J = 1.8$, $^5J = 0.9$, 1H, CH-1), 7.10 – 6.99 (m, 3H, CH-10;11;12), 6.96 – 6.90 (m, 1H, CH-13), 6.87 (td, $^3J = 7.7$, $^4J = 1.8$, 1H, CH-3), 6.76 (d, $^3J = 7.7$, 1H, CH-4), 6.54 (ddd, $^3J = 7.7$, 4.9, $^4J = 1.3$, 1H, CH-2), 5.29 (s, 2H, CH-7), 3.74 (s, 2H, CH-17), 0.87 (s, 9H, CH-19;20;21).

$^{13}\text{C-NMR}$ (C_6D_6): $\delta = 160.2$ (C-5), 149.5 (C-1), 144.1 (C-14), 142.1 (C-9), 136.3 (C-3), 121.9 (C-2), 121.1 (C-4), 118.6 (C-10/13), 118.2 (C-10/13), 110.6 (C-11/12), 110.5 (C-11/12), 56.8 (C-17), 52.0 (C-7), 33.0 (C-18), 28.6 (C-19;20;21).

HRMS (LIFDI, toluene): $m/z = 341.0976$ [**33** $^+$] (calcd. for $\text{C}_{17}\text{H}_{21}\text{N}_3\text{Ge}$: 341.0950).

Elemental analysis: calcd. for **33** (%): C 60.05, H 6.23, N 12.36; found: C 59.77, H 6.30, N 12.28.

5.2.19 *N*-Dichlorogermylene-*N,N'*-neopentyl(pyridin-2-ylmethyl)-benzimidazolin-2-germylene (**34**)

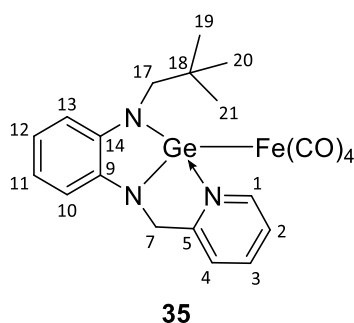


Germylene **33** (50.0 mg, 147 μmol , 1.0 eq.) is dissolved in 3 mL THF together with 34 mg GeCl_2 -dioxane (147 μmol , 1.0 eq.) and stirred overnight. The still yellow solution is filtered through a filter pad and layered with hexane. After several days, yellow crystals suitable for single crystal X-ray diffraction can be grown. The yield can be increased by precipitating the product with 5 mL diethyl ether (40.1 mg, 83 μmol , 57%). The product was not detectable *via* LIFDI MS, elemental analysis still contained impurities. The Product was not detectable *via* LIFDI MS.

$^1\text{H-NMR}$ (C_6D_6): δ = 8.70 (d, 3J = 4.2, 1H, CH-1), 7.82 (t, 3J = 7.7, 1H, CH-3), 7.43 – 7.36 (m, 2H, CH-2;4), 7.00 (d, 3J = 7.8, 1H, CH-10), 6.92 (d, 3J = 8.1, 1H, CH-12), 6.86 (t, 3J = 7.6; 1H, CH-12), 6.62 (t, 3J = 7.5, 1H, CH-11), 5.43 (s, 2H, CH-7), 3.77 (s, 2H, CH-17), 1.03 (s, 9H, $\text{C}(\text{CH}_3)_3$).

$^{13}\text{C-NMR}$ (C_6D_6): δ = 159.4 (C-5), 147.9 (C-1), 140.5 (C-3), 140.0 (C-9;14), 124.8 (C-2/4), 123.9 (C-2/4), 122.7 (C-13), 117.5 (C-11), 115.6 (C-10), 111.5 (C-12), 56.9 (C-17), 54.3 (C-7), 34.3 ($\text{C}(\text{CH}_3)_3$), 29.0 ($\text{C}(\text{CH}_3)_3$).

5.2.20 *N,N'*-Neopentyl(pyridin-2-ylmethyl)benzimidazolin-2-germylene[iron tetracarbonyl] (**35**)



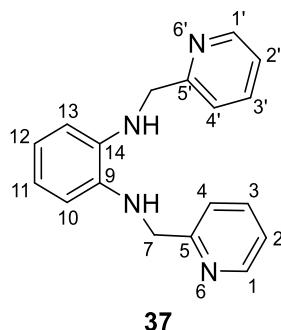
The germylene **33** (200 mg, 588 μmol , 1.0 eq.) and Fe_2CO_9 (214mg, 588 μmol , 1.0 equiv.) are dissolved in 10 mL THF and stirred overnight. The dark orange solution is filtered, reduced to 3 mL and layered with diethyl ether. Storage at -30°C for 2 d yields an orange crystalline solid, suitable for single crystal X-ray diffraction, which is washed with hexane and dried under vacuum (233mg, 459 μmol , 78%).

$^1\text{H-NMR}$ (C_6D_6): δ = 8.19 (dt, 3J = 5.5, 4J = 1.9, 1H, CH-1), 6.94 – 6.78 (m, 4H, CH-10;11;12;13), 6.46 (td, 3J = 7.6, 4J = 1.5, 1H, CH-3), 6.18 – 6.08 (m, 2H, CH-2;4), 4.67 (s, 2H, CH-7), 3.77 (s, 2H, CH-17), 1.07 (s, 9H, $\text{C}(\text{CH}_3)_3$).

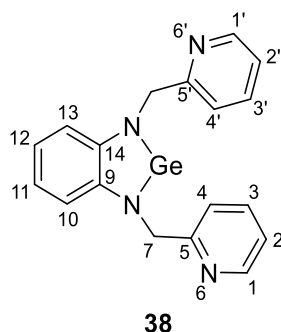
$^{13}\text{C-NMR}$ (C_6D_6): δ = 214.3 (CO), 155.3 (C-5), 144.3 (C-9), 143.9 (C-14), 143.7 (C-1), 140.3 (C-3), 124.1 (C-2), 122.1 (C-4), 120.1 ($\text{C}_{\text{arom.}}$), 117.9 ($\text{C}_{\text{arom.}}$), 114.2 ($\text{C}_{\text{arom.}}$), 110.3 ($\text{C}_{\text{arom.}}$), 55.4 (C-7/17), 55.4 (C-7/17), 34.1 ($\text{C}(\text{CH}_3)_3$), 29.0 ($\text{C}(\text{CH}_3)_3$).

HRMS (LIFDI, THF): m/z =508.5164 [**35** $^+$] (calcd. for $\text{C}_{21}\text{H}_{21}\text{O}_4\text{N}_3\text{GeFe}$: 509.0099).

Elemental analysis: calcd. for **35** (%): C 49.66, H 4.17, N 8.27; found: C 50.09, H 4.32, N 7.93.

5.2.21 *N,N'*-Di(pyridin-2-ylmethyl)-1,2-diaminobenzene (**37**)

In an adjusted procedure according to *Florián et al.*³²⁵ 10.0 g **37** (31.4 mmol, 1.0 eq.) are dissolved in 50.0 mL THF, cooled to 0 °C and 64.4 mL borane dimethyl sulfide (2 M in THF, 9.78 g, 129 mmol, 4.1 eq.) are added slowly. The suspension is heated to reflux for 2 d after which the reaction is stopped by addition of 20 mL MeOH and 20 mL 1 M HCl (slow, cooling bath!). The red solution is heated to reflux for 3 h. At room temperature NaOH_{aq.} 3 M is added until pH = 10. The organic layer is extracted with DCM (3 × 30 mL), washed with brine (2 × 20 mL) and dried over MgSO₄. After evaporation of the solvent under reduced pressure, the crude product (red oil) can be purified by flash chromatography (EtOAc/hexane: gradient from 0.3 to 0.7). After evaporation of the solvent and drying *in vacuo* the product can be isolated as grey solid (2.1 g, 7.22 mmol, 46%).

5.2.22 *N,N'*-Di(pyridin-2-ylmethyl)benzimidazolin-2-germylene (**38**)

702 mg of **37** (2.42 mmol, 1.0 eq.) are dissolved in 10 mL THF and a solution of Ge[N(SiMe₃)₂]₂ (952 mg, 2.42 mmol, 1.0 eq.) in 2 mL THF is added slowly. The reaction mixture is heated to reflux for 3 d after which the solvent is removed *in vacuo* (10⁻⁸ bar). The crude product can be purified by distillation in high vacuum at 250 °C. Crystals suitable for X-ray analysis can be grown from a THF solution at -32 °C. Exact yield has not been determined due to the high viscosity of the highly sensitive compound. Estimated yield 80% based on reused quantities (697 mg, 1.94 mmol).

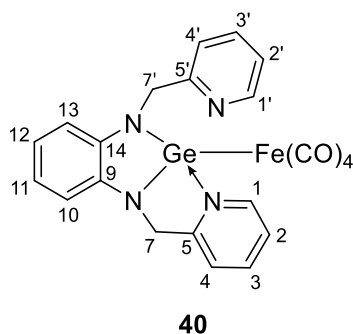
¹H-NMR (THF-d₈): δ = 8.53 (dd, ³J = 4.8, ⁴J = 1.7, 2H, CH-1;1'), 7.52 (td, ³J = 7.7, ⁴J = 1.8, 2H, CH-2;2'), 7.21 – 7.11 (m, 4H, CH-3;3';4;4'), 6.87 (m, 2H, CH-10;13), 6.73 – 6.67 (m, 2H, CH-11;12), 5.35 (s, 4H, CH-7;7').

¹³C-NMR (THF-d₈): δ = 161.2 (C-5;5'), 150.3 (C-1;1'), 143.8 (C-9;14), 137.6 (C-2;2'), 123.1 (C-4;4'), 122.3 (C-4;4'), 119.1 (C-11;12), 110.8 (C-10;13), 52.7 (C-7;7').

HRMS (LIFDI, THF): m/z = 361.9556 [**38**]⁺ (calcd. C₁₈H₁₆N₄Ge: 362.0590).

Elemental analysis: calcd. for 38 (%): C 59.89, H 4.47, N 15.52; found: C 59.43, H 4.78, N 15.54.

5.2.23 *N,N'*-Di(pyridin-2-ylmethyl)benzimidazolin-2-germylene[irontetracarbonyl] (**40**)



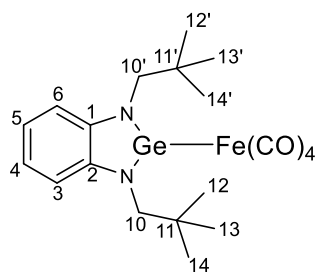
Diiron pentacarbonyl (24.1 mg, 66.5 μ mol, 1.2 eq.) is added to a solution of **38** (20.0 mg, 55.4 μ mol, 1.0 eq.) in 3 mL in toluene. The resulting dark orange suspension is stirred for 24 h at room temperature. The reaction mixture is filtered through a filter pad and the product precipitated by addition of hexane. The product can be isolated in form of a red, highly sensitive powder after filtration and drying *in vacuo*. (122.3 mg, 23.2 μ mol, 42%) Crystals suitable for X-ray analysis can be grown from the filtrate diluted in diethyl ether at -30°C . Impurities detected in the EA have not been assigned but likely arise from free ligand **38**.

¹H-NMR (THF-d₈): δ = 8.51 (d, ³J = 5.2, 2H, CH-1;1'), 6.84 (dd, ³J = 5.8, ³J = 3.3, 2H, CH-4;4'), 6.75 (s, 4H, CH-2;2';3;3'), 6.45 (d, ³J = 7.8, 2H, CH-10;13), 6.42 – 6.38 (m, 2H, CH-11;12), 4.79 (s, 4H, CH-7;7').

¹³C-NMR (THF-d₈): δ = 214.6 (CO), 156.9 (C-5;5'), 146.1 (C-1;1'), 142.9 (C-2), 138.1 (C-1), 122.6 (C-11;12), 122.0 (C-10;13), 118.6 (C-4;4'), 110.7 (C-2;2';3;3'), 51.6 (C-7;7').

HRMS (LIFDI, THF): m/z = 529.8566 [**40**]⁺ (calcd. for C₂₂H₁₆O₄N₄GeFe: 529.9738).

Elemental analysis: calcd. for 40 (%): C 49.96, H 3.08, N 10.59; found: C 52.32, H 3.49, N 10.81.

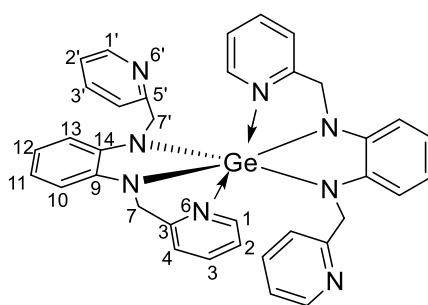
5.2.24 *N,N'*-Di(neopentyl)benzimidazolin-2-germylene[iron tetracarbonyl] (**41**)**41**

Diiron pentacarbonyl (20.5 mg, 56.4 μmol , 1.2 eq.) is added to a solution of **39** (15.0 mg, 47.4 μmol , 1.0 eq.) in 3 mL in THF and the reaction mixture is stirred for 24 h. After filtration, the clear yellow solution is concentrated *in vacuo* and the product precipitated by addition of hexane as brownish solid. Crystals suitable for X-ray diffraction analyses can be grown from the mother liquor at $-30\text{ }^\circ\text{C}$. Yield has not been determined as the product is still contaminated with side-products ($(\text{NeoGe})_2\text{Fe}(\text{CO})_3$).

$^1\text{H-NMR}$ (THF- d_8): δ = 8.01 (m, 4H, $\text{CH}_{\text{arom.}}$), 3.92 (s, 4H, $\text{CH-10;10}'$), 1.06 (s, 18H, $\text{C}(\text{CH}_3)_3$).

$^{13}\text{C-NMR}$ (THF- d_8): δ = 211.8 (CO), 142.2 (C-1;2), 118.1 (C-3;6), 110.0 (C-4;5), 55.7 (C-10;10'), 34.6 (C-11;11'), 29.0 ($\text{C}(\text{CH}_3)_3$).

HRMS (LIFDI, THF): m/z = 488.2829 [**41** $^+$] (calcd. for $\text{C}_{20}\text{H}_{26}\text{GeN}_2\text{FeO}_4$: 488.0459).

5.2.25 Bis[*N,N'*-di(pyridin-2-ylmethyl)benzimidazolin]-2-germane (**42**)**42**

To a solution of **38** (20.0 mg, 55.4 μmol , 1.0 eq.) in 3 mL THF GeCl_2 -dioxane (12.8 mg, 55.4 μmol , 1.0 eq.) is added slowly. The resulting orange suspension is stirred for 24 h at room temperature after which the precipitate can be filtered off and washed with 1 mL THF. The solution is stored at $-30\text{ }^\circ\text{C}$ for 2 days. Orange crystals, suitable for X-ray diffraction analysis, form, which can be separated off and dried *in vacuo* (12.6 mg, 19.4 μmol , 35%). The remaining precipitate was only soluble in pyridine partially and has not been fully characterized so far.

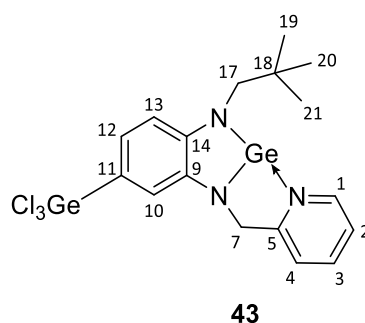
¹H-NMR (THF-d₈): δ = 8.03 (d, ³J = 5.1, 4H, CH-1;1'), 7.39 (td, ³J = 7.7, ⁴J = 1.8, 4H, CH-2;2') 6.98 (dd, ³J = 7.4, 5.1, 4H, CH-4;4'), 6.90 (d, ³J = 7.9, 4H, CH-3;3'), 6.33 (dd, ³J = 5.5, 3.3, 4H, CH-10;13), 6.20 (dd, ³J = 5.4, 3.4, 4H, CH-11;12); 4.49 (s, 8H, 7;7').

¹³C-NMR (THF-d₈): δ = 146.4 (C-1;1'), 140.1 (C-5;5'), 137.9 (C-9;14), 122.8, 122.7 (C-3;3'), 116.3 (C-4/4'), 105.8 (C-4/4'), 49.7 (C-7;7').

HRMS (LIFDI, THF): m/z =650.1086 [**42**⁺] (calcd. for C₃₆H₃₂GeN₈: 650.1970).

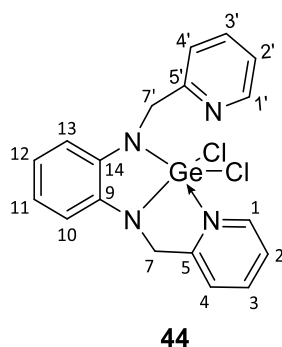
Elemental analysis: calcd. for 42·2 DME (%): C 63.10, H 6.18, N 12.26; found: C 62.6, H 6.7, N 10.97.

5.2.26 *N,N'*-Neopentyl(pyridin-2-ylmethyl)-4-trichlorgerman-benzimidazolin-2-germylene (**43**)



To a stirred solution of **33** (50.0 mg, 147 μ mol, 1.0 eq.) in 5 mL THF are added 16.8 μ L GeCl₄ (31.5 mg, 147 μ mol, 1.0 eq.) slowly at 0 °C giving a yellow solution. The reaction mixture is allowed to warm to room temperature and stirred for 3 d until full conversion is reached. The yellow suspension is filtrated, concentrated *in vacuo* and diluted with 2 mL hexane. The solution is stored at –32 °C for 48 h, after which crystals, suitable for single crystal X-ray diffraction, are formed. The crystals are filtered off, washed with pentane (2 \times 5 ml) and dried *in vacuo*. The product is isolated as a yellow crystalline solid. Conversion was observed only *via* LIFDI-MS.

HRMS (LIFDI, THF): m/z = 588.0911 [**43**⁺] (calcd. for C₁₇H₂₀N₄Ge₂Cl₅: 588.8501).

5.2.27 2,2-Dichloro-*N,N'*-di(pyridin-2-ylmethyl)benzimidazolin-2-germane (**44**)

To a stirred solution of **44** (40.0 mg, 111 μ mol, 1.0 eq.) in 2 mL THF are added 12.7 μ L GeCl_4 (23.8 mg, 111 μ mol, 1.1 eq.) slowly at 0 °C giving a yellow solution. The reaction mixture is allowed to warm to room temperature and stirred for 16 h giving a yellow suspension. The reaction mixture is filtrated, concentrated *in vacuo* and diluted with diethyl ether. After storage at -32 °C for 48 h a crystalline solid has formed, which is separated off, rinsed with pentane and dried *in vacuo* to yield the product as yellow solid. Crystals, suitable for X-ray diffraction analysis, can be grown from the mother liquor at -32 °C (19.6 mg, 44.3 μ mol, 41%).

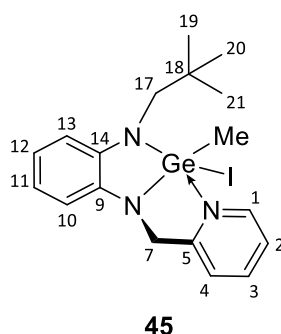
$^1\text{H-NMR}$ (CD_2Cl_2): δ = 8.81 (d, 3J = 5.4, 2H, CH-1;1'), 7.89 (s, 2H, CH-2;2'), 7.53 (d, 4H, 3J = 8.0, 2H, CH-4;4'), 7.47 (d, 3J = 6.5, 2H, CH-3;3'), 6.72 – 6.55 (m, 2H, CH-10;13), 6.52 (s, 2H, CH-11;12'), 4.92 (s, 4H, CH-7,7')-

$^{13}\text{C-NMR}$ (CD_2Cl_2): δ = 145.6 (C-1;1'), 138.9 (C-2;2'), 124.1 (C-3;3'), 123.0 (C-4;4'), 117.9 (C-11;12), 108.0 (C-10;13), 47.1 (C-7;7').

HRMS (LIFDI, THF): m/z = 432.2088 [**44**⁺] (calcd. for $\text{C}_{18}\text{H}_{16}\text{N}_4\text{GeCl}_2$: 431.9959).

Elemental analysis: calcd. for **44**·(0.4 GeCl_4 , 0.15 THF) (%): C 42.28, H 3.28, N 10.61; found: C 42.09, H 3.40, N 10.40.

5.2.28 2-Iodo-2-methyl-*N,N'*-neopentyl(pyridin-2-ylmethyl)benzimidazolin-2-germane (**45**)



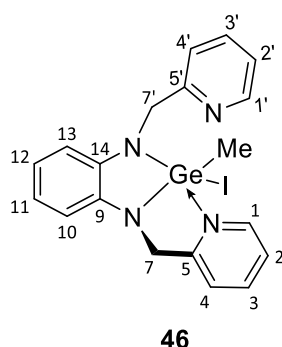
In an NMR tube equipped with a *J Young valve* are dissolved 15.0 mg **33** (44.1 μmol , 1.0 eq.) in 0.5 mL deuterated benzene and 2.3 μL MeI (6.3 mg, 44.1 μmol , 1.0 eq.) are added. The tube is placed in an ultrasonic bath for 48 h until full conversion is reached. The now yellow solution is diluted with 0.5 mL diethyl ether and stored at 0 °C to give yellow crystals, suitable for X-ray diffraction analysis, which can be filtrated off, rinsed with pentane and dried *in vacuo*.

$^1\text{H-NMR}$ (C_6D_6): δ = 8.20 (d, 3J = 5.2, 2H, CH-1), 7.13 – 7.00 (m, 3H, $\text{CH}_{\text{arom.}}$), 6.79 (td, 3J = 7.6, 4J = 1.6, 1H, CH-3), 6.73 (dd, 3J = 7.6, 4J = 1.4, 1H, $\text{CH}_{\text{arom.}}$), 6.52 – 6.48 (m, 1H, CH-2), 6.28 (d, 3J = 7.9, 1H, CH-4), 4.24 (s, 1H, CH-7), 3.49 (d, 2J = 15.0, 1H, CH-17), 3.39 (d, 2J = 15.0, 1H, CH-17), 1.51 (s, 2H), 1.07 (s, 9H, $\text{C}(\text{CH}_3)_3$).

$^{13}\text{C-NMR}$ (C_6D_6): δ = 152.3 (C-5), 143.5 (C-1;1'), 141.5 (C-9/14), 137.3 (C-9/14), 137.2 (C-3), 122.4 (C-2), 121.3 (C-4), 118.8 ($\text{CH}_{\text{arom.}}$), 116.3 ($\text{CH}_{\text{arom.}}$), 109.8 ($\text{CH}_{\text{arom.}}$), 108.9 ($\text{CH}_{\text{arom.}}$), 58.2 (C-17), 48.4 (C-7) 33.8 ($\text{C}(\text{CH}_3)_3$), 29.7 ($\text{C}(\text{CH}_3)_3$), 15.3 CH_3 .

HRMS (LIFDI, toluene): m/z =482.9219 [**45** $^+$] (calcd. for $\text{C}_{18}\text{H}_{24}\text{N}_3\text{GeI}$: 482.0230).

5.2.29 2-Iodo-2-methyl-*N,N'*-di(pyridin-2-ylmethyl)benzimidazolin-2-germane (**46**)



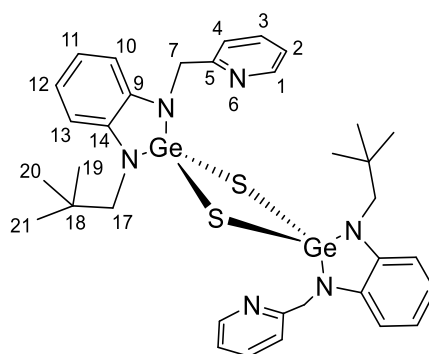
In an NMR tube equipped with a *J Young valve* are dissolved 10.0 mg **46** (27.7 μmol , 1.0 eq.) in 0.5 mL deuterated benzene and 2 μL MeI (3.9 mg, 27.7 μmol , 1.0 eq.) are added. The tube is placed in an ultrasonic bath for 48 h until full conversion is reached. The now yellow solution is diluted with 0.5 mL diethyl ether, filtrated with a filter pad and stored at 0 °C to give yellow crystals, suitable for X-ray diffraction analysis, which can be filtrated off, rinsed with pentane and dried *in vacuo*.

$^1\text{H-NMR}$ (C_6D_6): δ = 8.33 (ddd, 3J = 5.1, 4J = 1.7, 5J = 0.9, 2H, CH-1,1'), 6.93 (dd, 3J = 5.6, 4J = 3.3, 2H, CH_{arom.}), 6.88 (td, 3J = 7.6, 4J = 1.7, 2H, CH-3,3'), 6.72 (dt, 3J = 7.9, 4J = 1.1, 2H, CH-4,4'), 6.67 (dd, 3J = 5.6, 4J = 3.3 Hz, 2H, CH_{arom.}), 6.54 (ddd, 3J = 7.4, 3J = 5.1, 4J = 1.2, 2H, CH-2,2'), 4.64 (s, 2H, CH-7;7'), 1.31 (s, 3H, CH₃).

$^{13}\text{C-NMR}$ (C_6D_6): δ = 156.2 (C-5), 146.1 (C-1;1'), 138.1 (C-9;14), 136.7 (C-3;3'), 121.9 (C-2;2'), 121.3 (C-4;4'), 117.6 (CH_{arom.}), 108.2 (CH_{arom.}), 49.1 (CH₃), 15.3 (C-7;7').

HRMS (LIFDI, toluene): m/z =503.9493 [**46**⁺] (calcd. for C₁₉H₁₉N₄GeI: 503.9870).

5.2.30 Bis(*N,N'*-Neopentyl(pyridin-2-ylmethyl)benzimidazolin)-2,2'-dithiadigermetane (**47**)

**47**

In 2 mL deuterated benzene 30.0 mg **47** (88.2 μmol , 1.0 eq.) are dissolved and 2.8 mg (88.2 μmol , 1.0 eq.) elemental sulfur are added and mixture is stirred for 1 h. The product can be crystallized after filtration and dilution with diethyl ether (2 mL) at $-32\text{ }^{\circ}\text{C}$ after 48 h. The yellow crystalline solid can be filtrated off, rinsed with pentane and dried *in vacuo* (20.8 mg, 22.9 μmol , 63%). Crystals, suitable for X-ray diffraction analysis, can be grown from the mother liquor. A second species was still observed in the NMR spectra which is likely to be the configurational isomer, which always forms in solution in a ratio of circa 2:1. Thus, NMR signals are only given qualitatively.

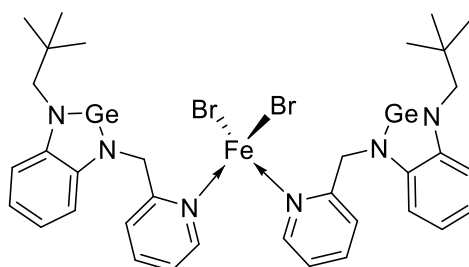
$^1\text{H-NMR}$ (C_6D_6): δ = 8.54 (d, 3J = 5.1), 8.42 (t, 3J = 4.4), 7.08 (d, 3J = 7.8), 7.05 (d, 3J = 7.9 Hz), 6.94 (td, 3J = 7.7, 4J = 1.9), 6.90 – 6.81 (m), 6.85 – 6.80 (m), 6.78 – 6.64 (m), 6.62 – 6.55 (m), 6.51 – 6.48 (m), 5.22 (s), 4.99 (s), 3.56 (s), 3.45 (s), 1.16 (s), 0.99 (s).

$^{13}\text{C-NMR}$ (C_6D_6): 159.3 ($C_{\text{arom.}}$), 159.1 ($C_{\text{arom.}}$), 149.7 ($C_{\text{arom.}}$), 149.3 ($C_{\text{arom.}}$), 140.1 ($C_{\text{arom.}}$), 139.8 ($C_{\text{arom.}}$), 137.8 ($C_{\text{arom.}}$), 137.8 ($C_{\text{arom.}}$), 136.6 ($C_{\text{arom.}}$), 136.4 ($C_{\text{arom.}}$), 122.0 ($C_{\text{arom.}}$), 121.9 ($C_{\text{arom.}}$), 121.1 ($C_{\text{arom.}}$), 120.6 ($C_{\text{arom.}}$), 118.6 ($C_{\text{arom.}}$), 118.6 ($C_{\text{arom.}}$), 118.5 ($C_{\text{arom.}}$), 118.2 ($C_{\text{arom.}}$), 110.3 ($C_{\text{arom.}}$), 110.2 ($C_{\text{arom.}}$), 109.6 ($C_{\text{arom.}}$), 109.5 ($C_{\text{arom.}}$), 57.3 (CH_2), 56.9 (CH_2), 50.1 (CH_2), 49.8 (CH_2), 34.4 ($\text{C}(\text{CH}_3)_3$), 34.1 ($\text{C}(\text{CH}_3)_3$), 29.5 ($\text{C}(\text{CH}_3)_3$), 29.2 ($\text{C}(\text{CH}_3)_3$).

HRMS (LIFDI, toluene): m/z = 743.9854 [**47** $^+$] (calcd. for $\text{C}_{34}\text{H}_{42}\text{N}_6\text{Ge}_2\text{S}_2$: 744.1355).

Elemental analysis: calcd. for **47**•**0.175 S₈** (%): C 51.76, H 5.37, N 10.65; found: C 52.15, H 5.28, N 10.26.

5.2.31 Bis[(1-(3-neopentyl)benzimidazolin-2-germylen)-pyridin-2-ylmethyl]iron(II)bromide (**48**)

**48**

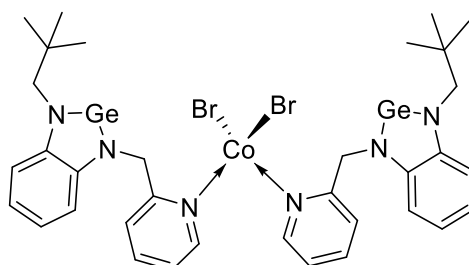
To a mixture of 200 mg **48** (588 μmol , 2.0 eq.) and 106 mg $\text{FeBr}_2(\text{dioxane})_2$ (294 μmol , 1.0 eq.) are added 10 mL THF. The yellow solution is stirred overnight, filtered through a filter pad and evaporated to dryness. The crude product is dissolved in toluene and stored at $-30\text{ }^\circ\text{C}$ giving a yellow precipitate which is washed with hexane and dried (137 mg, 247 μmol , 84%). Crystals, suitable for single crystal X-ray diffraction analysis, are grown from a concentrated toluene solution at $0\text{ }^\circ\text{C}$. The compound is paramagnetic and, thus, only $^1\text{H-NMR}$ shifts are given in the following.

$^1\text{H-NMR}$ (C_6D_6): δ = 20.75 (br), 15.19 (br), 8.27 (br), 7.01 (br), 6.69 (br), 6.30 (br), 5.37 (br), 3.49 (br), 0.63 (s, 18H).

HRMS (LIFDI, toluene): m/z = 405.0774 (calcd. for $[\text{C}_{17}\text{H}_{21}\text{N}_3\text{GeFeBr}]^{2+}$: 402.0270).

Elemental analysis: calcd. for **48** (%): C 45.59, H 4.47, N 9.38; found: C 45.75, H 4.61, N 9.12.

5.2.32 Bis[(1-(3-neopentyl)benzimidazolin-2-germylen)-pyridin-2-ylmethyl]cobalt(II)bromide(**50**)

**50**

To a mixture of 100 mg **33** (295 μmol , 2.0 eq.) and 32.3 mg CoBr_2 (148 μmol , 1.0 eq.) are added 10 mL THF. The dark green solution is stirred overnight, filtered through a filter pad and evaporated to

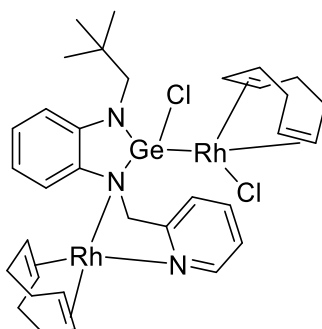
dryness. The crude product is dissolved in toluene and stored at $-30\text{ }^{\circ}\text{C}$ to give a green crystalline solid, suitable for single crystal X-ray diffraction analysis. The product is filtered off, washed with hexane and dried (119 mg, 133 μmol , 90%). The compound is paramagnetic and, thus, only $^1\text{H-NMR}$ shifts are given in the following.

$^1\text{H-NMR}$ (C_6D_6): $\delta = 7.31\text{--}7.11$ (m), 7.08 (br), 6.84 (br), 6.30 (br), 5.94 (br), 5.48 (br), 3.64 (s), 0.90 (s, 9H).

HRMS (LIFDI, toluene): $m/z = 408.1613$ (calcd. for $[\text{C}_{17}\text{H}_{21}\text{N}_3\text{GeCoBr}]^{2+}$: 405.0251).

Elemental analysis: calcd. for 50 (%): C 44.14, H 4.4, N 9.65; found: C 45.43, H 4.61, N 9.27.

5.2.33 $\text{Ge}, \text{N}, \text{N}_{\text{pyr}}\text{-}[(\mathbf{33})\text{Cl}]\text{Rh}_2(\text{cod})\text{Cl}$ (**52**)



52

To a solution of 25.0 mg **33** (73.5 μmol , 2.0 eq.) in 5.0 mL DCM are added 18.1 mg $[\text{Rh}(\text{cod})\text{Cl}]_2$ (36.8 μmol , 1.0 eq.) giving immediately a dark orange solution. The reaction mixture is heated to $50\text{ }^{\circ}\text{C}$ for 48 h and filtrated afterwards. The product is precipitated with 10 mL hexane and the solution is stored at $-30\text{ }^{\circ}\text{C}$ for 3 d to give an orange crystalline solid, suitable for X-ray diffraction analysis. The combined product is separated off the solution, rinsed with diethyl ether and dried *in vacuo* (37.4 mg, 41.9 μmol , 57%). The Product was not detectable *via* LIFDI MS.

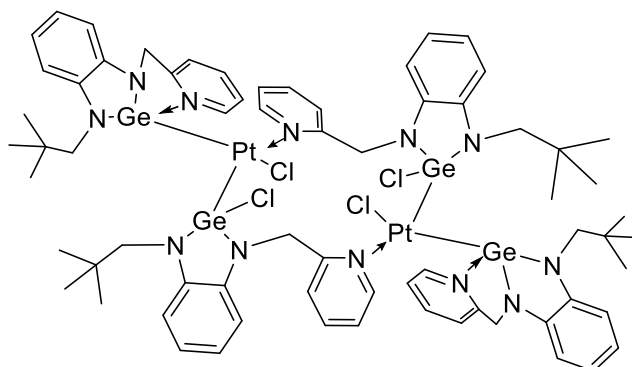
$^1\text{H-NMR}$ (C_6D_6): $\delta = 7.87$ (d, $^3J = 5.5$, 1H, $\text{CH}_{\text{pyr.}}$), 7.21 – 7.17 (m, 1H, $\text{CH}_{\text{arom.}}$), 7.05 (t, $^3J = 7.6$, 1H, $\text{CH}_{\text{pyr.}}$), 6.92 – 6.80 (m, 4H, $\text{CH}_{\text{arom.}}$), 6.47 (t, $^3J = 6.6$, 1H, $\text{CH}_{\text{pyr.}}$), 5.37 – 5.28 (m, 1H, CH_{cod}), 5.13 (d, $^2J = 13.8$, 1H, $\text{CH}_2\text{-pyr.}$), 4.83 – 4.71 (m, 1H, CH_{cod}), 4.55 (d, $^2J = 13.7$, 1H, $\text{CH}_2\text{-pyr.}$), 4.45 – 4.36 (m, 1H, CH_{cod}), 3.83 – 3.75 (m, 2H, CH_{cod}), 3.72 – 3.56 (m, 4H, $\text{CH}_2\text{C}(\text{CH}_3)_3$; CH_{cod}), 3.35 (d, $^2J = 14.6$, 1H, $\text{CH}_2\text{C}(\text{CH}_3)_3$), 2.71 – 2.57 (m, 2H, CH_2cod), 2.36 – 2.25 (m, 1H, CH_2cod), 2.17 – 1.94 (m, 4H, CH_2cod), 1.80 – 1.50 (m, 9H, CH_2cod), 1.33 (s, 9H, $\text{CH}_2\text{C}(\text{CH}_3)_3$).

$^{13}\text{C-NMR}$ (C_6D_6): $\delta = 161.5$ (s, $\text{C}_{\text{pyr.}}$), 149.5 (s, $\text{C}_{\text{pyr.}}$), 147.2 (s, $\text{C}_{\text{arom.}}$), 141.4 (s, $\text{C}_{\text{arom.}}$), 137.2 (s, $\text{CH}_{\text{arom.}}$), 122.8 (s, $\text{C}_{\text{pyr.}}$), 122.8 (s, $\text{CH}_{\text{arom.}}$), 122.7 (s, $\text{CH}_{\text{pyr.}}$), 114.9 (s, $\text{CH}_{\text{arom.}}$), 114.7 (s, $\text{CH}_{\text{pyr.}}$), 110.7 (s, $\text{CH}_{\text{arom.}}$).

98.79 – 98.63 (m, CH_{cod}), 81.03 – 80.76 (m, CH_{cod}), 78.14 (d, $^2J_{\text{Rh,C}} = 13.0$, CH_{cod}), 70.0 (d, $^2J_{\text{Rh,C}} = 13.6$, CH_{cod}), 68.7 (d, $^2J_{\text{Rh,C}} = 13.1$, CH_{cod}), 58.0 (s, $\text{CH}_2\text{C}(\text{CH}_3)_3$), 56.5 ($\text{CH}_2\text{-pyr.}$), 34.3 (s, $\text{CH}_2\text{C}(\text{CH}_3)_3$), 33.7 (s, $\text{CH}_{2,\text{cod}}$), 32.5 (s, $\text{CH}_{2,\text{cod}}$), 31.9 (s, $\text{CH}_{2,\text{cod}}$), 29.4 $\text{CH}_2\text{C}(\text{CH}_3)_3$, 28.8 (s, $\text{CH}_{2,\text{cod}}$).

Elemental analysis: calcd. for **52** (%): C 46.59, H 5.44, N 5.04; found: C 46.59, H 5.22, N 5.03.

5.2.34 $\text{Ge,Ge',N}_{\text{pyr}}\text{-}[(\mathbf{33})(\text{Cl-}\mathbf{33})\text{PtCl}]_2$ (**53**)



53

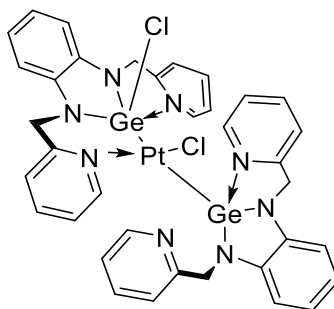
To a solution of 25.0 mg **33** (73.5 μmol , 2.0 eq.) in 5.0 mL DCM are added 13.8 mg $\text{Pt}(\text{cod})\text{Cl}_2$ (36.8 μmol , 1.0 eq.) giving a yellow solution. The reaction mixture is stirred overnight at room temperature and filtrated afterwards. The clear, yellow solution is diluted with 3.0 mL diethyl ether and stored at -30°C for 3 d to give a yellow crystalline precipitate which is separated from the solution, rinsed with diethyl ether and dried *in vacuo*. Yield has not been determined. Crystals, suitable for X-ray diffraction analysis, can be grown from the mother solution at -30°C . The Product was not detectable *via* LIFDI MS.

$^1\text{H-NMR}$ (C_6D_6): $\delta = 9.30$ (d, $^3J = 5.7$, 2H, $\text{CH}_{\text{pyr.}}$), 8.31 (dd, $^3J = 5.6$, $^3J = 1.6$, 2H, $\text{CH}_{\text{pyr.}}$), 7.04–6.70 (m, 16H, $\text{CH}_{\text{arom.}}$), 6.64–6.55 (m, 2H, $\text{CH}_{\text{arom.}}$), 6.26 (d, $^3J = 8.0$, 2H, $\text{CH}_{\text{arom.}}$), 6.11 (t, $^3J = 6.6$, 2H, $\text{CH}_{\text{arom.}}$), 6.07 - 5.97 (m, 2H, $\text{CH}_{\text{arom.}}$), 5.96–5.84 (m, 4H, $\text{CH}_{\text{arom.}}$), 5.48 (d, $^2J = 17.8$, 2H, CH_2), 5.43–5.24 (m, 4H, CH_2), 4.69–4.51 (m, 4H, CH_2), 3.92–3.78 (m, 2H, CH_2), 3.64–3.54 (m, 2H, CH_2), 3.46 (d, $^2J = 14.7$, 2H, CH_2), 1.16 (s, 9H, $\text{C}(\text{CH}_3)_3$), 1.10 (s, 9H, $\text{C}(\text{CH}_3)_3$).

$^{13}\text{C-NMR}$ (C_6D_6): $\delta = 156.5$ ($\text{C}_{\text{arom.}}$), 149.9 ($\text{C}_{\text{arom.}}$), 145.2 ($\text{C}_{\text{arom.}}$), 143.4 ($\text{C}_{\text{arom.}}$), 143.4 ($\text{C}_{\text{arom.}}$), 141.9 ($\text{C}_{\text{arom.}}$), 141.8 ($\text{C}_{\text{arom.}}$), 140.6 ($\text{C}_{\text{arom.}}$), 137.9 ($\text{C}_{\text{arom.}}$), 137.5 ($\text{C}_{\text{arom.}}$), 123.9 ($\text{C}_{\text{arom.}}$), 121.8 ($\text{C}_{\text{arom.}}$), 121.5 ($\text{C}_{\text{arom.}}$), 120.2 ($\text{C}_{\text{arom.}}$), 120.1 ($\text{C}_{\text{arom.}}$), 118.1 ($\text{C}_{\text{arom.}}$), 117.2 ($\text{C}_{\text{arom.}}$), 116.0 ($\text{C}_{\text{arom.}}$), 115.9 ($\text{C}_{\text{arom.}}$), 110.2 ($\text{C}_{\text{arom.}}$), 109.7 ($\text{C}_{\text{arom.}}$), 109.0 ($\text{C}_{\text{arom.}}$), 58.5 (s, CH_2), 55.2 (s, CH_2), 53.7 (s, CH_2), 52.7 (s, CH_2), 34.7 ($\text{C}(\text{CH}_3)_3$), 34.3 ($\text{C}(\text{CH}_3)_3$), 34.1 ($\text{C}(\text{CH}_3)_3$), 29.2 ($\text{C}(\text{CH}_3)_3$), 29.1 ($\text{C}(\text{CH}_3)_3$).

Elemental analysis: calcd. for 53·0.15 Pt(cod)Cl₂ (%): C 42.66, H 4.44, N 8.63; found: C 42.54, H 4.58, N 8.60.

5.2.35 *Ge,Ge',N_{pyr}-[(N4Ge)(Cl-33)PtCl] (54)*

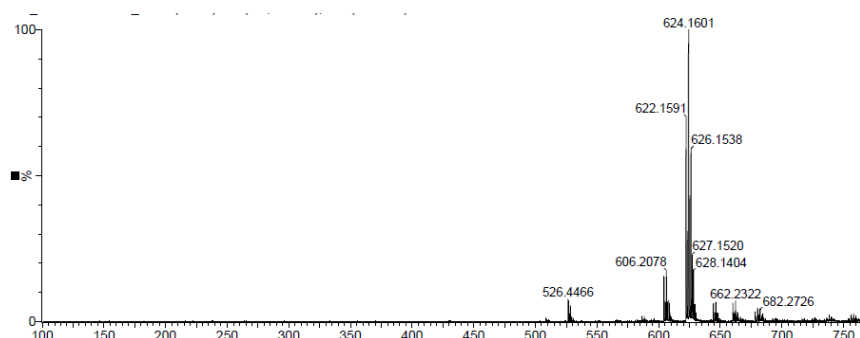


54

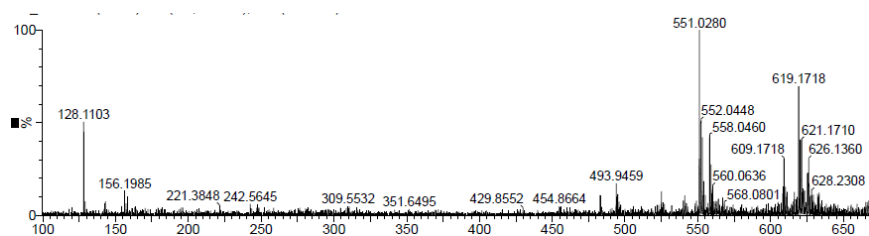
To a solution of 20.0 mg **54** (55.5 μmol , 2.0 eq.) in 5.0 mL DCM are added 10.4 mg Pt(cod)Cl₂ (27.7 μmol , 1.0 eq.) giving a yellow solution. The reaction mixture is stirred overnight at room temperature and filtrated afterwards. The clear, yellow solution is diluted with 3.0 mL diethyl ether and stored at $-30\text{ }^\circ\text{C}$ for 3 d to give a yellow crystalline precipitate that included crystals suitable for X-ray diffraction analysis. The solid is separated from the solution, rinsed with diethyl ether and dried *in vacuo*. Yield has not been determined as the product was still contaminated by side-products. The Product was not detectable *via* LIFDI MS.

6 SUPPLEMENTARY DATA

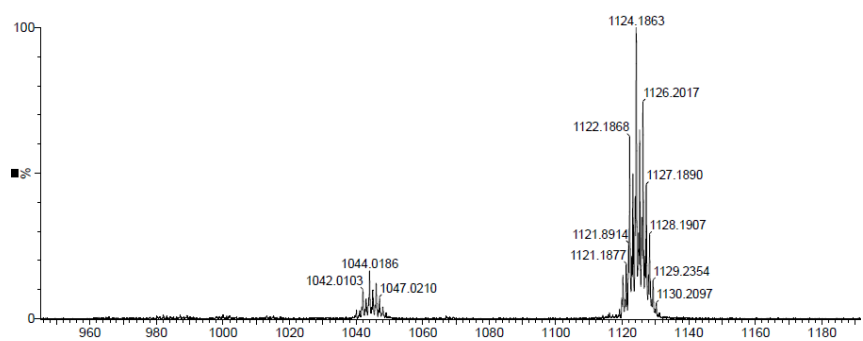
6.1 LIFDI Mass Spectrometry



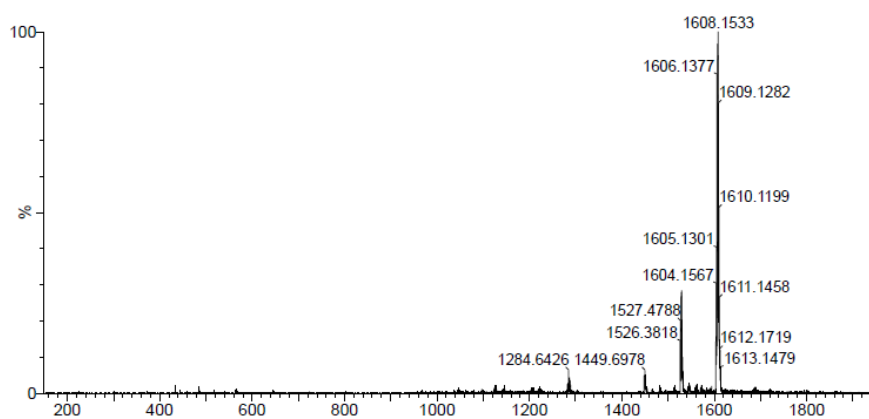
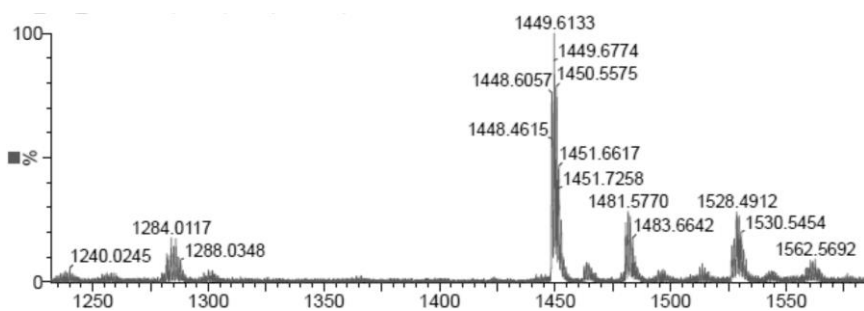
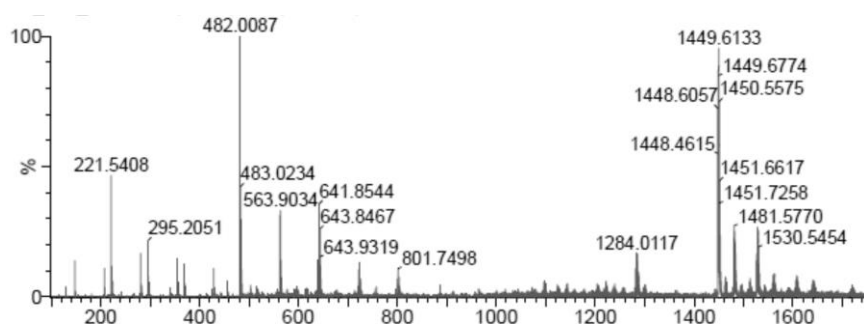
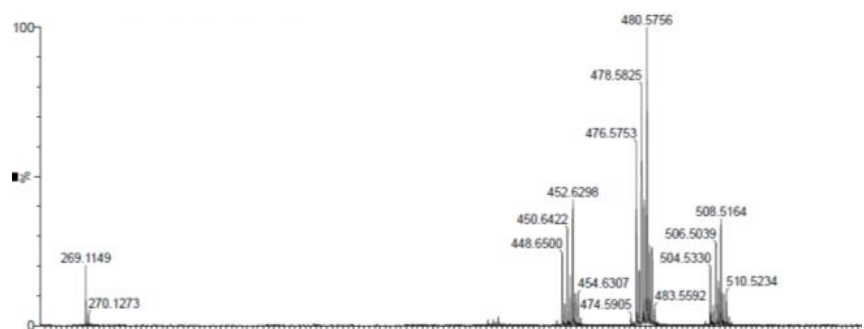
SD 1: LIFDI mass spectrum of **16** in toluene.

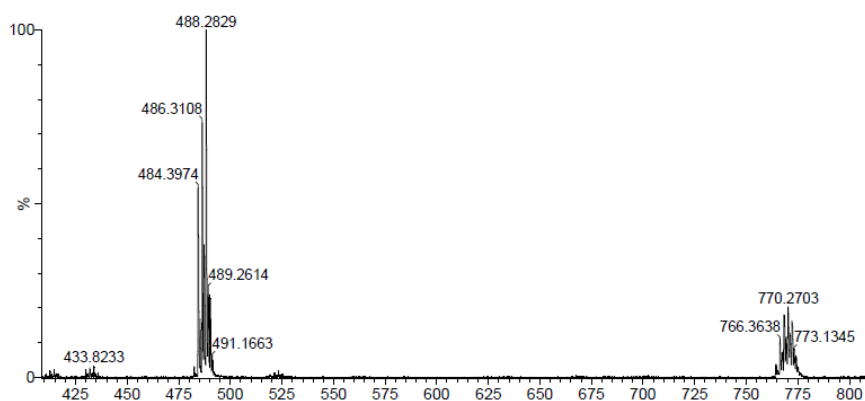
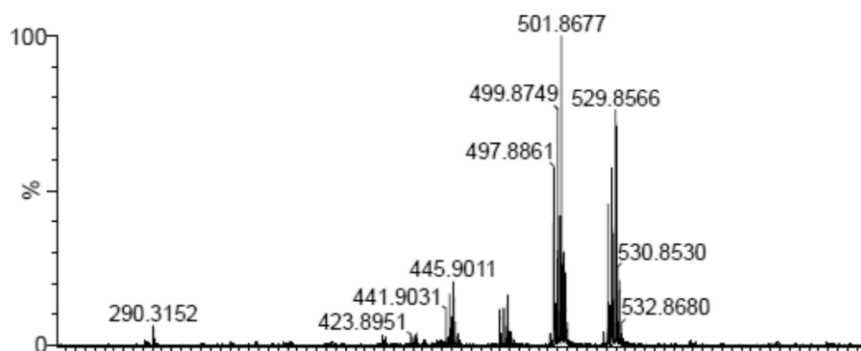
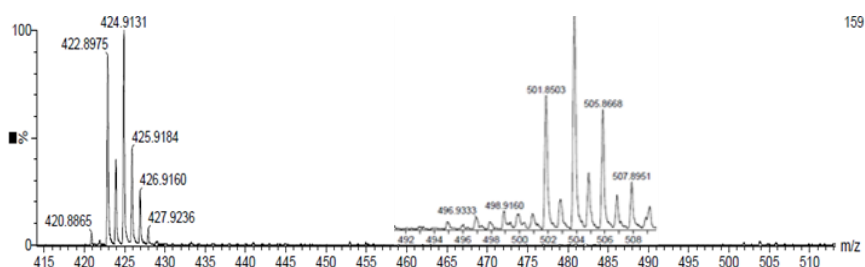
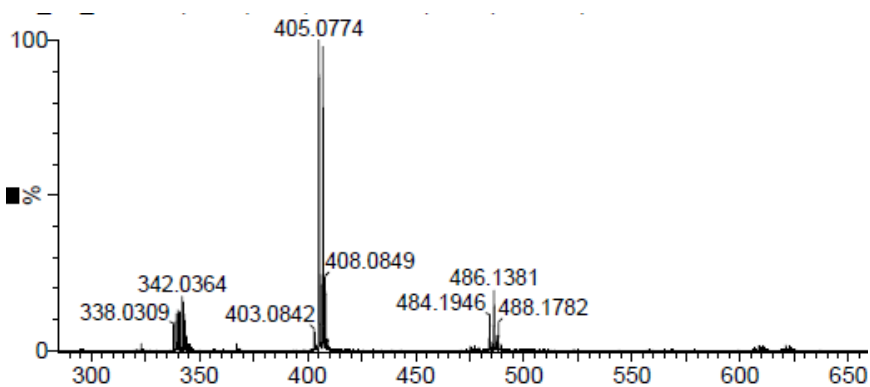


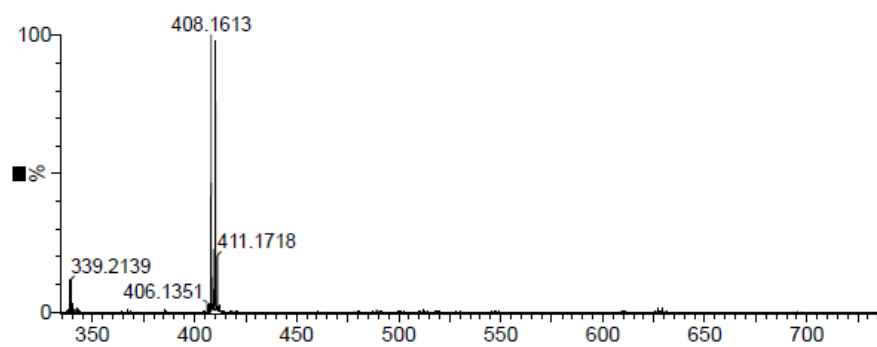
SD 2: LIFDI mass spectrum of the reaction mixture of **16** with lithium naphthalide in presence of excess of isoprene measured in THF.



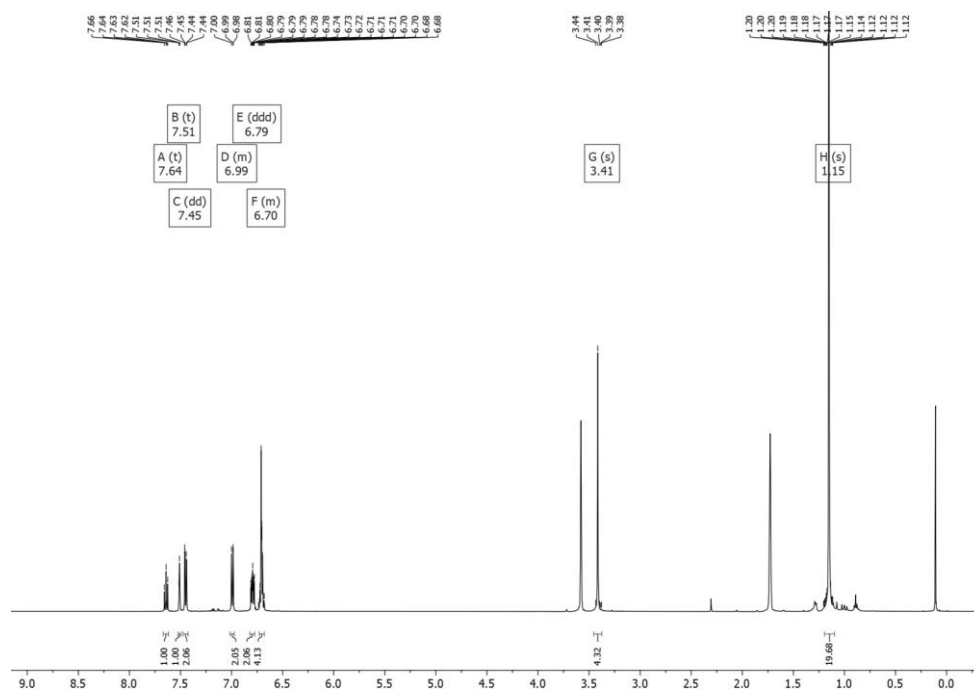
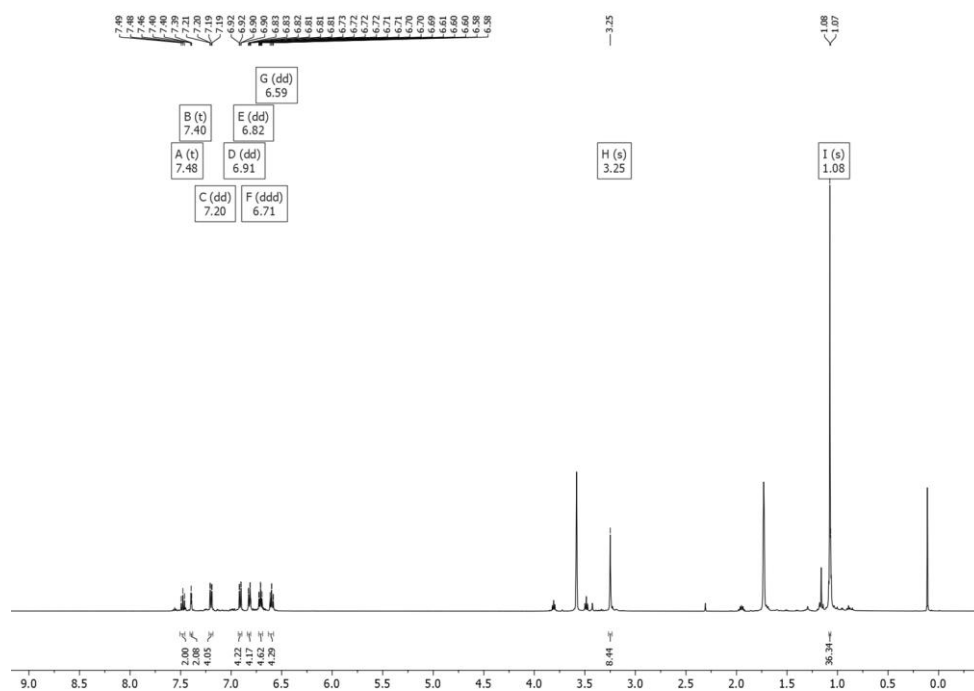
SD 3: LIFDI mass spectrum of the reaction mixture of **21** with 4.0 eq. KC_8 measured in toluene.

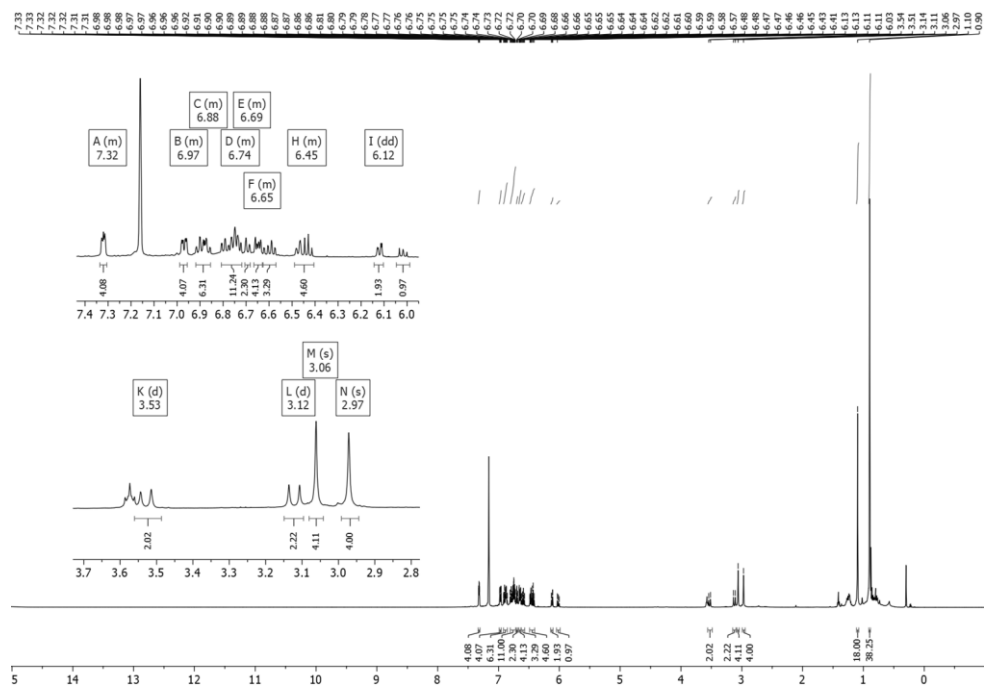
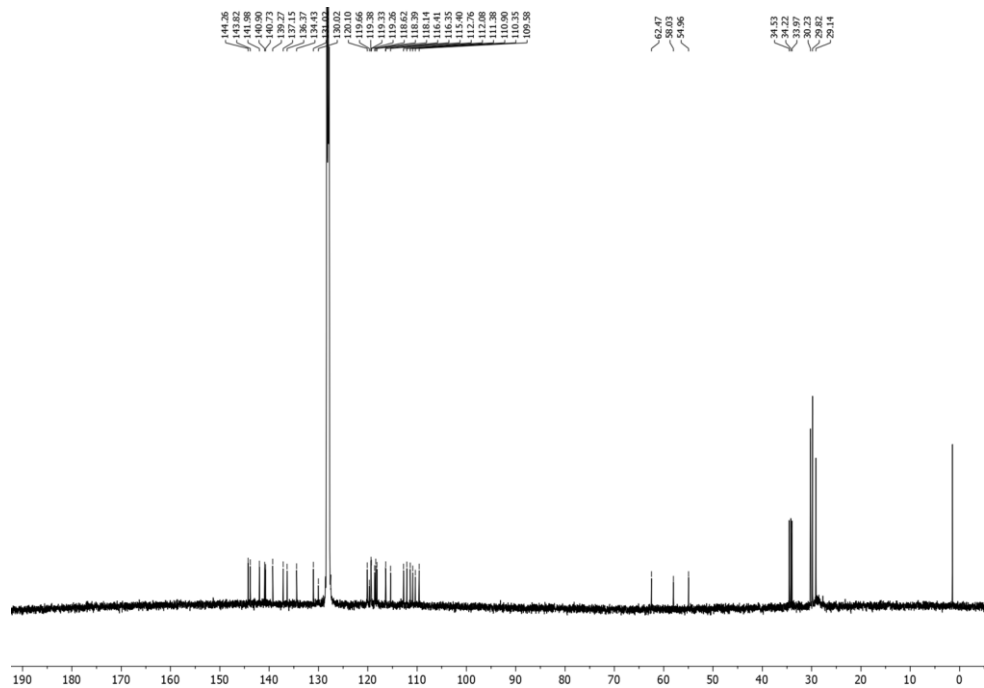
SD 4: LIFDI mass spectrum of the reaction mixture of **21** with 3.66 eq. KC_8 measured in toluene.SD 5: LIFDI mass spectrum of the filtrate of the reaction of **24** with 2.0 eq. KC_8 in DME (top: total; bottom: $m/z = 1200 - 1600$).SD 6: LIFDI mass spectrum of **35** measured in THF.

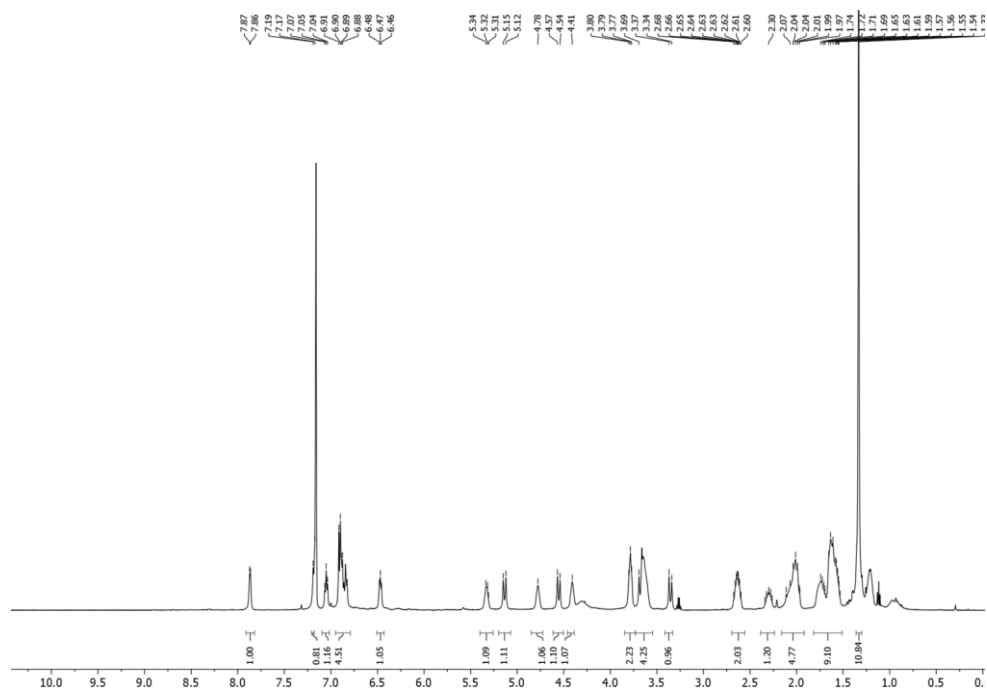
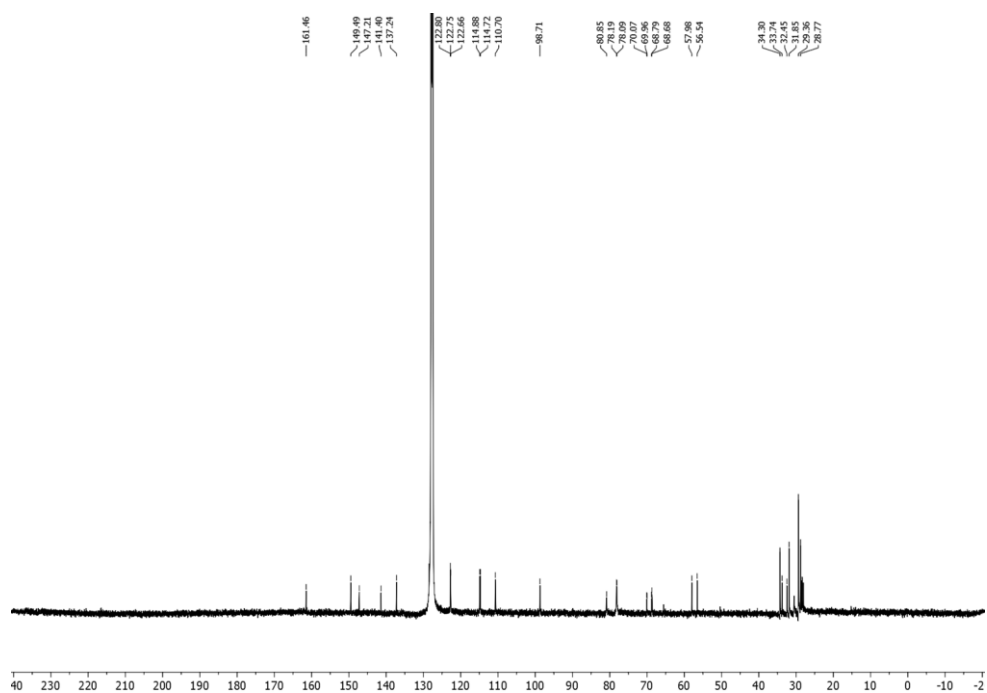
SD 7: LIFDI mass spectrum of **41** measured in THF, impurities can be assigned to $[(\mathbf{39})_2\text{Fe}(\text{CO})_3]$.SD 8: LIFDI mass spectrum of **40** measured in THF.SD 9: LIFDI mass spectrum of **49** measured in toluene.SD 10: LIFDI mass spectrum of **48** measured in toluene.

SD 11: LIFDI mass spectrum of **50** measured in toluene.

6.2 NMR Spectroscopy

SD 12: ^1H -NMR spectrum of **21** in THF- d_8 after 10 min.SD 13: ^1H -NMR spectrum of **21** in THF- d_8 after 24 h.

SD 14: ¹H-NMR spectrum of **24** in benzol-d₆.SD 15: ¹³C-NMR spectrum of **24** in benzol-d₆.

SD 16: $^1\text{H-NMR}$ spectrum of **52** in benzol- d_6 .SD 17: $^{13}\text{C-NMR}$ spectrum of **52** in benzol- d_6 .

6.3 DFT Calculations

SD 18: Atomic and group properties of Si₆H₁₄ predicted by QTAIM.

Si ₆ H ₁₄	ρ^a [Å ⁻³]	$\int A \cap B \rho(r)$ [Å ⁻¹]	$K_{\text{tot.}}^b$ [E _h]	$G_{\text{Kin.}}^c$ [E _h]	$V_{\text{Pot.}}^d$ [E _h]	ϵ
Si1-Si2	0.637549664	1.49746682	-0.048301	0.007185	-0.055486	0.024536
Si2-Si3	0.628911785	1.52836952	-0.047311	0.007635	-0.054947	0.051405
Si3-Si4	0.629552878	1.52854149	-0.047435	0.007655	-0.05509	0.049984
Si4-Si5	0.628911785	1.52836952	-0.047311	0.007635	-0.054947	0.051405
Si5-Si6	0.637549664	1.49746682	-0.048301	0.007185	-0.055486	0.024536
average	0.632495155	1.51604284	-0.0477318	0.007459	-0.0551912	0.0403732

SD 19: Atomic and group properties of Si₆Cl₁₄ predicted by QTAIM.

Si ₆ Cl ₁₄	ρ [Å ⁻³]	$\int A \cap B \rho(r)$ [Å ⁻¹]	$K_{\text{tot.}}$ [E _h]	$G_{\text{Kin.}}$ [E _h]	$V_{\text{Pot.}}$ [E _h]	ϵ
Si1-Si2	0.67919369	1.68602755	-0.052765	0.006372	-0.059137	0.026397
Si2-Si3	0.6624308	1.78058003	-0.050217	0.006537	-0.056754	0.047541
Si3-Si4	0.66264	1.84823981	-0.050304	0.006602	-0.056906	0.047522
Si4-Si5	0.6624308	1.78056491	-0.050217	0.006537	-0.056754	0.047541
Si5-Si6	0.67919369	1.68601432	-0.052765	0.006372	-0.059137	0.026397
average	0.6691778	1.75628533	-0.0512536	0.006484	-0.0577376	0.0390796

SD 20: Atomic and group properties of **24** predicted by QTAIM.

24	ρ [Å ⁻³]	$\int A \cap B \rho(r)$ [Å ⁻¹]	$K_{\text{tot.}}$ [E _h]	$G_{\text{Kin.}}$ [E _h]	$V_{\text{Pot.}}$ [E _h]	ϵ
Si1-Si2	0.64144346	1.73122226	-0.064453	0.043425	-0.107878	0.069644
Si2-Si3	0.60857903	1.55227457	-0.046165	0.007439	-0.053603	0.005653
Si3-Si4	0.61837087	n.a.	-0.047567	0.007428	-0.054995	0.010982
Si4-Si5	0.60855204	1.55343108	-0.04616	0.007439	-0.053599	0.005658
Si5-Si6	0.64142996	1.73223137	-0.064451	0.043423	-0.107875	0.06964
average	0.62367507	1.64228982	-0.0537592	0.0218308	-0.07559	0.0323154

^a Electron density

^b Hamiltonian form of kinetic energy density

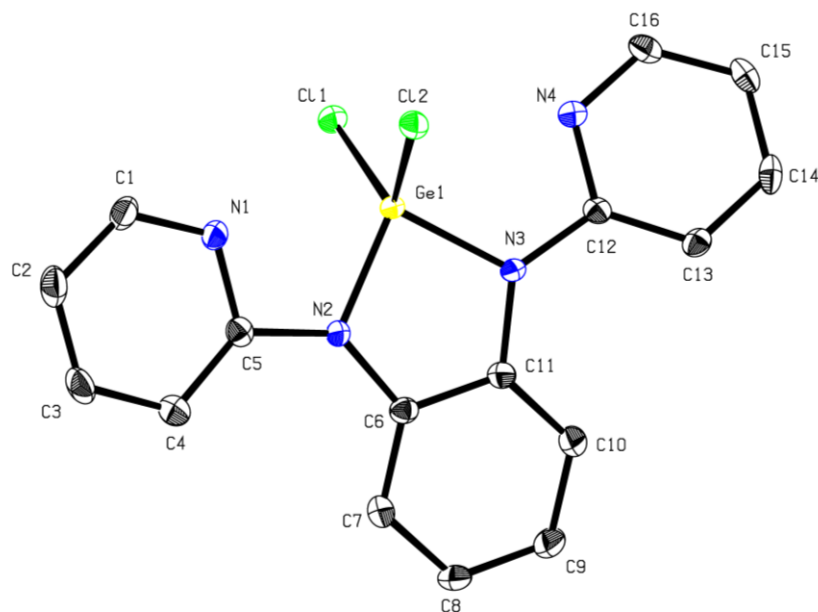
^c Lagrangian form of kinetic energy density

^d Potential energy density

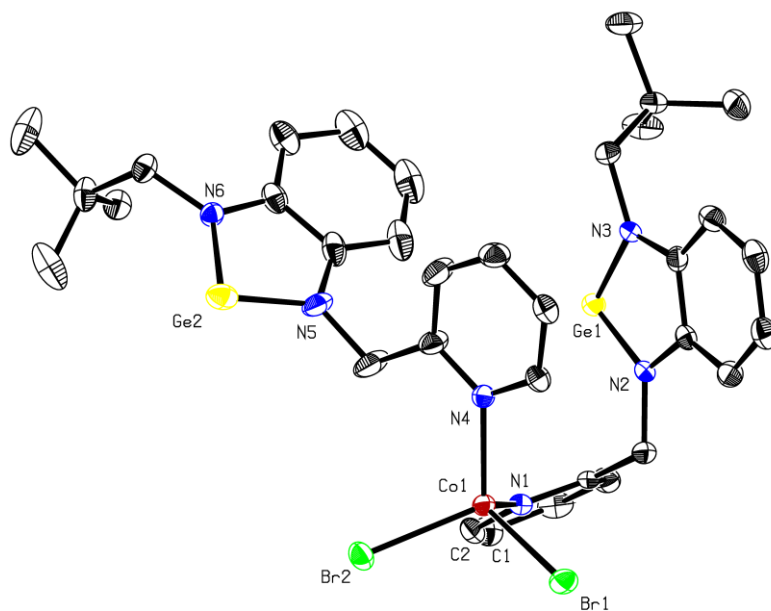
SD 21: Calculated NBO charges and bond lengths of Si₆H₁₄, Si₆Cl₁₄ and **24**.

NBO charges	Si ₆ H ₁₄	Si ₆ Cl ₁₄	24
Si1	0.44672	0.96839	1.46554
Si2	0.20945	0.62172	1.04913
Si3	0.23702	0.63969	1.08194
Si4	0.23702	0.63969	1.08197
Si6	0.44672	0.96839	1.46555
Si5	0.20945	0.62172	1.04914
average	0.29773	0.74327	1.19888
bond lengths [Å]			
Si1-Si2	2.33788	2.34101	2.356
Si2-Si3	2.33836	2.34968	2.40101
Si3-Si4	2.3376	2.34878	2.39662
Si4-Si5	2.33836	2.34968	2.40105
Si5-Si6	2.33788	2.34101	2.35602

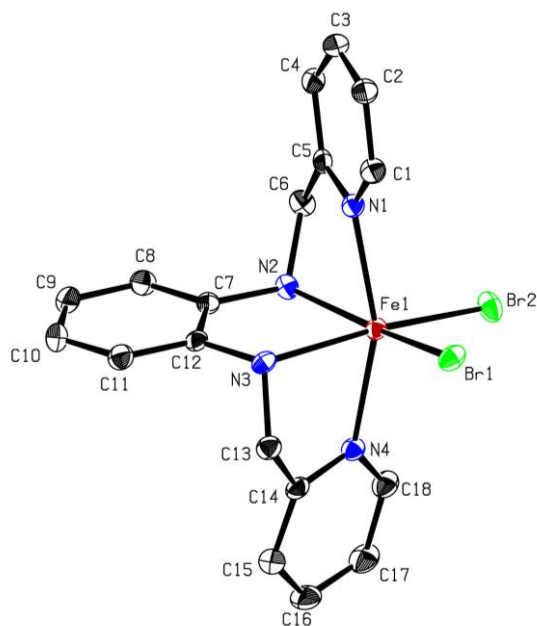
6.4 X-Ray Diffraction Analysis



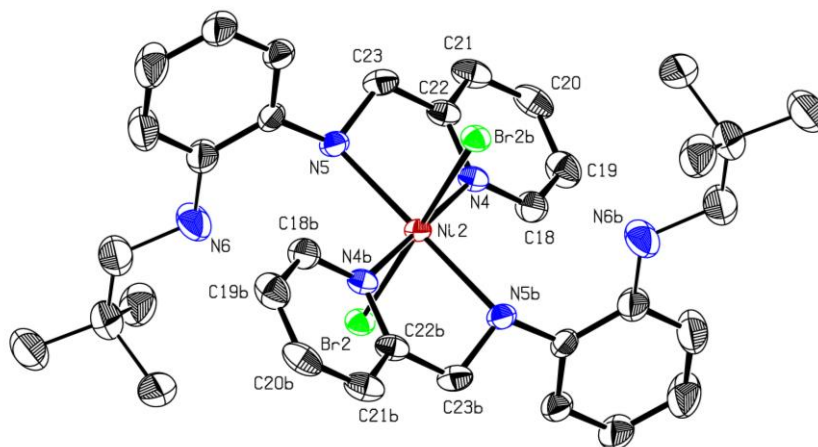
SD 22: Molecular structure of **30**. Ellipsoids are shown at the 50% probability level. Hydrogen atoms are omitted for clarity. Grey = carbon. blue = nitrogen. yellow = germanium. green = chloride.



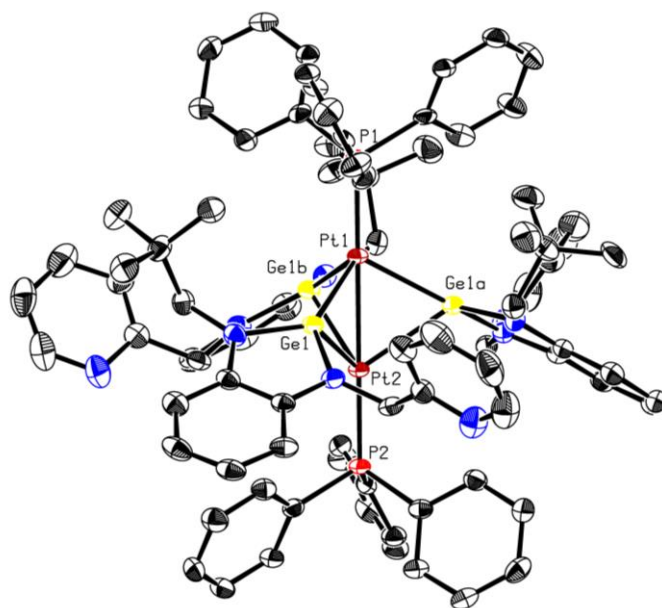
SD 23: Molecular structure of **51**. Ellipsoids are shown at the 50% probability level. Hydrogen atoms are omitted for clarity. Grey = carbon. blue = nitrogen. yellow = germanium. green = bromide. dark red = cobalt.



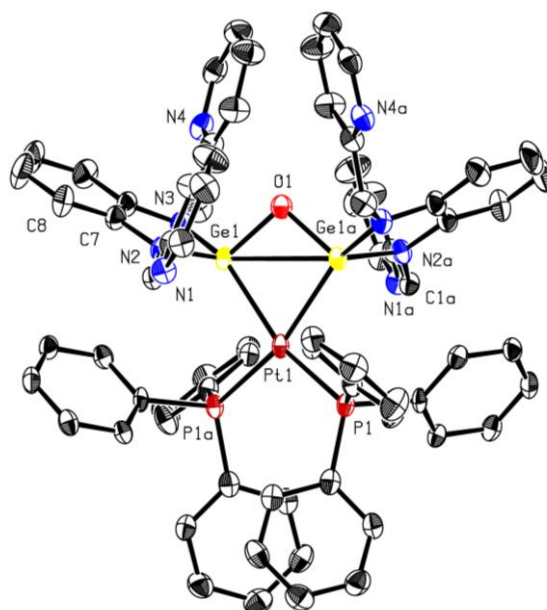
SD 24: Molecular structure of **49**. Ellipsoids are shown at the 50% probability level. Hydrogen atoms are omitted for clarity. Grey = carbon. blue = nitrogen. green = bromide. dark red = iron.



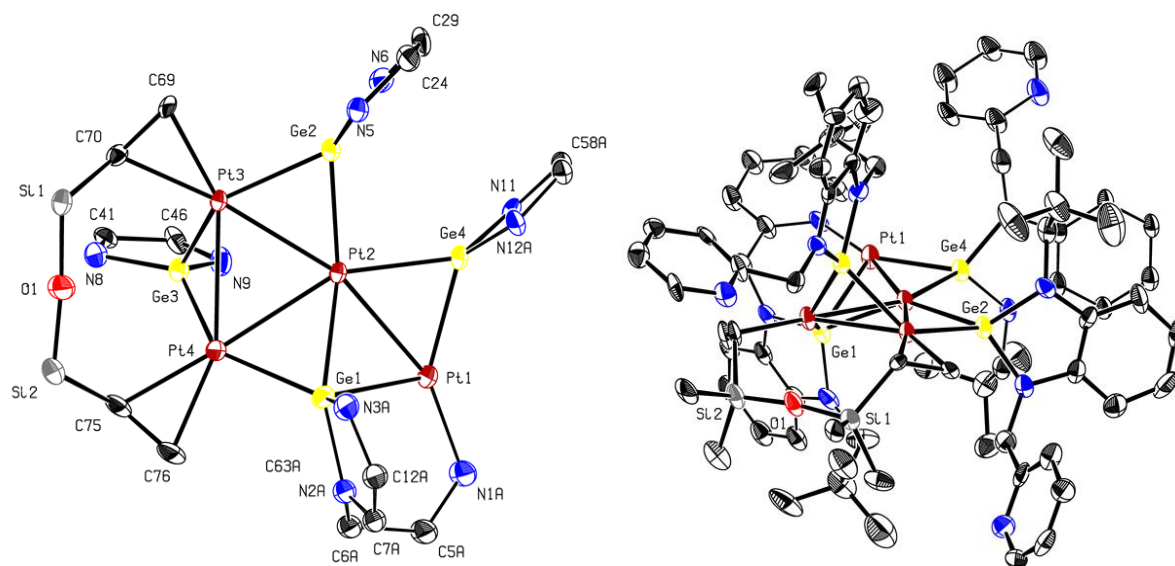
SD 25: Molecular structure of **51**. Ellipsoids are shown at the 50% probability level. Hydrogen atoms are omitted for clarity. Grey = carbon. blue = nitrogen. yellow = germanium. green = bromide. dark red = nickel.



SD 26: Molecular structure of **55**. Ellipsoids are shown at the 50% probability level. Hydrogen atoms are omitted for clarity. Grey = carbon. blue = nitrogen. yellow = germanium. red = phosphor. dark red = platinum.



SD 27: Molecular structure of **56**. Ellipsoids are shown at the 50% probability level. Hydrogen atoms are omitted for clarity. Grey = carbon. blue = nitrogen. yellow = germanium. orange = phosphor, red = oxygen, dark red = platinum.



SD 28: Cut-outs of the molecular structure of **57**. Ellipsoids are shown at the 50% probability level. Hydrogen atoms are omitted for clarity. Grey = carbon. blue = nitrogen. yellow = germanium. dark red = platinum. red = oxygen. light grey = silicon.

SD 29: Crystallographic data and structure refinement parameters of complexes **16**, **42** and **38**.

Substance identification	16	42	38
Chemical formula	C ₄₀ H ₄₆ Br ₄ N ₄ Si ₂	C ₃₅ H ₃₉ GeN ₉ O ₃	C ₂₂ H ₂₄ GeN ₄ O
Fw [g mol⁻¹]	958.63	706.34	433.04
T [K]	100(2)	100(2)	100(2)
Crystal system	orthorhombic	tetragonal	triclinic
Space group	<i>Pnma</i>	<i>P43</i>	<i>P-1</i>
a [Å]	17.2854(15)	9.647(5)	8.1479(7)
b [Å]	31.929(3)	9.647(5)	11.0518(10)
c [Å]	7.2610(7)	38.253(18)	11.8955(10)
α [deg]	90	90	77.233(3)
β [deg]	90	90	75.148(3)
γ [deg]	90	90	77.268(3)
V [Å³]	4007.4(6)	3560.(4)	994.44(15)
Z	4	4	2
Density (calcd) [g cm⁻³]	1.589	1.318	1.446
μ [mm⁻¹]	4.111	0.908	1.560
F (000)	1928	1472	448
Crystal size (mm³)	0.056 × 0.088 × 0.150	0.160 × 0.236 × 0.277	0.074 × 0.244 × 0.312
θ range for data collection [deg]	2.36 to 25.35	2.18 to 25.33	2.39 to 29.13
Reflections collected	184940	67624	57496
Independent reflections	3751	6458	5321
Data/restraints/parameters	3751 / 0 / 235	6458 / 1 / 436	5321 / 0 / 253
GOF on F²	1.034	1.853	1.053
Final R1	R1 = 0.0327	R1 = 0.0708	R1 = 0.0212
wR2 [I > 2σ(I)]	wR2 = 0.0424	wR2 = 0.2070	wR2 = 0.0515
Largest diff. peak and hole [eÅ⁻³]	0.338 and -0.252	0.480 and -1.651	0.512 and -0.318

SD 30: Crystallographic data and structure refinement parameters of complexes **47**, **40** and **41**.

Substance identification	47	40	41
Chemical formula	C ₃₄ H ₄₂ Ge ₂ N ₆ S ₂	C ₂₂ H ₁₆ FeGeN ₄ O ₄	C ₄₀ H ₅₂ Fe ₂ Ge ₂ N ₄ O ₈
Fw [g mol⁻¹]	744.03	528.83	973.73
T [K]	100(2)	100(2)	100(2)
Crystal system	triclinic	monoclinic	triclinic
Space group	<i>P</i> -1	<i>P</i> 121/ <i>c</i> 1	<i>P</i> -1
a [Å]	8.7952(7)	8.9469(5)	8.9871(7)
b [Å]	9.8039(7)	17.8118(8)	13.5426(10)
c [Å]	10.2004(8)	13.7044(7)	18.4903(13)
α [deg]	87.481(3)	90	104.349(3)
β [deg]	80.084(3)	102.742(2)	93.238(3)
γ [deg]	82.976(3)	90	92.884(3)
V [Å³]	859.67	2130.15(19)	2171.9(3)
Z	1	4	2
Density (calcd) [g cm⁻³]	1.437	1.649	1.389
μ [mm⁻¹]	1.903	2.130	2.078
F (000)	348	1064	1000
Crystal size (mm³)	0.050 × 0.075 × 0.198	0.067 × 0.088 × 0.113	0.234 × 0.263 × 0.317
θ range for data collection [deg]	2.37 to 27.87	2.29 to 29.57	2.15 to 27.48
Reflections collected	29172	118829	92956
Independent reflections	4099	5975	9982
Data/restraints/parameters	4099 / 0 / 202	5975 / 0 / 289	9982 / 0 / 517
GOF on F²	1.057	1.059	1.143
Final R1	0.0228	0.0331	0.0577
wR2 [I > 2σ(I)]	0.0470	0.0622	0.0822
Largest diff. peak and hole [eÅ⁻³]	0.375 to -0.318	0.608 and -0.494	0.896 and -0.814

SD 31: Crystallographic data and structure refinement parameters of complexes **49**, **54** and **46**.

Substance identification	49	54	46
Chemical formula	C ₂₂ H ₂₅ Br ₂ FeN ₄ O	C ₃₆ H ₃₂ Cl ₂ Ge ₂ N ₈ Pt	C ₁₉ H ₁₉ GeIN ₄
Fw [g mol⁻¹]	577.13	987.86	502.87
T [K]	100(2)	100(2)	100(2)
Crystal system	monoclinic	monoclinic	monoclinic
Space group	<i>P121/c1</i>	<i>P121/c1</i>	<i>P121/c1</i>
a [Å]	9.635(4)	11.7120(15)	7.3914(4)
b [Å]	15.354(5)	10.2396(12)	16.7703(10)
c [Å]	16.059(6)	31.895(4)	15.4348(9)
α [deg]	90	90	90
β [deg]	105.162(17)	97.786(4)	90.259(3)
γ [deg]	90	90	90
V [Å³]	2293.0(14)	3789.8(8)	1913.22(19)
Z	4	4	4
Density (calcd) [g cm⁻³]	1.672	1.731	1.746
μ [mm⁻¹]	4.164	5.436	3.224
F (000)	1156	1920	984
Crystal size (mm³)	0.028 × 0.074 × 0.136	0.172 × 0.178 × 0.312	0.100 × 0.103 × 0.201
θ range for data collection [deg]	2.56 to 27.10	2.03 to 30.03	2.43 to 25.68
Reflections collected	95250	206851	77729
Independent reflections	5053	11082	3614
Data/restraints/parameters	5053 / 180 / 317	11082 / 0 / 442	3164 / 33 / 257
GOF on F²	1.033	1.078	1.328
Final R1	0.0319	0.0416	0.0338
wR2 [I > 2σ(I)]	0.0682	0.0546	0.0816
Largest diff. peak and hole [eÅ⁻³]	2.007 and -0.632	1.533 and -1.561	0.808 and -0.937

SD 32: Crystallographic data and structure refinement parameters of complexes **45**, **33** and **32**.

Substance identification	45	33	32
Chemical formula	C ₁₈ H ₂₄ GeIN ₃	C ₁₇ H ₂₁ GeN ₃	C ₁₇ H ₂₁ Cl ₂ GeN ₃
Fw [g mol⁻¹]	481.89	339.96	410.86
T [K]	100(2)	100(2)	100(2)
Crystal system	monoclinic	triclinic	orthorhombic
Space group	<i>P121/c1</i>	<i>P-1</i>	<i>P212121</i>
a [Å]	11.5571(7)	8.1611(4)	8.0998(3)
b [Å]	7.1138(4)	9.9676(5)	11.1668(4)
c [Å]	23.6406(14)	10.0701(5)	19.6028(8)
α [deg]	90	81.978(2)	90
β [deg]	102.558(2)	75.307(2)	90
γ [deg]	90	78.531(2)	90
V [Å³]	1897.11(19)	773.12(7)	1773.05(12)
Z	4	2	4
Density (calcd) [g cm⁻³]	1.687	1.460	1.539
μ [mm⁻¹]	3.245	1.978	2.031
F (000)	952	352	840
Crystal size (mm³)	0.046 × 0.086 × 0.105	0.112 × 0.141 × 0.201	0.058 × 0.203 × 0.434
θ range for data collection [deg]	2.79 to 25.68	2.62 to 27.88	2.72 to 30.03
Reflections collected	47962	16284	91975
Independent reflections	3605	3684	5196
Data/restraints/parameters	3605 / 0 / 212	3684 / 0 / 193	5196 / 0 / 211
GOF on F²	1.148	1.067	1.115
Final R1	0.0369	0.0300	0.0233
wR2 [I > 2σ(I)]	0.0642	0.0535	0.0466
Largest diff. peak and hole [eÅ⁻³]	2.198 and -0.778	0.912 and -0.310	0.367 and -0.263

SD 33: Crystallographic data and structure refinement parameters of complexes **35**, **34** and **57**.

Substance identification	35	34	57
Chemical formula	C ₂₁ H ₂₁ FeGeN ₃ O ₄	C ₁₇ H ₂₃ Cl ₂ Ge ₂ N ₃	C ₇₆ H ₁₀₀ Ge ₄ N ₁₂ O ₁ Pt ₄ Si ₂
Fw [g mol⁻¹]	507.85	485.57	2324.57
T [K]	100(2)	100(2)	100(2)
Crystal system	triclinic	monoclinic	triclinic
Space group	<i>P</i> -1	<i>P</i> 121/ <i>c</i> 1	<i>P</i> -1
a [Å]	9.4653(5)	10.641(8)	14.1234(16)
b [Å]	9.8404(5)	8.763(5)	14.4084(17)
c [Å]	14.1371(7)	20.918(14)	22.628(3)
α [deg]	109.919(2)	90	91.456(3)
β [deg]	99.236(2)	97.50(2)	97.065(3)
γ [deg]	91.638(2)	90	114.258(3)
V [Å³]	1217.01(11)	1934.(4)	4151.5(8)
Z	2	4	2
Density (calcd) [g cm⁻³]	1.386	1.646	1.860
μ [mm⁻¹]	1.859	3.360	8.216
F (000)	516	968	2232
Crystal size (mm³)	0.070 × 0.082 × 0.268	0.074 × 0.127 × 0.167	0.025 × 0.046 × 0.094
θ range for data collection [deg]	2.19 to 27.10	2.52 to 26.44	2.29 to 25.03
Reflections collected	63521	61028	88271
Independent reflections	5370	4001	14669
Data/restraints/parameters	5370 / 378 / 405	4001 / 0 / 220	14669 / 1051 / 1156
GOF on F²	1.077	1.072	1.017
Final R1	0.0444	0.0446	0.1198
wR2 [I > 2σ(I)]	0.0571	0.0796	0.0907
Largest diff. peak and hole [eÅ⁻³]	0.340 and -0.473	2.118 and -0.701	2.579 and -1.674

SD 34: Crystallographic data and structure refinement parameters of complexes **55**, **52** and **43**.

Substance identification	55	52	43
Chemical formula	C ₈₇ H ₉₉ Ge ₃ N ₉ P ₂ Pt ₂	C ₃₄ H ₄₈ Cl ₅ GeN ₃ Rh ₂	C ₁₇ H ₂₀ Cl ₅ Ge ₂ N ₃
Fw [g mol⁻¹]	1940.64	960.42	588.79
T [K]	100(2)	100(2)	100(2)
Crystal system	trigonal	monoclinic	monoclinic
Space group	<i>P</i> -3	<i>C</i> 12/ <i>c</i> 1	<i>P</i> 121/ <i>c</i> 1
a [Å]	19.2658(11)	25.3371(11)	15.9907(12)
b [Å]	19.2658(11)	13.4814(6)	17.4553(13)
c [Å]	14.5964(8)	23.2531(10)	8.0793(6)
α [deg]	90	90	90
β [deg]	90	110.0880(10)	103.978(2)
γ [deg]	120	90	90
V [Å³]	4692.0(6)	7459.6(6)	2188.3(3)
Z	2	8	4
Density (calcd) [g cm⁻³]	1.374	1.710	1.787
μ [mm⁻¹]	3.998	2.063	3.366
F (000)	1932	3864	1168
Crystal size (mm³)	0.052 × 0.082 × 0.480	0.176 × 0.218 × 0.379	0.057 × 0.119 × 0.263
θ range for data collection [deg]	2.44 to 25.68	2.32 to 27.11	2.33 to 25.35
Reflections collected	80648	131912	25602
Independent reflections	5932	8237	4002
Data/restraints/parameters	5932 / 0 / 310	8237 / 165 / 482	4002 / 0 / 247
GOF on F²	6.938	1.030	1.043
Final R1	0.3981	0.0245	0.0688
wR2 [I > 2σ(I)]	0.7089	0.0410	0.0837
Largest diff. peak and hole [eÅ⁻³]	51.671 and -12.897	0.537 and -0.375	0.535 and -0.851

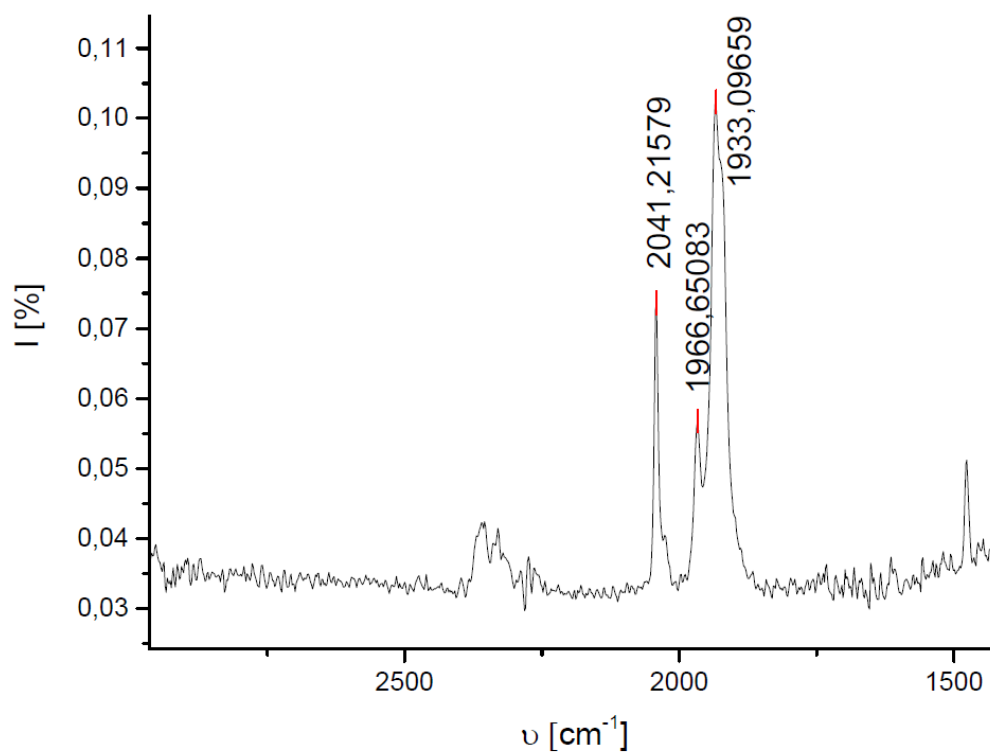
SD 35: Crystallographic data and structure refinement parameters of complexes **50**, **48** and **53**.

Substance identification	50	48	53
Chemical formula	C ₃₄ H ₄₂ Br ₂ CoGe ₂ N ₆	C ₄₁ H ₅₀ Br ₂ FeGe ₂ N ₆	C ₃₄ H ₄₂ Cl ₂ Ge ₂ N ₆ Pt
Fw [g mol⁻¹]	898.66	987.74	945.90
T [K]	100(2)	100(2)	100(2)
Crystal system	monoclinic	triclinic	triclinic
Space group	<i>P121/c1</i>	<i>P-1</i>	<i>P-1</i>
a [Å]	9.1018(17)	9.336(3)	15.181(5)
b [Å]	14.529(3)	13.203(4)	19.061(6)
c [Å]	27.377(6)	18.644(5)	21.069(7)
α [deg]	90	100.172(9)	106.231(10)
β [deg]	90.945(11)	101.896(9)	96.322(10)
γ [deg]	90	107.086(9)	99.749(10)
V [Å³]	3615.6	2079.3(10)	4
Z	4	2	1.104
Density (calcd) [g cm⁻³]	1.651	1.578	3.618
μ [mm⁻¹]	4.348	3.739	3.618
F (000)	1796	996	1856
Crystal size (mm³)	0.111 × 0.119 × 0.144	0.116 × 0.156 × 0.248	0.096 × 0.188 × 0.330
θ range for data collection [deg]	2.24 to 25.68	2.26 to 26.37	2.19 to 25.35
Reflections collected	80002	61902	175472
Independent reflections	6857	8505	20795
Data/restraints/parameters	6857 / 48 / 412	8505 / 0 / 476	20795 / 0 / 823
GOF on F²	1.015	1.050	1.019
Final R1	0.0569	0.0463	0.0459
wR2 [I > 2σ(I)]	0.0640	0.0685	0.0757
Largest diff. peak and hole [eÅ⁻³]	0.803 and -0.754	0.807 and -0.452	1.380 and -1.483

SD 36: Crystallographic data and structure refinement parameters of complexes **51** and **30**.

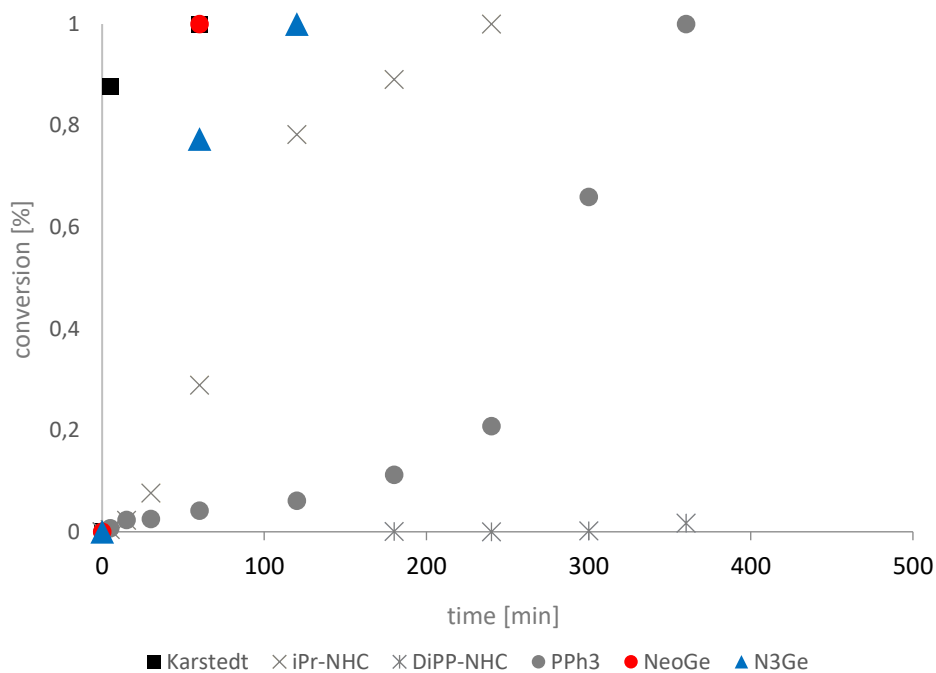
Substance identification	51	30	56
Chemical formula	C ₃₄ H ₄₆ Br ₂ N ₆ Ni	C ₁₆ H ₁₂ Cl ₂ GeN ₄	C ₇₂ H ₆₂ Ge ₂ N ₈ OP ₂ Pt
Fw [g mol⁻¹]	757.30	403.84	1457.50
T [K]	100(2)	100(2)	100(2)
Crystal system	triclinic	monoclinic	Monoclinic
Space group	<i>P</i> -1	<i>P</i> 121/ <i>c</i> 1	<i>C</i> 1 2/ <i>c</i> 1
a [Å]	9.9281(4)	9.7819(5)	20.785(3)
b [Å]	12.7902(6)	22.5815(10)	18.998(3)
c [Å]	16.4671(8)	7.0785(4)	18.306(2)
α [deg]	68.220(2)	90	90
β [deg]	80.186(2)	101.645(3)	96.778(5)
γ [deg]	89.931(2)	90	90
V [Å³]	1908.95(15)	1531.38(14)	7168.7(16)
Z	2	2	4
Density (calcd) [g cm⁻³]	1.318	1.751	1.350
μ [mm⁻¹]	2.630	2.352	2.870
F (000)	780	808	2920
Crystal size (mm³)	0.125 × 0.129 × 0.135	0.224 × 0.286 × 0.595	0.150 × 0.153 × 0.184
θ range for data collection [deg]	2.27 to 26.02	2.12 to 25.02	1.91 to 25.35
Reflections collected	50103	13215	147205
Independent reflections	7511	2711	6545
Data/restraints/parameters	7511 / 329 / 504	2711 / 0 / 208	6545 / 0 / 389
GOF on F²	1.018	1.066	1.129
Final R1	0.0436	0.0414	0.0562
wR2 [I > 2σ(I)]	0.0831	0.0907	0.1582
Largest diff. peak and hole [eÅ⁻³]	1.009 and -0.589	1.502 and -0.409	3.369 and -1.145

6.5 Infrared Spectroscopy

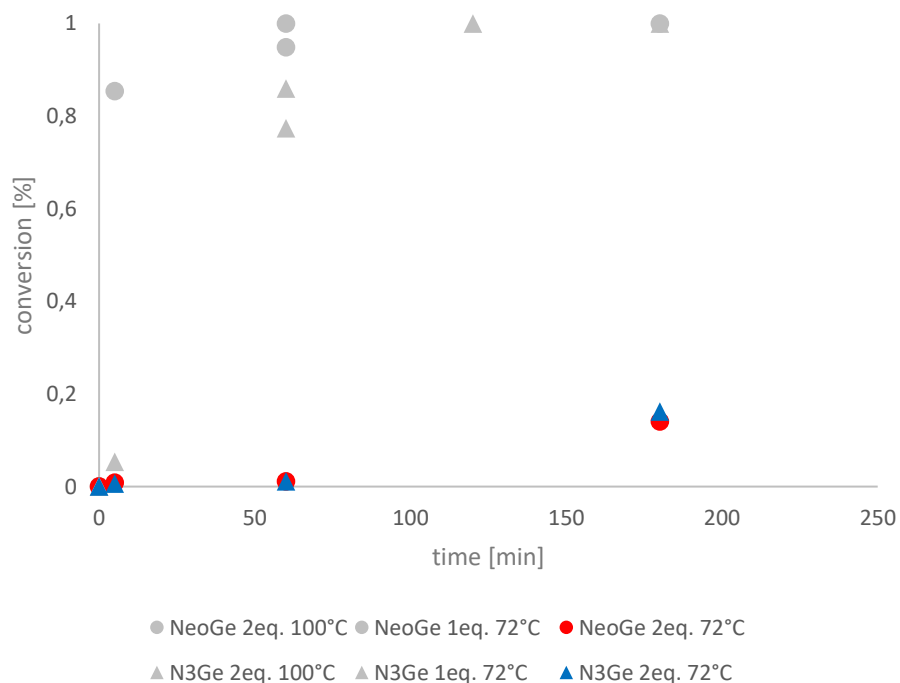


SD 37: Cut-out of the infrared spectrum of **35** (15 mg/mL). Reference spectrum of benzene has been subtracted.

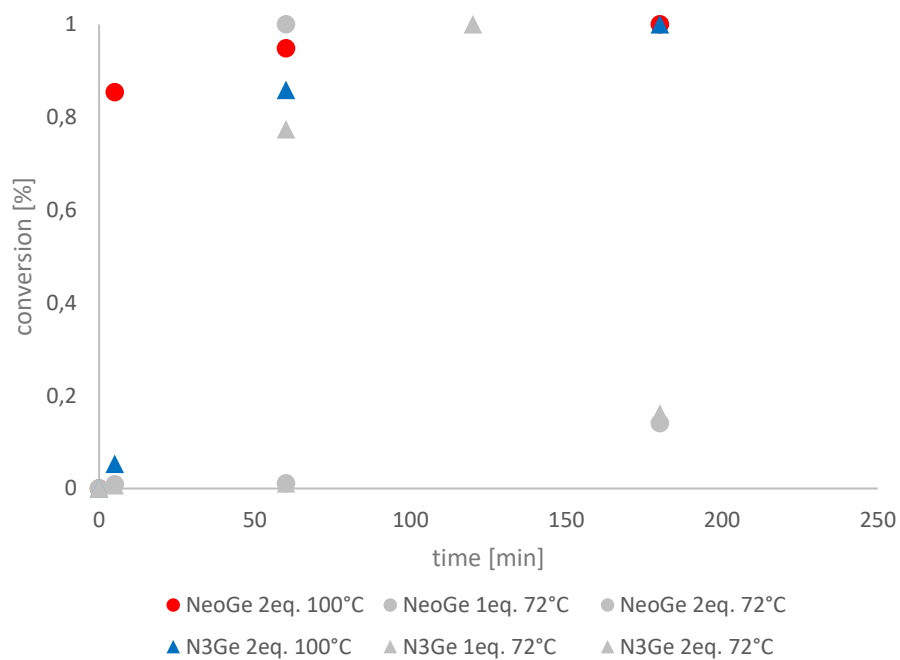
6.6 Catalytic Experiments



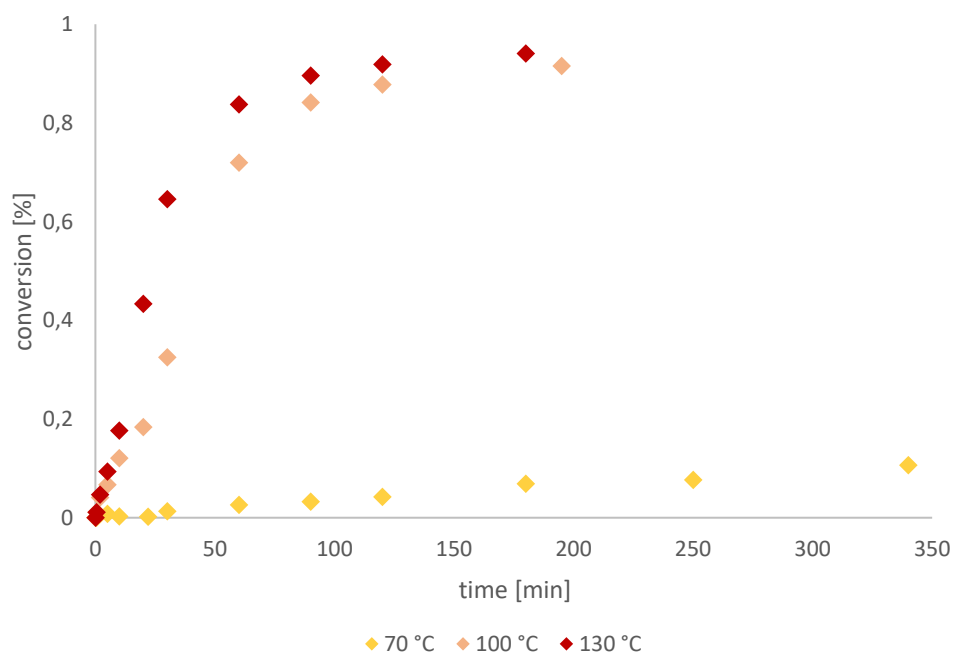
SD 38: Conversion versus time graphs of the platinum-catalyzed hydrosilylation reaction of *n*-octene and HSi with different additives in a 1:1 ratio (Pt:additive) at 72 °C.



SD 39: Conversion versus time graphs of the platinum-catalyzed hydrosilylation reaction of *n*-octene and HSi using NeoGe and N3Ge as additives in a 1:2 ratio (Pt:additive) at 72 °C.



SD 40: Conversion versus time graphs of the platinum-catalyzed hydrosilylation reaction of *n*-octene and HSi using NeoGe and N3Ge as additives in a 1:2 ratio (Pt:additive) at 100 °C.



SD 41: Conversion versus time graphs of the platinum-catalyzed hydrosilylation reaction of *n*-octene and HSi using N4Ge as additive in a 1:2 ratio (Pt:additive) at different temperatures.

7 REFERENCES

1. C. Betz, A. Hitzler, S. Hoffmann, T. Volkert and F. Wölfl, *Gesellschaft im 21. Jahrhundert: Entwicklungen und Herausforderungen*, Buchner, C.C. Verlag, 2013.
2. V. Brühl, *Wirtschaft des 21. Jahrhunderts: Herausforderungen in der Hightech-Ökonomie*, Springer Fachmedien Wiesbaden, 2015.
3. L. Lloyd, *Handbook of Industrial Catalysts*, Springer, New York, 2011.
4. *Catalytic Process Development for Renewable Materials*, Wiley-VCH, eds. P. Imhof and J. C. v. d. Waal, Weinheim, 2013.
5. J. A. Tyrell, *Fundamentals of Industrial Chemistry: Pharmaceuticals, Polymers, and Business*, Wiley, 2014.
6. W. Cabri, *Catalysis: A key technology for a green approach to pharmaceutical production*, 2007.
7. M. Beller, *Med. Chem. Rev.*, 1999, **19**, 357-369.
8. H.-J. Wernicke and R. W. Fischer, *CIT*, 2006, **78**, 825-834.
9. R. Van Santen, *NRSC-Catalysis*, 2009, **4**, 1-84.
10. M. Gürsoy and M. Karaman, *Surface Treatments for Biological, Chemical and Physical Applications*, Wiley, 2017.
11. A. A. Zagorodni, in *Ion Exchange Materials*, ed. A. A. Zagorodni, Elsevier, Oxford, 2007, pp. 377-395.
12. J. W. Erisman, M. A. Sutton, J. Galloway, Z. Klimont and W. Winiwarter, *Nat Geosci.*, 2008, **1**, 636-639.
13. R. A. Sheldon, *J. Chem. Technol. Biot.*, 1997, **68**, 381-388.
14. R. M. Heck, R. J. Farrauto and S. T. Gulati, *Catalytic Air Pollution Control: Commercial Technology*, Wiley, 2016.
15. G. J. K. Acres and B. Harrison, *Top. Catal.*, 2004, **28**, 3-11.
16. B. Marciniec, *Hydrosilylation: A Comprehensive Review on Recent Advances*, Springer Netherlands, 2009.
17. B. Marciniec, *Comprehensive Handbook on Hydrosilylation*, Pergamon Press, 1992.
18. L. N. Lewis, J. Stein, Y. Gao, R. E. Colborn and G. Hutchins, *Platinum Met. Rev.*, 1997, **41**, 66-75.
19. M. F. Lappert, T. A. Nile and S. Takahashi, *J. Organomet. Chem.*, 1974, **72**, 425-439.
20. A. Behr and P. Neubert, *Applied Homogeneous Catalysis*, Wiley-VCH, Weinheim, 2012.
21. J. G. Freeze, H. R. Kelly and V. S. Batista, *Chem. Rev.*, 2019, **119**, 6595-6612.
22. *World Refining Catalysts*, The Freedonia Group Inc., Cleveland, Ohio, 2016.
23. I. T. Horváth and P. T. Anastas, *Chem. Rev.*, 2007, **107**, 2169-2173.
24. K. Sanderson, *Nature*, 2011, **469**, 18-20.
25. P. van Leeuwen, *Homogeneous Catalysis – Understanding the Art*, Springer, Netherlands, 2004.
26. S. Zhang, L. Nguyen, Y. Zhu, S. Zhan, C.-K. Tsung and F. Tao, *Acc. Chem. Res*, 2013, **46**, 1731-1739.
27. J. Hagen, *Industrial Catalysis: A Practical Approach* Wiley-VCH, Weinheim, 2006.
28. R. Whyman, *Applied Organometallic Chemistry and Catalysis*, Oxford University Press, Oxford, 2001.
29. P. W. N. M. v. Leeuwen and J. C. Chadwick, in *Homogeneous Catalysts*, Wiley-VCH, Weinheim, 2011, pp. 1-49.
30. B. M. Murphy and B. Xu, *Prog. Energy Combust. Sci.*, 2018, **67**, 1-30.
31. N. Bahri-Laleh, A. Hanifpour, S. A. Mirmohammadi, A. Poater, M. Nekoomanesh-Haghighi, G. Talarico and L. Cavallo, *Prog. Polym. Sci.*, 2018, **84**, 89-114.
32. B. Cornils, W. A. Herrmann, M. Beller and R. Paciello, *Applied Homogeneous Catalysis with Organometallic Compounds: A Comprehensive Handbook in Four Volumes*, Wiley-VCH, Weinheim, 2017.
33. A. Thomas and M. Driess, *Angew. Chem. Int. Ed.*, 2009, **48**, 1890-1892.

34. Y. Liang, J. Wei, X. Qiu and N. Jiao, *Chem. Rev.*, 2018, **118**, 4912-4945.
35. M. I. Childers, J. M. Longo, N. J. Van Zee, A. M. LaPointe and G. W. Coates, *Chem. Rev.*, 2014, **114**, 8129-8152.
36. L. Hong, W. Sun, D. Yang, G. Li and R. Wang, *Chem. Rev.*, 2016, **116**, 4006-4123.
37. L. C. Wilkins and R. L. Melen, *Coord. Chem. Rev.*, 2016, **324**, 123-139.
38. A.-M. Caminade and R. Laurent, *Coord. Chem. Rev.*, 2019, **389**, 59-72.
39. The Nobel Prize in Chemistry 2001, nobelprize.org/prizes/chemistry/2001/summary/, (accessed 26.06.2019).
40. The Nobel Prize in Chemistry 2005, nobelprize.org/prizes/chemistry/2005/summary/, (accessed 25.06.2019).
41. The Nobel Prize in Chemistry 2010 nobelprize.org/prizes/chemistry/2010/summary/, (accessed 25.06.2019).
42. R. H. Crabtree, *New. J. Chem.*, 2011, **35**, 18-23.
43. K. Riener, S. Haslinger, A. Raba, M. P. Högerl, M. Cokoja, W. A. Herrmann and F. E. Kühn, *Chem. Rev.*, 2014, **114**, 5215-5272.
44. V. Y. Lee and A. Sekiguchi, *Organometallic Compounds of Low-Coordinate Si, Ge, Sn and Pb: From Phantom Species to Stable Compounds*, Wiley, 2011.
45. J. C. Chadwick, R. Duchateau, Z. Freixa and P. W. N. M. van Leeuwen, *Homogeneous Catalysts: Activity - Stability - Deactivation*, Wiley, 2011.
46. W. A. Herrmann, C. Köcher, L. J. Gooßen and G. R. J. Artus, *Chem. Eur. J.*, 1996, **2**, 1627-1636.
47. W. A. Herrmann and C. Köcher, *Angew. Chem. Int. Ed.*, 1997, **36**, 2162-2187.
48. F. Glorius and S. Bellemin-Laponnaz, *N-Heterocyclic Carbenes in Transition Metal Catalysis*, Springer, 2007.
49. C. S. J. Cazin, *N-Heterocyclic Carbenes in Transition Metal Catalysis and Organocatalysis*, Springer, Netherlands, 2011.
50. K. Izod, *Coord. Chem. Rev.*, 2013, **257**, 924-945.
51. S. Yao, Y. Xiong and M. Driess, *Organometallics*, 2011, **30**, 1748-1767.
52. M. Kira, *Chem. Commun.*, 2010, **46**, 2893-2903.
53. R. S. Ghadwal, R. Azhakar and H. W. Roesky, *Acc. Chem. Res.*, 2013, **46**, 444-456.
54. C.-W. So, H. W. Roesky, J. Magull and R. B. Oswald, *Angew. Chem. Int. Ed.*, 2006, **45**, 3948-3950.
55. S. Raoufmoğhaddam, Y.-P. Zhou, Y. Wang and M. Driess, *J. Organomet. Chem.*, 2016.
56. B. Blom, D. Gallego and M. Driess, *Inorg. Chem. Front.*, 2014, **1**, 134-148.
57. B. Blom, M. Stoelzel and M. Driess, *Chem. Eur. J.*, 2013, **19**, 40-62.
58. M. Asay, C. Jones and M. Driess, *Chem. Rev.*, 2011, **111**, 354-396.
59. S. K. Mandal and H. W. Roesky, *Chem. Commun.*, 2010, **46**, 6016-6041.
60. C. Boehme and G. Frenking, *Organometallics*, 1998, **17**, 5801-5809.
61. H. W. Roesky, *J. Organomet. Chem.*, 2013, **730**, 57-62.
62. T. A. N. Nguyen and G. Frenking, *Chem. Eur. J.*, 2012, **18**, 12733-12748.
63. H. Arp, J. Baumgartner, C. Marschner, P. Zark and T. Müller, *J. Am. Chem. Soc.*, 2012, **134**, 10864-10875.
64. J. T. York, V. G. Young and W. B. Tolman, *Inorg. Chem.*, 2006, **45**, 4191-4198.
65. G. Trinquier, *J. Am. Chem. Soc.*, 1990, **112**, 2130-2137.
66. S. S. Kostina, T. Singh and W. J. Leigh, *Organometallics*, 2012, **31**, 3755-3767.
67. L. Álvarez-Rodríguez, J. A. Cabeza, P. García-Álvarez and D. Polo, *Coord. Chem. Rev.*, 2015, **300**, 1-28.
68. A. Meltzer, C. Präsang and M. Driess, *J. Am. Chem. Soc.*, 2009, **131**, 7232-7233.
69. A. Meltzer, S. Inoue, C. Präsang and M. Driess, *J. Am. Chem. Soc.*, 2010, **132**, 3038-3046.
70. M. Driess, S. Yao, M. Brym, C. van Wüllen and D. Lentz, *J. Am. Chem. Soc.*, 2006, **128**, 9628-9629.
71. F. Lips, J. C. Fettinger, A. Mansikkamäki, H. M. Tuononen and P. P. Power, *J. Am. Chem. Soc.*, 2014, **136**, 634-637.

72. L. Sun, G. Jin, W. Feng, P. Lu, M. He and J. Xie, *J. Organomet. Chem.*, 2011, **696**, 841-845.
73. B. Blom, M. Pohl, G. Tan, D. Gallego and M. Driess, *Organometallics*, 2014, **33**, 5272-5282.
74. S. Yao, Y. Xiong, W. Wang and M. Driess, *Chem. Eur. J.*, 2011, **17**, 4890-4895.
75. A. K. Swarnakar, S. M. McDonald, K. C. Deutsch, P. Choi, M. J. Ferguson, R. McDonald and E. Rivard, *Inorg. Chem.*, 2014, **53**, 8662-8671.
76. E. Rivard, *Dalton Trans.*, 2014, **43**, 8577-8586.
77. W. Petz, *Chem. Rev.*, 1986, **86**, 1019-1047.
78. G. Schmid and E. Welz, *Angew. Chem. Int. Ed.*, 1977, **16**, 785-786.
79. K. Junold, J. A. Baus, C. Burschka and R. Tacke, *Angew. Chem. Int. Ed.*, 2012, **51**, 7020-7023.
80. K. Junold, J. A. Baus, C. Burschka, T. Vent-Schmidt, S. Riedel and R. Tacke, *Inorg. Chem.*, 2013, **52**, 11593-11599.
81. F. M. Mück, J. A. Baus, R. Bertermann, C. Burschka and R. Tacke, *Organometallics*, 2016, **35**, 2583-2588.
82. J. A. Baus, F. M. Mück, H. Schneider and R. Tacke, *Chem. Eur. J.*, 2017, **23**, 296-303.
83. R. Tacke and T. Ribbeck, *Dalton Trans.*, 2017, **46**, 13628-13659.
84. Y. Apeloig, R. Pauncz, M. Karni, R. West, W. Steiner and D. Chapman, *Organometallics*, 2003, **22**, 3250-3256.
85. M. Z. Kassae, H. Zandi, M. R. Momeni, F. A. Shakib and M. Ghambarian, *J. Mol. Struct.*, 2009, **913**, 16-21.
86. B. Gehrhuis, P. B. Hitchcock, R. Pongtavornpinyo and L. Zhang, *Dalton Trans.*, 2006, 1847-1857.
87. M. Haaf, T. A. Schmedake and R. West, *Acc. Chem. Res*, 2000, **33**, 704-714.
88. Y. Mizuhata, T. Sasamori and N. Tokitoh, *Chem. Rev.*, 2009, **109**, 3479-3511.
89. W. Levason, G. Reid and W. Zhang, *Coord. Chem. Rev.*, 2011, **255**, 1319-1341.
90. P. Zark, A. Schäfer, A. Mitra, D. Haase, W. Saak, R. West and T. Müller, *J. Organomet. Chem.*, 2010, **695**, 398-408.
91. N. Tokitoh, Y. Matsushashi, K. Shibata, T. Matsumoto, H. Suzuki, M. Saito, K. Manmaru and R. Okazaki, *Main Group Metal Chemistry*, 1994, **17**, 55.
92. M. E. Alberto, N. Russo and E. Sicilia, *Chem. Eur. J.*, 2013, **19**, 7835-7846.
93. T. J. Hadlington, T. Szilvási and M. Driess, *Angew. Chem. Int. Ed.*, 2017, **56**, 7470-7474.
94. Z. D. Brown and P. P. Power, *Inorg. Chem.*, 2013, **52**, 6248-6259.
95. D. Wendel, A. Porzelt, F. A. D. Herz, D. Sarkar, C. Jandl, S. Inoue and B. Rieger, *J. Am. Chem. Soc.*, 2017, **139**, 8134-8137.
96. D. Wendel, D. Reiter, A. Porzelt, P. J. Altmann, S. Inoue and B. Rieger, *J. Am. Chem. Soc.*, 2017, **139**, 17193-17198.
97. T. Hadlington, M. Driess and C. Jones, *Chem. Soc. Rev.*, 2018, **47**, 4176-4197.
98. Z. Benedek and T. Szilvasi, *RSC Adv.*, 2015, **5**, 5077-5086.
99. Z. Benedek and T. Szilvási, *Organometallics*, 2017, **36**, 1591-1600.
100. M. Denk, R. Lennon, R. Hayashi, R. West, A. V. Belyakov, H. P. Verne, A. Haaland, M. Wagner and N. Metzler, *J. Am. Chem. Soc.*, 1994, **116**, 2691-2692.
101. M. Denk, J. C. Green, N. Metzler and M. Wagner, *Dalton Trans.*, 1994, 2405-2410.
102. A. J. Arduengo, H. Bock, H. Chen, M. Denk, D. A. Dixon, J. C. Green, W. A. Herrmann, N. L. Jones, M. Wagner and R. West, *J. Am. Chem. Soc.*, 1994, **116**, 6641-6649.
103. W. A. Herrmann, M. Denk, J. Behm, W. Scherer, F.-R. Klingan, H. Bock, B. Solouki and M. Wagner, *Angew. Chem. Int. Ed.*, 1992, **31**, 1485-1488.
104. D. Bourissou, O. Guerret, F. P. Gabbaï and G. Bertrand, *Chem. Rev.*, 2000, **100**, 39-92.
105. F. E. Hahn, *Angew. Chem. Int. Ed.*, 2006, **45**, 1348-1352.
106. C. Heinemann, T. Müller, Y. Apeloig and H. Schwarz, *J. Am. Chem. Soc.*, 1996, **118**, 2023-2038.
107. C. Boehme and G. Frenking, *J. Am. Chem. Soc.*, 1996, **118**, 2039-2046.
108. A. K. Guha and A. K. Phukan, *J. Org. Chem.*, 2014, **79**, 3830-3837.
109. S. Krupski, R. Pöttgen, I. Schellenberg and F. E. Hahn, *Dalton Trans.*, 2014, **43**, 173-181.
110. F. Ullah, G. Bajor, T. Veszprémi, P. G. Jones and J. W. Heinicke, *Angew. Chem. Int. Ed.*, 2007, **46**, 2697-2700.

111. L. Pause, M. Robert, J. Heinicke and O. Kühn, *J. Chem. Soc., Perkin Trans. 1*, 2001, 1383-1388.
112. O. Kühn, P. Lönnecke and J. Heinicke, *Polyhedron*, 2001, **20**, 2215-2222.
113. P. J. Davidson, D. H. Harris and M. F. Lappert, *Dalton Trans.*, 1976, 2268-2274.
114. D. H. Harris, M. F. Lappert, J. B. Pedley and G. J. Sharp, *Dalton Trans.*, 1976, 945-950.
115. F. Ullah, O. Kühn, G. Bajor, T. Veszprémi, P. G. Jones and J. Heinicke, *Eur. J. Inorg. Chem.*, 2009, **2009**, 221-229.
116. X. Yun, Y. Shenglai and D. Matthias, *Chem. Asian J.*, 2012, **7**, 2145-2150.
117. S. K. Mandal and H. W. Roesky, *Acc. Chem. Res.*, 2012, **45**, 298-307.
118. G. Tan, W. Wang, B. Blom and M. Driess, *Dalton Trans.*, 2014, **43**, 6006-6011.
119. R. Dasgupta, S. Das, S. Hiwase, S. K. Pati and S. Khan, *Organometallics*, 2019, **38**, 1429-1435.
120. A. Fürstner, H. Krause and C. W. Lehmann, *Chem. Commun.*, 2001, 2372-2373.
121. M. Zhang, X. Liu, C. Shi, C. Ren, Y. Ding and H. W. Roesky, *Z. Anorg. Allg. Chem.*, 2008, **634**, 1755-1758.
122. G. Tan, S. Enthaler, S. Inoue, B. Blom and M. Driess, *Angew. Chem. Int. Ed.*, 2015, **54**, 2214-2218.
123. B. Blom, S. Enthaler, S. Inoue, E. Irran and M. Driess, *J. Am. Chem. Soc.*, 2013, **135**, 6703-6713.
124. A. Brück, D. Gallego, W. Wang, E. Irran, M. Driess and J. F. Hartwig, *Angew. Chem. Int. Ed.*, 2012, **51**, 11478-11482.
125. Y. Wang, M. Karni, S. Yao, Y. Apeloig and M. Driess, *J. Am. Chem. Soc.*, 2019, **141**, 1655-1664.
126. Z. Mo, A. Kostenko, Y.-P. Zhou, S. Yao and M. Driess, *Chem. Eur. J.*, 2018, **24**, 14608-14612.
127. Y.-P. Zhou, S. Raoufmoghaddam, T. Szilvási and M. Driess, *Angew. Chem. Int. Ed.*, 2016, **55**, 12868-12872.
128. S. Raoufmoghaddam, Y.-P. Zhou, Y. Wang and M. Driess, *J. Organomet. Chem.*, 2017, **829**, 2-10.
129. Y.-P. Zhou, M. Karni, S. Yao, Y. Apeloig and M. Driess, *Angew. Chem. Int. Ed.*, 2016, **55**, 15096-15099.
130. W. Wang, S. Inoue, S. Yao and M. Driess, *J. Am. Chem. Soc.*, 2010, **132**, 15890-15892.
131. D. Gallego, S. Inoue, B. Blom and M. Driess, *Organometallics*, 2014, **33**, 6885-6897.
132. P. Blakeman, B. Gehrhus, J. C. Green, J. Heinicke, M. F. Lappert, M. Kindermann and T. Veszprémi, *Dalton Trans.*, 1996, 1475-1480.
133. S. Krupski, J. V. Dickschat, A. Hepp, T. Pape and F. E. Hahn, *Organometallics*, 2012, **31**, 2078-2084.
134. A. V. Zabula and F. E. Hahn, *Eur. J. Inorg. Chem.*, 2008, **2008**, 5165-5179.
135. F. E. Hahn, A. V. Zabula, T. Pape and A. Hepp, *Eur. J. Inorg. Chem.*, 2007, **2007**, 2405-2408.
136. A. V. Zabula, F. E. Hahn, T. Pape and A. Hepp, *Organometallics*, 2007, **26**, 1972-1980.
137. S. S. Sen, S. Khan, S. Nagendran and H. W. Roesky, *Acc. Chem. Res.*, 2012, **45**, 578-587.
138. B. Gehrhus, P. B. Hitchcock and M. F. Lappert, *Z. Anorg. Allg. Chem.*, 2005, **631**, 1383-1386.
139. M. Driess, S. Yao, M. Brym and C. van Wüllen, *Angew. Chem. Int. Ed.*, 2006, **45**, 4349-4352.
140. M. A. Brook, *Silicon in Organic, Organometallic and Polymer Chemistry*, Wiley, New York, 2000.
141. B. Marciniak, *Silicon Chem. 1*, 2002, **1**, 155-174.
142. R. G. Jones, W. Ando and J. Chojnowski, *Silicon-Containing Polymers: The Science and Technology of Their Synthesis and Applications*, Springer Netherlands, 2013.
143. B. Marciniak, in *Applied Homogeneous Catalysis with Organometallic Compounds*, eds. W. A. Herrmann and B. Cornils, Wiley-VCH, 2017, pp. 569-620.
144. J. L. Speier, J. A. Webster and G. H. Barnes, *J. Am. Chem. Soc.*, 1957, **79**, 974-979.
145. B. D. Karstedt, General Electric Co., US3775452, 1973.
146. D. Troegel and J. Stohrer, *Coord. Chem. Rev.*, 2011, **255**, 1440-1459.
147. J. F. Harrod and A. J. Chalk, *J. Am. Chem. Soc.*, 1965, **87**, 1133-1133.
148. T. K. Meister, K. Riener, P. Giggler, J. Stohrer, W. A. Herrmann and F. E. Kühn, *ACS Catal.*, 2016, **6**, 1274-1284.
149. G. Chandra, P. Y. Lo, P. B. Hitchcock and M. F. Lappert, *Organometallics*, 1987, **6**, 191-192.
150. J. Stein, L. N. Lewis, Y. Gao and R. A. Scott, *J. Am. Chem. Soc.*, 1999, **121**, 3693-3703.

151. A. K. Roy and R. B. Taylor, *J. Am. Chem. Soc.*, 2002, **124**, 9510-9524.
152. M. A. Schroeder and M. S. Wrighton, *J. Organomet. Chem.*, 1977, **128**, 345-358.
153. J. C. Mitchener and M. S. Wrighton, *J. Am. Chem. Soc.*, 1981, **103**, 975-977.
154. C. L. Randolph and M. S. Wrighton, *J. Am. Chem. Soc.*, 1986, **108**, 3366-3374.
155. F. Seitz and M. S. Wrighton, *Angew. Chem. Int. Ed.*, 1988, **27**, 289-291.
156. T. Suzuki and P. Y. Lo, *J. Organomet. Chem.*, 1990, **396**, 299-305.
157. D. A. Armitage, in *Comprehensive Organometallic Chemistry*, Pergamon, Oxford, 1982, p. 117.
158. J. V. Obligacion and P. J. Chirik, *Nat. Rev. Chem.*, 2018, **2**, 15-34.
159. Y. Nakajima and S. Shimada, *RSC Adv.*, 2015, **5**, 20603-20616.
160. N. R. Council, *The Role of the Chemical Sciences in Finding Alternatives to Critical Resources: A Workshop Summary*, The National Academies Press, eds. D. Friedman, T. Masciangioli and S. Olson, Washington, DC, 2012.
161. I. E. Markó, S. Stérin, O. Buisine, G. Mignani, P. Branlard, B. Tinant and J. P. Declercq, *Science* 2002, **298**, 204-207.
162. S. Dierick and I. E. Markó, in *N-Heterocyclic Carbenes*, ed. S. P. Nolan, Wiley-VCH, Weinheim, 2014, pp. 111-150.
163. J. J. Dunsford, K. J. Cavell and B. Kariuki, *J. Organomet. Chem.*, 2011, **696**, 188-194.
164. M. A. Taige, S. Ahrens and T. Strassner, *J. Organomet. Chem.*, 2011, **696**, 2918-2927.
165. J. J. Hu, F. Li and T. S. A. Hor, *Organometallics*, 2009, **28**, 1212-1220.
166. G. F. Silbestri, J. C. Flores and E. de Jesus, *Organometallics*, 2012, **31**, 3355-3360.
167. S. Pisiewicz, K. Junge and M. Beller, *Eur. J. Inorg. Chem.*, 2014, **2014**, 2345-2349.
168. I. E. Markó, S. Stérin, O. Buisine, G. Berthon, G. Michaud, B. Tinant and J.-P. Declercq, *Adv. Synth. Catal.*, 2004, **346**, 1429-1434.
169. O. Buisine, G. Berthon-Gelloz, J.-F. Brière, S. Stérin, G. Mignani, P. Branlard, B. Tinant, J.-P. Declercq and I. E. Markó, *Chem. Commun.*, 2005, 3856-3858.
170. I. E. Markó, G. Berthon-Gelloz, O. Buisine, J.-F. Briere, G. Michaud, S. Stérin, G. Mignani, B. Tinant, J. P. Declercq and D. Chapon, *J. Organomet. Chem.*, 2005, **690**, 6156-6168.
171. A. M. Tondreau, C. C. H. Atienza, K. J. Weller, S. A. Nye, K. M. Lewis, J. G. P. Delis and P. J. Chirik, *Science*, 2012, **335**, 567-570.
172. T. K. Meister, J. W. Kück, K. Riener, A. Pöthig, W. A. Herrmann and F. E. Kühn, *J. Catal.*, 2016, **337**, 157-166.
173. V. César, S. Bellemin-Laponnaz, H. Wadepohl and L. H. Gade, *Chem. Eur. J.*, 2005, **11**, 2862-2873.
174. G. Berthon-Gelloz, Doctoral Thesis, Université Catholique de Louvain, 2007.
175. P. B. Glaser and T. D. Tilley, *J. Am. Chem. Soc.*, 2003, **125**, 13640-13641.
176. E. Calimano and T. D. Tilley, *J. Am. Chem. Soc.*, 2008, **130**, 9226-9227.
177. T. Troadec, A. Prades, R. Rodriguez, R. Mirgalet, A. Baceiredo, N. Saffon-Merceron, V. Branchadell and T. Kato, *Inorg. Chem.*, 2016, **55**, 8234-8240.
178. T. Iimura, N. Akasaka and T. Iwamoto, *Organometallics*, 2016, **35**, 4071-4076.
179. T. Iimura, N. Akasaka, T. Kosai and T. Iwamoto, *Dalton Trans.*, 2017, **46**, 8868-8874.
180. M. Tanabe, M. Kamono, K. Tanaka and K. Osakada, *Organometallics*, 2017, **36**, 1929-1935.
181. B. Marciniec, K. Posafa, I. Kownacki, M. Kubicki and R. Taylor, *ChemCatChem*, 2012, **4**, 1935-1937.
182. *Platinum Quarterly*, World Platinum Investment Council Ltd., London, 2019.
183. Price charts-Platinum, platinum.matthey.com/prices/price-charts, (accessed 26.06.2019).
184. A. N. Nesmeyanov, R. K. Freidlina, E. C. Chukovskaya, R. G. Petrova and A. B. Belyavsky, *Tetrahedron*, 1962, **17**, 61-68.
185. Y. Sunada, H. Tsutsumi, K. Shigeta, R. Yoshida, T. Hashimoto and H. Nagashima, *Dalton Trans.*, 2013, **42**, 16687-16692.
186. B. Marciniec and M. Majchrzak, *Inorg. Chem.*, 2000, **3**, 371-375.
187. R. D. Adams, U. Bunz, B. Captain, W. Fu and W. Steffen, *J. Organomet. Chem.*, 2000, **614-615**, 75-82.

188. F. Kakiuchi, Y. Tanaka, N. Chatani and S. Murai, *J. Organomet. Chem.*, 1993, **456**, 45-47.
189. S. C. Bart, E. Lobkovsky and P. J. Chirik, *J. Am. Chem. Soc.*, 2004, **126**, 13794-13807.
190. N. G. Léonard and P. J. Chirik, *ACS Catal.*, 2018, **8**, 342-348.
191. C. H. Schuster, T. Diao, I. Pappas and P. J. Chirik, *ACS Catal.*, 2016, **6**, 2632-2636.
192. C. C. H. Atienza, T. Diao, K. J. Weller, S. A. Nye, K. M. Lewis, J. G. P. Delis, J. L. Boyer, A. K. Roy and P. J. Chirik, *J. Am. Chem. Soc.*, 2014, **136**, 12108-12118.
193. C. C. Hojilla Atienza, A. M. Tondreau, K. J. Weller, K. M. Lewis, R. W. Cruse, S. A. Nye, J. L. Boyer, J. G. P. Delis and P. J. Chirik, *ACS Catal.*, 2012, **2**, 2169-2172.
194. A. C. Bowman, C. Milsmann, C. C. Hojilla Atienza, E. Lobkovsky, K. Wieghardt and P. J. Chirik, *J. Am. Chem. Soc.*, 2010, **132**, 1676-1684.
195. W. Wang, S. Inoue, E. Irran and M. Driess, *Angew. Chem. Int. Ed.*, 2012, **51**, 3691-3694.
196. J. V. Dickschat, D. Heitmann, T. Pape and F. E. Hahn, *J. Organomet. Chem.*, 2013, **744**, 160-164.
197. F. E. Hahn, A. V. Zabula, T. Pape and F. Hupka, *Z. Anorg. Allg. Chem.*, 2009, **635**, 1341-1344.
198. A. V. Zabula, T. Pape, A. Hepp, F. M. Schappacher, U. C. Rodewald, R. Pöttgen and F. E. Hahn, *J. Am. Chem. Soc.*, 2008, **130**, 5648-5649.
199. A. V. Zabula, T. Pape, A. Hepp and F. E. Hahn, *Dalton Trans.*, 2008, **43**, 5886-5890.
200. T. T. Metsanen, D. Gallego, T. Szilvasi, M. Driess and M. Oestreich, *Chem. Sci.*, 2015, **6**, 7143-7149.
201. W. Wang, S. Inoue, S. Enthaler and M. Driess, *Angew. Chem. Int. Ed.*, 2012, **51**, 6167-6171.
202. M. Schmidt, B. Blom, T. Szilvási, R. Schomäcker and M. Driess, *Eur. J. Inorg. Chem.*, 2017, **2017**, 1284-1291.
203. M.-P. Luecke, D. Porwal, A. Kostenko, Y.-P. Zhou, S. Yao, M. Keck, C. Limberg, M. Oestreich and M. Driess, *Dalton Trans.*, 2017, **46**, 16329-16714.
204. A. Kostenko, S. Yao, M. Driess and Y. Wang, *J. Am. Chem. Soc.*, 2017, **139**, 13499-13506.
205. F. E. Hahn, A. V. Zabula, T. Pape, A. Hepp, R. Tonner, R. Haunschuld and G. Frenking, *Chem. Eur. J.*, 2008, **14**, 10716-10721.
206. A. D. Ibrahim, K. Tokmic, M. R. Brennan, D. Kim, E. M. Matson, M. J. Nilges, J. A. Bertke and A. R. Fout, *Dalton Trans.*, 2016, **45**, 9805-9811.
207. A. D. Ibrahim, S. W. Entsminger, L. Zhu and A. R. Fout, *ACS Catal.*, 2016, **6**, 3589-3593.
208. C. Wasielewski, L. Dembkowski and M. Topolski, *Synthesis*, 1989, **1989**, 52-53.
209. H. C. Brown, S. Narasimhan and Y. O. N. G. M. Choi, *Synthesis*, 1981, **1981**, 441-442.
210. J. Heinicke, A. Oprea, M. K. Kindermann, T. Karpati, L. Nyulászai and T. Veszprémi, *Chem. Eur. J.*, 1998, **4**, 541-545.
211. R. D. Rieke, S. E. Bales, P. M. Hudnall, T. P. Burns and G. S. Poindexter, *Org. Synth.*, 1979, **59**, 85.
212. C. G. Screttas and M. Micha-Screttas, *J. Org. Chem.*, 1983, **48**, 153-158.
213. L. S. H. Dixon, A. F. Hill, A. Sinha and J. S. Ward, *Organometallics*, 2014, **33**, 653-658.
214. Chemcraft - graphical software for visualization of quantum chemistry computations, chemcraftprog.com, (accessed 05.07.2019).
215. S. S. Sen, S. Khan, P. P. Samuel and H. W. Roesky, *Chem. Sci.*, 2012, **3**, 659-682.
216. A. V. Zabula, I. A. Guzei, R. West, J. Li and A. Y. Rogachev, *Angew. Chem. Int. Ed.*, 2016, **55**, 13465-13469.
217. S. S. Sen, A. Jana, H. W. Roesky and C. Schulzke, *Angew. Chem. Int. Ed.*, 2009, **48**, 8536-8538.
218. A. C. Tomasik, A. Mitra and R. West, *Organometallics*, 2009, **28**, 378-381.
219. M. Haaf, T. A. Schmedake, B. J. Paradise and R. West, *Can. J. Chem.*, 2000, **78**, 1526-1533.
220. J. Koe, *Polym. Int.*, 2009, **58**, 255-260.
221. S. S. Bukalov, Y. V. Zubavichus, L. A. Leites, J. R. Koe and R. West, *Polymer*, 2009, **50**, 4845-4851.
222. W. Li, N. J. Hill, A. C. Tomasik, G. Bikzhanova and R. West, *Organometallics*, 2006, **25**, 3802-3805.
223. J. R. Koe, in *Comprehensive Organometallic Chemistry III*, eds. D. M. P. Mingos and R. H. Crabtree, Elsevier, Oxford, 2007, pp. 549-649.

224. S. M. Parke, E. Hupf, G. K. Matharu, I. de Aguiar, L. Xu, H. Yu, M. P. Boone, G. L. C. de Souza, R. McDonald, M. J. Ferguson, G. He, A. Brown and E. Rivard, *Angew. Chem. Int. Ed.*, 2018, **57**, 14841-14846.
225. E. Rivard, *Chem. Let.*, 2015, **44**, 730-736.
226. G. He, L. Kang, W. Torres Delgado, O. Shynkaruk, M. J. Ferguson, R. McDonald and E. Rivard, *J. Am. Chem. Soc.*, 2013, **135**, 5360-5363.
227. O. Köhl, *Coord. Chem. Rev.*, 2004, **248**, 411-427.
228. F. Walz, E. Moos, D. Garnier, R. Köppe, C. E. Anson and F. Breher, *Chem. Eur. J.*, 2017, **23**, 1173-1186.
229. M. Veith, S. Becker and V. Huch, *Angew. Chem. Int. Ed.*, 1989, **28**, 1237-1238.
230. M. Grosser and M. Veith, *Z. Naturforsch. B*, 1982, **37**, 1375-1381.
231. D. Lei, M. J. Hampden-Smith and E. N. Duesler, *Polyhedron*, 1990, **9**, 1127-1129.
232. B. Marciniak, H. Maciejewski and J. Mirecki, *J. Organomet. Chem.*, 1991, **418**, 61-67.
233. A. V. Zabula, A. Y. Rogachev and R. West, *Chem. Eur. J.*, 2014, **20**, 16652-16656.
234. F. Kaiser, R. M. Reich, E. Rivard and F. E. Kühn, *Organometallics*, 2018, **37**, 136-144.
235. F. Dyckhoff, F. Kaiser, S. Hölzl and F. E. Kühn, *Z. Anorg. Allg. Chem.*, 2019, **645**, 207-211.
236. H. Cui, Y. Shao, X. Li, L. Kong and C. Cui, *Organometallics*, 2009, **28**, 5191-5195.
237. H. Yoo, P. J. Carroll and D. H. Berry, *J. Am. Chem. Soc.*, 2006, **128**, 6038-6039.
238. D. Himmel, I. Krossing and A. Schnepf, *Angew. Chem. Int. Ed.*, 2014, **53**, 370-374.
239. A. Haaland, *Angew. Chem. Int. Ed.*, 1989, **28**, 992-1007.
240. E. K. Lermontova, M. Huan, A. V. Churakov, J. A. K. Howard, M. V. Zabalov, S. S. Karlov and G. S. Zaitseva, *Dalton Trans.*, 2009, 4695-4702.
241. W. P. Leung, C. W. So, Y. S. Wu, H. W. Li and T. C. W. Mak, *Eur. J. Inorg. Chem.*, 2005, **2005**, 513-521.
242. R. West, D. F. Moser, I. A. Guzei, G.-H. Lee, A. Naka, W. Li, A. Zabula, S. Bukalov and L. Leites, *Organometallics*, 2006, **25**, 2709-2711.
243. T. Chen, W. Hunks, P. S. Chen, C. Xu, A. G. DiPasquale and A. L. Rheingold, *Organometallics*, 2010, **29**, 501-504.
244. W.-P. Leung, Z.-X. Wang, H.-W. Li and T. C. W. Mak, *Angew. Chem. Int. Ed.*, 2001, **40**, 2501-2503.
245. C. Jones, R. P. Rose and A. Stasch, *Dalton Trans.*, 2008, 2871-2878.
246. B. Prashanth and S. Singh, *Dalton Trans.*, 2016, **45**, 6079-6087.
247. G. Ossig, A. Meller, C. Brönneke, O. Müller, M. Schäfer and R. Herbst-Irmer, *Organometallics*, 1997, **16**, 2116-2120.
248. Y.-L. Shan, B.-X. Leong, H.-W. Xi, R. Ganguly, Y. Li, K. H. Lim and C.-W. So, *Dalton Trans.*, 2017, **46**, 3642-3648.
249. Y.-L. Shan, W.-L. Yim and C.-W. So, *Angew. Chem. Int. Ed.*, 2014, **53**, 13155-13158.
250. S. M. I. Al-Rafia, M. R. Momeni, R. McDonald, M. J. Ferguson, A. Brown and E. Rivard, *Angew. Chem. Int. Ed.*, 2013, **52**, 6390-6395.
251. J. I. Schweizer, M. G. Scheibel, M. Diefenbach, F. Neumeyer, C. Würtele, N. Kulminkaya, R. Linser, N. Auner, S. Schneider and M. C. Holthausen, *Angew. Chem. Int. Ed.*, 2016, **55**, 1782-1786.
252. F. Uhlemann and A. Schnepf, *Chem. Eur. J.*, 2016, **22**, 10748-10753.
253. W.-P. Leung, H. Cheng, R.-B. Huang, Q.-C. Yang and T. C. W. Mak, *Chem. Commun.*, 2000, 451-452.
254. C. Drost, P. B. Hitchcock and M. F. Lappert, *Angew. Chem. Int. Ed.*, 1999, **38**, 1113-1116.
255. W.-P. Leung, W.-H. Kwok, F. Xue and T. C. W. Mak, *J. Am. Chem. Soc.*, 1997, **119**, 1145-1146.
256. A. Mcheik, N. Katir, A. Castel, H. Gornitzka, S. Massou, P. Rivière and T. Hamieh, *Eur. J. Inorg. Chem.*, 2008, **2008**, 5397-5403.
257. W. Yang, H. Fu, H. Wang, M. Chen, Y. Ding, H. W. Roesky and A. Jana, *Inorg. Chem.*, 2009, **48**, 5058-5060.

258. L. Álvarez-Rodríguez, J. A. Cabeza, P. García-Álvarez, E. Pérez-Carreño and D. Polo, *Inorg. Chem.*, 2015, **54**, 2983-2994.
259. P. Nie, Y. Li, Q. Yu, B. Li, H. Zhu and T.-B. Wen, *Eur. J. Inorg. Chem.*, 2017, **2017**, 3892-3899.
260. R. Azhakar, S. P. Sarish, H. W. Roesky, J. Hey and D. Stalke, *Inorg. Chem.*, 2011, **50**, 5039-5043.
261. L. W. Pineda, V. Jancik, J. F. Colunga-Valladares, H. W. Roesky, A. Hofmeister and J. Magull, *Organometallics*, 2006, **25**, 2381-2383.
262. I. Saur, G. Rima, K. Miqueu, H. Gornitzka and J. Barrau, *J. Organomet. Chem.*, 2003, **672**, 77-85.
263. R. Azhakar, H. W. Roesky, J. J. Holstein and B. Dittrich, *Dalton Trans.*, 2012, **41**, 12096-12100.
264. I. A. Portnyagin and M. S. Nechaev, *J. Organomet. Chem.*, 2009, **694**, 3149-3153.
265. G. Tavčar, S. S. Sen, R. Azhakar, A. Thorn and H. W. Roesky, *Inorg. Chem.*, 2010, **49**, 10199-10202.
266. S. Warratz, L. Postigo and B. Royo, *Organometallics*, 2013, **32**, 893-897.
267. M. Veith, S. Becker and V. Huch, *Angew. Chem. Int. Ed.*, 1990, **29**, 216-218.
268. A. Jana, P. P. Samuel, H. W. Roesky and C. Schulzke, *J. Fluor. Chem.*, 2010, **131**, 1096-1099.
269. T. Ochiai, D. Franz, X. N. Wu and S. Inoue, *Dalton Trans.*, 2015, **44**, 10952-10956.
270. A. R. Rossi and R. Hoffmann, *Inorg. Chem.*, 1975, **14**, 365-374.
271. R. W. Chorley, P. B. Hitchcock, M. F. Lappert, W.-P. Leung, P. P. Power and M. M. Olmstead, *Inorg. Chim. Acta*, 1992, **198-200**, 203-209.
272. S.-P. Chia, E. Carter, H.-W. Xi, Y. Li and C.-W. So, *Angew. Chem. Int. Ed.*, 2014, **53**, 8455-8458.
273. T. J. Marks, *J. Am. Chem. Soc.*, 1971, **93**, 7090-7091.
274. M. Weidenbruch, Z. Rappoport and Y. Apeloig, *The Chemistry of Organic Silicon Compounds*, Wiley, 2001.
275. J. Zheng, J. B. Sortais and C. Darcel, *ChemCatChem*, 2014, **6**, 763-766.
276. L. Álvarez-Rodríguez, J. Brugos, J. A. Cabeza, P. García-Álvarez and E. Pérez-Carreño, *Chem. Eur. J.*, 2017, **23**, 15107-15115.
277. S. Wu, X. Li, Z. Xiong, W. Xu, Y. Lu and H. Sun, *Organometallics*, 2013, **32**, 3227-3237.
278. J. Takaya, N. Kirai and N. Iwasawa, *J. Am. Chem. Soc.*, 2011, **133**, 12980-12983.
279. J. Takaya and N. Iwasawa, in *Pincer and Pincer-Type Complexes*, eds. K. J. Szabó and O. F. Wendt, Wiley-VCH, Weinheim, pp. 229-248.
280. L. Alvarez-Rodríguez, J. Brugos, J. A. Cabeza, P. Garcia-Alvarez, E. Perez-Carreno and D. Polo, *Chem. Commun.*, 2017, **53**, 893-896.
281. J. Brugos, J. A. Cabeza, P. García-Álvarez and E. Pérez-Carreño, *Organometallics*, 2018, **37**, 1507-1514.
282. J. Berthe, J. M. Garcia, E. Ocando, T. Kato, N. Saffon-Merceron, A. De Cózar, F. P. Cossío and A. Baceiredo, *J. Am. Chem. Soc.*, 2011, **133**, 15930-15933.
283. B. Çetinkaya, E. Çetinkaya, J. A. Chamizo, P. B. Hitchcock, H. A. Jasim, H. Küçükbay and M. F. Lappert, *J. Chem. Soc., Perkin Trans. 1*, 1998, 2047-2054.
284. T. Heidemann and S. Mathur, *Eur. J. Inorg. Chem.*, 2014, **2014**, 506-510.
285. T. A. Schmedake, M. Haaf, B. J. Paradise, A. J. Millevolte, D. R. Powell and R. West, *J. Organomet. Chem.*, 2001, **636**, 17-25.
286. K. M. Baines and W. G. Stibbs, *Coord. Chem. Rev.*, 1995, **145**, 157-200.
287. R. K. Siwatch, D. Yadav, G. Mukherjee, G. Rajaraman and S. Nagendran, *Inorg. Chem.*, 2014, **53**, 5073-5079.
288. S. Karwasara, M. K. Sharma, R. Tripathi and S. Nagendran, *Organometallics*, 2013, **32**, 3830-3836.
289. R. K. Siwatch and S. Nagendran, *Organometallics*, 2012, **31**, 3389-3394.
290. S. Sinhababu, R. K. Siwatch, G. Mukherjee, G. Rajaraman and S. Nagendran, *Inorg. Chem.*, 2012, **51**, 9240-9248.
291. S. S. Sen, R. S. Ghadwal, D. Kratzert, D. Stern, H. W. Roesky and D. Stalke, *Organometallics*, 2011, **30**, 1030-1033.
292. N. Tokitoh, T. Matsumoto, K. Manmaru and R. Okazaki, *J. Am. Chem. Soc.*, 1993, **115**, 8855-8856.

293. T. S. Piper, D. Lemal and G. Wilkinson, *Naturwissenschaften*, 1956, **43**, 129-129.
294. I. Buslov, J. Becouse, S. Mazza, M. Montandon-Clerc and X. Hu, *Angew. Chem. Int. Ed.*, 2015, **54**, 14523-14526.
295. A. M. Tondreau, C. C. H. Atienza, J. M. Darmon, C. Milsmann, H. M. Hoyt, K. J. Weller, S. A. Nye, K. M. Lewis, J. Boyer, J. G. P. Delis, E. Lobkovsky and P. J. Chirik, *Organometallics*, 2012, **31**, 4886-4893.
296. M. R. Friedfeld, G. W. Margulieux, B. A. Schaefer and P. J. Chirik, *J. Am. Chem. Soc.*, 2014, **136**, 13178-13181.
297. I. Pappas, S. Treacy and P. J. Chirik, *ACS Catal.*, 2016, **6**, 4105-4109.
298. N. M. Weliange, D. S. McGuinness, M. G. Gardiner and J. Patel, *Dalton Trans.*, 2016, **45**, 10842-10849.
299. P. Bag, S. U. Ahmad and S. Inoue, *Bull. Chem. Soc. Jpn.*, 2017, **90**, 255-271.
300. A. G. Avent, B. Gehrhus, P. B. Hitchcock, M. F. Lappert and H. Maciejewski, *J. Organomet. Chem.*, 2003, **686**, 321-331.
301. H.-X. Yeong, Y. Li and C.-W. So, *Organometallics*, 2014, **33**, 3646-3648.
302. J. M. García, E. Ocando-Mavárez, T. Kato, D. S. Coll, A. Briceño, N. Saffon-Merceron and A. Baceiredo, *Inorg. Chem.*, 2012, **51**, 8187-8193.
303. M. T. Whited, A. M. Deetz, J. W. Boerma, D. E. DeRoshia and D. E. Janzen, *Organometallics*, 2014, **33**, 5070-5073.
304. L. S. Bresler, N. A. Buzina, Y. S. Varshavsky, N. V. Kiseleva and T. G. Cherkasova, *J. Organomet. Chem.*, 1979, **171**, 229-235.
305. J. W. Grate and S. N. Kaganove, *Polym. News*, 1999, **24**, 149-155.
306. J. W. Sprengers, M. de Greef, M. A. Duin and C. J. Elsevier, *Eur. J. Inorg. Chem.*, 2003, 3811-3819.
307. J. W. Sprengers, M. J. Mars, M. A. Duin, K. J. Cavell and C. J. Elsevier, *J. Organomet. Chem.*, 2003, **679**, 149-152.
308. S. Ishida, R. Sugawara, Y. Misawa and T. Iwamoto, *Angew. Chem. Int. Ed.*, 2013, **52**, 12869-12873.
309. A. Leyva-Pérez and A. Corma, *Angew. Chem. Int. Ed.*, 2012, **51**, 614-635.
310. D. M. etGampe, S. Schramm, S. Ziemann, M. Westerhausen, H. Görls, P. Naumov and R. Beckert, *J. Org. Chem.*, 2017, **82**, 6153-6162.
311. M. Paul, P. Sudkaow, A. Wessels, N. E. Schlörer, J.-M. Neudörfl and A. Berkessel, *Angew. Chem. Int. Ed.*, 2018, **57**, 8310-8315.
312. *APEX suite of crystallographic software. APEX 2 Version 2008.4.*, Bruker AXS Inc., Madison, USA 2008.
313. *SAINT, version 7.56a, SADABS, version 2008.1*, Bruker AXS Inc., Madison, Wisconsin, USA 2008.
314. G. M. Sheldrick, *SHELXS-97 A Program for Crystal Structure Solution*, Göttingen, 1997.
315. C. B. Huebschle, G. M. Sheldrick and B. Dittrich, *J. Appl. Crystallogr.*, 2011, **44**, 1281-1284.
316. G. M. Sheldrick, *SHELXL-2014*, University of Göttingen, Göttingen, 2014.
317. A. J. C. Wilson, *International Tables for Crystallography, Vol. C, Tables 6.1.1.4 (pp. 500-502), 4.2.6.8 (pp. 219-222), and 4.2.4.2 (pp. 193-199)*, Kluwer Academic Publishers, Dordrecht, Netherlands, 1992.
318. A. L. Spek, *PLATON A Multipurpose Crystallographic Tool*, Utrecht University, Utrecht, Netherlands, 2010.
319. M. J. Frisch, G. W. Trucks, H. B. Schlegel, G. E. Scuseria, M. A. Robb, J. R. Cheeseman, G. Scalmani, V. Barone, G. A. Petersson, H. Nakatsuji, X. Li, M. Caricato, A. V. Marenich, J. Bloino, B. G. Janesko, R. Gomperts, B. Mennucci, H. P. Hratchian, J. V. Ortiz, A. F. Izmaylov, J. L. Sonnenberg, D. F. Williams, F. Lipparini, F. Egidi, J. Goings, B. Peng, A. Petrone, T. Henderson, D. Ranasinghe, V. G. Zakrzewski, J. Gao, N. Rega, G. Zheng, W. Liang, M. Hada, M. Ehara, K. Toyota, R. Fukuda, J. Hasegawa, M. Ishida, T. Nakajima, Y. Honda, O. Kitao, H. Nakai, T. Vreven, K. Throssell, M. J. J. A, J. E. Peralta, F. Ogliaro, M. J. Bearpark, J. J. Heyd, E. N. Brothers, K. N. Kudin, V. N. Staroverov, T. A. Keith, R. Kobayashi, J. Normand, K. Raghavachari, A. P. Rendell,

-
- J. C. Burant, S. S. Iyengar, J. Tomasi, M. Cossi, J. M. Millam, M. Klene, C. Adamo, R. Cammi, J. W. Ochterski, R. L. Martin, K. Morokuma, O. Farkas, J. B. Foresman and D. J. Fox, *Gaussian 16*, Gaussian, Inc., Wallingford CT, 2009.
320. S. Grimme, S. Ehrlich and L. Goerigk, *J. Comput. Chem.*, 2011, **32**, 1456-1465.
321. S. Grimme, *J. Comput. Chem.*, 2006, **27**, 1787-1799.
322. T. A. Keith, *AIMAll (Version 17.01. 25)*, Overland Park, KS, USA, 2017.
323. C. F. Matta and R. J. Boyd, *The Quantum Theory of Atoms in Molecules: From Solid State to DNA and Drug Design*, 2007, 1-30.
324. P. Macchi and A. Sironi, *Coord. Chem. Rev.*, 2003, **238-239**, 383-412.
325. J. Florián, C. C. McLauchlan, D. S. Kissel, C. C. Eichman and A. W. Herlinger, *Inorg. Chem.*, 2015, **54**, 10361-10370.

Complete List of Publications

- Parts of this work were submitted in an invention disclosure at TUM ForTe and are patented by Wacker Chemie AG.
- *Synthesis and Characterization of New N-Heterocyclic Silylazides*
F. Dyckhoff, F. Kaiser, S. Hölzl and F. E. Kühn, *Z. Anorg. Allg. Chem.*, 2019, **645**, 207-211.
- *A Bench Stable Cu(III) N-Heterocyclic Carbene Accessible from Simple Copper(II) Acetate*
S. M. Hölzl, M. R. Anneser, Fritz E. Kühn *256th ACS National Meeting & Exposition 2018*, Boston, USA, Poster.
- *Speciation in iron epoxidation catalysis: A perspective on the discovery and role of non-heme iron(III)-hydroperoxo species in iron-catalyzed oxidation reactions*
S. M. Hölzl,* P. J. Altmann,* J. W. Kück, F. E. Kühn, *Coordination Chemistry Reviews* **2017**, 352, 517-536.

Eidesstattliche Erklärung

Ich erkläre an Eides statt, dass ich die bei der promotionsführenden Einrichtung
TUM Graduate School

der TUM zur Promotionsprüfung vorgelegte Arbeit mit dem Titel:
Heavier N-Heterocyclic Tetrylenes in Platinum-Catalyzed Alkene Hydrosilylation

in der Fakultät für Chemie, Molekulare Katalyse

Fakultät, Institut, Lehrstuhl, Klinik, Krankenhaus, Abteilung

unter der Anleitung und Betreuung durch: Prof. Fritz E. Kühn ohne sonstige Hilfe erstellt und bei der Abfassung nur die gemäß § 6 Ab. 6 und 7 Satz 2 angebotenen Hilfsmittel benutzt habe.

Ich habe keine Organisation eingeschaltet, die gegen Entgelt Betreuerinnen und Betreuer für die Anfertigung von Dissertationen sucht, oder die mir obliegenden Pflichten hinsichtlich der Prüfungsleistungen für mich ganz oder teilweise erledigt.

Ich habe die Dissertation in dieser oder ähnlicher Form in keinem anderen Prüfungsverfahren als Prüfungsleistung vorgelegt.

Die vollständige Dissertation wurde in _____ veröffentlicht. Die promotionsführende Einrichtung

hat der Veröffentlichung zugestimmt.

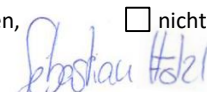
Ich habe den angestrebten Doktorgrad noch nicht erworben und bin nicht in einem früheren Promotionsverfahren für den angestrebten Doktorgrad endgültig gescheitert.

Ich habe bereits am _____ bei der Fakultät für _____ der Hochschule _____ unter Vorlage einer Dissertation mit dem Thema _____ die Zulassung zur Promotion beantragt mit dem Ergebnis: _____

Die öffentlich zugängliche Promotionsordnung der TUM ist mir bekannt, insbesondere habe ich die Bedeutung von § 28 (Nichtigkeit der Promotion) und § 29 (Entzug des Doktorgrades) zur Kenntnis genommen. Ich bin mir der Konsequenzen einer falschen Eidesstattlichen Erklärung bewusst.

Mit der Aufnahme meiner personenbezogenen Daten in die Alumni-Datei bei der TUM bin ich

einverstanden, nicht einverstanden.


München, 09.07.2019, Sebastian Hölzl